MODELING THE POWER REQUIREMENTS OF A ROTARY FEEDING AND CUTTING SYSTEM

A Thesis

Submitted to the College of Graduate Studies and Research

in Partial Fulfillment of the Requirements

for the Degree of

Doctor of Philosophy

in the

Department of Chemical and Biological Engineering

University of Saskatchewan

Saskatoon, Saskatchewan

By

Eric Veikle

July, 2011

COPYRIGHT

ABSTRACT

The purpose of this study was to develop an analytical model that could be used by the designers of a rotary feeding and cutting system (RFCS) to identify the power demand of the RFCS with limited or no required field or laboratory data. Two separate RFCS were investigated, incorporated with either a low-speed cutting process (LSCP) or a high-speed cutting process (HSCP). The results from the laboratory and field trials were used to create and validate the analytical model.

Laboratory tests were completed with the LSCP RFCS and these concluded that counter-knife sharpness, serrations and bevel angle all had significant effects on the specific energy required by the LSCP RFCS when processing cereal straw and alfalfa. The specific energy required by the LSCP RFCS, while processing cereal straw, increased by 0.35 kW·h/tonne (or 96%) when the sharpness of the counter-knives decreased from 0.13 to 0.63 mm (where the sharpness was recorded by the leading-edge-width of the counter-knives). With the same decrease in sharpness, the specific energy required by the LSCP RFCS while processing alfalfa increased by 0.04 kW·h/tonne (or 32%). The specific energy required by the LSCP RFCS while processing cereal straw with sharp counter-knives (counter-knives with a leading edge width of 0.13 mm) increased by 0.11 kW·h/tonne (or 51%) when serrated counter-knives were used instead of un-serrated counter-knives. However, counter-knife serrations did not have a significant effect on the specific energy demand of the LSCP RFCS when sharp counter-knives were used to process alfalfa. The increase in bevel angle from 15 to 90° caused the specific energy required to process cereal straw and alfalfa to approximately triple. The moisture content of alfalfa also had a significant effect on the specific energy required to process alfalfa with the LSCP RFCS. The specific energy demand of the LSCP RFCS was at a maximum when alfalfa at a moisture content of 53% on a wet basis (w.b.) was processed and decreased slightly (approximately 0.04 kW·h/tonne or 10%) when dryer and wetter alfalfa was processed.

Field tests were completed with the HSCP RFCS and it was concluded that in general, there was a direct relationship between the specific energy required by the HSCP RFCS and the moisture content of the straw, counter-knife engagement and throughput.

Further, it was also concluded that the specific energy requirements of the HSCP RFCS were more sensitive to counter-knife engagement when higher moisture content straw was processed. Depending on the type of chopper used, the specific energy required by the HSCP RFCS increased anywhere from 0.15 to 0.77 kW·h/tonne (or 22 to 61%) when the counter-knife engagement was increased from 0 to 100% (or fully removed to fully engaged). Again, depending on the type of chopper used, when the moisture content of the straw processed by the chopper increased from approximately 7 to 25% w.b. the specific energy required by the chopper increased by 0.14 to 0.96 kW·h/tonne (or 28 to 84%). The effect of throughput on the specific energy demand of the HSCP RFCS was dependent on the type of chopper used. For one of the choppers, an increase in throughput from 10.5 to 13.5 tonne/h caused the specific energy required by the HSCP RFCS to increase by 0.24 kW·h/tonne (or 35%); however for a different chopper, an increase in throughput from 12 to 13 tonne/h caused the specific energy demand of the HSCP RFCS to decrease by 0.16 kW·h/tonne (or 19%).

The analytical model was validated using a subset of the data that were collected while employing each cutting device under field conditions and the data collected with the use of a custom-designed material properties test stand. The output of the analytical model fell within the 95% confidence interval of the measured power demand for each of the rotary feeding and cutting systems, and the analytical model was therefore deemed sufficiently accurate.

Based on the analytical model, the total power demand of both the LSCP and HSCP rotary feeding and cutting systems was largely attributed to the power required to transport plant material. Further, the power required to transport the plant material along the sides of the counter-knives was much greater than the power required to transport the plant material along the rotor bed and along the leading edge of the tines. Because of the excessive power required to transport plant material along the sides of the counter-knives, three techniques were identified as potential strategies to decrease the power demand of the RFCS. The first technique involved removing half of the tines from the RFCS, and modifying the remaining tines to decrease the amount of plant material that is entrapped between sides of the counter-knives and the tines. The second technique involved

coating the inside surface of the tines with a baked Teflon, to decrease the coefficient of friction between the plant material and the RFCS. The third technique involved reshaping the counter-knives, to decrease the surface area over which plant material was transported along the side of the counter-knives. According to the analytical model, employing any of the three techniques would result in the total power demand of the RFCS to decrease by 15 to 26%.

For the HSCP RFCS, a stochastic model was developed to identify which of the four choppers tested during field trials would have the best performance when subjected to the same operating conditions. The chopper with the best performance was the WR chopper as its use resulted in the minimum geometric mean length of material exiting the combine harvester while also consuming the least amount of specific energy.

ACKNOWLEDGMENTS

The completion of this manuscript and of this project could not have been accomplished without the guidance and support of the following individuals:

- My supervisor, Dr. Martin Roberge for giving me the opportunity to grow as a researcher, and for giving me the opportunity to continue to conduct research in my area of interest.
- My supervisor, Dr. Trever Crowe, for the time you spent reviewing my manuscript and for the guidance you provided me during the project,
- All of the members of my supervisory committee, Dr. Scott Noble, Dr. Terrance Fonstad, Dr. Claude Lague, Dr. Greg Schoenau for your time invested in reviewing my thesis and the feedback provided during our meetings,
- The students in the Department of Agricultural and Bioresource Engineering, in particular Mr. Ryan Roberge and Mr. Lyndon Graff for your constructive criticisms and your help with the collection of field data,
- The individuals that assisted me during the collection of the field data with the HSCP RFCS, Mr. Jason Benes and Mr. Nathan Isaac, and
- Mr. Kevin Smith for helping collect the laboratory data with the LSCP RFCS.

Thank you all for the support you provided over the duration of this project!

Finally, I would also like to take this opportunity to thank the institutions for their financial support during this project. The financial support was provided by the Natural Science and Engineering Research Council (NSERC), the Department of Agricultural and Bioresource Engineering, The University of Saskatchewan Dean's Fund, The University of Saskatchewan College of Engineering Scholarships and CNH Canada Ltd. (part of CNH Global N.V).

DEDICATION

I dedicate this manuscript to my parents Lynn and Anita, and my brother Jason. Thank you for your love and support.

I dedicate this project to the persons who have literally saved my life (a few times over): Dr. N.J. Lowry, Dr. M.J. Tyrrell, Dr. A. Kakadekar, Ms. J. Cooper, Ms. L Zinger, Dr. W. G. Williams, Dr. R.M. Gow, Dr. R.M. Hamilton, Dr. I.M. Rebeyka, Dr. M.J. Kantoch, Dr. J.D. McMeekin, Dr. D.G. Wyse, Dr. J.M. Rothschild, Dr. J. Akhtar, Mr. K. Cornish and Mr. P. Runalls. It is amazing how time changes one's perspective. I once thought I was cursed with hypertrophic cardiomyopathy, now I realize how fortunate I am. I do not have the words to express how grateful I am for what you all have done for me. Without you all I would not be here today, nor would this project have been completed. Thank you!

TABLE OF CONTENTS

LIST OF TABLES

LIST OF FIGURES

LIST OF ABREVIATIONS

ANOVA	Analysis of variance
ASABE	American society of agricultural and biological engineers
ASAE	American society of agricultural engineers
ASTM	American society for testing and materials
CI	Confidence interval
CNH	Case new holland. An International company that designs and fabricates agricultural and industrial equipment.
GML	Geometric mean length
HSCP	High speed cutting process
LSCP	Low speed cutting process
LSM	Least squares means
LVDT	Linearly variable displacement transformer
MOG	Material other than grain
NA	Not applicable
N/A	Not available
RFCS	Rotary feeding and cutting system
rpm	Revolutions per minute
R^2	Represents the coefficient of determination
w.b.	Wet basis. Indicates that a moisture content is given with respect to the wet-mass of the specimen.
WR	Wide rotor. A chopper with tines that are mounted in a “V pattern” that is used in the combine harvester.

2X0.5 A chopper with two knives mounted in the same plane and the helical pattern of knives makes one half of a revolution across the width of the chopper.

2X3 A chopper with two knives mounted in the same plane and the helical pattern of knives makes three revolutions across the width of the chopper.

3X3 A chopper with three knives mounted in the same plane and the helical pattern of knives makes three revolutions across the width of the chopper.

LIST OF SYMBOLS

A	The cross-sectional area of compression (m^2)
A	The period before the crop entered the RFCS
$a_{3\ to\ 0}$	The coefficients of the third order polynomial used to define the Young's modulus of a given plant material (Pa)
AO_{MT}	The angular offset between the model and trial rotor (°)
AO_T	The angular offset between tines that cut on adjacent counter-knives (°)
AO_{T2}	The angular offset between the center and outside tines (°)
A_p	The cross-sectional area of the compression plate on the material properties test stand (m^2)
A_{punch}	The cross-sectional area of the punch used on the material properties test stand (m^2)
A_{shear}	The cross-sectional area of shear (m^2)
$A_{sm\ dull}$	The cross-sectional area of compression when dull counter-knives were used in the RFCS (m^2)
$A_{sm\ sharp}$	The cross-sectional area of compression when sharp counter-knives were used in the RFCS (m^2)
A_{sm}	The cross-sectional area of the plant material when it was cut (m^2)
A_v	Represents the allowable variation used to determine N_{um} (%)
avg	An intermediate averaging variable used in the analytical model
B	The period after the crop exited the RFCS
C	An indexing variable used in the analytical model
C_0	Represents the no-load power demand of a forage harvester header (kW)

C_1	Represents the constant power demand of a forage harvester header (kW·h/Mg)
C1	An indexing variable used in the analytical model
C2	An indexing variable used in the analytical model
CO1	Constant term used to quantify *ENLS* and is dependent on the coefficient of friction between the plant material being cut and the cutting device (kJ kg^{-1} m^{-1})
CO2	Constant term used to quantify *ENLS* and represents the power loss due to the friction of the chopped plant material and the housing, the movement of air, the pickup and the feeding mechanism (kJ/kg wet material)
d	Distance the body is moved (m)
E	The Young's modulus of the plant material (Pa)
E_a	The Young's modulus of the alfalfa processed by the RFCS (kPa)
EFC	Indicates the cutting efficiency of a rotary mower (decimal)
E_n	The Young's modulus of the plant material in the n^{th} zone (Pa)
ENC1	Indicates the cutting energy of a single cut made by a forager harvester (J)
ENCS	Indicates the specific cutting energy required by a forage harvester (kJ/kg dry matter)
ENCSAE	Indicates the specific energy per unit of field area required by a mower (kJ/m^2)
ENCSM	Indicates the specific cutting energy per material cut length (kJ·mm/kg dry material)
ENLS	Indicates the specific energy caused by the losses (kJ/kg wet material)
E_s	The Young's modulus of the cereal straw process by the RFCS (kPa)
F_{medium}	The average of the upper and lower limit of the factor of interest

F	The force required to transport the body (N)
F_{AP}	The average force required to pull the plant material across a steel surface (N)
F_{CM}	The maximum compressive force exerted by the hydraulic cylinder (N)
$F_{compress_{m_n}}$	The force required to compress the plant material in the n^{th} zone of the m^{th} cut (N)
$F_{cs_{m_n}}$	The force required to compress and cut plant material in n^{th} zone of the m^{th} cut made by the RFCS (N)
F_{cut_m}	The force required to cut the plant material of the m^{th} cut made by the RFCS (N)
F_{f_n}	The frictional force acting on the tine leading edge in the n^{th} zone (N)
$F_{f_{rb}}$	The frictional force between the plant material and the rotor bed (N)
F_{hc}	The force exerted on the plant material by the hydraulic cylinder on the material properties test stand (N)
F_{high}	The value of the upper limit of the factor of interest
F_{low}	The value of the lower limit of the factor of interest
F_N	The normal force exerted on the plant material (N)
F_{rb}	The normal force of the material on the rotor bed (N)
F_{shear}	The force applied parallel to the cross-sectional area A_{shear} (N)
F_{t_n}	The frictional force acting on the tine in the n^{th} zone (N)
F_t	The force required to achieve a given level of strain (N)
i	The rotor position which ranges from 0 to 359 (°)
Intsum	An intermediate summation variable used in the analytical model

J	The upper bound of the throughput of MOG (dry tonne/h)
k	The number of revolutions the rotor made during the trials while crop was being processed
l_i	The instantaneous depth of plant material in the compression box on the material properties test stand (m)
L_{BL}	The baseline power required to spin the rotor without crop in the RFCS
LLP	Indicates the theoretical length of cut of a device (mm)
lo	The initial depth of the plant material (m)
lo_m	The initial depth of plant material for the m^{th} cut made by the RFCS (m)
$lo_{m\ 2.5\ alfalfa}$	The initial depth of alfalfa for the m^{th} cut made by the RFCS when processing alfalfa at a throughput of 2.5 kg/s (m)
$lo_{m\ 2.5\ straw}$	The initial depth of cereal straw for the m^{th} cut made by the RFCS when processing cereal straw at a throughput of 2.5 kg/s (m)
$lo_{m\ 3.33\ straw}$	The initial depth of cereal straw for the m^{th} cut made by the RFCS at a throughput of 3.33 kg/s (m)
$lo_{m\ 3.75\ alfalfa}$	The initial depth of alfalfa for the m^{th} cut made by the RFCS when processing alfalfa at a throughput of 3.75 kg/s (m)
$lo_{m\ 3.75\ straw}$	The initial depth of cereal straw for the m^{th} cut made by the RFCS when processing cereal straw at a throughput of 3.75 kg/s (m)
$lo_{m\ 5.0\ alfalfa}$	The initial depth of alfalfa for the m^{th} cut made by the RFCS when processing alfalfa at a throughput of 5.0 kg/s (m)
$lo_{m\ 5.0\ straw}$	The initial depth of cereal straw for the m^{th} cut made by the RFCS when processing cereal straw at a throughput of 5.0 kg/s (m)
$lo_{m\ 5.55\ straw}$	The initial depth of cereal straw for the m^{th} cut made by the RFCS at a throughput of 5.55 kg/s (m)

l_{rb}	The rotor bed arc length (m)
LWD	Indicates the width of the cutting device (m)
m	The variable used to indicate cut number
m_{wet}	The wet-mass of plant material (kg)
M	The moisture content of straw processed by the harvester (% w.b.)
MAL	Indicates the material per unit length of a layer (dry g/mm)
MAT	Indicates the material flow rate (kg dry matter/s)
$MATWET$	Indicates the cutting capacity of a device (kg wet material/s)
MC	The moisture content of plant material on a wet basis (decimal)
ms_{s}	The maximum shear strength of cereal straw (MPa)
ms	The maximum shear strength of the plant material (Pa)
ms_{a}	The maximum shear strength of alfalfa (MPa)
N	The rotational speed of the rotor or chopper (rad/s)
n	The variable used to indicate the zone number
η	The sensitivity of the factor (%)
N_{um}	Represents the number of replicates required to achieve an acceptable level of variation based on a defined coefficient of variation
Num	An intermediate summation variable used in the analytical model
P_{m_n}	The compressive force caused by plant material between the tine pair and the sides of the counter-knife in the n^{th} zone of the m^{th} cut (N)
P	Matrix used in the analytical model
$P_{avg\ high}$	The average power demand of the rotor over 360° when the factor of interest is set to its upper limit (W)

$P_{avg\ low}$ The average power demand of the rotor over 360° when the factor of interest is set to its lower limit (W)

$P_{avg\ medium}$ The average power demand of the rotor over 360° when the factor of interest is set to the medium value (W)

P_{base} The power required to spin the rotor without crop flow through the RFCS (W)

P_c The power required to cut plant material with a non-row specific forage harvester header (kW)

$P_{chopper}$ The power required by the straw chopper on the combine harvester (W)

P_{cs_n} The power required to compress, cut and overcome the frictional force between the plant material and the leading edge of the tine in the n^{th} zone (W)

P_{CV} The power required to convey plant material with a non-row specific forage harvester header (kW)

P_D The pressure drop across the hydraulic motor driving the rotor (kPa)

P_{DS} Represents the down-stream pressure of the oil used to transfer power to the rotor motor on the LSCP test apparatus (kPa)

$P_{f\ alfalfa}$ The coefficient that relates the initial depth of alfalfa to the compressive force caused by alfalfa between the sides of a counter-knife and the tine pair (N/m)

$P_{f\ straw}$ The coefficient that relates the initial depth of cereal straw to the compressive force caused by cereal straw between the sides of a counter-knife and the tine pair (N/m)

P_f The coefficient that relates the initial depth of plant material to the compressive force caused by plant material between the sides of a counter-knife and the tine pair (N/m)

P_g	The power required to gather plant material with a non-row specific forage harvester header (kW)
$P_{i_{ave}}$	The position-specific power demand of the rotor at the angular position *i* (W)
P_{LR}	The power required by the rotor on the LSCP RFCS (kW)
P_o	The no-load power required by a non-row specific forage harvester header (kW)
POC	The power required to cut plant material with a forage harvester (kW)
POD	Indicates the total power required by a rotary mower (kW)
POL1	Indicates the constant portion of the power required by a forage harvester (kW)
POLS1,1	Indicates the specific power loss due to the air movement around the rotors and friction in the drive of a rotary mower (kW/m)
POLS1,2	Indicates the specific power loss due to the friction between the rotors and the stubble of a rotary mower (kW/m)
Power	Intermediate summation variable used in the analytical model
P_{pto}	Indicates the power-take-off power required by a forage harvester (kW)
P_{rb}	The power required to transport plant material along the rotor bed (W)
P_{t_n}	The power required to overcome the frictional force of sliding plant material along the sides of a counter-knife in the n^{th} zone (W)
P_{th}	Represents the total power required by a forage harvester header (kW)
P_{US}	Represents the up-stream pressure of the oil used to transfer power to the rotor motor on the LSCP test apparatus (kPa)
P_{wr}	The power required to transport a given body (W)

$Q_{Flow\ 1}$	Represents the oil flow rate through Meter 2 used to quantify the oil flow rate through the rotor motor on the LSCP test apparatus (L/min)
$Q_{Flow\ 2}$	Represents the oil flow rate through Meter 1 used to quantify the oil flow rate through the rotor motor on the LSCP test apparatus (L/min)
Q_{LSCP}	The flow rate of oil through the hydraulic motor used to drive the LSCP RFCS rotor (L/min)
R	The radius of curvature of the rotor bed (m)
Ro	An indexing variable used in the analytical model
Row	An indexing variable used in the analytical model
$\hat{r}$	Radial unit vector
r_5	The midpoint radius of the 5^{th} zone (m)
r_n	The midpoint radius of the n^{th} zone (m)
SE	Represents the specific energy required by a device based on the dry mass of material processed by the device (kW·h/tonne)
SLF	Represents the distance that the plant martial and the cutting device are in contact (m)
Sum	An intermediate summation variable used in the analytical model
sum1	An intermediate summation variable used in the analytical model
t	The period of time in which the body is moved (s)
$\hat{t}$	Tangent unit vector
T	The throughput of plant material on a wet-mass basis (kg/s)
T_1	Used to identify the beginning of the integration period used to quantify the energy consumed by the LSCP RFCS
T_2	Used to identify the end of the integration period used to quantify the energy consumed by the LSCP RFCS

$T_{chopper}$	The torque applied to the chopper shaft (N·m)
T_{dry}	Indicates the dry-mass throughput of plant material (tonne/h)
T_n	The torque that must be applied to the rotor to compress, cut and overcome the friction force between the plant material and the leading edge of the tine in the n^{th} zone (N·m)
T_{rq}	Represents the torque applied to any of the choppers (N·m)
t_s	Represents the value of a student's t for a two sided limit at a 95% probability level and infinite degrees of freedom used to determine N_{um}
T_{t_n}	The torque the must be applied to the rotor to overcome the frictional force of sliding plant material along the sides of a counter-knife in the n^{th} zone (N·m)
T_{wet}	Indicates the wet-mass throughput of plant material through the device (tonne/h)
v	The velocity of plant material tangential to the radius of curvature of the rotor bed (m/s)
$\mathbf{V}$	Matrix used in the analytical model
V	Represents the signal from the Wheatstone bridge on any of the straw choppers (V)
VLF	Indicates the forward velocity of a vehicle (m/s)
VLK	Represents the velocity of the cutter (m/s)
w	The width of compression (m)
w_{dull}	The width of compression when dull counter-knives were employed in the RFCS (m)
w_{sharp}	The width of compression when sharp counter-knives were employed in the RFCS (m)

x	Represents the signal from a pressure or flow sensor (V)
$\mathbf{X}$	Matrix used in the analytical model
$\mathbf{Z}$	Matrix used in the analytical model
α_n	The angle between the leading and lagging edge of the tine at the midpoint of the n^{th} zone (°)
γ_n	The angle between the datum and the midpoint on the leading edge of the counter-knife of the n^{th} zone (°)
Δl	The change in depth of the plant material (m)
Δl_n	The change in depth of plant material in the n^{th} zone (m)
δ_n	The arc length of the tine in the n^{th} zone (m)
ε	The strain of the plant material
ε_a	The strain experienced by the alfalfa
ε_{m_n}	The strain of the plant material in the n^{th} zone of the m^{th} cut
ε_s	The strain experienced by the cereal straw
ζ_n	The angle between the radial unit vector (which has an origin at the midpoint of the zone on the leading edge of the tine and is directed to the axis of rotation of the rotor) and $F_{cs\,n}$ in the n^{th} zone (°)
θ	The angle of the tine with respect to the datum (°)
Φ	An indexing variable used in the analytical model
λ_n	The angle between the datum and the lagging edge of the counter-knife in the n^{th} zone (°)
μ	The dynamic coefficient of friction between the plant material and steel
v_p	Represents an estimate of the coefficient of variation of the population used to determine N_{um} (%)

ρ	The coefficient that relates ρ_{dm} to lo_m (kg m^{-3} m^{-1})
$\rho_{dm\ a}$	The dry-mass density of the alfalfa (kg/m^3)
$\rho_{dm\ s}$	The dry mass-density of the cereal straw (kg/m^3)
ρ_{dm}	The dry-mass density of the plant material when it was cut (kg/m^3)
σ	The normal stress of the plant material (Pa)
τ	The shear stress of the plant material (Pa)
τ_{int}	The intercept of the linear equation that relates τ_{max} to ρ_{dm} (Pa)
τ_{max}	The maximum shear strength of the plant material (Pa)
τ_{slope}	The slope of the linear equation that relates τ_{max} to ρ_{dm} (Pa (kg m^{-3})$^{-1}$)
$\chi_{3.75\ alfalfa}$	The coefficient that relates the initial depth of alfalfa at a throughput of 2.5 kg/s to the initial depth of alfalfa at a throughput of 3.75 kg/s
$\chi_{3.75\ straw}$	The coefficient that relates the initial depth of cereal straw at a throughput of 2.5 kg/s to the initial depth of cereal straw at a throughput of 3.75 kg/s
$\chi_{5.0\ alfalfa}$	The coefficient that relates the initial depth of alfalfa at a throughput of 2.5 kg/s to the initial depth of alfalfa at a throughput of 5.0 kg/s
$\chi_{5.0\ straw}$	The coefficient that relates the initial depth of cereal straw at a throughput of 2.5 kg/s to the initial depth of cereal straw at a throughput of 5.0 kg/s
$\chi_{5.55\ straw}$	The coefficient that relates the initial depth of cereal straw at a throughput of 3.33 kg/s to the initial depth of cereal straw at a throughput of 5.55 kg/s

1 INTRODUCTION

A rotary feeding and cutting system (RFCS) has three main components: the rotor, the stationary knives, referred to as counter-knives, and the rotor bed. The axis of rotation of the rotor is perpendicular to the counter-knife leading edge. For each counter-knife, there is a pair of rotating elements that are attached to the rotor. The rotating elements, referred to as tines, have three "fingers" that are equally spaced around the circumference of the rotor. The counter-knives protrude through the rotor bed in a line, which is parallel to the axis of rotation of the rotor, and between the tine pairs. Each tine pair has the same angular offset, with respect to the axis of rotation of the rotor, however adjacent tine pairs have a relative angular offset. As the rotor rotates during operation, material that is fed into the RFCS is sheared between the tines on the rotor and the leading edge of the counter-knives. The RFCS has been implemented on both combine harvesters and balers. The main components of the RFCS are shown in Figure 1.1.

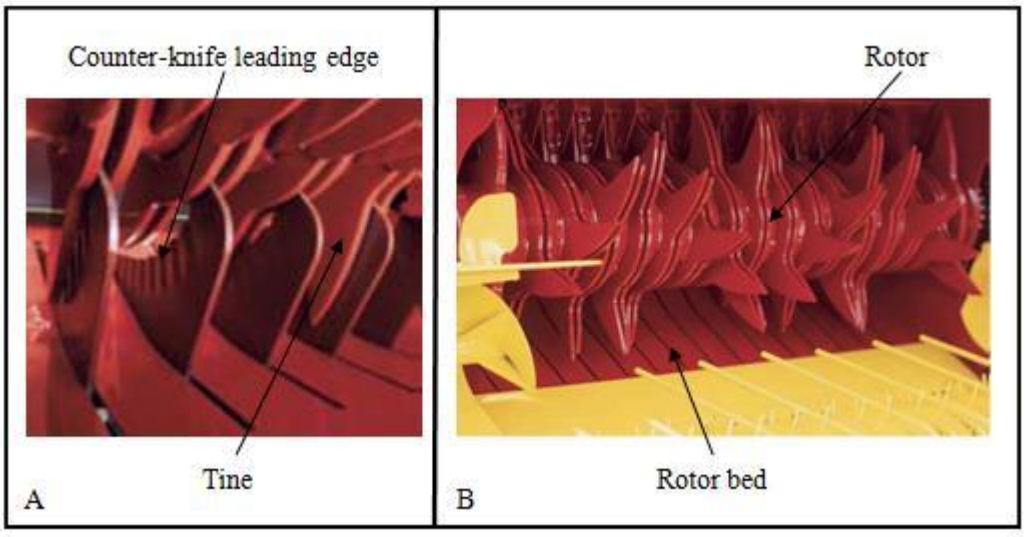

Figure 1.1 Photographs of the main components of a rotary feeding and cutting system (RFCS) (A) taken from behing the RFCS looking forward and (B) taken from infront of the RFCS looking backward (modified from New Holland BR7000 Series Roll-Belt™ Round Balers Brochure (CNH America LLC, 2008)).

In the case of the baler, the RFCS is located behind the pickup and ahead of the bale-forming chamber. The RFCS is used to reduce the geometric mean length (GML) of material entering the bale. Shorter material entering the bale-forming chamber allows for bales of higher crop density to be formed. For silage bales, a high-density bale is advantageous because a reduced amount of air in the bale aids in the fermentation process. Shorter hay aids in the mixing process of a total mixed ration. For straw bales, a shorter material length increases absorbency and aids in manure handling. Regardless of the crop being baled, the use of the RFCS increases the bale density, which results in fewer bales per field and fewer bales transported to storage.

In the case of the combine harvester, the RFCS is located behind the threshing rotor and ahead of the straw-spreading system. The RFCS is used to reduce the mean length of the material other than grain (MOG). There are two advantages of a reduced mean length of MOG. During subsequent seeding operations, the short MOG will pass through the ground-engaging tools of a seeding drill with less plugging. A reduced mean particle length, also results in a reduced variation of the length of MOG, which allows the MOG to be more uniformly spread across the working width of the combine. After the MOG has been spread on the field by the harvester it is referred to as residue. Uniform distribution of residue facilitates homogenous seed germination (Siemens and Wilkins, 2005).

The RFCS is an optional system on both balers and combine harvesters, and the capital cost of the machine increases if the component is installed. Regardless of its application, the RFCS has an operational and capital cost. The operational cost includes the energy consumption of the system as well as the maintenance of the system. The RFCS can require up to 20% of the total energy consumption of the baler or combine harvester. During operation, the counter-knives and drive components of the rotor become worn and/or fatigued, and must be replaced at the operator's expense. The RFCS has generally been accepted in industry because the cost associated with the system is believed to be recovered.

The cost associated with the RFCS on the baler is offset by the increase in the quality of feed and a decrease in handling and transportation cost. Denser silage bales are of

higher feed quality, because of the elimination of air pockets which would otherwise hinder the fermentation process. The quality of silage bales is potentially further improved by an increase in plant sugar made available from cutting the plant material (Shinners, 2003). The machine used to produce a total mixed ration performs two functions. It mixes and reduces the GML of the feed. The reduction in length is proportional to the operation time of the machine. By using baled feed previously processed with the RFCS, the operation time and cost of the mixer is decreased because the optimum feed particle length can be obtained following a shorter processing time. Perhaps the single aspect that has the greatest potential for recovering the cost of the RFCS is the decrease of the cost associated with transporting and storing the bales. A significant decrease of the cost associated with transporting biomass was observed by increasing the bulk density of biomass (Kadam et al., 2000).

The cost associated with the RFCS on the combine is offset by the reduction in the frequency or the elimination of seed equipment plugging. Siemens and Wilkins (2005) concluded that a seeding drill could operate without plugging when the residue was uniformly spread, and cut into pieces less than 0.18-m in length. Drill plugging causes operator frustration, reduced field capacity and large piles of residue that form behind the drill which cover the seed row and suppress plant growth. Further, when residue is spread uniformly across the working width of the combine harvester, an increase in plant establishment, growth and yield are obtained (Siemens and Wilkins, 2005). Thus, the cost associated with the RFCS on the combine is recovered by an increase of productivity during future seeding operations and a potential increase in revenue due to higher crop yields in future years.

Although the RFCS has been generally accepted in industry, there is a lack in the understanding of what factors affect the energy consumption of the system. The need exists for further study, documenting the factors that affect the energy consumption of the RFCS. Further, a model that could be used to quantify the energy consumption of the RFCS, in terms of its design parameters, would be advantageous. It would reduce the need for costly laboratory and field trials which would otherwise be required to improve the efficiency of the system.

2 LITERATURE REVIEW

The literature survey revealed that the RFCS has not been studied in the past, however cutting of plant material in general, and more specifically cutting of plant material with a sickle-type and rotary-type cutter has been extensively studied. The RFCS is somewhat of a hybrid rotary cutter because it has characteristics of a rotary cutter in which material is cut both parallel and perpendicular to the axis of rotation. Even though the RFCS is not a sickle-type cutter, but a unique rotary cutter, published data on the factors that affect the performance of both sickle-type and rotary-type cutters are applicable and informative, as the fundamentals of the cutting process are similar for each cutting device.

A sickle-type cutter employs a series of sharp knives that reciprocate between a series of stationary knife guards. Plant material is sheared between the reciprocating knife and the countershear or stationary guard. There are two types of rotary cutters, high-velocity impact cutters, and lower velocity cutters which employ a countershear. Rotary cutters can also be classified by the orientation of the rotating axes with respect to the orientation of the cut they make through the plant material. Plant material is either cut parallel or perpendicular to the axis of rotation of the cutter. An example of a rotary cutter that cuts parallel to the axis of rotation is a forage harvester cutterhead, which also employs a countershear. A forage harvester cutterhead has a series of knives that are attached to the circumference of a rotating drum, and the edge of the knives are oriented parallel to the drum's axis of rotation or in a spiral pattern around the axis of rotation. As plant material is fed into the cutter, it is sheared between the stationary countershear and the rotating knives. A disk mower is an example of a rotary-type impact cutter which cuts perpendicular to the axes of rotation. For a disk mower, the knives are attached to a disk and during rotation, the knives are in a radial orientation with respect to the disk's axes of rotation. No countershear is used to support the material during the cutting process, instead the support comes from the plant stem. For a disk mower, the plant stem is sheared when the high velocity knife passes through the plant stem. A typical sickle-type cutter, forage harvester cutterhead and disk mower are shown in Figure 2.1.

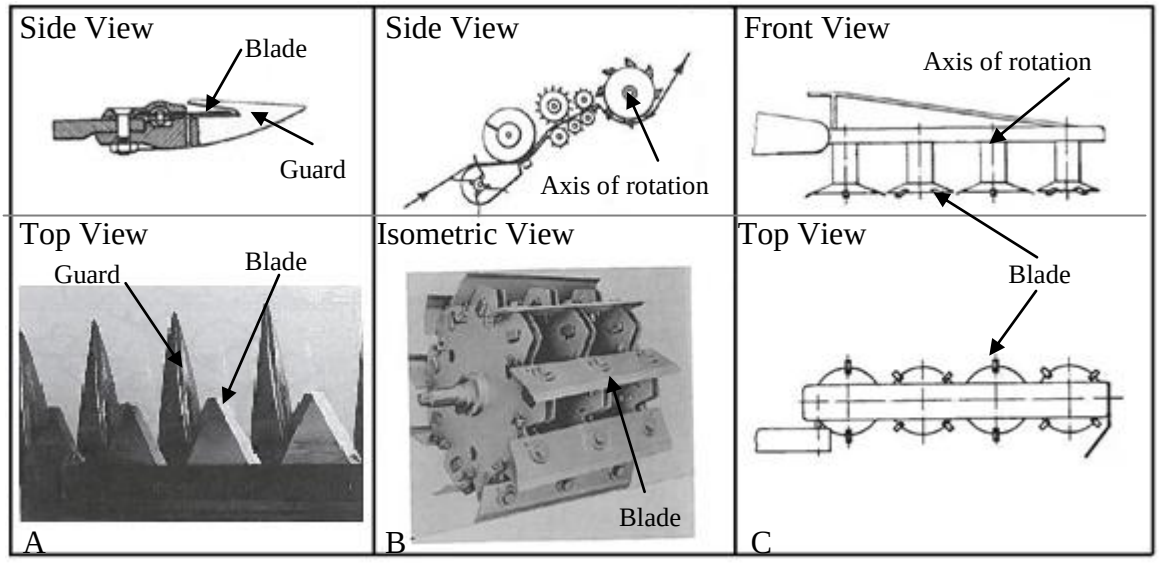

Figure 2.1 Cutter type (A) sickle (B) forage harvester cutterhead (C) disk mower (modified from Persson (1987)).

Literature related to factors that affect the performance of cutting mechanisms has been extensively researched and documented. The most common mechanisms studied were rotary cutters and sickle-type cutters. In this review, the factors that were deemed to be the most dominant were identified and their effects quantified. An understanding of plant material's physical properties was essential to the development of an analytical model to predict the power requirements of any mechanism that interacts with plant material. Thus, a section has been included in this review which identifies the physical properties of plant material. The models that have been developed to predict the power and energy requirements of rotary and sickle-type cutters were identified. Literature related to the factors that affect the performance of cutting mechanisms, mechanical properties of plant material and energy and power requirements of sickle and rotary-type cutters are topics covered in this chapter.

2.1 Factors that affect the performance of cutting mechanisms

Previous research completed on the factors that affect the performance of sickle and rotary-type cutters is extensive. The following subsections provide a survey of the previous studies and their findings. The factors that will be discussed are blade speed,

bevel angle, sharpness, thickness, oblique angle, serrations, clearance between cutting edges, material moisture content and depth and density of material. The term blade, which was typically used in the reviewed literature to refer to the cutting element, is analogous to the counter-knives of the RFCS. The factors listed above are not a comprehensive list of factors that affect the performance of a cutting mechanism, however they are the factors that are under review in this study.

2.1.1 Blade speed

In terms of the factors that affect the performance of cutting mechanisms, according to Chancellor (1988) the most common variable studied in the period of 1953 to 1985 was blade speed. Based upon a review of 26 papers Chancellor (1988) concluded that there was either no change or a slight increase (10 to 15% when blade speed was doubled) in cutting energy requirements as blade speed increased for devices that cut between two elements. Chancellor (1988) also concluded that, in general, devices that cut efficiently were not influenced by blade speed over a range of quasi-static to 60 m/s. Unfortunately, the specific devices that Chancellor (1988) was referring to were not defined.

Persson (1987) indicated that an increase in blade velocity often increased the power losses, so even if the cutting power stayed relatively constant, the total power requirement of the cutter likely increased as cutting speed increased. The power losses were associated with several factors including: accelerating the material to exit velocity, overcoming friction between the material and the housing while still being pushed by the cutting device, sustaining air movement in the cutting device and overcoming mechanical friction in the driving mechanism. Persson (1987) reviewed the work done by Berge (1951) and concluded that the energy required by a flywheel-type cutterhead was linearly related to the cutting speed in the range 20 to 50 m/s. However, the published work of Berge (1951) alone does not support this conclusion. Chancellor (1957) examined the effect of cutting speed on the force and energy required to cut timothy at a moisture content of 54% on a wet basis (w.b.) with a mower. He concluded that there was very little change in cutting energy when the cutting speed was changed from 1.8 to 5.2 m/s.

The blades on the RFCS are the counter-knives, and because they are stationary, the speed of cutting is proportional to the rotational speed of the rotor and the radial

dimension of the tines. During normal operation, the speeds at the tip and base of the cutting elements on the baler RFCS differ by 1.3 m/s (3.0 m/s at the tip vs. 1.7 m/s at the base). For the combine, the nominal cutting speeds at the tip and base of the cutting elements are 23.3 and 11.0 m/s, respectively. The previous research completed on the effect of blade speed suggests that in general, the cutting energy consumed by the RFCS will change very little, especially for the baler RFCS because of its relatively low cutting speed. However, even if the cutting energy is unaffected by the cutting speed it is likely that the total power to process plant material will increase as a function of cutting speed due to an increase in the power losses as observed with the other cutting devices.

2.1.2 Blade bevel angle

The definition of blade bevel angle is shown in Figure 2.2. As the blade bevel angle decreases the amount of deformation that the material being cut experiences (in the area of the cut) decreases. However, the durability of the blade decreases when the blade bevel angle decreases. Therefore, a blade with a smaller bevel angle will wear faster and become duller sooner than a blade with a larger bevel angle. Further, a blade with a small bevel angle is more susceptible to damage or failure when subject to foreign material (like stones or lost metal objects in the field). According to Ige et al. (1976), a blade with a bevel angle of 22 to 55° was best suited for cutting corn and alfalfa with a forage harvester cutterhead. According to Chancellor (1988), a bevel angle of 20 to 30° was best suited for cutting a wide range of plant material, as there was very little reduction in cutting energy when the bevel angle was decreased below 20°, and there was a substantial increase in the rate of wear with a small bevel angle. A blade bevel angle greater than 30° resulted in higher cutting forces and an increased amount of energy consumed to cut plant material. For example, a bevel angle of 70 to 80° required approximately double the energy to cut plant material than a 25° bevel angle (Chancellor, 1988). Chancellor (1988) also indicated that the effect of bevel angle is more pronounced as the thickness or depth of plant material being cut increased.

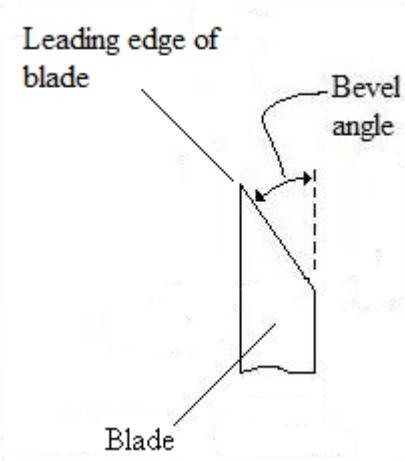

Figure 2.2 The definition of blade bevel angle.

According to Persson (1987) in general (for all cutting devices and different type of plant materials) the bevel angle had a significant effect on the cutting force, the cutting energy and the lifetime of the blade. A small bevel angle, in general, reduced the cutting force. Persson (1987) suggested that a bevel angle as small as 20° was desirable from a cutting energy standpoint, however with such a small bevel angle, the durability of the blade was compromised. In some instances, blades with bevel angles of 45° have been used to cut forage material. This sacrificed the efficiency of the cutting process, but improved the lifetime of the blade significantly. A strategy of this nature would likely be adopted if there were excessive amounts of foreign material in the forage.

According to Chancellor (1957), the maximum cutting force for cutting timothy stems at low speeds was significantly affected by the blade bevel angle. Chancellor (1957) also concluded that the maximum cutting force changed very little with a bevel angle less than 30°, and the energy requirement changed very little at a bevel angle of less than 35°. This would suggest that there is no advantage in having a bevel angle of less than 35° as there is no benefit in the way of a reduction in cutting energy or forces and the smaller bevel angle will likely reduce the service life of the blade.

All of the previous research suggests that in order to minimize the energy consumption to cut plant material, the bevel angle must also be minimized. However, the durability of the blade limits the minimum bevel angle. In general, unless there is an issue with an

excessive amount of foreign material combined with the plant material the optimum bevel angle for all cutting devices is between 20 and 30°. The RFCS implemented in a baler made by CNH Global N.V. (or CNH) under the brand names of Case IH™ 454 Silage and New Holland™ BR7060 Silage Special uses a bevel angle of 30°. The previous research presented in this section does not identify a direct relationship between bevel angle and energy consumption to process plant material with the RFCS. The literature simply implies that this trend exists. Further experiments are needed to identify whether or not the bevel angle has a significant effect on the energy consumption of an RFCS.

2.1.3 Blade sharpness

The force and energy required to cut plant material has a direct relationship with the blade-edge radius. Experiments completed, comparing the effect of blade sharpness, revealed that a blade with a 0.25-mm edge radius had double the force and energy requirements than a blade with a 0.05 to 0.1-mm edge radius (Reznik, 1979). The reason that a sharp blade required less energy than a dull blade when used to cut a given plant material is that a very sharp blade causes more localized cell failure and compression in the material. In contrast, a dull blade caused cell failure and compression over a greater area, thereby requiring more force and energy. Prince et al. (1958) found that the energy required to cut alfalfa approximately doubled when a dull blade was used instead of a sharp blade (where the leading edge width of a sharp and dull blade was less than 0.03 mm and equal to 0.25 mm, respectively). The reason that a sharp blade required less energy than a dull blade has application to all cutting devices. Thus, it is expected that a dull counter-knife will consume more energy than a sharp counter-knife when plant material is processed with the RFCS. However, the magnitude of the effect of counter-knife sharpness on the energy requirements of the RFCS is unknown and needs to be quantified.

The minimum peripheral speed (which was required to cut plant material) increased 40% as the blade edge radius changed from 0.1 to 0.25 mm (Bockhop et al., 1965) for a high-velocity impact cutter. During the same trials, the cutting forces also increased by 25%. The RFCS is not an impact-type cutting device, because plant material is cut

between the tines and the counter-knives. Thus, the results reported by Bockhop et al. (1956) have limited relevance to the RFCS.

Studies by Tuck (1976; 1977; 1978) on power requirements of mowers indicated that the specific cutting energy per unit field area was 1.5 kJ/m^2 for a sharp blade and 2.1 kJ/m^2 for a worn blade. It should be noted that these values included the energy used for cutting and transporting the material. The conclusions drawn by Tuck (1976; 1977; 1978) agreed with what Reznik (1979) concluded in that dull blades consume more energy to cut plant material than sharp blades. However, the conclusions reached by Tuck (1976; 1977; 1978) have limited relevance to the energy requirement of the RFCS because they were conclusions observed for a mower.

Liljedahl et al. (1961) concluded that the energy requirements for a dull blade were twice that of a sharp blade when the clearance between the cutting edges was small (0.05 mm) and three times as high for a larger clearance (0.41 mm). The same author found that the interaction between blade sharpness and the clearance between cutting edges had a reduced effect when sharp blades were used. The RFCS implemented in the CNH RB454 Silage and Rotor Cutter used a 4.5 mm clearance between the shearing surfaces. Based upon the conclusions drawn by Liljedahl et al. (1961), the effect of counter-knife sharpness on the energy required to cut plant material with the RFCS will be substantial, because of the relatively large clearance between the shearing surfaces on the RFCS.

2.1.4 Blade thickness

Blade thickness has little effect when cutting thin layers, however when cutting thick layers of material, a thicker blade will displace more material, increasing the amount of energy used to cut the material (Chancellor 1988). According to Chancellor (1988), the energy required to cut a 100-mm thick layer of corn stalks was 46% higher when an 8-mm thick blade was used as opposed to a 2-mm thick blade. The counter-knives used in the CNH RB454 Silage and Rotor Cutter are 5 mm thick, and the depth of material, depending on the throughput, can vary from zero to 15 cm. Thus, based on the conclusions of Chancellor (1988), the thickness of the counter-knives will likely have a significant effect on the energy required to cut plant material with the RFCS when high throughputs of plant material are processed. However, when lower throughputs are

processed, the effect of counter-knife thickness will likely be insignificant because of a thinner layer of plant material being cut. Further, research needs to be completed to confirm whether or not counter-knife thickness affects the energy consumption of the RFCS, and if there is a material-layer thickness at which counter-knife thickness does not have a significant effect.

2.1.5 Oblique angle

The oblique angle is the angle between the blade edge and the counter shear edge measured in the plane that is created by the blade motion. According to Persson (1987), an oblique angle (of approximately 15 to 60 degrees) is used to reduce the peak cutting forces. However, if the oblique angle is too large, the material will be expelled from between the shearing surfaces instead of being sheared. According to Kepner (1952), an oblique angle of 27 to 34° was required to retain straw between smooth shearing surfaces. During the same study, it was determined that an angle of 32 to 40° was required to retain grass between the same smooth shearing surfaces. Serrated edges allow for a greater oblique angle, typically 66 to 84° for straw and 84 to 90° for grass (Kepner, 1976). According to Chancellor (1988), the maximum cutting force decreased as the oblique angle increased, at a rate of approximately 1% per degree. The minimum cutting energy was typically achieved with an oblique angle in the range of 25 to 50° (Chancellor, 1988), unfortunately Chancellor (1988) did not specify whether these values applied to smooth or serrated shearing surfaces. Thus, in general, both rotary and sickle-type cutters benefit from an increased oblique angle, because an increased oblique angle increases the time over which a mat of material is cut, which results in lower peak cutting forces. However, both types of cutters can expel material from between the shearing surfaces if an excessive oblique angle is used. Blade serrations are used to allow for greater oblique angles, as the presence of serrations increases the tangential force between the blade edge and the material being cut.

The oblique angle of the RFCS changes with the angular position of the rotor and the radial distance of the tine. The oblique angle on the RFCS is the angle between the tine leading edge and the counter-knife leading edge. The oblique angle is at a maximum at the base of the tine (closest to the axis of ration) at the initial stages of a cut, and is equal

to approximately 50°. As a cut progresses, or the rotor rotates, the oblique angle decreases to approximately 0°. The counter-knives used on the RFCS are serrated which likely allow for the oblique angle to have a relatively high maximum value at the early stages of a cut. However, even without serrated counter-knives, the RFCS may not suffer from material expulsion, as the geometry of the tine and counter-knife are such that the material between the tine and counter-knife become trapped and forced to the base of the tine as the rotor rotates.

2.1.6 Blade serrations

Serrations increase the forces tangential to the blade cutting edge by effectively increasing the contact angle (measures from the blade edge) between the blade edge and the crop material. The increase in tangential force is due to the protrusions or crevasses on the blade edge, which are perpendicular to the blade cutting edge. A greater tangential force permits a larger oblique angle, the relative angle between two shearing surfaces, which has been found to decrease peak cutting forces. Without serrations, an excessive oblique angle would cause the material to be expelled from between the two shearing surfaces, leaving the material uncut and the cutting device ineffective. When comparing a smooth and serrated blade, the oblique angle of a cutter that uses a serrated blade can be approximately double the oblique angle of a smooth blade and ensures that no material will be expelled (Persson, 1987).

During tests where hay was cut by slicing, serrated blades required less than half the energy of smooth blades, but the slicing force (with a given normal force) was approximately 40% greater (McClelland et al., 1958). According to Chancellor (1988) the presence of serrations on a blade resulted in higher cutting forces and cutting energy except when material was cut by a slicing action. Chancellor suggested that “the reason is that at the root of the serration groove, the cutting plane has more clearance than at the outer blade edge, and thus cutting tends to take place over a zigzag line through the material”. Thus Chancellor is attributing the increased cutting energy to the combined effect of a larger clearance between the shearing surfaces as well as a longer length of cut through the material. A slicing cut refers to a cut with a large oblique angle, but unfortunately neither of the authors indicated what oblique angle they considered to be

sufficient to cause a slicing cut. The oblique angle of the RFCS is constantly changing as a function of the rotor position, however the average oblique angle during a single cut is approximately 15°. This would suggest that the RFCS does not cut plant material by slicing, and therefore serrated counter-knives will require more energy to process plant material than un-serrated counter-knives.

It is also important to note that a blade with serrations will remain sharper for a longer period of use than an un-serrated blade. When a serrated blade is used, the material being cut will slide a shorter distance on a blade edge, which in turn results in less wear on the blade edge. Therefore, using serrated counter-knives may be a valid strategy to minimize the long-term energy requirements of the RFCS, as the serrated counter-knives will stay sharper for a longer period, and consume less energy to process plant material.

2.1.7 Clearance between cutting edges

Liljedahl et al. (1961) determined that when blades are sharp, with an edge radius of less than one thousandth of a millimeter, there is little effect on cutting force and energy, when dealing with clearances ranging from 0.26 to 2.32 mm. However, when the clearance was examined over a greater range, or when dull blades were used (edge radius of 7.0×10^{-3} to 30.0×10^{-3} mm), the cutting energy was affected to a larger degree. Liljedahl et al. (1961) found that the cutting energy increased by 67% as clearance increased from 2 to 10 mm when sharp blades were used to cut corn stalks. Chancellor (1958) found that a clearance of 0.13 to 0.64 mm had very little effect on the maximum cutting force. Chancellor (1988) found that in general, a combination of large clearances and dull blades resulted in approximately twice as much cutting force and energy required to cut plant material. It was concluded that the increase in cutting force and energy was due to the material being torn apart which was observed in the resulting ragged cuts. All of the previous studies followed the same trend. If a sharp blade was used, the effect of clearance between shearing surfaces on the energy required to cut plant material was reduced. However, if dull blades were used, (with an edge radius on the order of 7.0 μm) the clearance between shearing surfaces became significant.

The clearance between the shearing surfaces on the RFCS, or more specifically the clearance between the tines and the counter-knife, is approximately 4.5 mm which is a

large clearance relative the studies completed by Chancellor (1988), Liljedahl et al. (1961) and Chancellor (1958). Thus counter-knife sharpness will likely have a significant effect on the energy requirements of the RFCS.

Clearance between shearing surfaces has also been found to affect the rate of wear on the shearing surfaces. Wilkes (1985) suggested that even if sharp blades are used, the clearance should not be excessive because excessive clearances lead to accelerated wear of the countershear and rapid deterioration of blade sharpness. Wilkes (1985) did not indicate what clearance would be considered excessive, however based upon the previously examined clearances the RFCS's 4.5 mm clearance would likely be considered excessive. By decreasing the clearance of the shearing surfaces on the RFCS, the effect of counter-knife sharpness may be reduced, and the counter-knife will likely remain sharper for a longer period of time.

2.1.8 Moisture content

Chancellor (1957) found that the maximum force to cut timothy occurred at a moisture content of 40% w.b., and forces were reduced at lower and higher moisture contents. Chancellor (1988) performed a comprehensive review of the research that has been done on the factors that affect the cutting process. Chancellor (1988) concluded that in general, a major decrease in plant moisture content causes cutting forces to increase slightly. For example, various researchers have observed a 20 to 50% increase in cutting forces when the plant moisture content was decreased from 80 to 10% w.b. (Chancellor, 1988). Moustafa et al. (1978) determined that the total cutting energy, of a forage harvester cutterhead, (including the energy to cut and accelerate the alfalfa) was a maximum at 28 to 43% w.b. and decreased at higher and lower levels of alfalfa moisture content. However the effect of moisture content was largely attributed to variations in the energy required to accelerate and not to cut the alfalfa. Liljedahl et al. (1961) concluded that moisture content of hay had little effect on shear energy when a sharp blade was employed, however as the blade became dull the effect of moisture was more pronounced. When dull blades were used, the energy needed to shear hay was a maximum when 20 to 30% moisture content hay was sheared, and decreased at higher and lower levels of moisture content. Persson (1987) suggested that the reason some

plant material exhibits a maximum cutting force at a moisture content in the range of 35 to 40% was that the plant material excreted a sticky substance which builds up on the cutting surfaces. Thus, the increase in cutting energy observed by Moustafa et al. (1978), Liljedahl et al. (1961) and Chancellor (1957) may not have been attributed to a difference in the structural properties of the plant material at varying moisture levels but instead an increase in the frictional forces between the plant material and the cutting elements or between the cutting components themselves.

There is somewhat of a contradiction between the conclusions drawn by Hennen (1971) and Moustafa et al. (1978). Hennen (1971) investigated the effect of moisture content on the specific energy requirements of a forage harvester. He concluded that the specific cutting energy was not affected by the moisture content, if the specific energy was calculated on dry material basis. According to Moustafa et al. (1978), the total energy required to cut alfalfa with a forage cutterhead was influenced by the moisture content. The difference in conclusions could be attributed to the fact that Hennen (1971) was investigating the effect of material moisture content on the specific energy required to process plant material while Moustafa et al. (1978) was looking at the effect of material moisture content on the total energy to process plant material with a forage cutterhead.

Halyk et al. (1968) found that the shear strength of individual alfalfa stems had an indirect relationship with moisture content. It was also indicated that the relationship between shear strength and moisture content could not be described well by a linear equation. Unfortunately, Halyk et al. (1968) did not present the raw data from the study, and therefore the results could not be compared to the previously established trend. The difference in conclusions drawn by Halyk et al. (1968) and the other authors presented in this section could be attributed to the fact that the material interaction present when a mat of material is cut caused the maximum cutting force to occur when the material moisture content was between 20 and 30% w.b..

During normal operation, the RFCS on a baler could be used to process plant material at a wide range of moisture contents. Silage bales can be formed with material moisture contents as high as 60% on a wet basis. Conversely, hay bales can be formed with

material moisture contents as low as 20% on a wet basis. Based upon previous studies, and because the RFCS typically cuts through a mat of plant material instead of individual plant stems, it is expected that the specific energy requirements of the RFCS would be a maximum when plant material at a moisture content of 20 to 40% on a wet basis is processed by the device. Furthermore, it is expected that the specific energy requirements will decrease at higher and lower levels of moisture content. Also, the effect of moisture content on the specific energy requirements of the RFCS may not be apparent or at least substantially reduced if the moisture content of the material is reported on a dry basis.

2.1.9 Depth and density of material

There are two ways that the amount of energy used to cut plant material is affected by the depth of the material. The first is that as the thickness of material being cut increases, the stress concentrations near the blade decrease, resulting in an increased amount of material being compressed, which ultimately results in an increased amount of energy used to compress the material before it is cut. For example, as the depth of corn stalks increased from 25 to 120 mm, the portion of total energy used to compress the corn increased from 35 to 69% (Reznik, 1975). Springer et al. (1976) found that the total energy to process alfalfa and corn with a forage harvester cutterhead increased as depth of material increased. The increase in total energy was attributed to an increase in the energy to compress the material, acceleration the particles and air and mechanical friction. Chancellor (1958) stated that "with greater aggregate thickness of materials, a greater force is required to compress the pile of stems to a firmness that will permit continued cutting. The greater forces needed before and during result in a greater energy consumption". The second is that the maximum shear strength of material has a direct relationship with the dry-matter density of the material being cut. Halyk and Hurlbut (1968) found that the maximum shear strength of individual alfalfa stems was directly proportional to dry-matter density. As the depth of material increases the dry-matter density will also increase, which ultimately results in an increased amount of energy consumed to cut the material.

Chancellor (1957) investigated the effect of material thickness, specifically timothy, on the maximum specific cutting force. It was concluded that the maximum specific cutting force in units of N/mm, which is the cutting force per unit length of cutting width, had a direct linear relationship with the dry-matter density of the material on the countershear, expressed in units of mg/mm^2. Bright and Kleis (1964) also concluded that the energy to shear silage material was directly proportional to the amount of dry matter in the cross section to be sheared.

Based upon the conclusions of Bright and Kleis (1964), Halyk and Hurlbut (1968) and Chancellor (1957), there would be no advantage in decreasing the depth of material or density of material at shear in terms of the energy consumption to shear plant material with the RFCS. However, based upon the conclusions drawn by Springer et al. (1976), Reznik (1975) and Chancellor (1958), the amount of energy consumed to compress the material before it is cut could be decreased by increasing the rotational speed of the rotor, or increasing the operational width of the RFCS while maintaining a constant throughput.

2.2 Mechanical properties of plant material

The previous research that has been completed on the Young's modulus, dynamic coefficient of friction and the maximum shear strength of cereal straw and forages is reviewed in the next three subsections. These are not a comprehensive list of the mechanical properties of plant material, however they are believed to be the factors that have the greatest effect on the power requirements of the RFCS.

2.2.1 Young's modulus

The Young's modulus is the relationship between stress and strain when a material experiences recoverable deformation. Thus, the Young's modulus provides an indication of the force required to compress a material with a known cross section. Plant material is viscoelastic in nature, which means that the force required to achieve a given level of deformation is a function of the rate at which the material is loaded. Negi et al. (1987) studied the stress-strain relationship of whole-plant corn at a moisture content of 66% on a wet basis and determined that, "The faster the rate of deformation, the greater was the stress developed in the material." Thus, it is expected that the Young's modulus of plant

material would have a direct relationship with the rate at which it was loaded. In order to accurately quantify the Young's modulus of the material processed by the RFCS, the material will need to be loaded at (or as close as possible to) the rate at which the material is loaded in the RFCS during normal operation.

The Young's modulus reported by Esehaghbeygi et al. (2009), Tavakoli et al. (2009), Galedar et al. (2008), Tavakoli et al. (2008), O'Dogherty et al. (1995) and O'Dogherty et al. (1989) was determined for individual stems and is shown in Table 2.1. To determine the Young's modulus using this method, the stems were subject to a load between two supports. The values reported for alfalfa were based on tests completed with alfalfa at a moisture content of 10 to 80% on a wet basis.

Table 2.1 Young's modulus for individual stems of wheat straw, alfalfa stems and barley straw.

Material	**Young's modulus (GPa)**	**Author(s)**
Barley Straw	0.33 to 0.62	Tavakoli et al. (2009)
Wheat Straw	3.13 to 3.75	Esehaghbeygi et al. (2009)
Alfalfa Stem	0.79 to 3.99	Galedar et al. (2008)
Wheat Straw	0.98 to 1.80	Tavakoli et al. (2008)
Wheat Straw	4.76 to 6.58	O'Dogherty et al. (1995)
Wheat Straw	1.59 to 2.15	O'Dogherty et al. (1989)

Usrey et al. (1992) investigated the compressibility of rice straw. To accomplish this task, a material properties testing machine along with a rectangular steel plate and box were employed. The length, width and height of the box were 576, 207 and 205 mm, respectively. The steel plate was undersized by approximately 5 mm to fit within the box. The loading rate of the plate was 127 mm/min with a maximum load of 4448 N. During testing, the rice straw was placed in the box parallel to the longest axes and the stems were manually arranged to minimize the lodging of the stems. It was concluded that the orientation of the stems in the compression box were critical to the outcome of the test.

The Young's modulus of plant material has been reported for both individual stems (particle properties), and for a mat of plant material (bulk properties). According to Hall and Husman (1981), particle interactions have a significant effect on the mechanical properties of plant material. The interaction of plant particles would likely have an effect on the Young's modulus of the plant material because the Young's modulus is a mechanical property. During normal operation, a mat of material enters the RFCS. Therefore, in order to accurately quantify the Young's modulus of the material processed by the RFCS the bulk properties should be quantified. The values of the Young's modulus given in Table 2.1 are for individual stems, and will likely not accurately represent the Young's modulus of the material in the RFCS. Furthermore, based upon the observations of Usrey et al. (1992), it will be important to mimic the orientation of the plant stems during normal operation of the RFCS, while quantifying the Young's modulus.

2.2.2 Dynamic coefficient of friction

The energy consumed to cut plant material is typically only a fraction of the total energy consumed by a cutting mechanism. The majority of the energy consumption goes towards satisfying what are considered parasitic losses. The parasitic losses are not solely attributed to friction but a large portion of the losses can be attributed to frictional losses. Friction between the material being cut and the housing of the cutter or friction between uncut material in the field and the cutter head both contribute to frictional losses caused by crop-and-machine interaction. In order for a model to be developed that predicts the energy or power requirements of a cutting mechanism one must take into account the frictional forces between the plant material and the cutter. Therefore, the remainder of the discussion in this section will focus on the previous research completed on the coefficient of friction between alfalfa and steel and cereal straw and steel.

Richter (1954) determined the static and dynamic coefficient of friction between four different crops and galvanized steel. The crops studied were chopped hay, chopped straw, corn silage and grass silage. According to the author, there was not a significant difference, in terms of friction coefficients, between the chopped hay and straw nor between the corn and grass silage. The static and dynamic coefficients of friction for

chopped hay and straw had a range of 0.17 to 0.42 and 0.28 to 0.33, respectively. The static and dynamic coefficients of friction for corn and grass silage ranged from 0.52 to 0.82 and 0.57 to 0.78, respectively. Therefore, it is expected that the dynamic coefficient of friction between straw and the RFCS will be in the range of 0.28 to 0.33.

Shinners et al. (1991) investigated the effect of surface type, moisture content, sliding velocity, normal pressure and the water lubrication rate on the dynamic coefficient of friction of alfalfa. It was determined that the surface type, moisture content and water lubrication had a significant effect on the coefficient of friction, but the sliding velocity and normal pressure did not. The ranges of normal pressure and velocity tested were 37 to 207 kPa and 16.7 to 38.1 m/s, respectively. The friction coefficient between alfalfa and polished steel, glass-coated steel, polyethylene, iron oxide-coated steel, and Teflon were 0.53, 0.49, 0.42, 0.40, and 0.38, respectively. The friction coefficient had a direct relationship with moisture content. For some but not all of the surfaces under review, the friction coefficient increased slightly as the moisture content increased from 33 to 77% on a wet basis. Water lubrication reduced the friction coefficient on all surfaces by an average of 67%.

The ASABE Standard D251.2 (ASABE Standards, 2008) defined the relationship between moisture content and the dynamic coefficient of friction between stainless steel and alfalfa. Figure 2.3 shows this relationship. According to this standard, the dynamic coefficient of friction for chopped straw at an unknown moisture content sliding on galvanized steel was 0.30. The coefficient was found to be independent of normal pressure over a pressure range of 0.68 to 2.73 kPa. Huisman (1978) reported that the coefficient of kinetic friction between wheat straw was 0.19, 0.23 and 0.31 for moisture contents of 8.7, 16.9 and 26.3 % on a wet basis, respectively.

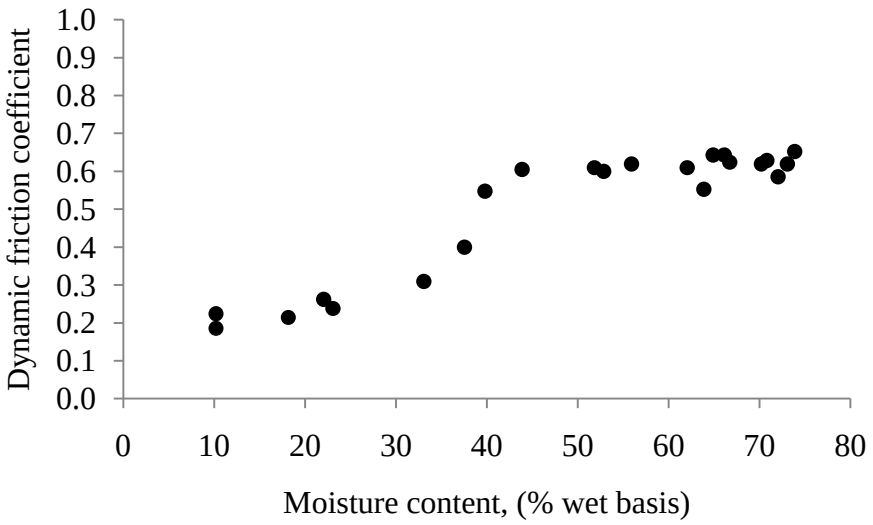

Figure 2.3 Dynamic friction coefficient of alfalfa and stainless steel as a function of moisture content (recreated from ASABE D251.2 (ASABE Standards, 2008)).

Based on the conclusions drawn by Shinners et al. (1991), when determining the dynamic coefficient of friction of the material processed by the RFCS, it will not be necessary to match the speed or pressure applied to the material in the RFCS. However, it will be important, when quantifying the dynamic coefficient of friction, to match the moisture content of the material to the moisture content of the material processed by the RFCS. Also, it will be important to quantify the dynamic coefficient of friction between the biological-material processed by the RFCS and a material with a similar type of surface as the RFCS with which the biomaterial is in contact. The dynamic coefficient of friction determined with the testing device may not accurately reflect the dynamic coefficient of friction even if the proper material moisture content is used. The friction coefficient determined by the testing device could indicate a higher coefficient of friction than what is present in the RFCS, as there may be a release of water from high-moisture-content plant material in the RFCS which has been found to decrease the coefficient of friction. Conversely, the friction coefficient determined by the testing device could indicate a lower coefficient of friction than what is present in the RFCS, as there may be a buildup of a sticky substance (caused by plant material excretions) on the RFCS cutting surfaces when forage with a moisture content of 30 to 40% on a wet basis is processed.

2.2.3 Maximum shear strength

A true shearing test involves the application of a force and a reaction force in parallel planes that are separated by a small distance. When reporting the tests on mechanical properties of biological material, sometimes the term "shearing" has been used for the process which is actually a cutting process and not true shear. The shear under investigation in this study pertains to the cutting process therefore the following articles are also referring to shear as a cutting process.

Bright and Kleis (1964) completed a study to determine the mass shear strength of haylage. The study investigated the effect of storage length in a silo, forage type and dry-matter density on the bulk shear strength of haylage. They used a punch-and-die method throughout the test. The punch that was used for the majority of the tests had a diameter of 11.2 mm and a clearance of 0.05 mm with the die. The punch speed used during all trials was 25.4 mm per minute. Three different types of forage were tested: orchard grass, a mixture of timothy and ladino clover, and alfalfa at two levels of moisture content. The two levels of moisture content of the alfalfa were 43 and 57% on a wet basis. The moisture content of the orchard grass and the timothy mixture was 26 and 48% on a wet basis, respectively. Prior to shearing, the forages were stored in laboratory-scale silos for a 3, 6, 9, or 12 month period. All forages were tested at four levels of bulk density including 320, 400, 481 and 561 kg/m^3 on a wet basis which corresponded to a dry-matter density ranging from approximately 144 to 400 kg/m^3. It was concluded that storage period, forage type and dry-matter density had a significant effect on the shear strength. A highly linear relationship between shear strength and dry-matter density was observed, however no equations were given to describe the relationship. Based upon the data presented in the article, the relationship between dry-matter density and shear strength, for alfalfa at 57% moisture content after 3 months of storage, could be described by a linear equation with a slope of 44 MPa (kg m^{-3})$^{-1}$ and an intercept of 0.87 MPa. Similarly, the relationship between forage type and shear strength was defined as significant but the relationship itself was not defined. The authors questioned the significance of the storage period, as they were unable to define any pattern between the storage duration and the shear strength.

Halyk and Hurlbut (1968) found that the maximum shear strength of individual alfalfa stems was inversely proportional to moisture content and directly proportional to dry-matter density. Ultimate shear strength of individual alfalfa stems varied from 0.4 to 18.0 MPa. Galedar et al. (2008) measured the maximum shear strength of individual alfalfa stems, and found that the location along the stems had a significant effect on the maximum shear strength. Galedar et al. (2008) found that the largest maximum shear strength of alfalfa was 28.16 MPa which was observed at the lower region of the alfalfa stem, and typically the maximum shear strength of the stem was the lowest at the top of the stem.

O'Dogherty et al. (1989) found that the mean ultimate shear strength was in the range of 5.39 to 6.98 MPa for five varieties of winter wheat and was equal to 8.53 MPa for spring wheat with a moisture content that ranged from 10 to 15% on a wet basis. The values O'Dogherty arrived at for the maximum shear strength were based on data obtained from shearing individual stems of wheat. O'Dogherty (1995) found that the shear strength of individual wheat stems at varying positions along the length of the stem at maturity ranged from 4.91 to 7.26 MPa.

Kushwaha et al. (1983) investigated the effect of straw moisture content, bevel angle and shear velocity on the maximum shear strength of wheat straw. The moisture content and bevel angle were found to be significant however the shear velocity was not. The shear velocity used varied from 0.005 to 0.02 mm/s. Across all factor levels the maximum shear strength was found to vary from 6.95 to 29.57 MPa. These values were obtained by shearing 2 to 10 wheat straw stems at a time perpendicular to their axial direction.

The maximum shear strength of both alfalfa and wheat straw has been found to be affected by dry-matter density. Thus, it will be important to quantify the maximum shear strength of the material processed by the RFCS over varying levels of dry-matter density. The maximum shear strength has been quantified for individual stems (particle properties), and for a mat of plant material (bulk properties). During normal operation, the location and orientation of the plant stems that are cut by the RFCS are random. Further, individual stems are not cut by the RFCS. A mat of plant material with

randomly oriented stems is processed. Therefore, to obtain a representative maximum shear strength of the material processed by the RFCS, the bulk properties should be quantified, and the orientation and location of the cut with respect to the plant stems should be random. The speed at which that the maximum shear strength has been quantified by previous researchers is relatively slow (0.03 to 5.0×10^{-6} m/s) compared to the cutting speed in the RFCS (1.5 to 74 m/s). The maximum shear strength of plant material is likely affected by the speed at which it is cut. Thus, when quantifying the maximum shear strength, the speed of the die should be equal to the speed of the cutting device, or as close as practically possible.

2.3 Energy and power requirements of sickle and rotary type cutters

The two most commonly studied cutters are sickle-type and rotary-type cutters. In the following sections the research completed on the power requirements of these common mechanisms will be discussed. Previous research on the cutters has also included the creation of models to predict power requirements of these common cutting mechanisms.

The energy requirements of a cutting mechanism can be separated into two categories, cutting energy, and losses. The cutting energy is the total energy used to compress and cut plant material. Kepner et al. (1978), McRandal and McNulty (1978), as well as Ige and Finner (1976b) have indicated that the cutting energy is only a small fraction of the total energy used by the cutting mechanism, sometimes as little as 10 to 15%. According to Persson (1987) the energy losses of a cutting machine can be separated into the following categories: accelerating the material to exit velocity, overcoming friction between the material and the housing while it is still pushed by the cutting device, overcoming the friction between the cutting disk or knife and the stubble on the ground, sustaining air movement in the cutting device, and overcoming mechanical friction in the driving mechanism and in the feeding mechanism.

2.3.1 Sickle cutter

Baird (1956) found that the energy requirement for cutting alfalfa with a sickle-bar mower ranged between 0.078 and 0.139 kJ/m^2 of field area. Elfes (1954) found that a total of 0.890 kW per meter of cutter bar was required to cut mixed hay at a machine

travel speed of 2.1 m/s. Of the 0.89 kW/m, 66%, or 0.59 kW/m, was used to operate the mower without cutting. According to ASABE Standard D497.6 (ASABE Standards, 2006) the power requirement of a sickle-bar mower was 1.20 kW per meter of cutter width, which corresponded to 0.56 kJ/m^2, assuming a forward velocity of 2.1 m/s. The value that Baird (1956) reported was a result of cutting alone while the ASABE value indicated the total power requirement of the mower, which explained the differing values. The difference in these values reported by Elfes (1954) and ASABE Standard D497.6 (ASABE Standards, 2006) was likely attributed to differing crop conditions or machine design. Colzani (1968) found when cutting alfalfa at a forward speed of 2.2 m/s that the total power requirement to propel the tractor and operate the mower was 4.25 kW per meter of cutter bar. Of this, 1.6 kW/m was delivered to the power-take-off when crop was being cut and 0.3 kW/m when no crop was being cut. This meant that 1.3 kW/m was used for cutting the crop. The power requirement reported by Colzani (1968) was in agreement with ASABE Standard D497.6 (ASABE Standards, 2006).

The RFCS is not classified as a sickle-type cutter, and thus the work completed by Baird (1956), Elfes (1954) and Colzani (1968) does not have a direct application to the energy consumption of the RFCS. However, work by Elfes (1954) supports the conclusion reached by Kepner et al. (1978), McRandal and McNulty (1978), as well as Ige and Finner (1976b) in that the majority of the energy consumed to cut plant material is attributed to losses as opposed to compressing and cutting the plant material.

2.3.2 Rotary cutter

According to Persson (1987), there was typically a linear relationship between the total power requirement of a rotary mower and cutting capacity. However, Klinner et al. (1971) have found instances when the total power of a rotary mower was not quite linear, with the power increasing faster at lower feedrates than at higher feedrates. According to ASABE Standard D497.6 (ASABE Standards, 2006) the power requirements of a disk mower were 5.00 kW per meter of cutter bar width, and was independent of feedrate. However, the power requirement indicated by ASABE Standard D497.6 (ASABE Standards, 2006) had a range of ± 30%. Tuck (1976; 1977; 1978) studied the power

requirements of mowers and suggested the following equation can be used to describe the power requirements for rotary mowers of drum-and disk-type,

$$POD/LWD = POLS1,1 + POLS1,2 + (ENCSAE/EFC) \times VLF, \quad \textbf{(2.1)}$$

where:

POD is the total power required by the mower (kW),

POLS1,1 is the specific power loss due to air movement around the rotors and friction in the drive (kW/m),

POLS1,2 is the specific power loss due to friction between the rotors and stubble (kW/m),

LWD is the width of the cutting device (m),

VLF is the forward velocity of the mower (m/s) and

ENCSAE/EFC is the specific energy per unit field area required by a mower, divided by cutting efficiency (kJ/m^2).

The coefficient *POLS1,1* was found to be approximately proportional to the square of the rotor tip speed, and was quantified during stationary testing by rotating the cutting elements at a normal operating speed. The coefficient *POLS1,2* was determined using the following process. The linear portion of the total power curve at higher forward velocities was projected back to a forward speed of zero as shown in Figure 2.4. Then, the difference between the projected value and the actual total power at zero forward velocity was calculated giving the value of *POLS1,2*. Figure 2.4 gives a graphical representation of how *POLS1,1* and *POLS1,2* can be calculated.

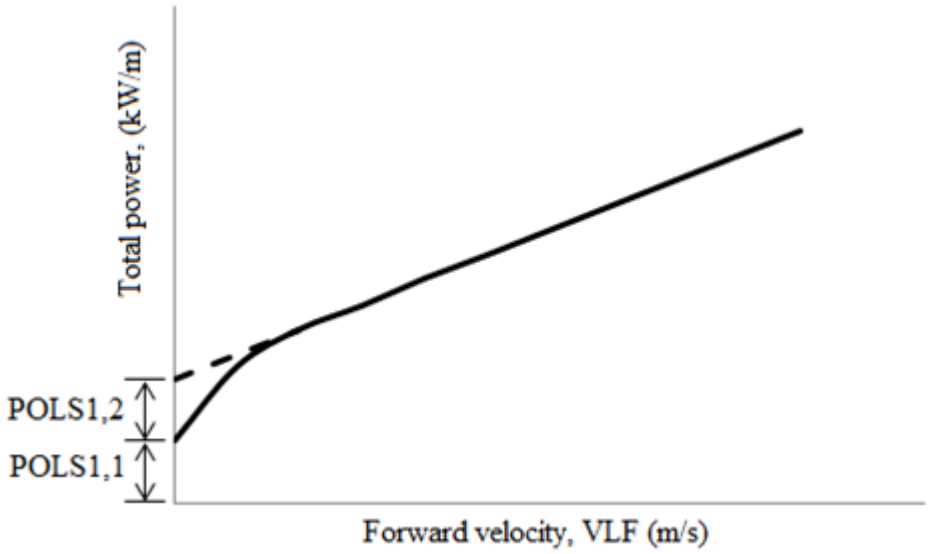

Figure 2.4 Typical relationship between total power and forward speed for rotary mowers (recreated from (Persson, 1987)) where POLS1,1 and POLS1,2 are terms representing the power loss of the mower.

Persson (1987) concluded that one of two phenomena or both will occur with an increase in feedrate of a forage harvester. If the mean particle length was held constant, the number of cuts per unit time will increase, or the material layer thickness will increase, both of which result in increased cutting power requirements. Blevins (1954) concluded that the specific energy requirements to cut alfalfa was a function of feedrate and a constant for a given moisture content and length of cut. According to Persson (1987), the power requirement to cut plant material with a forage harvester can be described by,

$$POC = ENCS \times MAT, \quad \textbf{(2.2)}$$

where:

POC is the power of cutting (kW),

MAT is the material flow rate (kg dry matter/s) and

ENCS is the specific cutting energy required by a forage harvester (kJ/kg dry matter).

It is apparent from equation (2.2) that the power required to cut material was linearly related to the dry mass flow rate. The model presented by Persson (1987) only quantifies the power requirements to cut plant material, however the total power requirements of a forage harvester can be quantified with a slightly more complex relationship given by ASABE Standard EP496.3 (ASABE Standards, 2006). The ASABE standard suggests that the power requirement of a forage harvester used to process wilted alfalfa to a 9 mm length of cut can be described by the following equation,

$$P_{pto} = 6.0 + 4.0T_{dry}\ , \qquad \textbf{(2.3)}$$

where:

P_{pto} is the power-takeoff power required by the forage harvester (kW) and

T_{dry} is the dry-mass throughput of plant material (tonne/h).

The power requirement indicated by the ASABE standard had a relatively large range of ± 40%. Like the ASABE model, Persson (1987) developed a model that can be used to quantify the total power requirements of a forage harvester. Persson (1987) concluded that the total power requirement of a forage harvester can be quantified by,

$$POD = POL1 + ENLS * MATWET + (ENCSM/LLP) * MAT, \qquad \textbf{(2.4)}$$

where:

POD is the total power (kW),

POL1 is the constant portion of the power requirement (kW),

ENLS is the specific energy caused by losses (kJ/kg wet material),

MATWET is the cutting capacity (kg wet material per second),

ENCSM is the specific cutting energy per material cut length (kJ·mm/kg dry material),

LLP is the theoretical length of cut (mm) and

MAT is the capacity (kg dry material per second).

The specific cutting energy per material cut length can be calculated by identifying the theoretical cut length, *LLP*, and the specific cutting energy, *ENSC*, using equation (2.5),

$$ENCSM = ENC1/MAL = ENSC \times LLP, \quad \textbf{(2.5)}$$

where:

ENC1 is the cutting energy for a single cut made by a forage harvester (J),

MAL is the material per unit length of layer, expressed as dry mass per unit length of cut material in (g/mm) and

ENSC is the specific cutting energy (kJ/kg).

An approximate calculation for the specific energy caused by losses can be made using equation (2.6),

$$ENLS = 0.5 * VLK^2/1000 + CO1 * SLF + CO2\ , \quad \textbf{(2.6)}$$

where:

VLK is the velocity of the cutter (m/s),

CO1 is a constant depending on the coefficient of friction (kJ kg^{-1} m^{-1}),

SLF is the distance that the plant martial and the cutting device are in contact (m) and

CO2 is a factor that represents the power loss due to friction of chopped material in housing, air movement, and pickup and feed mechanism (kJ/kg wet material).

The power loss in equation (2.6), *C02*, was assumed to be caused mostly by the energy needs for transporting material to and from the cutting area. Therefore the specific energy caused by losses, *ENLS*, was proportional to the total transported mass or the total transported wet mass. Blevins and Hansen (1956) found that the transport energy was a function of moisture content, feed rate and the square of the speed.

Persson (1987) admitted that equation (2.6) could be improved as the values for *CO1* and *CO2* were approximated, however he added that the equation described the power requirement of a forage harvester well. Persson (1987) also suggested that further work needs to be completed to validate the equation. Roberge (1999) performed laboratory experiments with a forage harvester. The power requirements of the forage harvester were measured when corn and grass were processed at varying levels of moisture content and throughput. It was found that Persson's model, equation (2.4), could predict the power requirements of the forage harvester with an R^2 value in excess of 0.97 regardless of crop type, throughput and crop moisture content.

The model presented by ASABE Standard EP496.3 (ASABE Standards, 2006) was only a function of the dry-matter feed rate, however the accuracy of the model was poor because the variation between the power requirements indicated by the model and an actual forage harvester can vary by up to 40%. Persson (1987) concluded that the power required to transport material was proportional to the total wet mass of material, and the power required to cut plant material was proportional to the dry mass of the material. Based on the conclusions drawn by Roberge (1999), the model developed by Persson (1987) very accurately described the power requirements of a forage harvester, given the large R^2 value. Relatively simple and complex models have also been developed to predict the power requirement and specific energy requirements of a forage harvester header. As with the forage harvester models, a simple model has been developed to approximate the power requirement of a forage harvester header, and a more complex model has been developed which has a higher degree of accuracy.

Goering et al. (1993) suggested a model to describe the power requirements of a forage harvester header. This model consisted of a term corresponding to the no-load power and a second term proportional to the throughput,

$$P_{th} = C_0 + C_1 T_{wet}, \quad \textbf{(2.7)}$$

where:

P_{th} is the total power of a forage harvester header (kW),

C_0 is the no-load power (kW),

C_1 is the constant for any given header (kW·h/Mg) and

T_{wet} is the wet-mass throughput of plant material through the device (tonne/h).

Nieuwenhof (2003) investigated the specific energy requirements of a prototype non-row-specific corn header. It was determined that the header type, throughput and input speed had a significant effect on the specific energy requirements of the non-row specific corn header. In order to predict the energy requirements of the header the following model was created,

$$SE = \frac{P_o + P_c + P_g + P_{cv}}{T(1-MC)}, \quad \textbf{(2.8)}$$

where:

SE is the specific energy of the header (kW·h/Mg),

P_0 is the no-load power (kW),

P_c is the cutting power (kW),

P_g is the gathering power (kW),

P_{cv} is the conveying power (kW),

T is the throughput of plant material on a wet-mass basis (kg/s) and

MC is the crop moisture content on a wet basis (decimal).

The model developed required particular machine-plant interaction properties to be measured, such as cutting energy and crush resistance. After completing trials with a non-row specific forage harvester header, Nieuwenhof (2003) compared the accuracy of the model developed by Goering et al. (1993) and his own model. It was determined that the strength of the model developed by Nieuwenhof (2003) was slightly higher than the one developed by Goering et al. (1993), with R^2 values of 0.90 and 0.88, respectively. The advantage of the more complex model developed by Nieuwenhof (2003) is that the power required to convey, gather and cut the plant material are individually quantified.

Relatively simple models have been developed to predict the power required for all types of cutting devices previously discussed. The simple models typically include a

constant power term, which corresponds to the no-load power of the cutting device, with the addition of a power term which is proportional to the throughput of the cutting device. Though the simple models quantifies the power requirements of the cutting devices, the variation of the actual power requirements of the cutting device and the modeled power can be in excess of 40%, as indicated by the ASABE standards. Successful attempts have been made to improve the accuracy of the simple models, which has been accomplished by including more factors in the model. However, the simple models, and to some extent the more complex models, are limited in the sense that the power required is not defined in terms of the design parameters of the cutting device. Therefore, the models have limited application for a designer of the cutting devices, because the designer cannot quantify the effect of changing a design parameter on the power requirements of the device. Like the power requirements of the rotary cutting devices discussed in this section, the power requirements of the RFCS will likely be able to be predicted, to a limited degree, with a linear equation. However, a model which incorporates the design parameters that have a significant effect on the power requirements of the RFCS, would be of greater value, as a designer of the RFCS could adjust the design parameters of the model and quantify the power requirements of the RFCS.

2.4 Summary

The factors that have a documented influence on the performance of cutting mechanisms have been extensively researched. The factors that were of interest for this study include blade speed, bevel angle, sharpness, thickness, oblique angle, serrations as well as clearance between cutting edges, material moisture content, and depth and density of material. The power required and or energy consumption of a cutting mechanism typically increases with an increase in blade speed, bevel angle, dullness, and thickness. The presence of serrations also typically increases the power required and or energy consumption of a cutting mechanism. An increase in the clearance between cutting edges typically increases the power and or energy requirements especially when a dull blade is employed. The energy required to cut material is typically only slightly affected by moisture content. However, an increase in the dynamic coefficient of friction due to an increase in moisture content of the material causes an increase in the total energy

consumed to transport the material. An increase in material depth and density causes an increase in the energy required to cut material. An increase in oblique angle typically reduces the maximum cutting forces but does not always translate to a decrease in the energy required to cut the material.

The material properties that are of interest for the study include the Young's modulus, maximum shear strength and the dynamic coefficient of friction for alfalfa and cereal straw. The Young's modulus for individual cereal straw is between 0.3 and 6.6 GPa and between 0.8 and 4.0 GPa for individual alfalfa stems. The dynamic coefficient of friction for cereal straw ranged from 0.19 to 0.33 and 0.2 to 0.6 for alfalfa. For both materials, there is a direct relationship between dynamic coefficient of friction and moisture content. The maximum shear strength of individual stems of cereal straw ranged from 4.9 to 8.5 MPa and 0.4 to 18.0 MPa for alfalfa. The bulk maximum shear strength of cereal straw has been found to range from 7.0 to 30.0 MPa and 0.9 MPa to 17.0 GPa for alfalfa. For both materials, there is a direct relationship between maximum shear strength and dry-matter density.

The power requirements of sickle and rotary-type cutters can be predicted based upon ASABE standards. The models presented by ASABE are relatively simple however the range of predicted power is in excess of ± 40%. Successful attempts have been made to improve the accuracy of the models used to predict the power requirements of rotary cutters. To achieve a higher degree of accuracy, the complexity of the models has increased.

During the survey of literature no publications were found that identified the factors that have an effect on the energy requirements of an RFCS. Furthermore, no models that predict the energy consumption of the RFCS were found. The RFCS is a unique rotary cutter and as such will likely have many of the same performance characteristics as the common cutting devices, yet the lack of published research prevents one from drawing any certain conclusions on the RFCS' performance.

3 OBJECTIVES

The lack of published information identifying the factors that affect the performance of a RFCS gave rise to the general objective. The general objective is to determine the effect of various parameters on the performance of the RFCS, and once the significant parameters are defined, to develop a model that can be used to predict the power requirements of the RFCS. The parameters included in the study are counter-knife sharpness, counter-knife width, counter-knife bevel angle, counter-knife serrations, counter-knife engagement, rotor speed, plant-material throughput and plant-material moisture content. The specific objectives have been separated based on the speed of cutting because, the geometry of the two RFCS is different and the physical process that the plant material goes through when cut at low speeds is different than when the plant material is processed as high speeds. The specific objectives relating to the low speed cutting process (LSCP) and the high speed cutting process (HSCP) are identified in this chapter. None of the factors that that were investigated with the LSCP RFCS were expected to affect the geometric mean length (GML) of the plant material exiting the system. However, counter-knife engagement was expected to affect the GML of the plant material exiting the HSCP RFCS. Therefore GML was included as a dependent factor for the HSCP RFCS and not the LSCP RFCS.

The research objectives associated with the LSCP (objective 1-4) were originally completed to partially satisfy the requirements of a Master of Science degree. Originally, the motivation of the study was to identify what could be done to decrease the energy requirements of the RFCS. After completing the LSCP objectives (1-4 in section 3.1), the scope of the project changed because the requirement from the project shifted from a Master of Science degree to a doctoral program. The scope of the project broadened to include the development of an analytical model that could be used to predict the power demand of the RFCS. The analytical model was developed after the LSCP objectives 1 to 4 were completed. The development of the analytical model revealed that further testing was required to validate the model. Thus, additional laboratory experiments (with the LSCP RFCS), or model validation experiments, were completed so that the analytical model could be validated. The HSCP RFCS analytical model was developed before any

field trials were completed with the HSCP RFCS, thus no additional field trials needed to be completed with the HSCP RFCS to validate the model.

3.1 Low speed cutting process (LSCP)

The specific LSCP objectives are to:

1. Determine the effect of rotor speed (low, medium, and high), throughput (low, medium and high), and counter-knife sharpness (dull and sharp) on the specific energy requirements (kW·h/tonne) to process cereal straw.

2. Determine the effect of counter-knife serrations (serrated and un-serrated), counter-knife thickness (thick and thin), and throughput (low, medium and high) on the specific energy requirements to process cereal straw.

3. Determine the effect of counter-knife bevel angle (beveled and un-beveled) and throughput (low, medium and high) on the specific energy requirements to process cereal straw.

4. Determine the effect of counter-knife thickness (thick and thin), counter-knife bevel angle (beveled and un-beveled), moisture content (low, medium and high) and throughput (low, medium and high) on the specific energy requirements to process alfalfa. Also identify the specific energy requirements of the production counter-knife, to process alfalfa at the same three levels of throughput and moisture content.

5. Develop an analytical model to predict the power requirements of the RFCS.

6. Use the analytical model to identify the significance of each factor on the specific energy requirement.

3.2 High speed cutting process (HSCP)

The specific HSCP objectives are to:

1. Determine experimentally, by way of field trials, the effect of moisture content (low and high), throughput (low and high) and counter-knife engagement (low, medium and high) on the corresponding GML of material other than grain (MOG) exiting the combine and the specific energy requirements to process cereal straw with various chopper types.

2. Develop an analytical model to predict the power requirements of the RFCS using the data from the field trials.

3. Develop a stochastic model to predict the particle length distribution of the material exiting the RFCS using the data from the field trials.

4. Use the analytical model to identify the significance of each factor on the specific energy requirement.

5. Use the stochastic model to identify which chopper results in the minimum GML for the same specific energy.

4 EXPERIMENTAL EQUIPMENT

In order for the low speed cutting process (LSCP) objectives 1 to 4 and the high speed cutting process (HSCP) objective 1 to be complete, the effect of various parameters on the specific energy requirement of the rotary feeding and cutting systems needed to be quantified. To accomplish this task two separate apparatuses were used, the LSCP and HSCP Apparatus. A detailed description of the LSCP and HSCP Apparatus is given in this chapter. The instrumentation that was used on each apparatuses and the calibration of the instruments is also discussed in this chapter.

The objectives of this project also included the development of an analytical model that could be used to quantify power demand of the RFCS. After the development of the analytical model it became apparent that the mechanical properties of the plant material processed by the RFCS needed to be quantified. A test stand was designed and fabricated so that the dynamic coefficient of friction, maximum shear strength and Young's modulus of the plant material processed with the RFCS could be quantified. A detailed description of the material properties test stand is given in this chapter.

4.1 Low speed cutting process test equipment

A test stand with five counter-knives was created by modifying a production RFCS. A production RFCS on a CNH baler has fifteen counter-knives. The test stand was created by shortening the width of the rotor housing, and length of the rotor. The modification was accomplished by cutting the center-section out of a production RFCS, and welding the two end pieces together. As on the production RFCS, the counter-knives on the test stand protrude into a pair of tines. The distance between adjacent counter-knives, and tine pairs on the test stand was equal to the production value of 71.4 mm. Similarly, a pair of tines at each end of the rotor was used to maintain material flow through the rotor housing. The rotor housing, counter-knives and tines are shown in Figure 4.1.

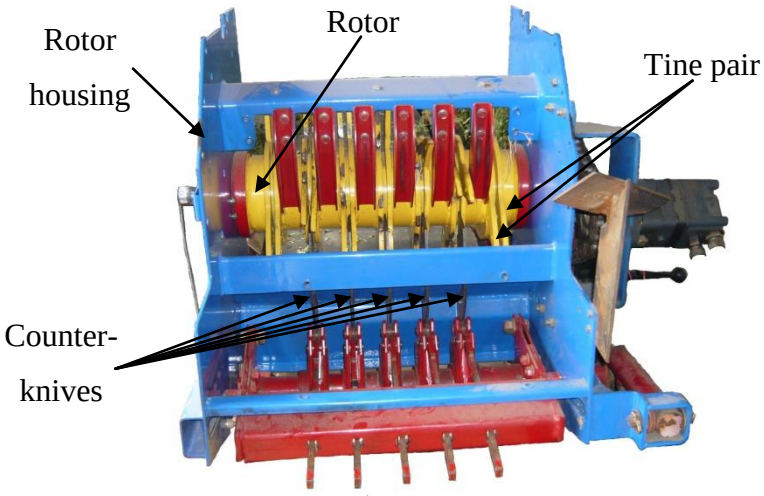

Figure 4.1 Rear view of the LSCP test stand, showing five counter-knives which protrude through the blue rotor bed and between the tines attached to the yellow rotor.

A 2-m long conveyor was used to feed material into the RFCS. The width of the conveyor was equal to the width of the rotor housing. The rotor and conveyor were driven with hydraulic motors. The conveyor used to feed the material into the RFCS as well as the hydraulic motors used to drive the rotor and conveyor are shown in Figure 4.2.

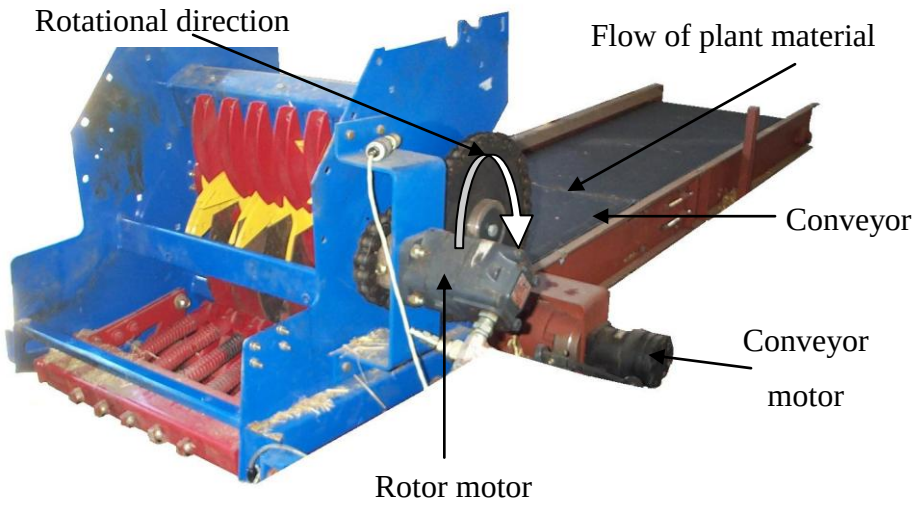

Figure 4.2 Isometric view of the RFCS test stand, showing the conveyor used to feed material into the RFCS.

The five different sets of prototype counter-knives used in the test stand included the following: 3-mm thick serrated, 3-mm thick un-serrated, 5-mm thick serrated, 5-mm thick un-serrated and 3-mm thick un-beveled. A single set of 5-mm thick production counter-knives was also used in the test stand. There were two subtle differences between the production counter-knives and the prototype counter-knives. The production counter-knives had a different type of serration than the rest of the serrated counter-knives. The production and prototype serrations are shown in Figure 4.3. The production counter-knives also had a different type of bevel than the other beveled counter-knives. The production counter-knives were beveled on both sides, causing the knife edge to be centered in relation to the knife width. Conversely, the prototype counter-knives were beveled on one side, which caused the knife edge to be offset to one side. The bevel angle on the production and prototype counter-knives is shown in Figure 4.4. The differing bevels also caused the clearance between the shearing edges to be 4.5 mm for the production counter-knives and 1 mm for the prototype counter-knives. The clearance of the shearing surfaces for the production and prototype counter-knives is shown in Figure 4.4.

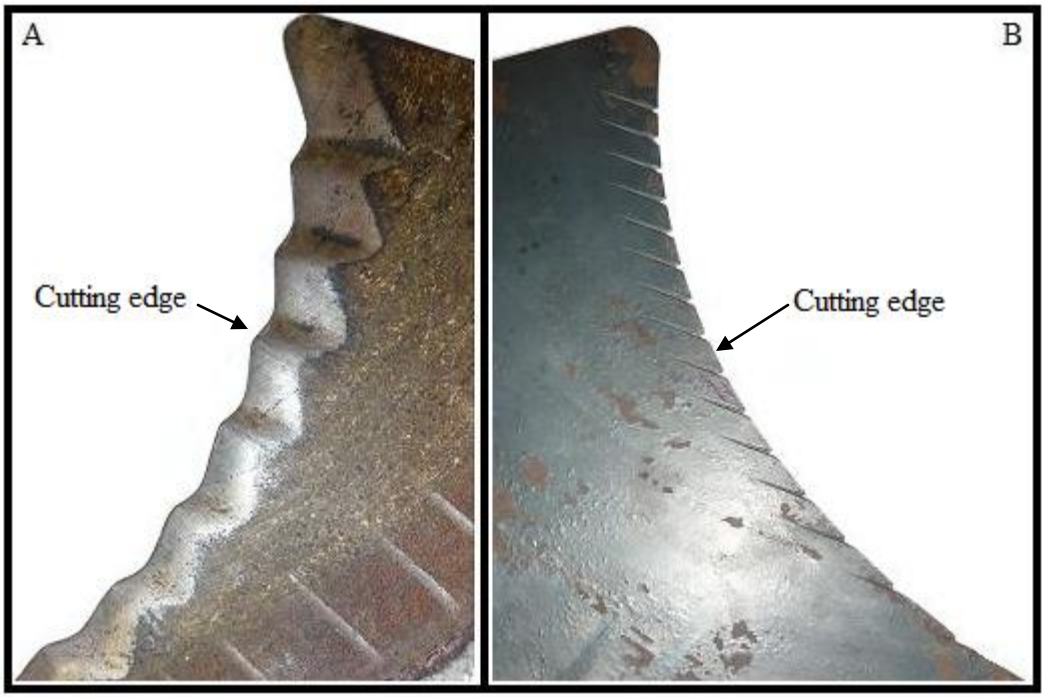

Figure 4.3 Photograph showing the differences between the type of serrations on the production counter-knives (A) and 3 and 5-mm thick serrated counter-knives (B).

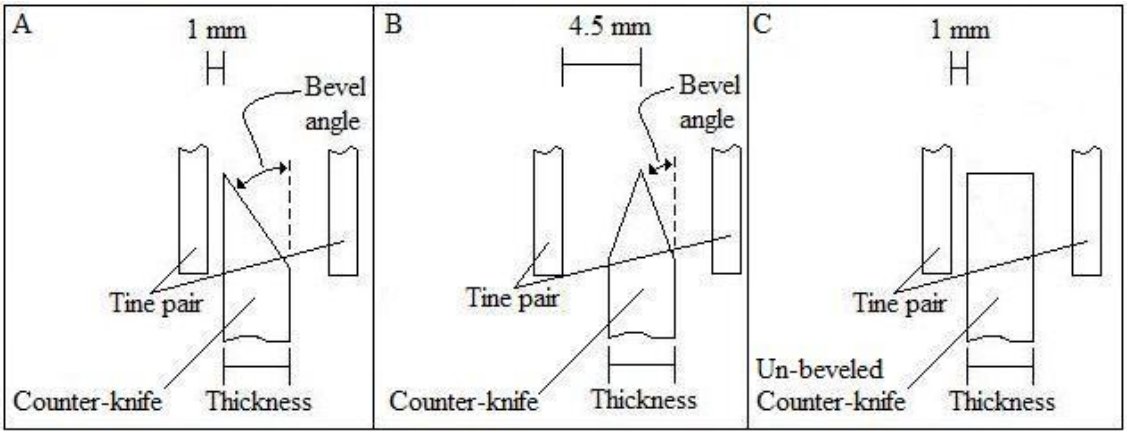

Figure 4.4 Bevel angle and clearance between shearing edges for the (A) prototype counter-knives, (B) production counter-knives and (C) prototype un-beveled counter-knives.

The standard tine-pair gap was 9.0 mm, which was used for all of the experiments except the one that investigated the effect of counter-knife bevel angle, the third LSCP objective. For these trials, inserts were welded to the tines to decrease the tine-pair gap from 9.0 mm to 4.5 mm. The location of the inserts used to reduce the tine to counter-knife gap is shown in Figure 4.5.

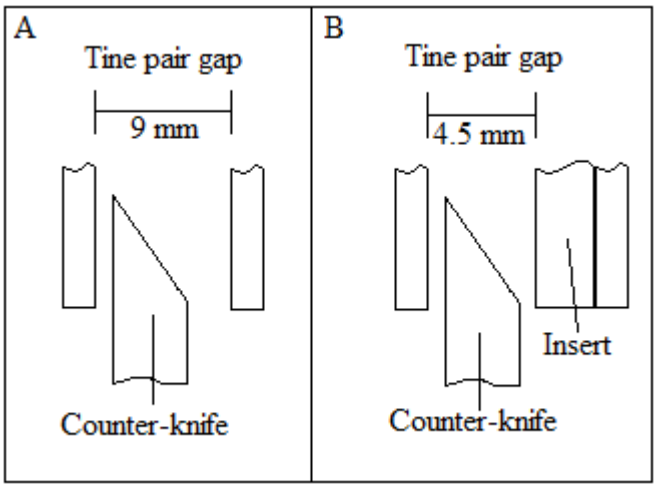

Figure 4.5 Tine-pair gap for the (A) standard gap and (B) reduced gap with insert.

Counter-knife sharpness was determined by measuring the width of the leading edge of the counter-knife (measured perpendicular to the cutting edge). The sharpness of each counter-knife used was measured in triplicate at three locations on the leading edge of the counter-knife before and after the trials were completed. The location of the measurement on the leading edge of the counter-knife is shown in Figure 4.6. The measurements were taken before and after the completion of the trials, to ensure that there was not a significant change in the sharpness, over the duration of the trials. A 10-bit color camera (Q-Imaging, 01-GO-3-CLR-10, Surrey, BC) was used in conjunction with a stereoscope (Ancansco, 076850, Toronto, ON) to take pictures of the leading edge of the counter-knives. A software package, Q Capture Pro (Q- Imaging® ,QCapture Pro, Version 6.0.0.412, Surrey, BC) was used to take pictures of, and measure the width of the counter-knife leading edge.

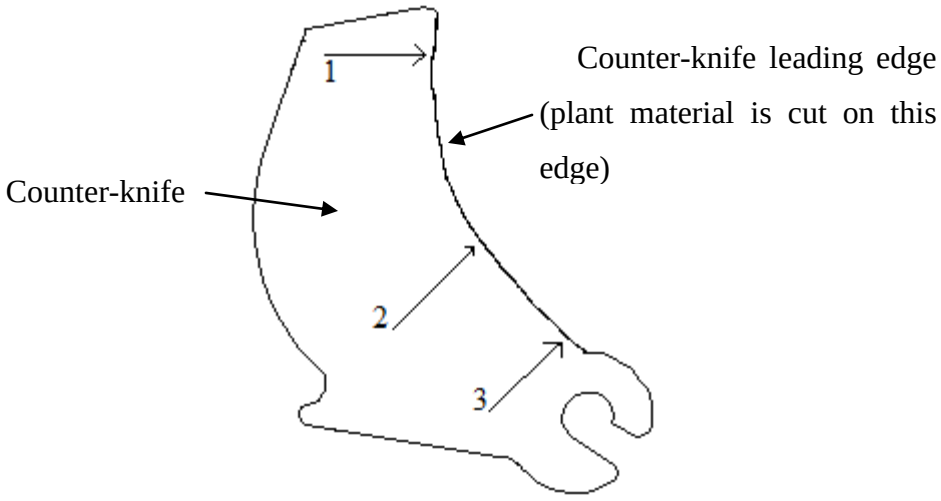

Figure 4.6 Locations of the measurements taken on the leading edge of the counter-knives to quantify the sharpness of the counter-knives.

Both the conveyor and the rotor of the test stand were powered hydraulically. The oil delivered to the conveyor and rotor motor came from an agricultural tractor (Case IH, STX-375, Racine, WI), which had the ability to deliver up to 113 liters per minute (L/min) at 20 MPa. The speeds of the rotor and the conveyor were controlled by two separate bypass-type, pressure-compensated flow control valves. The directions of oil flow through the rotor and conveyor motors were controlled by two separate directional control valves. The rotor and conveyor hydraulic motors were both fixed displacement motors. For safety purposes, a valve was used to allow oil flow in parallel with the rotor motor. During normal operation the valve was closed, preventing the oil from bypassing the motor. A schematic of the hydraulic circuit that was used to power the conveyor motor and rotor motor is shown in Figure 4.7 and Figure 4.8, respectively.

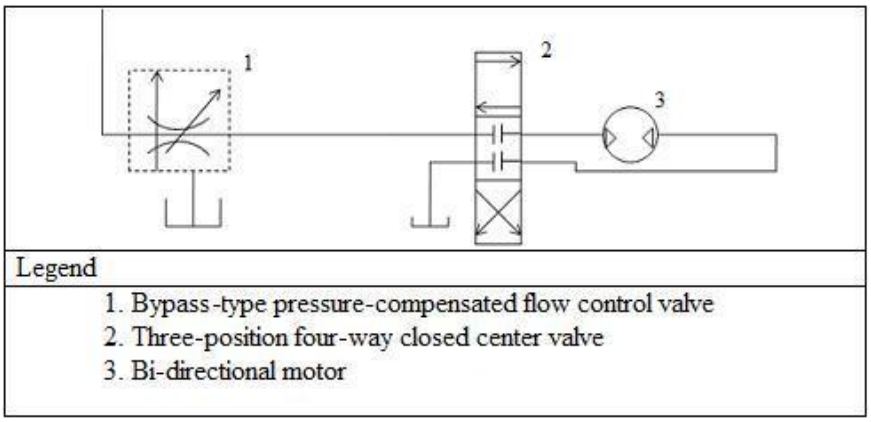

Figure 4.7 Conveyor motor hydraulic schematic.

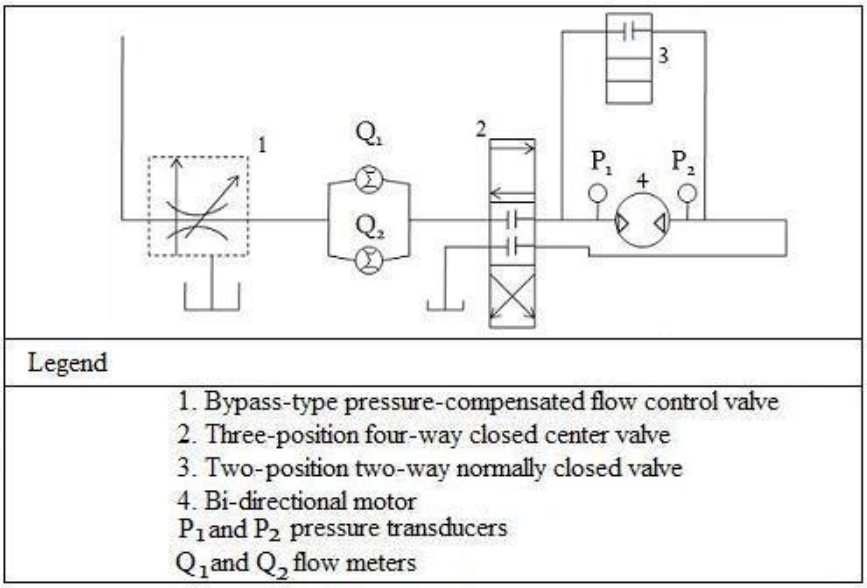

Figure 4.8 Rotor motor hydraulic schematic.

An optical encoder (AutomationDirect, TRD-SH360VD, Cumming, GA) was attached to the rotor. The optical encoder was used to determine the rotor speed and position. The sensor had three output channels A, B, and Z. The A and B channels had an output of 360 pulses per revolution, and the Z channel had one pulse per revolution. The signals from the A and Z channels were logged during the trials. The signal from the A channel

was used to determine the position and speed of the rotor. The Z channel, in conjunction with the A channel, was used to identify the absolute position of the rotor.

The pressure drop, and oil flow through the rotor motor was measured using pressure transducers and flow meters. Two pressure transducers (Stellar Technology Inc., GT 1600-5000G-233, Amherst, NY) were used to measure the pressure up-stream and down-stream of the rotor motor. Two flow meters (Hersey, Ramapo Mark V-1/2-SB, Cleveland, NC) were used to measure the oil flow through the rotor motor. The flow meters used could measure a maximum flow rate of 57 L/min, thus two were placed in parallel so that the maximum deliverable flow rate of the system could be measured. The signals from the pressure transducers and flow meters were connected to a signal conditioner and amplifier (Validyne Engineering Corp., MC 170-X, Northridge, CA).

The signals from the signal conditioner and amplifier and the optical encoder were recorded using a data logger (National Instruments, NI-DAQ 6015, Austin, TX) at a sample rate of 10 kHz. Signals were recorded for a total of 10 seconds for each trial, however the actual time during which the crop was processed by the RFCS was approximately 2 seconds. A schematic of the data acquisition system is shown in Figure 4.9. A detailed description of the process used to calibrate the sensors used on the LSCP RFCS is given in Appendix A.1.

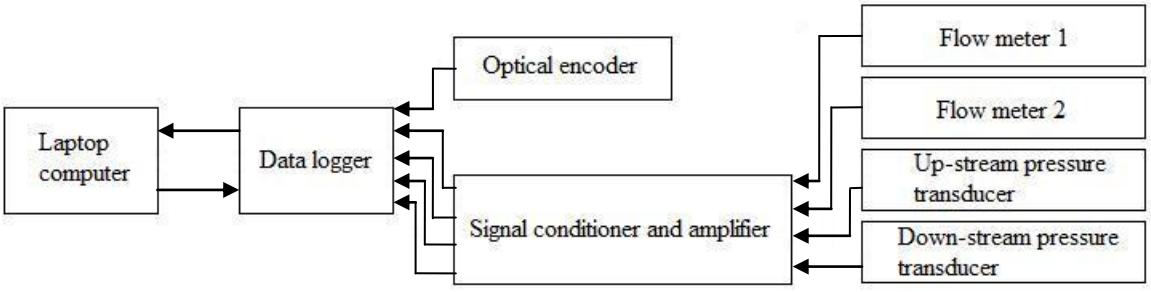

Figure 4.9 Schematic of the data logging system used on the LSCP test stand.

4.2 High speed cutting process test equipment

A combine harvester (Case IH, AFX 6.5 C4 (7010), year 2002, serial number 009770009, Grand Island, NE) was used to complete the trials. The combine harvester used to complete the trails was a class seven combine, with 354 hp. Case combine harvesters are rotary-type combines, which means that they use a threshing rotor to separate the grain from the plant material. A schematic of the combine harvester used is shown in Figure 4.10.

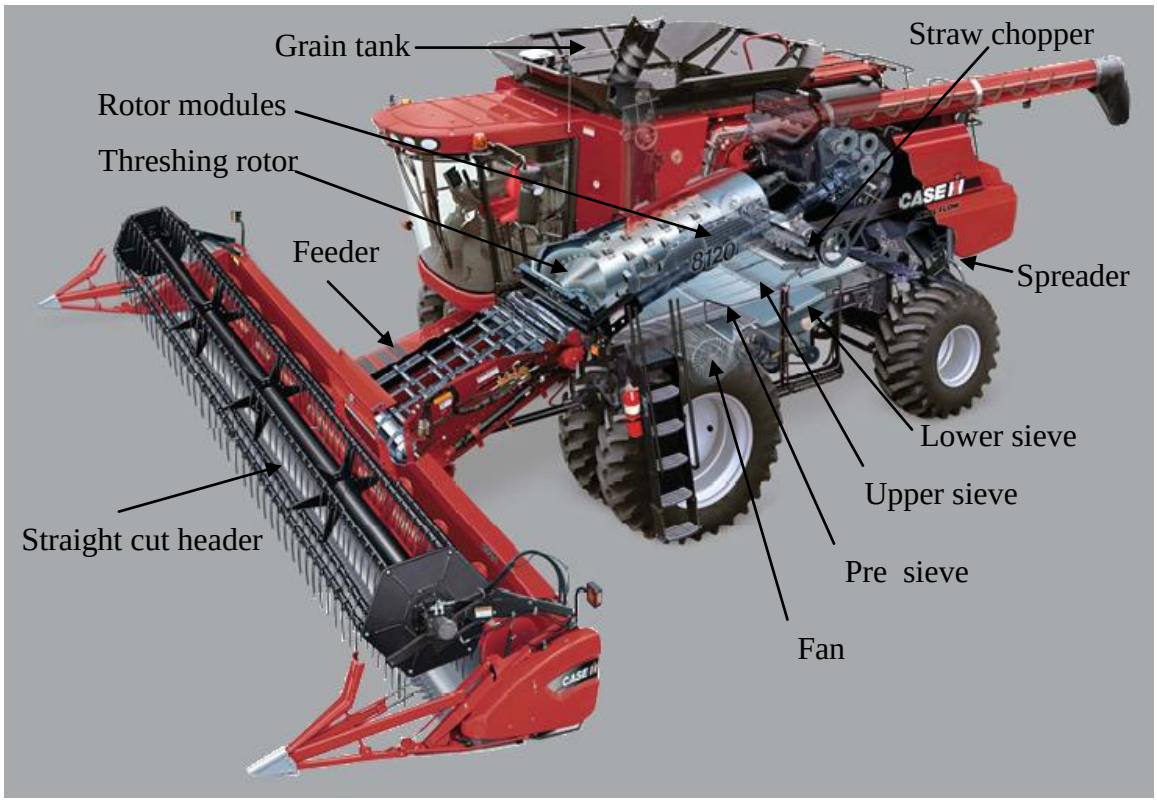

Figure 4.10 Schematic of the Case IH combine harvester used to complete field trials (modified from Axial-Flow® Combines Class V-IX Brochure (CNH America LLC, 2009)).

Plant material enters the front of the combine through the feeder, and the material other than grain, (MOG) exits at the rear of the combine through the spreader. A straight cut header is used to cut the plant stems in the field, and transport the cut plant material to the combine feeder. The feeder transported the material from the header to the threshing rotor. While in the threshing area, between the threshing rotor and rotor modules, the

grain is separated from the plant material. The longer MOG is transported to the rear of the threshing area, and to the straw chopper. The grain and shorter MOG exits the threshing area, and is subsequently processed by the cleaning system. The MOG from the cleaning system and the MOG from the straw chopper converge at the rear of the combine. The MOG is spread uniformly behind the combine by the spreader. The clean grain is transported into the grain tank. The flow of material through the combine is shown in Figure 4.11.

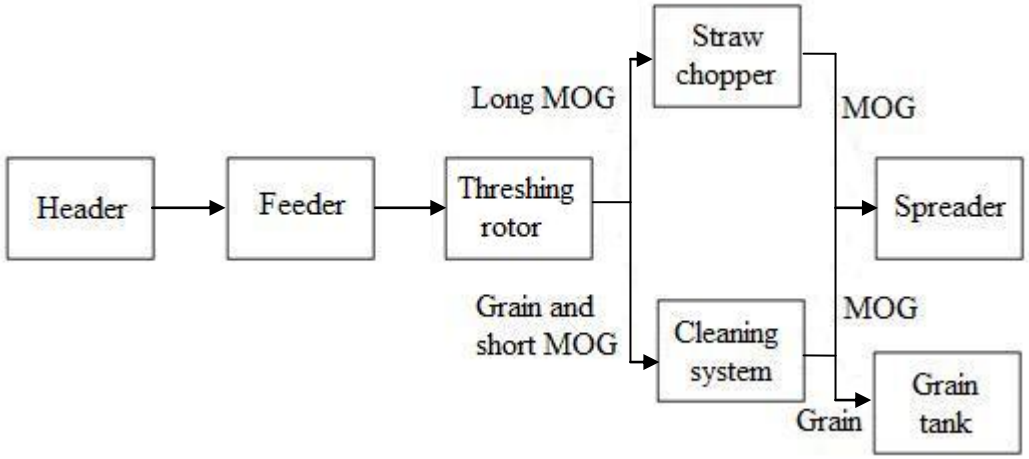

Figure 4.11 Path of plant material through a rotary combine harvester.

There are some similarities and differences between the LSCP RFCS and the HSCP RFCS. The HSCP RFCS on the combine, shown in Figure 4.12, is fed by the threshing rotor, while the LSCP RFCS is fed by a conveyor. Both RFCS have a rotor bed, through which stationary knives protrude. They both have a rotor, in the case of the LSCP RFCS the rotor is referred to as the rotor, however the rotor on the HSCP RFCS is referred to as the straw chopper. The "wide rotor" (WR) straw chopper has tines attached to the rotor, which is similar to the LSCP RFCS. However, the other straw choppers have knives attached to the rotor. The production rotational speed of the LSCP RFCS rotor is 120 rpm, while the production rotational speed of the straw chopper is either 940 or 2900 rpm. Therefore the average peripheral speed of cutting on the LSCP RFCS is approximately 2.0 m/s, while the average peripheral speed of the HSCP RFCS is

approximately 17 or 60 m/s. The rotating knives achieve impact cutting on the HSCP RFCS, while the LSCP RFCS and the WR straw chopper shear material between the tines and the stationary counter-knives.

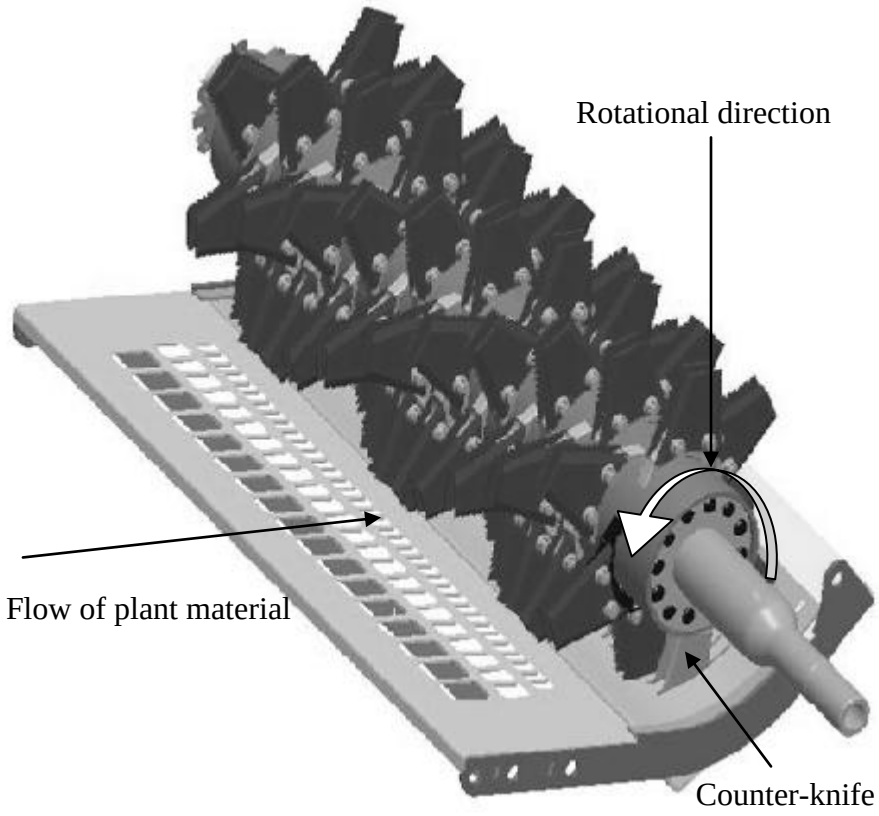

Figure 4.12 Isometric drawing of the HSCP RFCS, showing the direction of rotation of the rotor and the path of plant material thought the RFCS.

The throughput of total MOG was quantified by collecting the MOG that exited the rear of the combine. The straw spreader of the combine harvester was disengaged, and removed from the flow of material that exited the rear of the combine. Thus, the material that exited the combine was dropped into a windrow. A tarp system was mounted on the rear of the combine, so that the windrow of MOG could be collected. A 3-m long section of the windrow was collected with the tarp. The mass of material on the 3-m long tarp, and the forward velocity of the combine harvester were used to quantify the total MOG

throughput. The total MOG throughput is greater than the rate of MOG passing through the straw chopper, but it was used as a reasonable approximation.

The throughputs of MOG through the straw chopper and the combine are affected, to some degree, by the operational parameters of the combine harvester. The operational parameters include the following: header cut height and width, crop yield, forward travel speed, threshing rotor speed, rotor module type (both front and rear), the clearance between the threshing rotor and the front rotor module, the pre-sieve gap, upper sieve gap, lower sieve gap and fan speed. The pre-sieve, upper sieve, lower sieve and fan are all components of the cleaning system. The components of the cleaning system affect the path the plant material (MOG and grain) takes through the rear of the combine harvester. If the pre-sieve and upper sieve were closed so the gap was zero, or if the fan speed was increased to its maximum with the pre-sieve, upper sieve and lower sieve open, all of the plant material would have exited the rear of the combine, causing the measured throughput to increase substantially. The measured throughput would increase because instead of the grain and a limited amount of MOG being transported to the clean grain tank on the combine harvester it would be transported out the rear of the combine. Conversely the pre-sieve, upper sieve and lower sieve could have been opened and the fan speed decreased to a minimum, which would cause all of the grain and the majority of the MOG to be transported into the clean grain tank of the combine harvester, which would have decreased the measured throughput.

The threshing rotor and rotor modules are part of the threshing system. The rotor modules form a barrier around the circumference of the threshing rotor. The modules are used to hold the crop material against the threshing rotor long enough to be thoroughly threshed. The modules must also allow the threshed grain to separate from the MOG. Different types of modules are available to change how long the crop material is held against the threshing rotor. The front rotor module type, threshing rotor speed and the clearance between the front rotor module and the threshing rotor affects the aggressiveness of the threshing process. The rear rotor module is largely responsible for the separation of the grain from the longer MOG.

Before any trials of the study were completed, the operational parameters of the combine were set to the suggested initial values, and slightly modified to optimize the threshing, separating and cleaning performance of the combine. The suggested initial values of for the operational parameters were taken from the 7010 Operators Manual (CNH America LLC, 2004). This was accomplished by minimizing the seed loss, while maintaining a clean grain sample and not exceeding the capacity of the re-threshing system. The optimum values for each of the operational parameters are shown in Table 4.1. These parameters remained constant during all of the trials. It is important to note that although these were the optimum settings for the conditions present during the initial field setup, they may not have been the optimum setting for the conditions present during the completion of all of the field trials. The settings were not adjusted during the completion of the trials as the adjustment may have caused the performance of the combine to be altered. To prevent the operational parameters from being factors in the experiment they were held constant.

Table 4.1 Operational parameters of the combine harvester used during the field trials.

Operating parameter	**Settings**
Threshing rotor rotational speed (rpm)	1100
Front rotor module type	Small wire
Front rotor module and threshing rotor clearance (mm)	10
Rear rotor module type	Large skip wire
Pre-sieve gap (mm)	5
Upper sieve gap (mm)	13
Lower sieve gap (mm)	8
Fan rotational speed (rpm)	1000

The rotor module types used during the field trials were Small Wire and Large Skip Wire shown in Figure 4.13. The Small Wire modules have 5-mm thick wire with approximately a 5 mm gap between the wires. The Large Skip Wire modules have 6-mm thick wire with an alternating 13 and 26 mm gap between the wires. The Small Wire modules have a relatively low porosity, which prevents the crop material from exiting the

threshing area while the Large Skip Wire modules have a relatively high porosity which allows crop material to exit the threshing area. The Small Wire modules are most commonly used in small grain crops, while the Large Skip Wire modules are typically used in corn, soybean and rice crops.

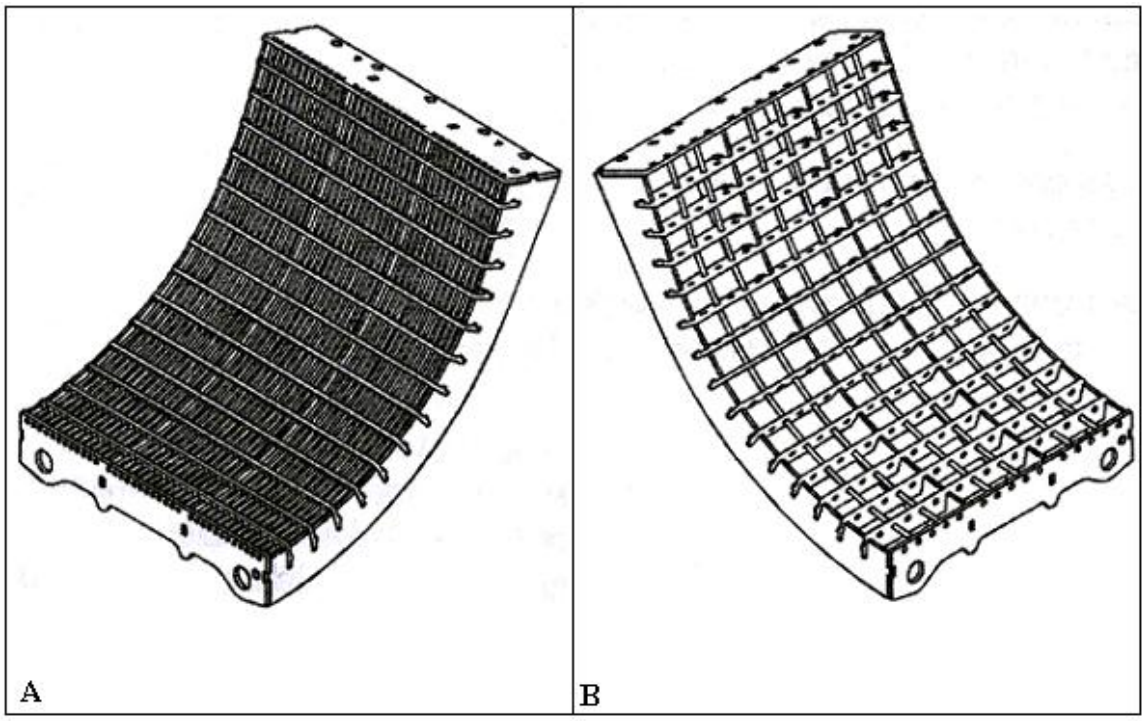

Figure 4.13 Drawing of the threshing rotor modules used in the combine harvester during the completion of the field trials, (A) Small Wire, (B) Large Skip Wire. (copied from 7010 Operators Manual (CNH America LLC, 2004)).

Four different choppers were tested, including a 2X0.5, 2X3, 3X3 and WR, shown in Figure 4.14. For the first three choppers (2X0.5, 2X3 and 3X3) the knives were attached in a helical pattern to the circumference of the choppers. The first index indicated the number of rotating knives mounted on the circumference of the chopper in the same plane (the plane being perpendicular to the axis of rotation of the chopper). The second index indicated the number of rotations the helix pattern made around the axis of rotation of the chopper, across the width of the chopper. For example, the 2X0.5 chopper had two

knives that were mounted to the circumference of the chopper in a single plane, and the helical pattern in which the knives were placed on the outside of the chopper made half of a revolution across the width of the chopper, as shown in Figure 4.14 A. WR is an abbreviation for "wide rotor". The WR chopper does not have rotating knives, like the other three choppers. Instead it had tines similar to the LSCP test stand.

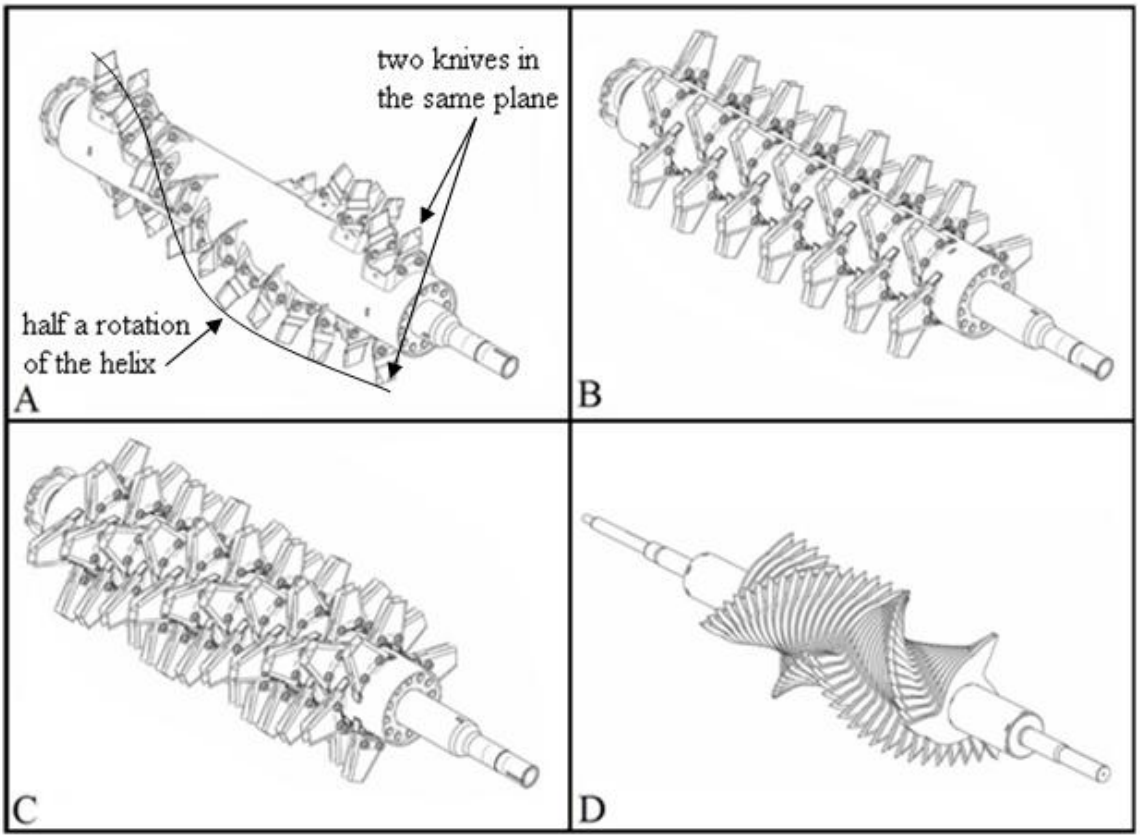

Figure 4.14 Drawings of the four choppers tested in the HSCP RFCS, (A) 2X0.5, (B) 2X3, (C) 3X3 and (D) WR.

The geometry was not the only difference between the choppers tested; the operational speed and counter-knives also differed. The 2X0.5, 2X3 and 3X3 choppers were designed to operate at 2900 rpm, and the WR was designed for a lower speed of 940 rpm. The average peripheral speed of the 2X0.5, 2X3 and 3X3 choppers was 60.4 m/s, it was 17.2 m/s for the WR. The average peripheral speed was defined as the tangential speed of the tine at the midpoint of the tine (half way between the tip and base of the tine). The

difference in the peripheral speed of the choppers is attributed mainly to the varying rotational speed, as the tip radii of the cutting elements on all choppers were approximately the same. The tip and base peripheral speed, average speed and radii for each chopper used in the combine along with the chopper rotational speed are given Table 4.2.

Table 4.2 Rotational and peripheral speed of the cutting elements on the choppers and the tip and base radii of the cutting elements.

Chopper type	**Rotational speed (rpm)**	**Tip speed (m/s)**	**Base speed (m/s)**	**Average speed (m/s)**	**Tip radius (m)**	**Base radius (m)**
2X0.5	2900					
2X3	2900	73.8	47.1	60.4	0.243	0.155
3X3	2900					
WR	940	23.8	11.2	18.1	0.242	0.114

The 2X3 and 3X3 choppers had the same type of rotating knives which were designed to be used with the same type of counter-knives. The number of counter-knives used with the 2X3 and 3X3 choppers was 42, and the spacing between the counter-knives was 27.0 mm. The number of counter-knives used with the 2X0.5 chopper was 41, and the spacing between the counter-knives was 27.0 mm. The 2X0.5 counter-knives were similar to sickle sections one would find on a sickle-type cutting device. The number of counter-knives used during the WR trials was 26 and the spacing between counter-knives was 40.6 mm. The WR counter-knives were the same as the counter-knives used in the LSCP test stand. The number, profile and spacing between counter-knives for each chopper, were selected based upon the recommended configuration given in the 7010 Operators Manual (CNH America LLC, 2004). The profile of the counter-knives used with the four different choppers tested, and the orientation of the counter-knives with respect to the chopper and crop flow is shown in Figure 4.15.

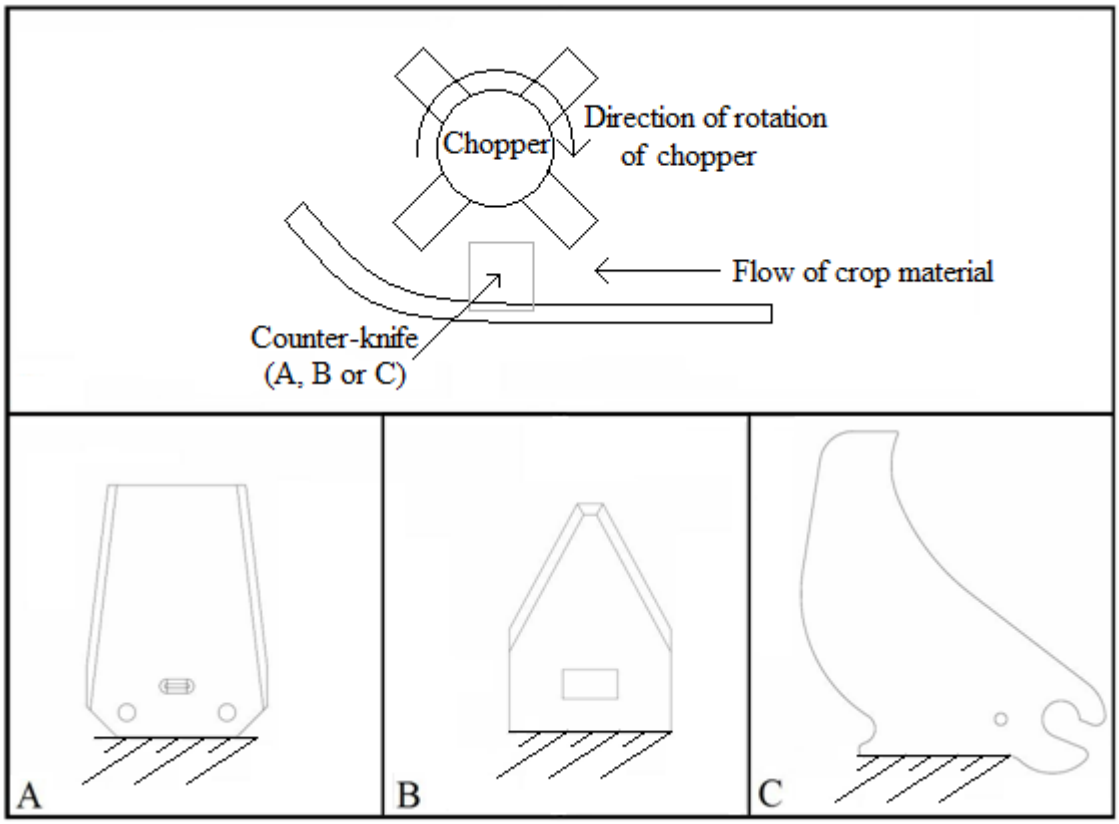

Figure 4.15 Drawings of the counter-knives used with the (A) 2X3 and 3X3 choppers, (B) 2X0.5 chopper and (C) WR chopper.

The counter-knife engagement on all choppers was adjusted using a mechanical detent. The locked position of the detent for the 2X0.5, 2X3 and 3X3 choppers was adjusted so that the counter-knives could be set at three different levels of engagement. The three levels of counter-knife engagement used during the 2X0.5, 2X3 and 3X3 trials was 0, 50 and 100%. A 100% counter-knife engagement was achieved by inserting the counter-knives, as far as possible, through the rotor bed and between the rotating elements of the chopper. Conversely, 0% engagement was achieved when the counter-knives were fully removed from between the rotating elements of the chopper and the rotor bed. The same levels of counter-knife engagement were not investigated with the WR chopper. The WR counter-knives could not be fully removed from the chopper because of the lack of clearance between the upper sieve and the counter-knives. Thus, counter-knife engagements of 100, 89, and 78% were examined with the WR chopper.

The distance the counter-knives protruded past the rotor bed and into the chopper, for all choppers tested is given in Table 4.3.

Table 4.3 The relationship between the level of counter-knife engagement and the distance the counter-knives protruded into the chopper.

		Chopper			
		2X3	**3X3**	**2X0.5**	**WR**
		Distance (mm)			
Counter-knife engagement	High	78	78	33	165
	Medium	39	39	17	147
	Low	0	0	0	129

High 100% engaged, or fully inserted for all choppers
Medium 50% engaged (2X3, 3X3 and 2X0.5) 89% (WR)
Low 0% engaged or fully removed (2X3, 3X3 and 2X0.5) 78% engaged (WR)

Strain gauges were oriented on the straw chopper shaft to facilitate the measurement of torque experienced by the chopper. Four active gauges were mounted on the 2X0.5, 2X3 and 3X3 chopper drive shafts. These three choppers were driven independently from the cleaning system of the combine. A shaft inside of the straw chopper was used to transfer power to the cleaning system. The WR chopper did not employ the shaft-in-shaft design. Therefore in order to measure the torque experienced by the WR chopper eight gauges were used. Four gauges were mounted on each of the drive and driven sides of the chopper. The location of the strain gauges on the chopper is shown in Figure 4.16.

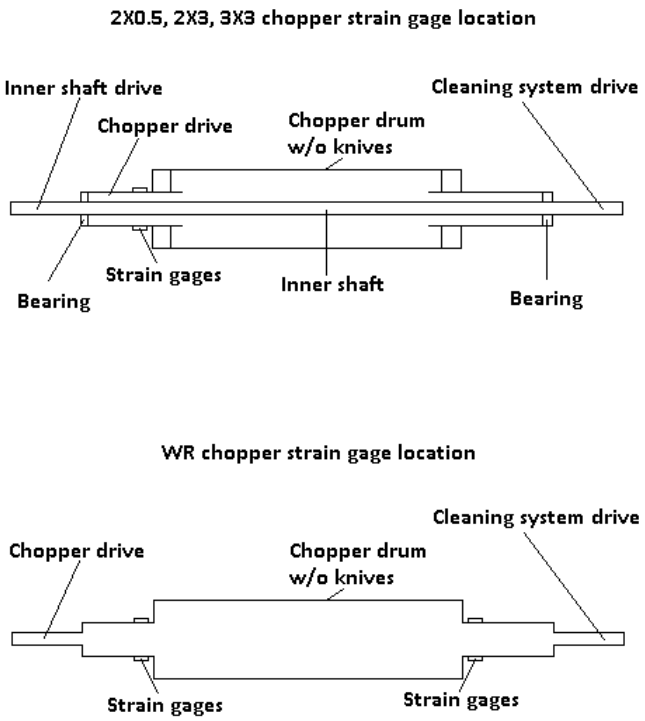

Figure 4.16 Location of strain gages on the straw choppers.

The strain gauges were mounted on the shaft at a 45° angle from the axis of rotation of the chopper. The gauges were placed in the Wheatstone bridge so that the output was sensitive only to torsional strain and not bending strain. The location of the gauges within the Wheatstone bridge is shown in Figure 4.17.

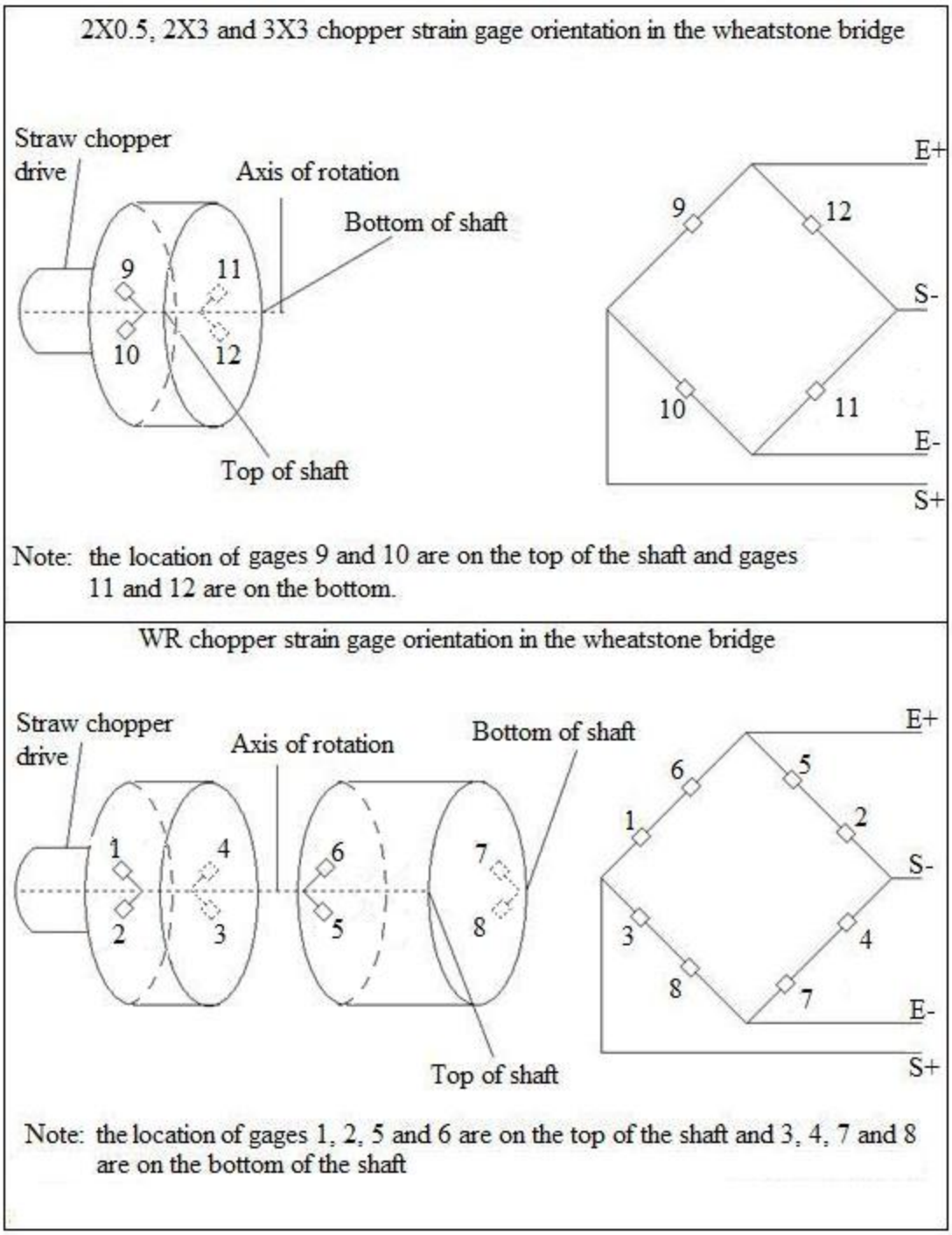

Figure 4.17 Strain gauge orientation within the Wheatstone bridge for all four choppers.

The signals from the bridges on the straw choppers were transferred by way of a telemetry system (Accumetrics Associates Inc., AT-5001, Schenectady, NY). The components of the telemetry system used included a Kevlar strap, strap tightening mechanism, transmitter and receiver. The components of the telemetry system are shown in Figure 4.18.

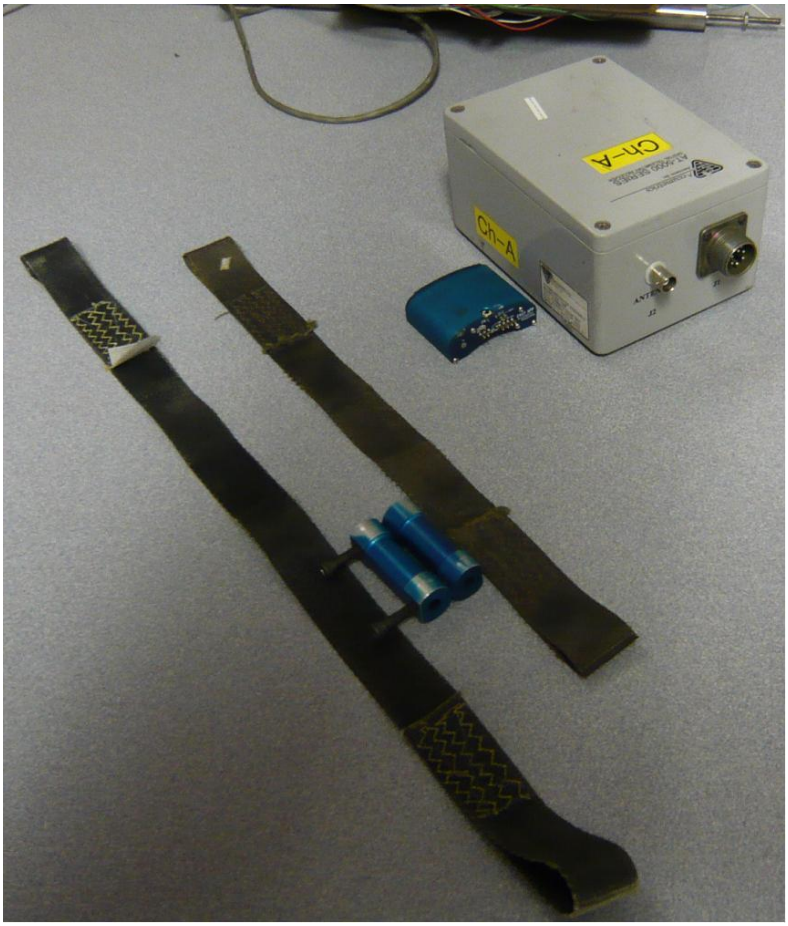

Figure 4.18 Photograph of the components of the telemetry system including the Kevlar straps, strap fastening mechanism (blue cylinders), transmitter (blue box) and receiver (gray box).

The transmitter was fastened to the shaft of the chopper using a Kevlar strap and strap fastening mechanism. The excitation and signal wires from the Wheatstone bridge were connected to the transmitter. A radio frequency pickup coil, which was a loop of coaxial

cable, was placed around the circumference of the chopper shaft within 30-mm of the transmitter. A data logger was used to record the output signal from the receiver.

The same optical encoder that was used on the LSCP test stand, described in section 4.1, was attached to the chopper shaft to determine the chopper's rotational speed and position. Because of the shaft-in-shaft design of the 2X0.5, 2X3 and 3X3 choppers, the optical encoder could not be mounted on the end of the chopper shaft. Therefore, a sprocket was modified so that it could be attached to either the 2X0.5, 2X3, or 3X3 chopper. This was done by welding a hub to a sprocket, boring the sprocket and hub assembly to the outside diameter of the chopper shaft and cutting the sprocket and hub assembly in half. Two bolts were used to fasten the sprocket hub to the chopper shaft. The modified sprocket was linked to another sprocket of the same diameter with a roller chain. The second sprocket was attached to a short shaft that was mounted on the combine in parallel with the axis of rotation of the chopper. The optical encoder was attached to the end of the short shaft. The location of the optical encoder, modified sprocket and hub assembly, roller chain and short shaft with the second sprocket is shown in Figure 4.19. The WR chopper did not use the shaft-in-shaft design, which allowed the sensor to be mounted directly to the end of the straw chopper shaft.

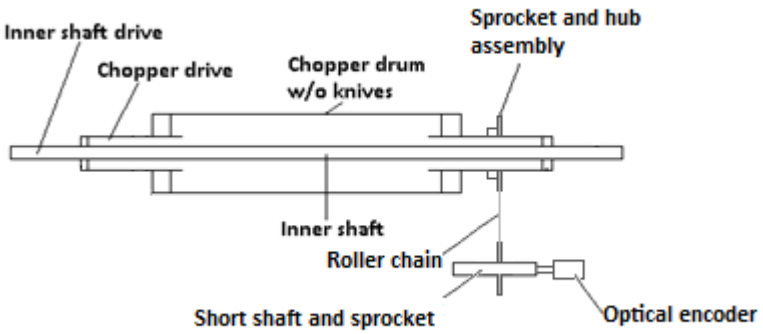

Figure 4.19 Cross-sectional sketch of a chopper, showing the location that the sprocket and hub assembly was attached to the 2X0.5, 2X3 and 3X3 chopper, along with the roller chain, short shaft and sprocket used to indirectly attach the optical encoder.

A data logger (National Instruments, NI-DAQ 6216, Austin, TX) was used to record the position of the chopper and the torque on the straw chopper. The output from the receiver of the telemetry system, as well as the output from the optical encoder were connected directly to the data logger. Both of the signals were sampled at a rate of 36 kHz. A total of 5 seconds was logged for each trial, which was limited by the buffer size of the data logger. The block diagram of the data logging system used on the combine harvester is shown in Figure 4.20. A detailed description of the process used to calibrate the sensors used on the HSCP RFCS is given in Appendix A.2.

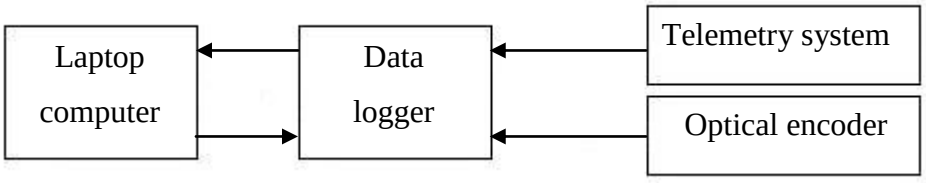

Figure 4.20 Schematic of the data logging system used on the combine harvester.

4.3 Material properties test stand

A test stand was fabricated to determine the material properties of the plant material that was processed by the RFCS. The material properties of interest were the Young's modulus, maximum shear strength and dynamic coefficient of friction between plant material and steel. Because of the visco-elastic nature of plant material, it was important to quantify the mechanical properties of plant material at a loading rate equal to (or as close as possible to) the loading rate it experienced in the RFCS (particularly for quantifying the Young's modulus and maximum shear strength). A material properties testing machine (Instron, Grove City, PA) was not used to determine the material properties of the plant material because of its relatively slow crosshead speed (8.0×10^{-3} m/s). Instead, a test stand was designed and built to subject the plant material to a loading rate of up to 0.5 m/s, which was two orders of magnitude faster than other available testing systems (for example the Instron) and closer to the loading rate that the plant material experienced in the RFCS. The loading rate that the plant material experienced in the LSCP RFCS was on the order of 1.5 to 3.4 m/s and in the HSCP RFCS

from 11.2 to 73.8 m/s. As discussed in sections 2.2.1 and 2.2.3 the bulk material properties (for Young's modulus and maximum shear strength) needed to be quantified because the interaction of the plant material with itself has an effect on the properties the plant material exhibit. The procedure used to quantify the Young's modulus, maximum shear strength and dynamic coefficient of friction of plant material is given in Appendix B.

A calibration section was not included for the sensors used on the material properties test stand because both of the sensors were new and they were calibrated by the manufacturer. The calibration curve for each sensor was validated, and the relationship recorded during the manufacture calibration was mirrored during the validation process. The relationship between position of the core in the linearly variable displacement transformer (LVDT) and the signal of the LVDT was highly linear. Similarly, the relationship between the force subject to the load cell and signal from the load cell was highly linear.

The test stand had three main components: the structural support, the plant-material engaging tools and the hydraulic system used to control the tools. A data logger was used to control the tool operation, as well as record information from a load cell and a LVDT. Three different material-engaging tools were made so that the Young's modulus, maximum shear strength and dynamic coefficient of friction of alfalfa and cereal straw could be quantified.

The mast and mast support provided the structural support to the test stand. The mast of the test stand was fabricated from channel iron, and the mast support was fabricated from angle iron. A linear hydraulic actuator (The Sheffer Corp., JJSL12ADKY, Cincinnati, OH) was attached to the mast of the structural support. The dual-rod actuator had a 305-mm stroke, and a bore of 29-mm. The speed and position of the hydraulic cylinder was measured with a LVDT (Macro Sensor, DC-750-1000, Pennsauken, NJ). The force exerted by the actuator was measured using a rod-end load cell (Honeywell, AL428-DJ, Columbus, OH). The capacity of the load cell was 8.9 kN. The structural support, hydraulic actuator, LVDT and load cell are shown in Figure 4.21.

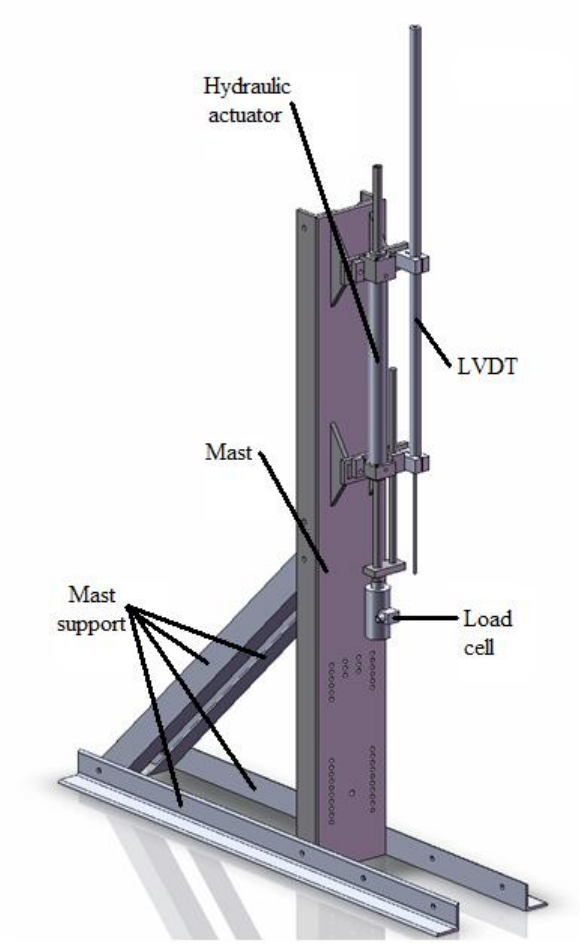

Figure 4.21 The material properties test stand structural components, hydraulic actuator and sensors.

An electrically powered hydraulic unit was used to deliver oil to the test stand at a rate of up to 26.0 L/min at a pressure of 18.0 MPa. The rate of oil flow to the actuator, and thus the actuator speed, was controlled with a pressure-compensated flow control valve. The pressure-compensated flow control valve was critical in the operation of the test stand, as it maintained a constant loading rate while quantifying the properties of the plant material. A globe valve was installed downstream of the flow-control valve, for safety purposes. The globe valve was turned off, when the operator manipulated the tools on the end of the actuator. The direction of the cylinder was controlled with a solenoid operated three-position four-way closed center valve. Solenoid operation was controlled with a data logger (National Instruments, NI-DAQ 6015, Austin, TX). A needle valve

was placed in parallel with the ports on the actuator. The needle valve was installed to allow the actuator to be moved, by hand, when the hydraulic pump or the electronic control system was off. The hydraulic components of the material properties test stand are shown in Figure 4.22.

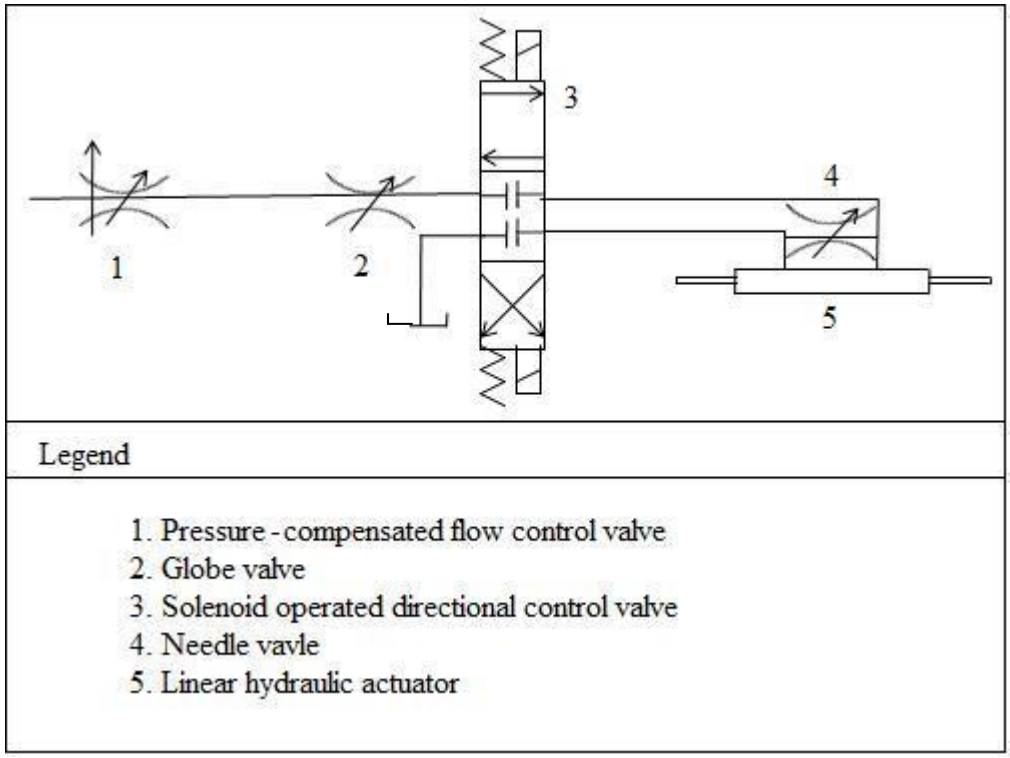

Figure 4.22 Hydraulic circuit used to control the linear actuator on the material properties test stand.

The signals from the LVDT, and the load cell were recorded using a data logger (National Instruments, NI-DAQ 6015, Austin, TX), at a sample rate of 10 kHz. The solenoids on the directional control valve were also controlled with the same data logger. A schematic of the data-acquisition and control systems is shown in Figure 4.23.

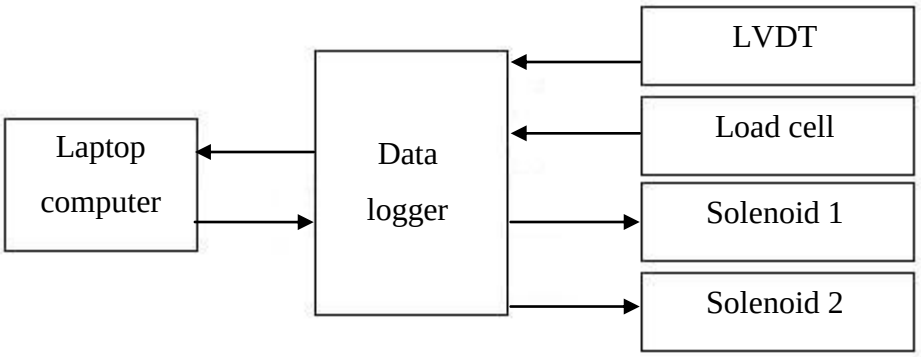

Figure 4.23 Schematic of the data logging system used on the material properties test stand.

The punch and die assembly used to quantify the maximum shear strength of cereal straw and alfalfa is shown in Figure 4.24 A. The punch and die assembly that was used to quantify the bulk maximum shear strength of the plant material was similar to the punch and die used by Bright and Kleis (1964). The maximum shear strength of plant material was determined by placing the plant material in the die and recording the force required to push the punch through the mat of plant material inside the die. The punch was a cylinder with a diameter of 12.1 mm and length of 152.0 mm. The punch was threaded at one end so that it could be fastened to the load cell. The die consisted of two components - a base and a lid. The lid was fastened onto the base with three bolts, and a hole was bored through the lid and base to accommodate the punch. The volume of the chamber made by the die base and lid was 297×10^3 mm^3. The base was fastened to the mast of the test stand with four bolts. A photograph of the punch and die used to quantify the maximum shear strength of plant material processed by the RFCS is shown in Figure 4.24 B.

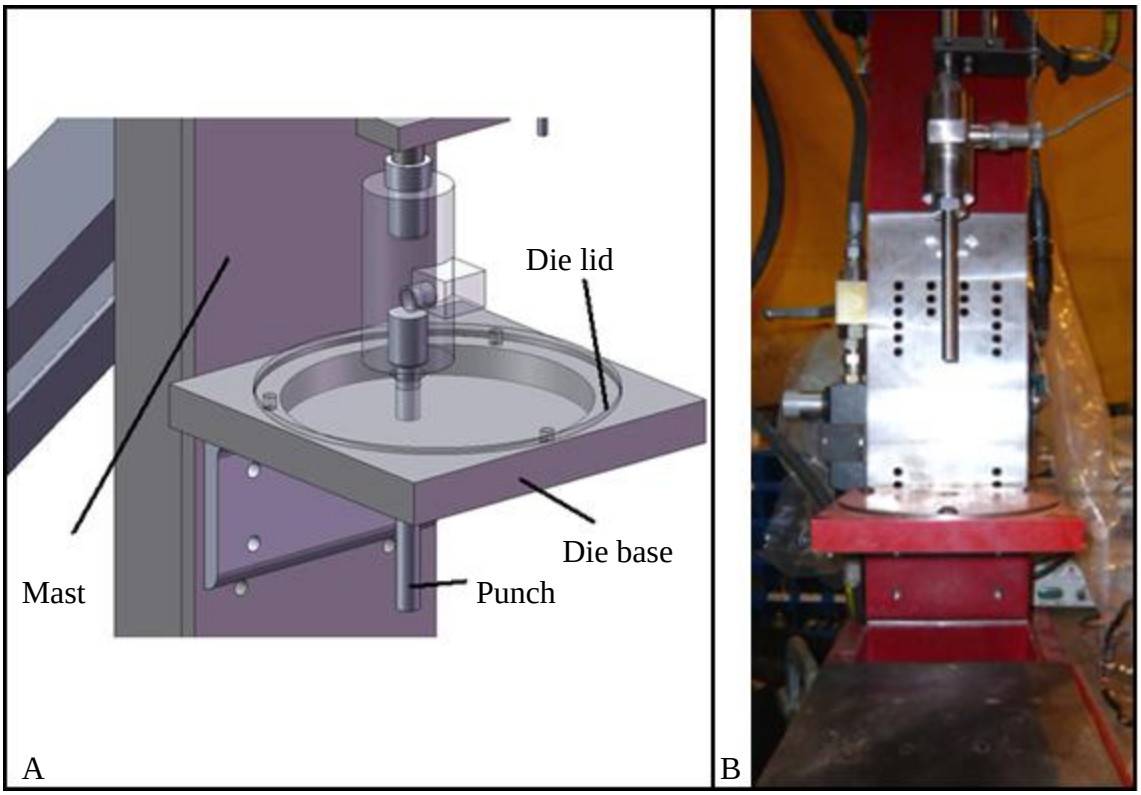

Figure 4.24 Punch and die used to determine the maximum shear strength of plant material (Computer-aided design drawing (A), Photograph (B)).

A box and compression plate were used to determine the bulk Young's modulus of plant material, as was done by Usrey et al. (1992). The height, width and length of the box was 180.0, 620.0 and 140.0 mm, respectively. The compression plate length and width were 170.0 and 610.0 mm, respectively. The compression plate was threaded into the load cell and the box was supported by the mast using four bolts. The compression plate and box are shown in Figure 4.25 A. A photograph showing the box and compression plate used to determine the bulk Young's modulus of the plant material processed by the RFCS is shown in Figure 4.25 B.

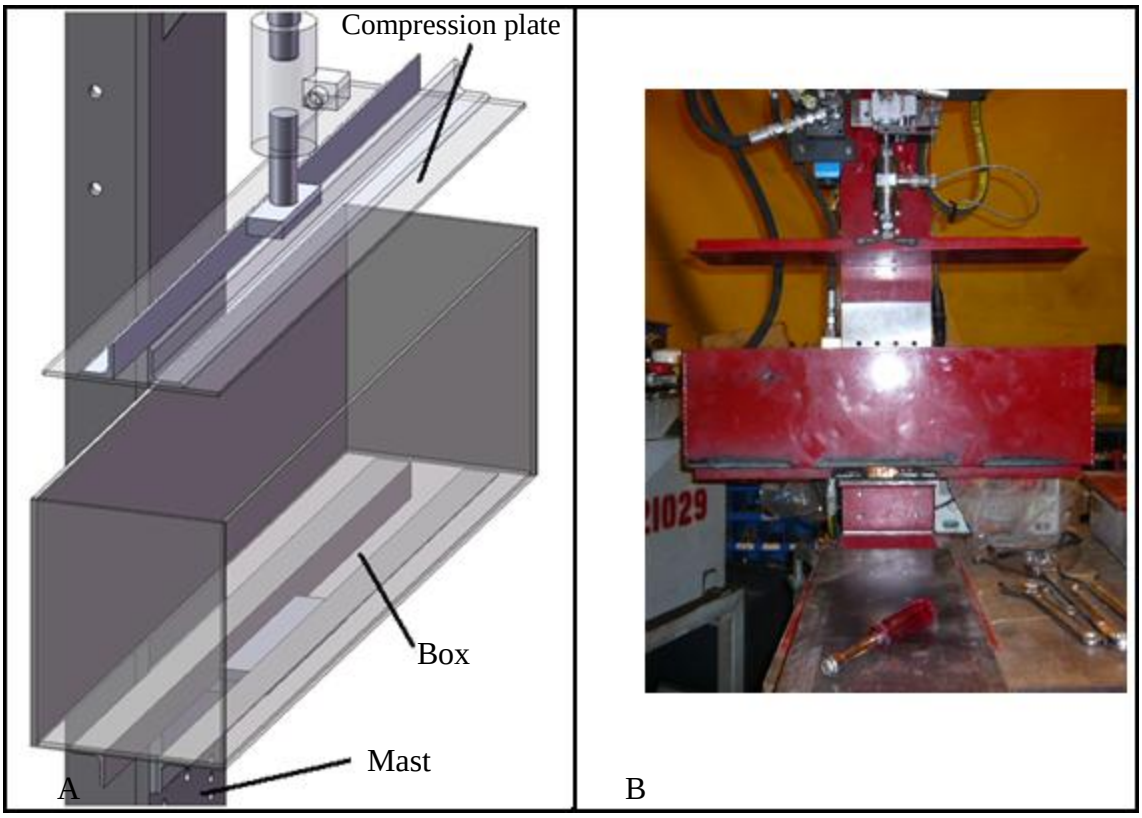

Figure 4.25 Compression plate and box used to determine the Young's modulus of plant material (Computer-aided design drawing (A), Photograph (B)).

The dynamic coefficient of friction of the plant material was determined by sliding the plant material across a polished steel surface. The box that was used to contain the plant material during the trials was suspended from the steel surface by four ball bearings. The bearings were used to minimize the effect of the steel box sliding on the polished steel surface. A plate and load of known mass were placed on top of the plant material during the trials. The box containing plant material was pulled by the hydraulic actuator using a cable and pulley. The box, plate, and pulley are shown in Figure 4.26. The cable, which was supported by the pulley and connected to the load cell and the material box is not shown in Figure 4.26 A. A photograph showing the box, sliding surface, pulley and cable used to quantify the dynamic coefficient of friction of plant material processed by the RFCS is shown in Figure 4.26 B.

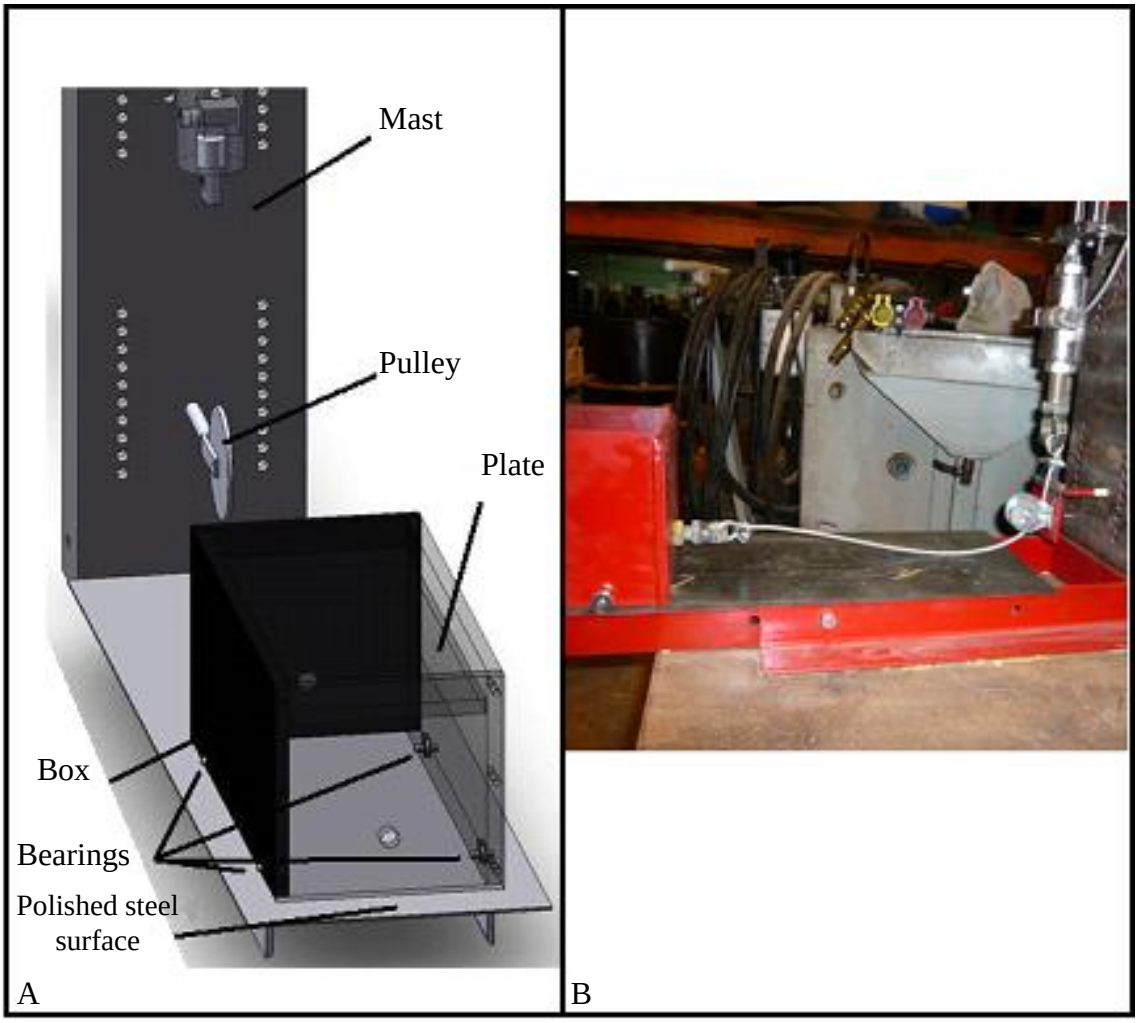

Figure 4.26 Box, plate and pulley system used to determine the dynamic coefficient of friction of plant material (Computer-aided design drawing (A), Photograph(B)).

5 LOW SPEED CUTTING PROCESS (LSCP)

To complete the LSCP objectives 1-4 in section 3.1, which were to determine the effect of various operational, design and crop factors on the specific energy requirements of the RFCS, laboratory experiments were completed. Objectives 1 to 3 (section 3.1) were completed with cereal straw because, at the time the experiments were completed, this was the only material available. After the completion of the laboratory experiments with cereal straw, fresh alfalfa became available. The results of the experiments completed with cereal straw were used to identify the factors that would likely affect the specific energy requirements of the RFCS when used to process alfalfa. For example, the effect of rotor speed did not have a significant effect on the specific energy requirements of the RFCS when used to process cereal straw. Thus it was assumed that the rotor speed, over the same range tested with cereal straw, would not have a significant effect on the specific energy requirements of the RFCS when used to process alfalfa. Therefore, the effect of rotor speed was not investigated when the RFCS was used to process alfalfa.

The development of the analytical model revealed that further testing was required to validate the model. Thus, additional laboratory experiments, or model validation experiments, were completed so that the analytical model could be validated. In this chapter, the methodology used to complete the experiments as well as the results and conclusions drawn from the experiments will be discussed.

5.1 Laboratory experiments – significant parameter identification

5.1.1 Methodology

The LSCP testing apparatus described in section 4.1 was used to determine the effect of counter-knife sharpness, bevel angle, thickness, rotor speed, material moisture content and throughput on the specific energy requirements of the RFCS. The materials processed with the testing apparatus were cereal straw and alfalfa.

For all trials completed with the LSCP testing apparatus the same method was used to achieve varying levels of throughput. The throughput during the trials was determined by placing a known mass of material on the conveyor which operated at a constant velocity. The rotational speed of the conveyor motor was measured with an optical tachometer, and set with a bypass-type pressure-compensated flow control valve. The rotational speed of the conveyor motor was set so that the velocity of the conveyor belt was constant. Thus, varying levels of throughput were achieved by adjusting the mass density (mass per length of conveyor) of material placed on the conveyor at the start of each trial. The mass of material was quantified using a digital scale and it was spread uniformly over the length of the conveyor.

The method used to quantify the moisture content of the material processed by the LSCP testing apparatus was the same for all trials. The moisture content was determined according to ASABE Standard S358.2 (ASABE, 2008) where 50-g samples were dried in a convection oven at 103ºC for 24 h. Moisture was determined in triplicates and expressed in percent wet basis (% w.b.).

The experimental design used for all trials completed with the LSCP testing apparatus was the same. A split-plot experiment design was used to minimize the number of times the counter-knives needed to be changed in the test stand. The ASTM Standard D3108 (ASTM, 1992c) was used to determine the required number of replicates,

$$N_{um} = \frac{\left(t_s v_p\right)^2}{{A_v}^2}, \qquad \textbf{(5.1)}$$

where:

N_{um} is sample size,

t_s is the value of a student's t for a two sided limit at 95% probability level and infinite degrees of freedom, 1.96 (for population)

v_p is an estimate of the coefficient of variation, CV, and

A_v is 15% of average, the value for allowable variation.

Preliminary tests were completed to determine a value for an estimate of the coefficient of variation. By using equation (5.1), the number of replicates that needed to be completed was 3 with a 15% value for the allowable variation.

LSCP Objective 1: The first LSCP objective was to determine the effect of rotor speed, throughput, and counter-knife sharpness on the specific energy required to process cereal straw with the RFCS. Thus trials were completed with the LSCP testing apparatus. The rotor speed was determined by using an optical tachometer. The speed of the rotor was adjusted by a bypass-type pressure-compensated flow control valve. During normal operation the counter-knives on the RFCS were stationary. Thus, the speed of cutting was dependent on the rotational speed of the rotor, and the dimension from the axis of rotation of the rotor to the cutting surface on the tine. The average peripheral speed of the tine was determined at the midpoint between the tip and base of the tine, a radius of 0.160 m. The average peripheral speeds of the tines were 2.0, 2.4 and 3.4 m/s at a rotational speed of 120, 140 and 200 rpm, respectively. The tine tip and base peripheral speed, average speed, and radii are given in Table 5.1.

Table 5.1 Rotational and peripheral speed of the rotor and tines on the test stand used to complete the LSCP objectives and the tip and base radii of the tines.

Rotor speed (rpm)	**Tine tip speed (m/s)**	**Tine base speed (m/s)**	**Average tine speed (m/s)**	**Tine tip radius (m)**	**Tine base radius (m)**
120	2.6	1.5	2.0	0.205	0.115
140	3.0	1.7	2.4		
200	4.3	2.4	3.4		

Two levels of counter-knife sharpness were investigated with the production counter-knives, sharp and dull, which corresponded to a leading edge width of 0.13±0.05 mm and 0.63±0.07 mm, respectively. Three levels of throughput were investigated: 2.5, 3.75 and 5.0 kg/s. The levels of rotor speed investigated were 120, 140 and 200 rpm. The normal operational speed of the rotor on a production RFCS was 140 rpm.

LSCP Objective 2: The second LSCP objective was to determine the effect of counter-knife serrations, counter-knife thickness and cereal straw throughput on the

specific energy requirements of the RFCS. Four sets of counter-knives were used to determine the effect of counter-knife thickness and serrations including: 3-mm thick serrated, 3-mm thick un-serrated, 5-mm thick serrated and 5-mm thick un-serrated. Three levels of throughput were investigated: 2.5, 3.75 and 5.0 kg/s.

LSCP Objective 3: The third LSCP objective was to determine the effect of counter-knife bevel angle and cereal straw throughput on the specific energy requirements of the RFCS. The two sets of counter-knives used were the 3-mm thick un-serrated and the 3-mm thick un-beveled. Inserts were also welded onto the tines so that the gap between tines was 4 mm instead of the standard 9 mm. The only experiments that were completed with the rotor inserts, which decreased the gap between the tine pairs, were the experiments completed to satisfy the third LSCP objective. Three levels of throughput were investigated: 2.5, 3.75 and 5.0 kg/s.

LSCP Objective 4: The fourth LSCP objective was to determine the effect of counter-knife thickness and bevel, alfalfa moisture content and throughput, on the specific energy requirements of the RFCS. In addition the objective was also to determine the specific energy requirements of the RFCS, when the production counter-knives were used to process alfalfa at the same three levels of throughput and moisture content. Four sets of counter-knives were used including the: 3-mm thick un-beveled un-serrated, 3-mm thick un-serrated side-beveled, 5-mm thick un-serrated side-beveled, and 5-mm thick serrated center-beveled (the production counter-knives). The production counter-knives were excluded from the statistical analysis because the experiment did not have sufficient degrees of freedom to include counter-knife serrations as a factor. The experiments with the production counter-knives were done simply to provide a benchmark for the specific energy requirements of the current system. Three levels of throughput were investigated: 2.5, 3.75 and 5.0 kg/s. The target levels for the moisture content were 60, 40 and 20% w.b. to represent silage, haylage and hay, respectively. However, the average moisture content at the three levels was 65, 53 and 25% w.b.

5.1.2 Data processing and analysis

In order for the specific energy requirement of the RFCS to be quantified, the power demand of the rotor needed to be calculated. The power required by the RFCS was quantified by,

$$P_{LR} = \frac{P_D * Q_{LSCP}}{60\ 000}, \qquad \textbf{(5.2)}$$

where:

P_{LR} is the power required by the rotor on the LSCP RFCS (kW),

P_D is the pressure drop across the hydraulic motor driving the rotor (kPa) and

Q_{LSCP} is the flow rate of oil through the hydraulic motor driving the LSCP RFCS rotor (L/min).

A theoretical power curve, shown in Figure 5.1, was created based on a point by point multiplication of the pressure drop across the rotor motor and the flow rate of oil through the rotor motor. The energy consumed during each trial was determined by integrating the power curve using the trapezoidal method.

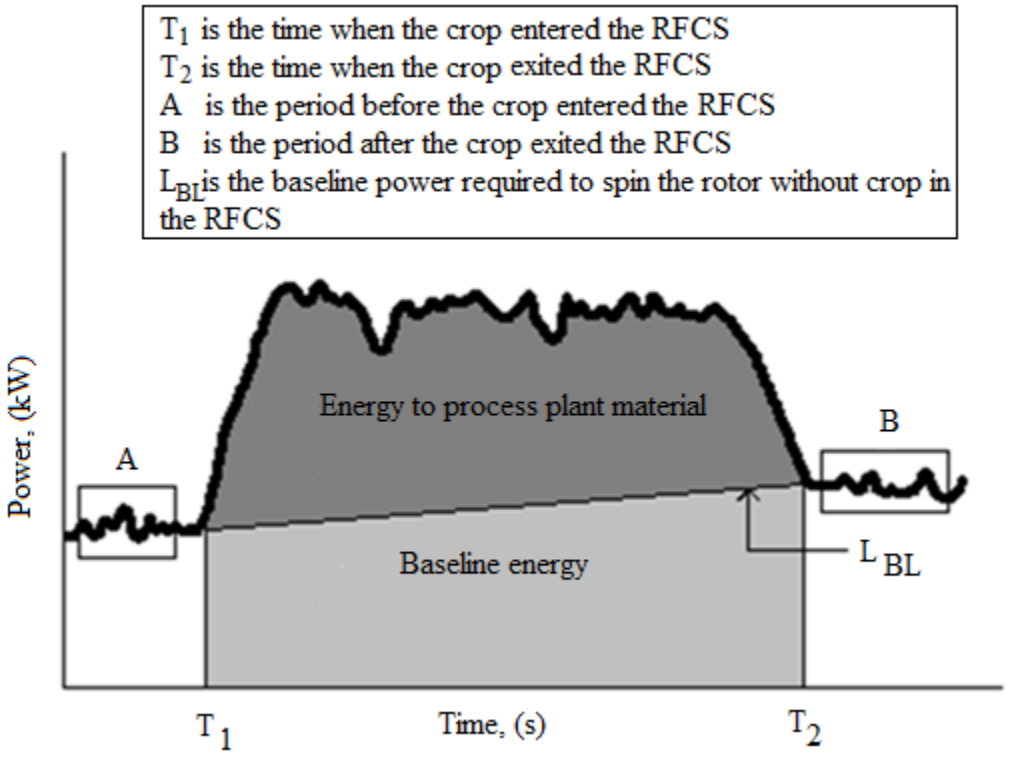

Figure 5.1 A theoretical power curve created by a point by point multiplication of the pressure drop across and the flow of oil through the hydraulic motor that was used to drive the rotor on the RFCS.

The period that was logged for each trial did not start when the crop entered the RFCS, and did not end when the crop exited the RFCS. Therefore the period of integration needed to be defined in an objective manner. The beginning of the integration period, T_1, was defined for each trial as the time when the power demand first exceeded the mean plus two standard deviations of period A. Similarly, the end of the integration period, T_2, was defined for each trial as the time when the power demand of the RFCS first dropped below the mean plus two standard deviations of period B. Period A was selected before plant material was processed by the RFCS, and period B was selected after the plant material had passed through the RFCS. The pre- and post-plant-processing periods, (periods A and B) and the beginning and end of the integration period, (T_1 and T_2) are shown in Figure 5.1.

Integration of the power curve from T_1 to T_2 quantified the total energy consumed by the RFCS. To quantify the energy consumed to process the plant material, the energy consumed to spin the rotor was subtracted from the total energy. The energy required to spin the rotor was quantified by integrating the baseline power, L_{BL}, from T_1 to T_2 using the trapezoidal method. The baseline power was approximated with the assumption that, if there was a change in the baseline power from T_1 to T_2 it was linear. To define the baseline power, L_{BL}, two points were needed. The start of the line was defined as the time T_1 and a power equal to the mean power of period A. The second point on the line was defined as the time T_2 and a power equal to the mean power of period B. The specific energy was calculated by dividing the energy required to process the material by the dry mass of material processed. Thus, the units of the specific energy were reported as kW·h/dry tonne.

Stata 9.0 (StatCorp, College Station, TX), a statistical software package, was used to complete an analysis of variance (ANOVA) to determine which factors had a statistically significant effect on the specific energy requirements of the RFCS. A custom univariate general linear model was defined in the statistical software package to account for the split-plot experiment structure. The model was defined so that the estimation of the experimental error could be partitioned between the whole-plot and sub-plot factors. The first error term was used to quantify the significance at the whole-plot level, while the second error term was used to quantify the significance of the sub-plot factors. A probability of 0.05 was used as the criterion to accept or reject the null hypothesis. The least square means were calculated with an alternate statistical software package, JMP 8.0 (SAS Institute, Cary, NC).

5.1.3 Results and discussion

LSCP Objective 1: The average specific energy required to process cereal straw with sharp and dull production counter-knives at three levels of throughput and rotor speed is given in Table 5.2. Note that the average specific energy, given in Tables 5.2 to 5.5 is an average of the three replicates, unless otherwise specified. The statistical analysis revealed that counter-knife sharpness was the only factor that was significant at a 0.05 level. The summary of the analysis of variance of the data showing the effect of counter-

knife sharpness, rotor speed and throughput on the specific energy requirement of the RFCS is presented in Table C.1 (shown in Appendix C). The average and standard deviation of the specific energy required to process cereal straw with sharp counter-knives was found to be 0.39±0.16 kW·h/dry tonne, and for dull counter-knives 0.74±0.08 kW·h/dry tonne.

Table 5.2 The average specific energy consumed by the RFCS at three levels of throughput and rotor speed while using sharp and dull counter-knives to process cereal straw.

Rotor speed (rpm)	**Throughput (kg/s)**	**Counter-knife sharpness**	**Average specific energy (kW·h/dry tonne)**
120	2.50	Sharp	0.421
		Dull	0.775
	3.75	Sharp	0.378
		Dull	0.849
	5.00	Sharp	0.387
		Dull	*
140	2.50	Sharp	0.461
		Dull	0.690
	3.75	Sharp	0.372**
		Dull	0.822
	5.00	Sharp	0.388
		Dull	*
200	2.50	Sharp	0.328
		Dull	0.707
	3.75	Sharp	0.325
		Dull	0.698
	5.00	Sharp	0.428
		Dull	0.826

** average of two replicates
* data were unavailable (only one trial was completed)

The specific energy requirements of the RFCS with dull counter-knives and rotor speeds of 120 and 140 rpm with a throughput of 5.0 kg/s are not given because the power requirements during these trials exceeded the available power of the test apparatus. The

specific energy requirements of these trials are not known, however it is reasonable to assume that the specific energy requirements of these trials exceeded all other specific energy requirements of the experiment.

The results of this experiment, specifically the effect of counter-knife sharpness, are in agreement with the conclusions drawn from previous research. Experiments completed comparing the effect of blade sharpness revealed that a blade with a 0.25-mm edge radius had double the force and energy requirements than a blade with a 0.05-mm to 0.1-mm edge radius (Reznik, 1979). Studies by Tuck (1976; 1977; 1978) on power requirements of mowers indicated that the specific cutting energy per unit field area was 1.5 kJ/m^2 for a sharp blade, and 2.1 kJ/m^2 for a worn blade. Liljedahl et al. (1961) concluded that the energy requirements for a dull blade were twice that of a sharp blade when the clearance between shearing edges was small (0.05 mm) and three times as high for a larger clearance (0.41 mm). All of these studies have revealed the same trend; a dull blade requires more energy to cut material than a sharp blade. This can be physically explained by the fact that a very sharp blade causes localized cell failure and compression in the material, in contrast to a dull blade that will cause cell failure and compression over a greater area.

According to Persson (1987) there is typically a linear relationship between the total power requirement of a rotary mower and capacity. The increase in cutting power can be explained by the fact that at a higher throughput, given the same cutting speed, the material layer thickness increases. As the thickness of material being cut increases the stress concentrations near the blade decreases resulting in increased amounts of pre-compression occurring before the material is cut. This phenomenon was observed during the completion of the LSCP objective one trials. The power required to process straw with a dull counter-knife at a high throughput (5.0 kg/s) and a lower rotational speed (120 and 140 rpm) exceeded the available power of the LSCP test apparatus.

The average cutting speed of the cutting elements at 120, 140, and 200 rpm were 2.0, 2.4 and 3.4 m/s, respectively. The effect of rotor speed, which is proportional to the cutting speed, was not a significant factor in this experiment. This conclusion has also been observed in previous research. Chancellor (1988) completed a comprehensive

review of the research that had been published on the effect of various parameters on the performance of cutting devices and concluded that in general the energy demand changed very little as a function of cutting speed over a range of quasi-static to 60 m/s for all devices. Chancellor (1957) examined the effect of cutting speed on the force and energy required to cut timothy at a moisture content of 54% wet basis. He concluded that there was very little change in cutting energy when the cutting speed was changed from 1.8 to 5.2 m/s.

Not all published research arrived at the same conclusion. According to Persson (1987) Berge (1951) concluded that a flywheel-type cutterhead required more energy to cut hay at a speed of 50 m/s as opposed to 20 m/s. However it is unclear how Persson (1987) arrived at this conclusion, based solely on the information presented by Berge (1951). The difference in the results of this study and the conclusions of Berge (1951) is likely attributed to the higher range of speed investigated by Berge (1951). According to Persson (1987), the power losses of a cutting device increase when the cutting speed increases, thus the losses become more prevalent at higher cutting speeds. The power losses to which Persson (1987) was referring included accelerating the material to exit velocity, overcoming friction between the material and the housing while still being pushed by the cutting device, sustaining air movement in the cutting device and overcoming mechanical friction in the driving mechanism.

LSCP Objective 2: The specific energy required to process cereal straw with thick and thin serrated and un-serrated counter-knives at three levels of throughput is given in Table 5.3. The statistical analysis revealed that counter-knife serrations had a significant effect at a 0.05 level, on the specific energy required to process cereal straw with the RFCS. The results of the analysis of variance for the effect of counter-knife thickness, serrations and throughput are presented in Table C.2. Throughput was on the verge of significance ($p=0.046$). The average and standard deviation of the specific energy required to process cereal straw with serrated and un-serrated counter-knives was 0.33 ± 0.08 and 0.22 ± 0.07 kW·h/dry tonne, respectively.

Table 5.3 The average specific energy consumed by the RFCS at three levels of throughput while using four different types of counter-knives to process cereal straw.

Throughput (kg/s)	Counter-knife thickness (mm)	Counter-knife edge type	Average specific energy (kW·h/tonne)
2.50	3	Serrated	0.313
	5	Serrated	0.390
	3	Un-serrated	0.174
	5	Un-serrated	0.235
3.75	3	Serrated	0.285
	5	Serrated	0.275
	3	Un-serrated	0.175
	5	Un-serrated	0.223
5.00	3	Serrated	0.355
	5	Serrated	0.369
	3	Un-serrated	0.195
	5	Un-serrated	0.313

Contrary to the previous research completed by Chancellor (1988), counter-knife thickness did not have a significant effect on the specific energy required to process cereal straw with the RFCS, nor was there a significant interaction between throughput (direct relationship with material layer thickness) and counter-knife thickness. It is possible that a 2-mm difference between the two levels of counter-knife thickness was not large enough to cause a statistically significant effect. However, it is also interesting to note that the average specific energy requirement of the thicker counter-knives was slightly higher than the thinner counter-knives. Thus the trend observed in previous research is prevalent in the data, however the effect of thickness was not large enough to be statistically significant.

The presence of serrations caused, on average, a 0.11 kW·h/dry tonne increase in the specific energy required to process cereal straw with the RFCS. The physical phenomenon that could explain the increased energy required to process cereal straw with serrated blades is the radial location, with respect to the rotating axes of the RFCS rotor, at which the material was cut. The presence of serrations increased the tangential force between the material being cut and the counter-knives. The presence of serrations likely

limited the degree to which the cereal straw slid along the leading edge of the counter-knives, causing the majority of the material to be cut at the base of the counter-knife. Alternatively, the location at which the majority of the cutting occurred was at the tip of the tines, the location farthest away from the rotating axis of the RFCS rotor. In contrast, the un-serrated counter-knives allowed material to slide farther up the counter-knife edge before being cut, causing the majority of the cutting to occur at the base of the tines, the location closest to the rotating axis of the RFCS rotor. All else being equal, cutting plant material at the tip of the tine required more energy than when it was cut at the base of the tine, due to the increased moment arm.

The least squares means (LSM) of the specific energy required by the RFCS was determined because the analysis of variance indicated that throughput was significant, however the average specific energy requirements of the RFCS at each level of throughput tested was very similar. Therefore it was difficult to identify the relationship between throughput and the average specific energy requirements of the RFCS. The LSM indicated that the specific energy required by the RFCS was at a minimum when material was processed at a throughput of 3.75 kg/s. The LSM of the specific energy required to process cereal straw at a throughput of 2.5, 3.75 and 5.0 kg/s was 0.27, 0.24 and 0.31 kW·h/dry tonne, respectively, with a standard error of 0.02 kW·h/dry tonne. Though the statistical analysis indicated that the three levels of throughput were distinct, the maximum difference between the least squares means was only 0.07 kW·h/dry tonne, which is a relatively small effect compared to the effect of counter-knife sharpness, serrations or bevel angle. Further, the other experiments completed to investigate the effect of throughput on the specific energy requirements of the RFCS indicated that throughput was not significant at a 0.05 level. Therefore, it was assumed that the specific energy requirements of the RFCS were not affected by throughput, because throughput was on the verge of significance, the magnitude of the effect of throughput was relatively small and the other experiments indicated that throughput was not a significant factor.

LSCP Objective 3: The specific energy required to process cereal straw with rotor inserts, while using 3-mm thick un-serrated and 3-mm thick un-beveled counter-knives is given in Table 5.4. A statistical analysis was not completed with this data because of the

lack of replications that were completed when the un-beveled counter-knives were used in the RFCS. The lack of replications was due to the power demand of the RFCS, when the un-beveled counter-knives were employed, exceeding the available power of the RFCS. None of the trails at a throughput of 5.0 kg/s, while using un-beveled counter-knives, could be completed without the rotor plugging, therefore no specific energy is given for the combination of the factors in Table 5.4. It is reasonable to assume that the specific energy requirement of the RFCS, when the un-beveled counter-knives were used to process cereal straw at 5.0 kg/s, was in excess of 0.760 kW·h/dry tonne. The average and standard deviation of the specific energy required to process cereal straw with 3-mm thick beveled and 3-mm thick un-beveled counter-knives was found to be 0.33±0.03 and 0.88±0.17 kW·h/dry tonne, respectively.

Table 5.4 The average specific energy consumed by the RFCS at three levels of throughput while using beveled and un-beveled counter-knives to process cereal straw.

Throughput (kg/s)	**Counter-knife sharpness**	**Counter-knife edge type**	**Average specific energy (kW·h/tonne)**
2.50	Sharp	Un-serrated	0.320
	NA	Un-beveled	*
3.75	Sharp	Un-serrated	0.311
	NA	Un-beveled	0.760**
5.00	Sharp	Un-serrated	0.367
	NA	Un-beveled	*

** average of two replicates
* data are unavailable (only one trial was completed)
not applicable (NA)

Chancellor (1988) found that an increase in bevel angle from 25 to 80° caused the energy required to cut plant material to double. The bevel angle of the beveled counter-knives and un-beveled counter-knives used in the RFCS test stand was 15 and 90°, respectively. The increase in bevel angle of 75° caused the specific energy required to process cereal straw to approximately triple. Persson (1987) and Chancellor (1957) also determined that there was an indirect relationship with the energy consumed to cut plant material and bevel angle. The reason that there is an indirect relationship between bevel

angle and cutting energy is likely very similar to the effect of knife sharpness. Like a sharp knife, a beveled knife causes localized cell failure and compression in the material, in contrast to a dull or un-beveled knife which will cause cell failure and compression over a greater area.

LSCP Objective 4: The specific energy required to process alfalfa at varying levels of moisture content, throughput and with four different counter-knives is given in Table 5.5. The statistical analysis revealed that counter-knife thickness and bevel angle as well as alfalfa moisture content were factors that had a significant effect on the specific energy requirements of the RFCS. The magnitude of the effect of bevel angle was the largest of all the factors tested. The results of the analysis of variance for the effect of counter-knife thickness, bevel angle and alfalfa moisture content and throughput are presented in Table C.3. The average and standard deviation of the specific energy required to process alfalfa with beveled and un-beveled counter-knives was 0.20±0.03 and 0.49±0.06 kW·h/dry tonne, respectively. The magnitude of the effect of counter-knife thickness was far less than that of the counter-knife bevel. The average and standard deviation of the specific energy required to process alfalfa with a 3-mm and 5-mm thick counter-knife was 0.20±0.03 and 0.24±0.03 kW·h/dry tonne, respectively. The magnitude of the effect of alfalfa moisture content was similar to that of counter-knife thickness. The specific energy requirement of the RFCS was at a maximum when alfalfa at 53% w.b. was processed and decreased at higher and lower moisture levels. The average and standard deviation of the specific energy required to process alfalfa at an average moisture content of 28, 53 and 65% w.b. was 0.30±0.16, 0.33±0.14 and 0.29±0.11 kW·h/dry tonne, respectively.

Table 5.5 The average specific energy consumed by the RFCS at three levels of throughput and moisture content while using four different types of counter-knives to process alfalfa.

Moisture content (% wet basis)	Throughput (kg/s)	Counter-knife thickness (mm)	Counter-knife edge type	Average specific energy (kW·h/tonne)
28	2.5	3	Un-serrated	0.173
		3	Un-beveled	0.492
		5	Un-serrated	0.196
		5	Production	0.300
	3.75	3	Un-serrated	0.175
		3	Un-beveled	0.538
		5	Un-serrated	0.206
		5	Production	0.290
	5	3	Un-serrated	0.215
		3	Un-beveled	0.51
		5	Un-serrated	0.212
		5	Production	0.327
53	2.5	3	Un-serrated	0.231
		3	Un-beveled	0.594
		5	Un-serrated	0.275
		5	Production	0.371
	3.75	3	Un-serrated	0.217
		3	Un-beveled	0.466
		5	Un-serrated	0.238
		5	Production	0.329
	5	3	Un-serrated	0.233
		3	Un-beveled	0.472
		5	Un-serrated	0.268
		5	Production	0.315
65	2.5	3	Un-serrated	0.177
		3	Un-beveled	0.433
		5	Un-serrated	0.260
		5	Production	0.382
	3.75	3	Un-serrated	0.175
		3	Un-beveled	0.448
		5	Un-serrated	0.242
		5	Production	0.327
	5	3	Un-serrated	0.203**
		3	Un-beveled	0.432
		5	Un-serrated	0.249
		5	Production	0.313

** average of two replicates

On average, when the production counter-knives were used to process alfalfa at three levels of moisture content and at three levels of throughput, the specific energy requirement of the RFCS was larger than when the 3-mm and 5-mm thick counter-knives were used. However, the specific energy requirement of the RFCS was the largest when the un-beveled counter knives were used. The average and standard deviation of the specific energy requirement of the 3-mm thick un-beveled, production, 5-mm thick beveled and 3-mm thick beveled counter-knives was 0.49±0.06, 0.33±0.05, 0.24±0.03 and 0.20±0.03 kW·h/dry tonne, respectively.

The bevel on the production counter-knife caused the cutting edge to be centered in relation to the width of the counter-knife, while the bevel on the 3-mm and 5-mm thick counter-knives caused the cutting edge to be offset to one side of the counter-knife (with respect to the width of the counter-knife), as shown in Figure 4.4. The difference in the bevel on the counter-knives resulted in the clearance between the shearing surfaces to be 1 mm and 4.5 mm for the production and the 3-mm and 5-mm thick counter-knives, respectively. According to Liljedahl et al. (1961) and Chancellor (1988), the energy consumed by cutting devices that use blades that have an edge width in excess of 0.06 mm will be sensitive to the clearance between the shearing surfaces. Thus, it was expected that the RFCS would be sensitive to the clearance between the shearing surfaces, (the tines and the counter-knives) because the width of the leading edge of the counter-knives (counter-knife sharpness) was in excess of 0.06 mm.

As discussed earlier in this section, serrations were found to have a significant effect on the specific energy to process cereal straw with a RFCS. Chancellor (1988) also found that the presence of serrations on a blade resulted in higher cutting energy. Thus it was expected that the presence of serrations on the production counter-knives would increase the specific energy required to process alfalfa with the RFCS. However, due to the structure of the experiment, the effect of serrations and clearance between shearing surfaces could not be isolated. Previous research by Liljedahl et al. (1961) and Chancellor (1988) indicated that the presence of serrations and increased clearance between shearing surfaces result in increased energy required to cut plant material. Therefore, it was expected that the specific energy requirements of the RFCS would be

higher when the production counter-knives were used as opposed to the 3-mm and 5-mm thick counter-knives. The 3-mm and 5-mm thick counter-knives were un-serrated and had a side bevel which resulted in a smaller clearance between shearing surfaces.

The specific energy consumed to process alfalfa with the production counter-knives was higher than when the 3-mm and 5-mm thick un-serrated counter-knives were used. The larger energy requirements of the RFCS, when the production counter-knives were used, can be attributed to the presence of serrations and the larger clearance between the shearing surfaces. However, when the un-beveled counter-knives were used, the specific energy requirements of the RFCS were larger than when the production counter-knives were used. Thus the coupled effect of an increased clearance between shearing surfaces and serrations (when the production counter-knives were used in the RFCS) was not as large as the effect of counter-knife bevel angle.

Chancellor (1988) found that an increase in blade thickness caused an increase in the energy consumed to cut a thick mat of plant material. The amount of material that is displaced with a thick blade is greater than a thin blade thus, the thicker blade will compress a greater amount of plant material before it is cut. This results in an increased amount of energy being consumed per cut. Counter-knife thickness was found to have a significant effect ($p=0.013$) on the specific energy requirements of the RFCS, and the trend identified by Chancellor (1988) was also observed. When the 5-mm thick counter-knives were used, the specific energy required to process alfalfa was greater than when the 3-mm thick counter-knives were used. The same levels of counter-knife thickness were examined for both alfalfa and cereal straw. However, counter-knife thickness did not have a significant effect ($p= 0.072$) on the specific energy required to process cereal straw with the RFCS.

A build up of a sticky substance (caused by plant material excretions) on the sides of the counter-knives, when alfalfa was processed, was likely the reason that counter-knife thickness was found to be significant when alfalfa was processed, and not when cereal straw was processed. There was no visible build-up of a sticky substance on the counter-knives when the cereal straw was processed. The sticky substance on the sides of the counter-knife would have likely increased the coefficient of friction between the plant

material and the counter-knife. The thicker counter-knife also resulted in less clearance between the tines and counter-knife. The decreased clearance forced the plant material between the tines and counter-knife into a smaller void, which would increase the normal force between the tines and the counter-knife. Therefore, the larger specific energy required to process alfalfa with thick counter-knives was likely due to the combination of the increased friction coefficient between the counter-knives and plant material, and the increased force of plant material between the thicker counter-knives and tines. This also suggests that the increase in specific energy requirement of the thicker counter-knife is not only due to an increased amount of energy to compress the material but also to transport the material.

The same trend was observed in the alfalfa data as was observed with straw data, in that the specific energy requirement of the RFCS was greater when un-beveled counter-knives was used as opposed to beveled counter-knives. Chancellor (1988), Persson (1987) and Chancellor (1957) all found that decreasing the bevel angle of the blade resulted in a decreased energy consumption to cut plant material. As previously discussed in this section, the reason that there is an indirect relationship between bevel angle and cutting energy is likely very similar to the effect of knife sharpness. Like a sharp knife, a beveled knife causes localized cell failure and compression in the material, in contrast to a dull or un-beveled knife that will cause cell failure and compression over a greater area.

Even by reporting the specific energy requirement of the RFCS on a dry matter basis, it was found to be significantly affected by alfalfa moisture content. The specific energy requirement was at a maximum when material at an average moisture content of 53% w.b. was processed, and decreased when higher and lower moisture content alfalfa was processed. Liljedahl et al. (1961), Moustafa et al. (1978) and Chancellor (1957) all observed a similar phenomenon, in that the energy and force required to shear plant material was at a maximum when 30 to 40% w.b. plant-material was processed and decreased at higher and lower moisture levels. The testing completed with the RFCS indicated that the maximum specific energy requirement occurred when the plant material moisture content was at 53% w.b. Further tests with the RFCS are needed to

determine if the maximum specific energy requirements of the RFCS would occur when processing plant material in the range of 30 to 40% w.b. Regardless, the effect of moisture content on the specific energy requirement of the RFCS does follow the trend previously identified by Liljedahl et al. (1961), Moustafa et al. (1978) and Chancellor (1957). Persson (1987) suggested that the reason some plant material exhibits a maximum cutting force at a moisture content in the range of 35 to 40% on a w.b. was that the plant material excreted a sticky substance which builds up on the cutting surfaces. A build up of a sticky substance (caused by plant material excretions) on the counter-knives was observed when alfalfa was processed with the RFCS. However, the buildup of the sticky substance was not only observed when alfalfa at 53% on a w.b. was processed, but at all levels of moisture content investigated. Even though the sticky substance was observed at all levels of moisture content, the friction coefficient between the plant material and the counter-knives could have been a maximum when alfalfa at a moisture content of 53% w.b. was processed. Unfortunately, at the time of processing the friction coefficient between the alfalfa and the counter-knives was not quantified, a task that would need to be completed to validate the previous hypothesis.

5.1.4 Summary

The following is a summary of the results obtained from the LSCP RFCS laboratory trials:

1. Counter-knife sharpness had a significant effect on the specific energy required to process cereal straw with the RFCS. The average and standard deviation of the specific energy required to process cereal straw with sharp and dull counter-knives (leading edge width of 0.13±0.05 and 0.63±0.07 mm, respectively) was 0.39±0.16 and 0.74±0.08 kW·h/dry tonne, respectively.

2. The effect of rotor speed over a range of 120 to 200 rpm, which corresponded to an average cutting speed of 2.0 to 3.4 m/s, did not have a significant effect on the specific energy required by the RFCS to process cereal straw.

3. Throughput did not have a significant effect on the specific energy required to process cereal straw or alfalfa with the RFCS for throughputs ranging from 2.5 to 5.0 kg/s.

4. Counter-knife serrations had a significant effect on the specific energy required to process cereal straw with the RFCS. The average and standard deviation of the specific energy required to process cereal straw with sharp serrated and sharp un-serrated counter-knives was 0.33±0.08 and 0.22±0.07 kW·h/dry tonne, respectively.

5. Counter-knife thickness did not have a statistically significant effect on the specific energy required to process cereal straw, however it did have a statistically significant effect on the specific energy required to process alfalfa with the RFCS.

6. The magnitude of the effect of bevel angle was relatively large compared to the other factors investigated. The specific energy required to process alfalfa and cereal straw with the RFCS was much higher when un-beveled counter-knives were used as opposed to beveled counter-knives. A statistical analysis could not be completed on the cereal straw data because the power required to process cereal straw with un-beveled counter-knives exceeded the available power of the RFCS which caused the rotor to plug, and limited the number of repeated trials. The same issue was not encountered with the alfalfa trials. There were sufficient replicates to complete a statistical analysis and bevel angel did have a statistically significant effect ($p < 0.05$). The average and standard deviation of the specific energy required to process cereal straw with beveled and un-beveled counter-knives was 0.33±0.03 and 0.88±0.17 kW·h/dry tonne, respectively. The average and standard deviation of the specific energy required to process alfalfa with beveled and un-beveled was 0.20±0.03 and 0.49±0.06 kW·h/dry tonne, respectively.

7. Alfalfa moisture content was found to have a statistically significant effect ($p < 0.05$) on the specific energy required to process alfalfa with the RFCS. The specific energy requirement of the RFCS was a maximum when alfalfa at a

moisture content of 53% w.b. was processed, and decreased when higher and lower moisture content alfalfa was processed. However, the magnitude of the effect of alfalfa moisture content on the specific energy requirement of the RFCS was relatively small. The maximum difference in the average specific energy requirement of the RFCS was on the order of 0.04 kW·h/dry tonne.

5.1.5 Conclusions

The objective (first, second, third and fourth LSCP objectives) of the laboratory experiments was to determine if counter-knife thickness, serrations, sharpness, bevel angle and material throughput, moisture content and rotor speed had a significant effect on the specific energy requirements of the RFCS. The reason that these tests were completed was to identify the factors that ought to be included in an analytical model.

For all of the tests completed with the LSCP RFCS the effect of counter-knife sharpness, serrations and bevel angle were found to be significant and, the magnitude of their effect was relatively large. Even when the typical materials that are used to make the counter-knives are hardened, during the operation of the RFCS the counter-knives will experience wear on the leading edge and become dull. Therefore, counter-knife sharpness should be included as a parameter in the analytical model if the intent of the model is to predict the power demand of the RFCS over the life span of the counter-knives.

The bevel angle and serrations on the counter-knives will also be affected by the wear that the counter-knives experience over their life span, however these factors are not as sensitive to wear as counter-knife sharpness. Previous research completed by Chancellor (1988) has indicated that an optimum bevel angle is in the range of 20 to 30°. Further, the tests completed with the LSCP RFCS indicated that the effect of bevel angle on the energy required to cut plant material followed the same relationship that Chancellor (1988) observed with other cutting devices. Bevel angle does not need to be included in the analytical model because the bevel angle of the counter-knives are currently in the optimum range of 20 to 30° and, the bevel angle on the counter-knives will change very little over the life span of the counter-knives.

In order to minimize the long-term energy requirements of the RFCS serrated counter-knives should be used, as the serrated counter-knives will stay sharper for a longer period, and consume less energy to process plant material (in the long term). The wear rate of the leading edge of the counter-knives was not quantified during these experiments and therefore the period of use in which the counter-knives become dull cannot be reported. When cereal straw was processed, the presence of counter-knife serrations did cause the specific energy requirements of the RFCS to increase on average approximately 0.11 kW·h/dry tonne. However, the use of dull counter-knives instead of sharp counter-knives caused the specific energy requirements of the RFCS to increase by 0.35 kW·h/dry tonne. In the short-term, the use of serrated counter-knives does increase the specific energy requirements of the RFCS, however the serrated counter-knives stay sharper for a longer period of use. Therefore the use of serrated counter-knives will result in the RFCS specific energy requirements to be lower in the long-term. Counter-knife serration does not need to be included as a parameter in the analytical model if this long-term energy saving strategy is adopted by the future designers of the RFCS.

Counter-knife thickness was only found to have a significant effect on the specific energy requirement of the LSCP RFCS when alfalfa was processed but not when cereal straw was processed. The magnitude of the effect of counter-knife thickness was also relatively small when alfalfa was processed with the RFCS. An increase in counter-knife thickness of 2 mm caused the specific energy required by the RFCS to increase by approximately 0.04 kW·h/dry tonne. Counter-knife thickness does not need to be included as a parameter in the analytical model because the effect of the parameter is relatively small and only significant when alfalfa was processed.

Throughput was not found to have a significant effect on the specific energy requirement of the LSCP RFCS. This indicates that the specific energy required to compress, cut and transport the plant material was not affected by the throughput of plant material. However, the power required by the RFCS is directly related to throughput because at higher throughputs a grater mass of plant material is transported in a given period of time. This conclusion is not based on data presented in this section but on rudimentary laws of physics.

Rotor speed did not have a significant effect on the specific energy requirement of the LSCP RFCS. Therefore, based on the laboratory trials there is no need to include rotor speed as a parameter in the analytical model.

Alfalfa moisture content did have a significant effect on the specific energy requirement of the LSCP RFCS. However the magnitude of the effect of alfalfa moisture content was relatively small. The maximum difference between the specific energy required by the RFCS to process alfalfa with a moisture content of 28 to 65% w.b. was only 0.04 kW·h/dry tonne. Therefore alfalfa moisture content does not need to be included as a parameter in the analytical model.

5.2 Laboratory experiments - model validation

In order to satisfy the 5th LSCP objective, an analytical model was developed to predict the power requirements of the RFCS. After the development of the analytical model, it became apparent that three material properties needed to be quantified in order to validate the model. These three material properties were Young's modulus, maximum shear strength, and the dynamic coefficient of friction (friction coefficient between the plant material and steel). It was believed that the material properties of the alfalfa change with time, because the alfalfa was actively growing when it was cut in the field. The same variety of cereal straw processed with the RFCS could be obtained and because the cereal straw had senesced and had dried prior to processing, it was assumed that the material properties of the cereal straw would not change with time. Therefore additional trials with cereal straw were not needed because the mechanical properties of the cereal straw that was processed by the RFCS could be quantified. The results of the tests completed with the material properties test stand are presented in section 7.2.1.

To allow for model validation with both cereal straw and alfalfa an additional set of laboratory experiments was completed with the LSCP RFCS. Alfalfa at one level of moisture content was processed with the LSCP RFCS. Counter-knife serrations and sharpness were included in the abbreviated test because both parameters were found to have a significant effect on the specific energy requirements of the RFCS. Although throughput did not have a significant effect on the specific energy requirements of the

RFCS it was expected that the power consumption of the RFCS would be influenced by throughput.

5.2.1 Methodology

The LSCP testing apparatus described in section 4.1 was used to determine the effect of counter-knife sharpness, serrations, and throughput on the average power required to process alfalfa at an average moisture content of 54.0% (w.b.) with the RFCS. The methods used to achieve varying levels of throughput, quantify the alfalfa moisture content and to quantify the required number of replicates were the same as was done for the previous laboratory experiments. The detailed description of how varying levels of throughput were achieved, material moisture content was quantified, and how the required number of replicates was quantified were discussed in section 5.1.1. The same type of experiment design, a split-plot, was also used during the second set of laboratory experiments to minimize the number of times the counter-knives were changed in the test stand.

The objective was to determine the effect of counter-knife sharpness, serrations and throughput on the average power required to process alfalfa with a RFCS. Two levels of counter-knife sharpness were investigated. A sharp counter-knife had a leading edge width of 0.13±0.05 mm and a dull counter-knife had a leading edge width of 0.63±0.07 mm. Two levels of serrations were investigated, serrated and un-serrated. The type of serration used is shown in Figure 4.3B. Three levels of throughput were investigated: 2.5, 3.75 and 5.0 kg/s.

Immediately after the trials were completed with the LSCP test apparatus, the mechanical properties of the unprocessed alfalfa were quantified with the material properties test stand. The mechanical properties of the alfalfa were determined using the material properties test stand described in section 4.3. The material properties that were determined included Young's modulus, maximum shear strength, and the dynamic coefficient of friction between alfalfa and steel. The procedure used to quantify these material properties is described in detail in Appendix B.

5.2.2 Data processing and analysis

The power consumption of the RFCS was determined by a point by point multiplication of the pressure drop across the rotor motor and the oil flow through the motor, using equation (5.2). The same method identified in section 5.1.2 was used to define the period over which the RFCS was processing plant material.

Stata 9.0 (StatCorp, College Station, TX), a statistical software package, was used to complete an ANOVA to determine which factors had a significant effect on the average power requirements of the RFCS. A custom univariate general linear model was defined in the statistical software package to account for the split-plot experiment structure. The model was defined so that the estimation of the experimental error could be partitioned between the whole-plot and sub-plot factors. The first error term was used to quantify the significance at the whole-plot level, while the second error term was used to quantify the significance of the sub-plot factors. A probability of 0.05 was used as the criterion to accept or reject the null hypothesis. The least square means (LSM) was calculated with an alternate statistical software package, JMP 8.0(SAS Institute, Cary, NC).

5.2.3 Results and discussion

The average power (including the no-load power, or the power required to spin the rotor without crop flow) required to process alfalfa with sharp and dull counter-knives, serrated and un-serrated counter-knives and at three levels of throughput is given in Table 5.6. The statistical analysis revealed that the counter-knife sharpness, serrations and throughput were statistically significant at a 0.05 level. The summary of the analysis of variance of the effect of counter-knife sharpness, serrations and throughput is shown in Table C.4. The average power required to process alfalfa with dull counter-knives was higher than when sharp counter-knives were used. The average and standard deviation of the power required to process alfalfa with sharp and dull counter-knives in the RFCS was 1.96±0.19 and 2.62±0.30 kW, respectively. The average power also increased as the throughput of alfalfa through the RFCS increased. The average and standard deviation of the power required to process alfalfa at a throughput of 2.5, 3.75 and 5.0 kg/s was 2.10±0.40, 2.27±0.39 and 2.51±0.37 kW, respectively. The interaction of counter-knife

serrations and sharpness was also found to be significant. When sharp counter-knives were used the presence of serrations had little effect on the average power demand of the RFCS. However the average power demand of the RFCS was higher when dull un-serrated counter-knives were used as opposed to dull serrated counter-knives. The LSM of the average power demand of the RFCS was determined because the average power demand of the RFCS when sharp and dull, serrated and un-serrated counter-knives were used was very similar. The LSM of the average power demand of the RFCS while using sharp serrated and un-serrated counter-knives was 1.99 and 1.98 kW, respectively with a standard error of 0.04 kW. Conversely, the LSM of the average power demand of the RFCS while using dull serrated and un-serrated counter-knives was 2.42 and 2.74 kW, respectively with a standard error of 0.04 kW.

Table 5.6 The average power demand of the RFCS at three levels of throughput while using dull and sharp, and serrated and un-serrated counter-knives to process alfalfa.

Throughput (kg/s)	**Counter-knife edge type**	**Counter-knife sharpness**	**Average power (kW)**
2.50	Serrated	Sharp	1.89
	Serrated	Dull	2.12
	Un-serrated	Sharp	1.80
	Un-serrated	Dull	2.66
3.75	Serrated	Sharp	1.89
	Serrated	Dull	2.53
	Un-serrated	Sharp	1.93
	Un-serrated	Dull	2.58
5.00	Serrated	Sharp	2.19
	Serrated	Dull	2.61
	Un-serrated	Sharp	2.22
	Un-serrated	Dull	3.00

Past research has shown that the power required to process plant material with rotary cutting devices is affected by the throughput of plant material through the device. Persson (1987), Klinner et al. (1971) and Tuck (1976; 1977; 1978) all found that there

was an increase in the total power of a rotary mower with an increase in the throughput. Georing et al. (1993) developed a model to predict the power requirements of a forage harvester header which was proportional to throughput. The results from this study indicated that the average power required by the RFCS to process alfalfa also increased with an increase in throughput. The increase in power with an increase in throughput is believed to be attributed to two phenomena. First, an increase in throughput all else being equal, caused an increase in the depth of material being cut, which increased the dry-mass density of the material being cut. The increase in dry-mass density has been found to increase the maximum shear strength of plant material (Bright et al., (1964); Halyk and Hurlbut, (1968)). The increase in maximum shear strength result in an increase in cutting forces and ultimately an increase in the power consumption of the cutting device, with a constant cutting speed. Second, the parasitic power losses associated with rotary cutting devices have been found to be proportional to the total mass of material transported by the device (Blevins and Hansen, 1956; Persson, 1987).

The average power requirements of the RFCS were higher when dull counter-knives were employed relative to when sharp counter-knives were used. Tuck (1976; 1977; 1978) also found that the power requirements of a mower were higher when dull blades were used as opposed to sharp blades. The increased power demand with a dull cutting element is believed to be attributed to an increase in the amount of material being compressed, because a dull cutting element causes cell failure and compression over a greater area.

Serrations did not have a significant effect on the average power consumption of the RFCS when the counter-knives were sharp. However, when dull counter-knives were used in the RFCS the average power demand of the RFCS was affected by serrations. The average power consumption of the RFCS was higher when dull un-serrated counter-knives were used, as opposed to dull serrated counter-knives. The reason that the average power of the RFCS when dull-serrated counter-knives were used was less than when the dull-un-serrated counter-knives were used could be explained by one of two phenomena. First, the trials completed with serrated blades were on average 12% longer than the trials completed with un-serrated blades. The increased trial time resulted in a slight decrease

in the average throughput. As previously observed, throughput had a significant effect on the average power demand of the RFCS, with higher throughputs resulting in higher power demand. Thus, the increased trial time of the serrated counter-knives resulted in a slight decrease in the average throughput, which ultimately decreased the average power demand of the RFCS. The increased trial time associated with the serrated counter-knives could be attributed to higher tangential forces between the plant material and the counter-knives, which impeded the flow of plant material through the RFCS. Second, the presence of serrations on the leading edge of the counter-knife caused localized sharp zones (where the blade was thin due to the serrations), which resulted in the serrated counter-knives being slightly sharper than the un-serrated counter-knives. As previously observed, counter-knife sharpness had a significant effect on the average power demand of the RFCS. The relationship between counter-knife sharpness and the average power demand of the RFCS was inverse.

5.2.4 Summary

The following is a summary of the results obtained from the LSCP RFCS laboratory trials:

1. Counter-knife sharpness had a significant effect on the average power demand of the RFCS to process alfalfa at an average moisture content of 54.0% w.b. The average and standard deviation of the average power demand of the RFCS to process the alfalfa with sharp and dull counter-knives (leading edge width of 0.13±0.05 and 0.63±0.07 mm, respectively) was 1.96±0.19 and 2.62±0.30 kW, respectively.

2. Throughput had a significant effect on the average power demand of the RFCS to process alfalfa at an average moisture content of 54.0% w.b. The average and standard deviation of the average power demand of the RFCS to process the alfalfa at a throughput of 2.5, 3.75 and 5.0 kg/s was 2.10±0.40, 2.27±0.39 and 2.51±0.37 kW, respectively.

3. The interaction between counter-knife serrations and sharpness was found to be significant. When sharp counter-knives were used in the RFCS the power

demand to process alfalfa at an average moisture content of 54.0% w.b. was not affected by counter-knife serrations. However, when dull counter-knives were used in the RFCS the counter-knife serrations affected the average power demand of the RFCS. When dull serrated and un-serrated counter-knives were used the LSM power demand of the RFCS was 2.42 and 2.74 kW, respectively with a standard error of 0.04 kW.

5.2.5 Conclusions

The purpose of completing the laboratory trials discussed in section 5.2 was so that the analytical model could be validated when processing both cereal straw and alfalfa. The mechanical properties of the cereal straw processed during the trials discussed in section 5.1 could be quantified, and therefore no additional trials were completed during which cereal straw was processed. However, the mechanical properties of the alfalfa processed during the trials discussed in section 5.1 could not be quantified, and therefore additional trials were completed during which alfalfa was processed with both the LSCP RFCS and the material properties test stand.

It was concluded in section 5.1 that throughput would affected the power demand of the RFCS. The results of the information presented in section 5.2 supports this conclusion and therefore throughput should be included as a parameter in the analytical model.

The sharpness of counter-knives had a significant effect on the power demand of the RFCS while processing alfalfa and the magnitude of the effect was relatively large. Thus, as concluded in section 5.1 counter-knife sharpness should be included as a parameter in the analytical model.

The effect of counter-knife serrations did not have a significant effect on the average power demand of the RFCS when alfalfa was processed with sharp counter-knives. However, the average power demand of the RFCS was affected by the presence of serrations when dull counter-knives were used to process alfalfa. When alfalfa was processed the presence of serrations caused the average power demand of the RFCS to be

less than when un-serrated counter-knives were used. In order to minimize the energy requirements of the RFCS serrated counter-knives should be used to process alfalfa, as the serrated counter-knives will stay sharper for a longer period, and consume less energy to process plant material than dull un-serrated counter-knives. Therefore counter-knife serration does not need to be included as a parameter in the analytical model.

6 HIGH SPEED CUTTING PROCESS (HSCP)

To complete the first HSCP objective, field trials were completed. The trials were completed to determine the effect of plant moisture-content, throughput, and counter-knife engagement on the corresponding GML of MOG and the specific energy required to process cereal straw with various choppers. The field data was also used to validate the analytical model developed to predict the power required by the chopper. The methodology used to complete the experiments, as well as the results and conclusions drawn from the experiments are discussed in this chapter.

6.1 Field experiments

6.1.1 Methodology

The HSCP testing apparatus described in section 4.2, was used to determine the effect of counter-knife engagement, straw moisture-content and throughput on the specific energy requirements of four different choppers. The objective also included the investigation of the effect of counter-knife engagement, straw moisture content and throughput on the GML of the MOG. The material that was processed with the combine harvester was cereal straw.

For all trials completed with the HSCP testing apparatus, the same method was used to achieve varying levels of throughput. Preliminary field trials were completed to determine the maximum sustainable throughput with the combine harvester. The maximum sustainable throughput occurred when the combine harvester was traveling at a forward velocity of 7.0 km/h. All high-level throughput trials were completed at 7.0 km/h, while all low-level throughputs were completed at 4.5 km/h. The implicit assumption that forward velocity was directly related to throughput was that the crop yield was uniform and constant throughout the field, and the header cut width and height was constant. As discussed in section 4.2, the throughput was quantified by collecting the windrow of MOG that exited the rear of the combine.

Field trials with varying levels of plant moisture were accomplished by performing field trials at different times throughout the day. Trials conducted with material at a high moisture content were completed in the early morning or late evening, while trials

conducted with dry material were completed in the early or late afternoon. An effort was made to avoid performing trials during mid-afternoon, because that is when the moisture content of the test material was lowest. It was also suspected that extremely dry plant material would undergo extensive particle length reduction in other areas of the combine harvester, and the effect of the straw chopper on the GML of MOG may have been minimal when extremely dry plant material was processed. The method used to quantify the moisture content of the material processed by the HSCP testing apparatus was the same for all trials. The moisture content was determined according to ASAE Standard S358.2 (ASABE, 2008) where 50-g samples were dried in a convection oven at 103ºC for 24 h. Moisture was expressed in percent wet basis (% w.b.).

Three levels of counter-knife engagement were investigated for each of the four choppers tested. The method of achieving varying levels of counter-knife engagement; and the levels of counter-knife engagement used for each of the four choppers tested is discussed in detail in section 4.2. The rotational speed, counter-knife type and spacing for each of the choppers tested is also identified in section 4.2.

The GML of MOG was determined by sieving samples that were collected from the windrow during the trials. The procedure used to quantify the GML was similar to the ASAE S424.1 Standard (ASABE, 2007). However, the actual procedure used was the CNH standard titled "Quality of Chopped Straw using a Windrow Collection Procedure". The only difference between the two methods is the average particle length associated with the sieve openings. Because samples were only collected at the exit of the combine, the particle length reduction due to the chopper could not be quantified, as other components in the combine harvester may have reduced the particle length of straw.

The experiments completed with each chopper followed a full factorial, completely randomized design. A total of 36 trials were completed with each chopper (2X0.5, 2X3, 3X3 and WR); a result of two levels of throughput and moisture content, three levels of counter-knife engagement and three replicates. The required number of replicates was determined using equation (5.1), with a 15 % allowable variation and the approximate coefficient of variation of the specific energy requirements of the 2X0.5 chopper determined during preliminary field trials. The chopper speed and torque were measured

and recorded during each trial. A throughput in excess of 11 dry tonne/h was the target for a high-level throughput trial, and a throughput less than 11 dry tonne/h was the target for the low-level throughput trials. The high-level straw moisture content trials had a target moisture content in excess of 13% w.b., while the low-level straw moisture content trials had a target moisture content below 13% w.b. For all choppers except the WR, the level of counter-knife engagement investigated was 0, 50 and 100%. The counter-knife engagement investigated with the WR chopper was 100, 89 and 78%. The reason that the counter-knife engagement investigated with the WR was different than the other choppers and, the distance the counter-knives were inserted into the choppers was discussed in section 4.2.

In order for the trials to be completed at two distinct levels of moisture content, the average trial time needed to be less than 5 minutes. In an ideal situation, samples would have been taken during each of the 36 trials, for each chopper tested, to determine throughput, moisture content and GML however, the time required to sample during each trial would have caused the average trial time to exceed 5 minutes. If the trial time exceeded 5 minutes it would not have been reasonable to assume that each of the choppers were subject to the same crop material, because the maturity of the crop changed with time. Thus, to achieve the targeted average trial time, the sampling frequency was decreased so that 12 out of 36 trials for each chopper tested were sampled. The trials that were sampled were strategically chosen so that measurements of throughput, moisture content and GML were completed for each combination of the factors under study.

There were 24 trials completed with each chopper during which the throughput, moisture content and GML of MOG were not sampled and subsequently quantified, these trials were referred to as the non-measured trials. For these trials, the throughput, moisture content and GML of MOG was approximated from the 12 measured trials. The moisture content of the straw processed during the non-measured trials was approximated by taking the average of the straw moisture content of the measured trials that were completed immediately preceding and following the non-measured trial. The delay between the occurrence of the measured and non-measured trials was at most 10 minutes.

The moisture content of the non-measured trials was quantified based on the assumption that the moisture content of the straw in the field was homogeneous and that it changed only as a function of time (during the morning and afternoon the straw moisture content would decrease and during the evening and night the straw moisture content would increase). The high-level throughput and low-level throughput of the non-measured trials were assumed to be equal to the average of the measured high-level and low-level throughputs, respectively. This assumption was made based on the assumption that the cut width and height of the header on the combine was constant and the straw yield in the field was homogeneous. Ultimately, it was assumed that the forward velocity of the combine harvester was directly related to the throughput of MOG. Because the high-level throughput trials were all completed at the same forward velocity it was assumed that they all had the same throughput of MOG. Similarly, the low-level throughput trials were all completed at the same forward velocity and it was assumed that they all had the same throughput. The GML of MOG was assumed to be the same for each replicate at a given throughput, moisture content and counter-knife engagement. The implicit assumption with this approach of quantifying the GML of MOG is that the GML of MOG is only affected by the throughput of MOG, the MOG moisture content and the level of counter-knife engagement.

Immediately after the trials were completed with the combine harvester the mechanical properties of the unprocessed cereal straw were quantified with the material properties test stand. The mechanical properties of the cereal straw were determined using the material properties test stand described in section 4.3. The material properties that were determined included Young's modulus, maximum shear strength, and the dynamic coefficient of friction between cereal straw and steel. The procedure used to quantify these material properties is described in detail in Appendix B.

6.1.2 Data processing and analysis

In order for the specific energy requirement of the straw chopper to be quantified, the power demand of the chopper needed to be calculated. The power required by the straw chopper on the combine harvester was quantified by,

$$P_{chopper} = T_{chopper} \times N \quad \textbf{(6.1)}$$

where:

$P_{chopper}$ is the power required by the straw chopper on the combine harvester (W),

$T_{chopper}$ is the torque applied to the chopper shaft (N·m) and

N is the rotational speed of the chopper (rad/s).

The power required by the chopper was determined for each trial by a point-by-point multiplication of the torque experienced by the chopper shaft and the rotational speed of the chopper. For each trial, the total energy consumed by the straw chopper was determined by integrating the power required by each chopper using the trapezoidal method.

The signal from the Wheatstone bridge on the chopper was zeroed (when the chopper was stationary) before the completion of each trial to mitigate any drift in the signal. During the LSCP trials, the data-logging event started before crop was flowing through the RFCS, and continued until after crop had been processed by the RFCS. Unlike the LSCP trials, the data-logging event during the HSCP trials was taken during the targeted steady-state throughput. The almost constant throughput during the HSCP trials eliminated the need for quantifying the period of integration on a per trial basis, as was done with the LSCP RFCS trials. The period of integration used to determine the energy consumption of the HSCP RFCS was the total length of the trial, which was five seconds.

The energy consumed to process the plant material with the straw choppers was determined by subtracting the energy required to spin the chopper without crop flowing through the chopper from the total energy consumption of the chopper. The total power required by the chopper was quantified by a point-by-point multiplication of the torque the chopper experienced by the operational speed of the chopper during a five second interval. The total energy required by the chopper was quantified by integrating the total energy over a five-second interval, using the trapezoid method. The energy required to spin the choppers without crop flow was determined before and after the completion of all the trials with a given chopper. The energy required to spin the choppers without crop flow did not change from before to after the completion of the trials for any of the choppers tested. The power required to spin the rotor without crop flow through the

RFCS, P_{base}, was determined by a point-by-point multiplication of the torque the chopper experienced by the operational speed of the chopper during a five second interval without crop flow. The energy required to spin the chopper without crop flow was quantified by integrating P_{base} over a five-second interval, using the trapezoid method.

The specific energy was determined by dividing the energy consumed to process plant material by the mass of material processed by the chopper. The mass of material processed by the chopper was determined by multiplying the trial throughput by the trial period, which was five seconds.

A statistical software package (SPSS Statistics 17.0, IBM Corporation, Somers, NY) was used to complete an analysis of variance to determine which factor or factors had a significant effect on the specific energy required to process cereal straw. A univariate general linear model was defined in the statistical software package to account for the fully factorial, completely random experiment design structure. Thus only a single experimental error term was quantified and used to determine the significance of the independent factors. A probability of 0.05 was used as the criterion to accept or reject the null hypothesis. A statistical analysis was not completed to determine which factors had a significant effect on the GML of material exiting the combine harvester because no repeated GML measurements were made.

6.1.3 Results and discussion

The specific energy requirements of the 2X0.5 chopper could not be calculated, because the optical encoder used to determine the speed of the chopper malfunctioned. Therefore, the effect of counter-knife engagement, cereal straw throughput and moisture content on the specific energy requirements of the 2X0.5 chopper could not be quantified. It was impossible to complete tests with the 2X0.5 chopper again, because the maturity of the crop changed with time and in order to compare the performance of all choppers the field trials needed to be completed in the least amount of time. However, the effects of the aforementioned factors on the GML of MOG when the 2X0.5 chopper was used will be discussed.

The results of the field trials will be discussed on an individual chopper basis, and the general trend of the effect of counter-knife engagement, cereal straw throughput and moisture content on all choppers are stated. However, the performance of the choppers will not be compared, because each chopper was not subject to the same operating conditions, in terms of the cereal straw throughput and moisture content; and the specific energy requirement of all of the choppers tested was affected by both cereal straw throughput and moisture content.

The average high and low throughput in units of dry tonnes per hour, to which each chopper was subjected was not the same. Because the choppers were not subject to the same throughput and because their performance was typically found to be affected by throughput, the performance of the choppers is not compared. Recall that the varying levels of throughput were achieved by varying the forward velocity of the combine harvester. The average high and low-level throughputs that the 2X0.5, 3X3, 2X3, and WR choppers were subject to were 14.0 & 7.0, 12.5 & 9.0, 13.5 & 10.5 and 13.0 & 12.0, respectively. These throughputs were not the same because of the variation in crop yield. Further, the variation of the high and low-level throughputs was also due to the variation in crop yield. A box-and-whisker plot of the throughputs is shown in Figure 6.1. The whiskers identify the upper and lower quartiles of throughput, the box indicated the middle quartiles, and the thick horizontal line (labeled with a number) indicates the median. The circles shown on the 2X0.5 and 2X3 choppers are trials that were considered outliers.

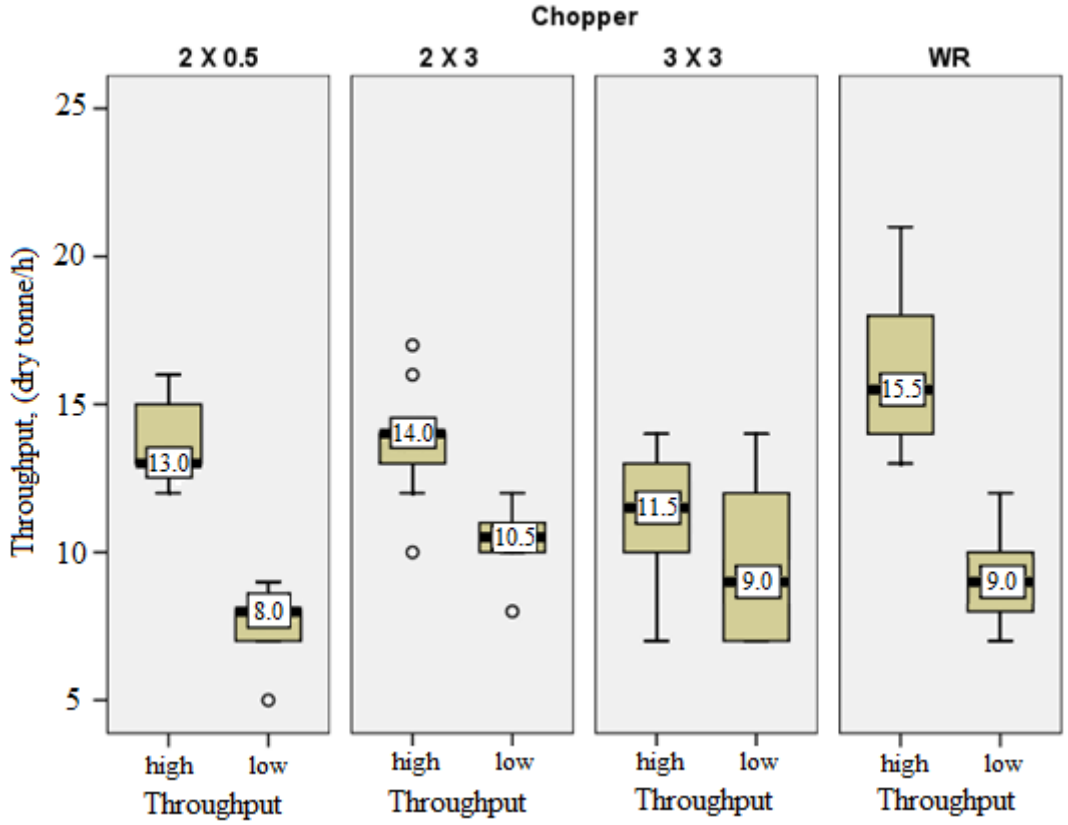

Figure 6.1 Box-and-whisker plot showing the range of the high-level and low-level throughput that each chopper was subject to during the field trials.

The moisture content of the straw processed with the 3X3 choppers during the high-level moisture content trials was higher than the high-level straw moisture content trials completed with all other choppers, as shown in Figure 6.2. The relatively high level of the straw moisture content caused the threshing rotor to plug when subject to the targeted high-level throughput. Therefore to complete the 3X3 trials, the target high-level throughput of the high-level straw moisture content trials was decreased to prevent the threshing rotor from plugging. Grouping all of the 3X3 trials together, the decrease in the high-level throughput of the trials completed with the 3X3 chopper prevented the high and low-level throughputs from being statistically separable.

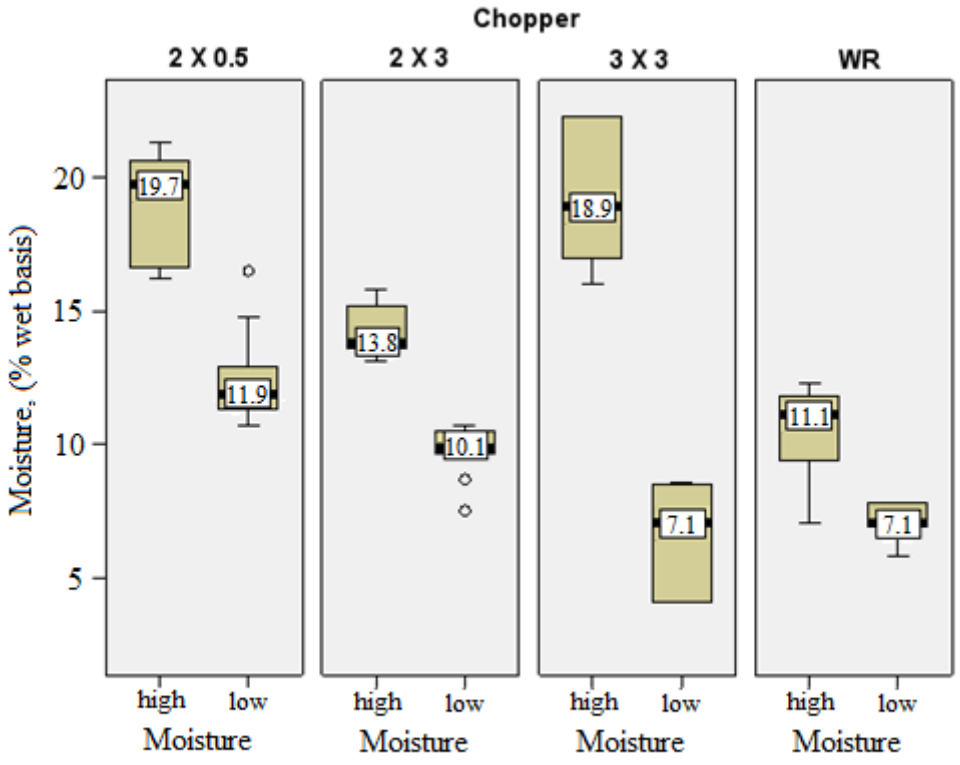

Figure 6.2 Box-and-whisker plot showing the range of the high-level and low-level straw moisture content processed by each chopper.

It was by chance that the 3X3 chopper was used to process straw with a higher than normal moisture content. The weather during the trials dictated, by in large, the moisture content of the straw that was processed by each chopper. Efforts were made to expose each chopper to the same range of high-level and low-level straw moisture contents by performing the trials at different times throughout the day. It just so happened that the high-moisture-content-straw trials of the 3X3 chopper occurred during an evening when the relative humidity rose faster than expected which in turn caused the moisture content of the straw to increase faster than expected. The 3X3 high-moisture-content-straw trials could not be postponed to the next day because the maturity of the crop changed with time, and in order to compare the performance of all choppers the field trials needed to be completed in the least amount of time.

Just like throughput, the average high and low straw moisture content that each chopper was subject to was not the same. Because the choppers were not subject to the same straw moisture content, and the choppers' performance was typically found to be affected by straw moisture content the performance of the choppers will not be compared. The average high and low-level straw moisture content that was processed by the 2X0.5, 3X3, 2X3, and WR choppers in % w.b. are 18.8 & 12.3, 19.2 & 6.7, 14.3 & 9.9 and 10.7 & 7.1, respectively. The moisture content of the straw processed by the choppers was not a controlled factor; the high and low-level straw moisture content trials were achieved by performing the trials at different times throughout the day. The reason that each chopper was not subject to the same high and low-level straw moisture content was a result of varying weather conditions during the trials. Also, the variation of straw moisture content that each chopper was subject to was a result of varying weather conditions during the completion of the trials. A box-and-whisker plot of straw moisture levels that each chopper was subject to is shown in Figure 6.2. The circles shown on the 2X0.5 and 2X3 choppers are trials that were considered outliers.

The specific energy requirement of the 3X3 chopper was significantly influenced at the 0.05 level by the counter-knife engagement and straw moisture content. The analysis of variance of the data collected to test the effect of counter-knife engagement and straw throughput and moisture content on the specific energy requirement of the 3X3 chopper is shown in Table C.5. The interaction of counter-knife engagement and straw moisture content was also significant. The specific energy requirement of the 3X3 chopper as a function of counter-knife engagement, and moisture content are given in Figure 6.3.

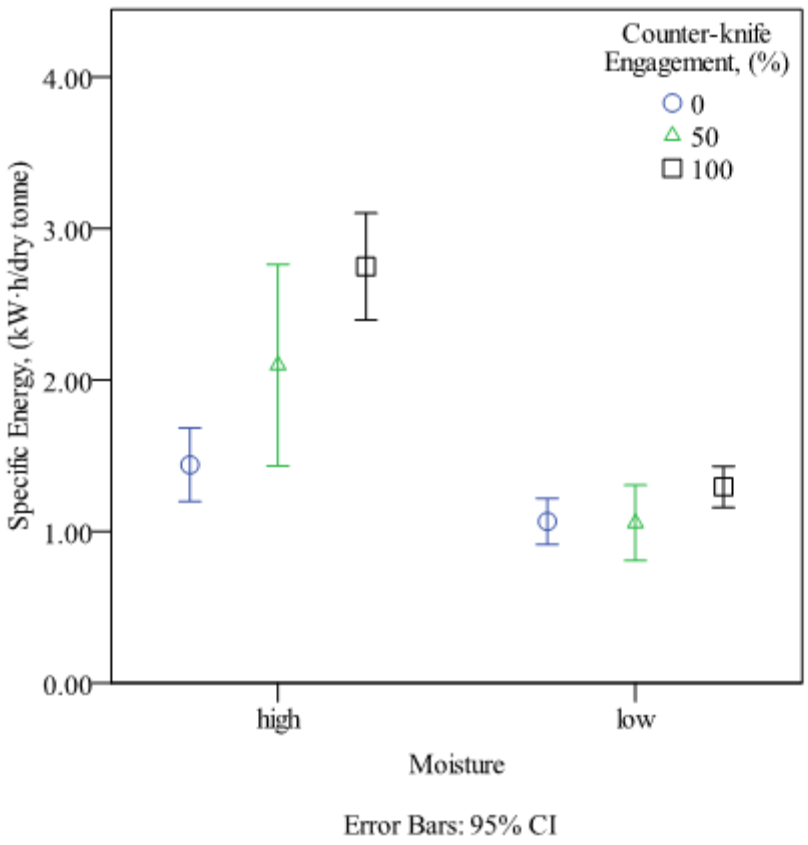

Figure 6.3 The average and 95% confidence interval (CI) of the specific energy consumed by the 3X3 chopper as a function of counter-knife engagement and moisture content.

The specific energy of the 3X3 chopper varied from 0.69 to 3.12 kW·h/dry tonne. The average specific energy requirement for the 3X3 chopper with a counter-knife engagement of 0, 50 and 100% was 1.25, 1.58 and 2.02 kW·h/dry tonne, respectively. Thus, by changing the counter-knife engagement from 0 to 50%, the specific energy increased on average by approximately 0.33 kW·h/dry tonne. However, changing the counter-knife engagement from 50 to 100% yielded approximately a 0.44 kW·h/dry tonne average increase in specific energy requirement. The average specific energy for the high and low throughput trials was 1.63±0.67 and 1.60±0.74 kW·h/tonne, respectively. The moisture content had the greatest effect out of the three factors

investigated. The high and low-level moisture content trials had an average specific energy of 2.10 and 1.14 kW·h/dry tonne, respectively, approximately a 0.96 kW·h/dry tonne difference. The interaction between counter-knife engagement and straw moisture content is apparent in Figure 6.3, as the magnitude of the effect of counter-knife engagement was larger when high moisture content straw was processed.

The specific energy required by the 2X3 chopper was affected by the same factors that affected the 3X3 chopper, with the addition of throughput which had a significant effect on the specific energy requirements of the 2X3 chopper. The specific energy required by the 2X3 chopper was significantly influenced at the 0.05 level by counter-knife engagement, throughput, and moisture content. The analysis of variance of the data collected to test the effect of counter-knife engagement and straw throughput and moisture content on the specific energy requirement of the 2X3 chopper is shown in Table C.6. The interaction of counter-knife engagement and moisture content was also statistically significant at the 0.05 level. The specific energy required by the 2X3 chopper as a function of throughput, counter-knife engagement, and moisture content is shown in Figure 6.4.

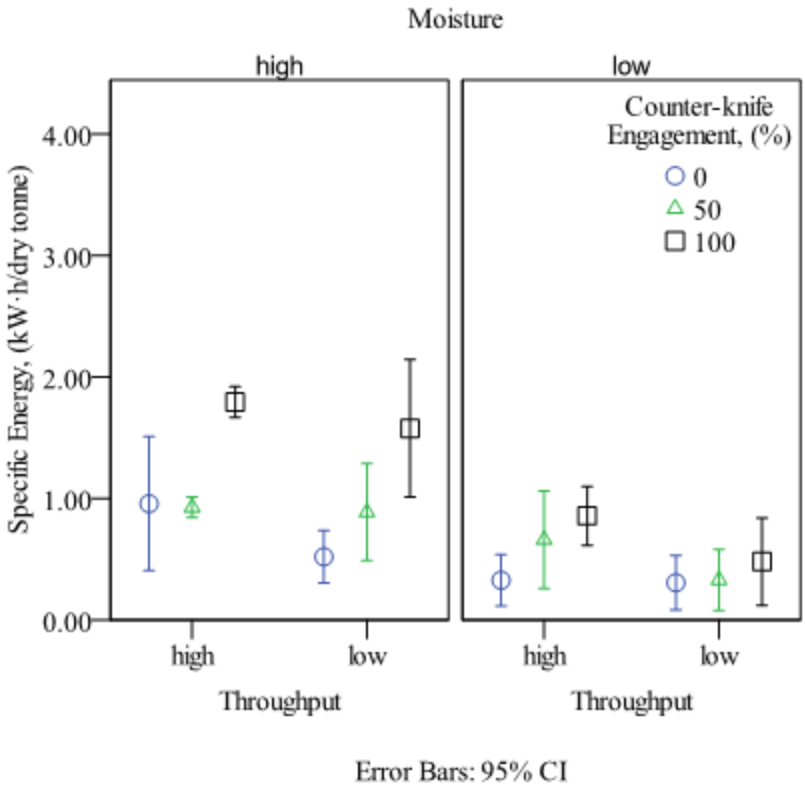

Figure 6.4 The average and 95% confidence interval (CI) of the specific energy consumed by the 2X3 chopper as a function of counter-knife engagement, throughput, and moisture content.

The specific energy required by the 2X3 chopper varied from 0.07 to 2.10 kW·h/dry tonne. The average specific energy required by the 2X3 chopper with a counter-knife engagement of 0, 50 and 100% was 0.53, 0.70 and 1.18 kW·h/dry tonne, respectively. Thus by changing the counter-knife engagement from 0 to 50% the specific energy increased on average by approximately 0.23 kW·h/dry tonne, and changing the counter-knife engagement from 50 to 100% yielded approximately a 0.48 kW·h/dry tonne average increase in specific energy. The average specific energy for the high and low-level throughput trials was 0.92 and 0.68 kW·h/dry tonne, respectively. Just like the 3X3 chopper, the magnitude of the effect of moisture content on the specific energy required by the 2X3 was the largest of all the factors investigated. The high and low-level

moisture content trials had an average specific energy of 1.11 and 0.49 kW·h/dry tonne respectively, approximately a 0.62 kW·h/tonne difference.

The specific energy of the WR chopper was affected by the same factors that had a significant effect on the specific energy requirements of the 2X3 chopper, with the exception of counter-knife engagement. Counter-knife engagement had a significant effect on the specific energy requirements of the 2X3 chopper but not on the WR chopper. The specific energy requirements of the WR chopper was significantly influenced at the 0.05 level by the throughput and moisture content. The analysis of variance of the data collected to test the effect of counter-knife engagement and straw throughput and moisture content on the specific energy requirement of the WR chopper is shown in Table C.7. The interaction of counter-knife engagement and moisture content was statistically significant at the 0.05 level. The specific energy required by the WR as a function of throughput and moisture content is shown in Figure 6.5.

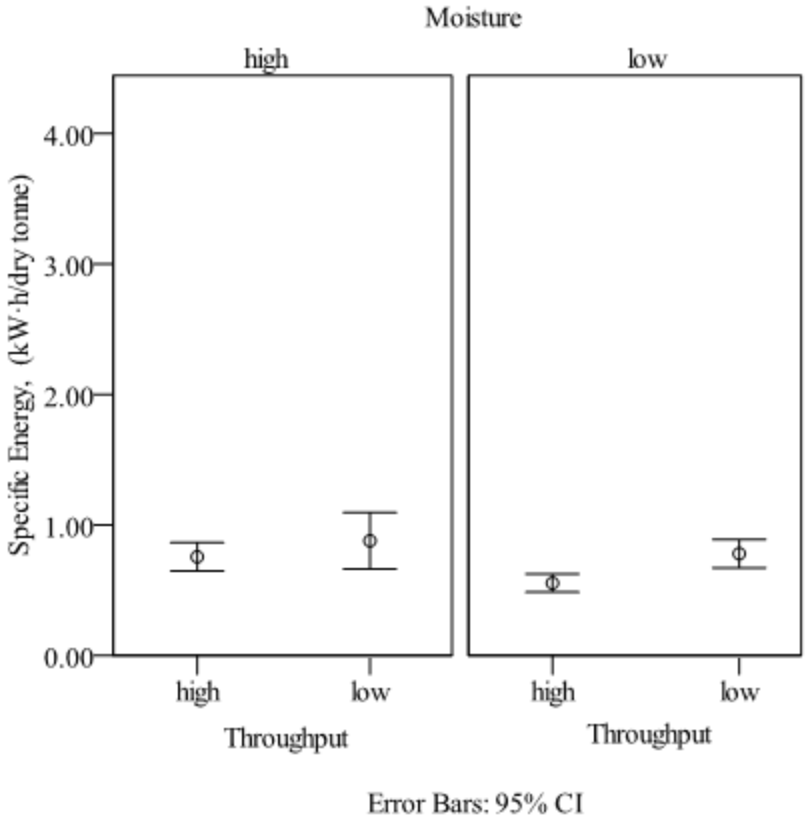

Figure 6.5 The average and 95% confidence interval (CI) of the specific energy consumed by the WR chopper as a function of throughput and moisture content.

The specific energy required by the WR chopper varied from 0.44 to 1.39 kW·h/dry tonne. The average specific energy required by the WR chopper with a counter-knife engagement of 78, 89 and 100% engagement was 0.63, 0.66 and 0.78 kW·h/dry tonne, respectively. Thus, by changing the counter-knife engagement from 78 to 89% the specific energy increased on average by approximately 0.03 kW·h/tonne, and changing the counter-knife engagement from 89 to 100% yielded approximately a 0.12 kW·h/dry tonne average increase in specific energy. Contrary to the 2X3 and 3X3 choppers, the specific energy of the WR had an inverse relationship with throughput. The average specific energy for the low and high throughput trials was 0.83 and 0.67 kW·h/dry tonne, respectively, approximately a 0.16 kW·h/dry tonne difference. The high and low-level

moisture content trials had an average specific energy of 0.81 and 0.67 kW·h/dry tonne, respectively, approximately a 0.14 kW·h/dry tonne difference.

The GML of the MOG was only measured once with each combination of straw throughput, moisture content and counter-knife engagement. Thus, no statistical analysis could be completed to determine which factors had a significant effect on the GML of the MOG. For all of the choppers tested, it appears that the there was an inverse relationship between GML of MOG and counter-knife engagement, and a direct relationship between GML and straw moisture content for all four choppers tested. Conversely, throughput had little or no effect on the GML of the MOG for all of the choppers tested. The GML of MOG as well as the specific energy requirements of the choppers as a function of straw throughput, moisture content and counter-knife engagement is shown in Table 6.1.

Table 6.1 Average specific energy requirements of each chopper, and the geometric mean length of the material other than grain exiting the combine harvester at two levels of throughput, straw moisture content and three levels of counter-knife engagement.

Chopper	Counter-knife engagement (%)	Throughput (dry tonne/h)	Moisture content (% wet basis)	Specific energy (kW·h/dry tonne)	Geometric mean length (mm)
3X3	0	10[a]	6.6	1.01	42.4
		10[a]	19.1	1.59	65.7
		11[a]	7.6	1.13	41.8
		11[a]	17.5	1.29	67.8
	50	10[a]	4.8	0.93	41.7
		10[a]	20.2	2.03	54.0
		11[a]	8.4	1.19	39.4
		11[a]	17.9	2.17	57.3
	100	9	6.3	1.24	47.0
		9	19.9	2.84	47.0
		12	6.5	1.35	42.8
		12	19.1	2.66	50.2
2X3	0	11	8.9	0.31	46.6
		11	13.7	0.52	51.9
		14	9.9	0.33	43.3
		14	14.7	0.95	51.6
	50	10	10.4	0.33	42.8
		10	14.1	0.89	48.3
		13	9.8	0.66	40.7
		13	14.6	0.93	48.9
	100	10	10.3	0.48	43.9
		10	14.4	1.58	41.8
		14	10.1	0.86	39.4
		14	14.4	1.80	48.8
2X0.5	0	8	12.3	N/A	46.3
		8	17.9	N/A	55.6
		14	12.4	N/A	42.4
		14	18.2	N/A	52.0
	50	8	11.0	N/A	41.6
		8	20.8	N/A	54.8
		14	13.7	N/A	40.4
		14	18	N/A	44.5
	100	7	11.7	N/A	41.8
		7	19.1	N/A	45.5
		13	12.7	N/A	42.1
		13	18.7	N/A	49.4
WR	78	9	7.5	0.79*	41.3
		9	10.4	0.80	45.8
		17	6.7	0.52	43.3
		17	10.4	0.68	41.3
	89	9	7.7	0.78	41.6
		9	11	0.72	43.3
		16	6.6	0.62	42.0
		16	9.9	0.73	39.8
	100	9	7.1	0.78	41.7
		9	11.2	1.24*	43.7
		16	7.2	0.44**	42.6
		16	11.1	0.85	46.8

* average of two replicates

** no replicates

not available (N/A)

[a] not statistically separable

The GML of MOG did not appear to be affected by throughput for any of the choppers tested. The difference between the GML corresponding to the high-level and low-level throughput for each chopper tested was approximately the same as the standard deviation of the GML. The standard deviation of the GML was not determined from repeated measurements but rather, from the method used to quantify the GML of a single sample. The fact that the GML of MOG was not affected by throughput suggests that the orientation and distribution of the straw particles across the width of the straw chopper never changed as a function of throughput.

Throughput did not have a significant effect on the specific energy requirements of the 3X3 chopper. However, this conclusion is questionable because the high-level and low-level throughputs were not statistically separable. At a counter-knife engagement of 0 and 50%, the two levels of throughput to which the 3X3 chopper was subjected to were not statistically separable. However at a counter-knife engagement of 100%, the high and low-level throughputs that the 3X3 chopper experienced were on the verge of being statistically separable ($p = 0.053$).

The specific energy requirements of the 2X3 chopper increased with an increase in the throughput of plant material through the chopper. It was expected that the energy consumed to process material would increase as throughput increased because of two reasons. First the rotational speed of the chopper was constant during the trials, thus an increase in throughput caused an increase in the depth of material being cut by the chopper. Springer et al. (1976), Reznik (1975) and Chancellor (1958) all found that as the depth of material processed by a cutting device increased, the energy required to compress the material also increased. Second, the increase in the depth of material caused the density of material being sheared to increase, which has been found to increase the maximum shear strength of the plant material (Halyk and Hurlbut, 1968).

The specific energy required by the WR chopper was inversely related to throughput. However, the energy consumed to process cereal straw with the WR chopper was directly related to throughput. Therefore, the WR chopper also followed the expected trend, in terms of the relationship between energy consumption and throughput. Thus for the WR

chopper, the rate of increase in the energy consumed (as a function of throughout) was less than the rate of increase in throughput.

The specific energy requirement of all choppers tested increased with increasing straw moisture content, and the GML of MOG also increased with increasing straw moisture content. According to Chancellor (1988) the energy required to process cereal straw should have decreased as the straw moisture content increased. Chancellor (1988), concluded that a major increase in plant-material moisture content typically caused a slight decrease in cutting forces. However, Chancellor (1988) was focused on cutting alone, while the RFCS was also used to transport the plant material. The added mass of the water in the straw, during the high-level straw moisture content trials would have caused the specific energy requirement of the RFCS to increase.

The direct relationship between straw moisture content and the specific energy requirements of the straw choppers is also attributed to two other phenomena. First, dry cereal straw behaved as a brittle material, and when processed by the combine harvester the dry straw underwent extensive particle length reduction in the threshing rotor and feeder. Thus, by the time the straw reached the chopper the straw particle length may have been short enough that the majority of the straw passed through the chopper without being cut. Second, the increase in moisture content caused the dynamic coefficient of friction of the straw to increase. The increase in the dynamic coefficient of friction (between the straw and steel) resulted in a greater amount of energy used to transport the straw through the chopper. The direct relationship between GML and straw moisture content is attributed to the fact that the wet straw was more ductile and underwent less particle length reduction in the threshing rotor, feeder and chopper.

There were a few exceptions to the direct relationship between straw moisture content and the GML of the MOG. There were cases when the GML of MOG was shorter when high-moisture-content straw was processed. For example, as shown in Table 6.1 when the 2X3 chopper was used to process straw at a throughput of 10 tonne per hour with fully inserted counter-knives, the GML with low-moisture straw was approximately 2.1 mm longer than when high-moisture straw was processed. However, a difference of 2.1 mm is approximately equal to the standard deviation of the GML of the MOG, which

suggests that there is not a significant difference between the GML of MOG in this case. The exceptions to the trend typically occurred when relatively low moisture content straw was processed by the choppers, thus the indirect relationship between GML and straw moisture content could be attributed to a greater degree of particle length reduction occurring in the threshing rotor and feeder.

Counter-knife engagement had a significant effect on the specific energy required by the 2X3 and 3X3 choppers, and with each chopper tested the GML of MOG typically decreased as counter-knife engagement increased. Counter-knife engagement did not have a significant effect on the specific energy requirements of the WR chopper. There are two reasons why the WR chopper was not affected by counter-knife engagement. First, the range of counter-knife engagement examined with the WR chopper was much smaller than the range examined with the 2X3 and 3X3 choppers. The counter-knife engagement examined with the WR varied from 78 to 100% engaged. Conversely the counter-knife engagement investigated with the 2X3 and 3X3 choppers was from 0 to 100% engaged. Second, the interaction between counter-knife engagement and straw moisture content had a significant effect on the specific energy requirement of the WR chopper. The specific energy required by the WR chopper was more sensitive to counter-knife engagement when higher moisture content straw was processed. The significant interaction, coupled with the fact that the moisture content of the straw processed with the WR chopper was relatively low compared to the other choppers, specifically the high-level straw moisture content trials as shown in Figure 6.2, was likely the reason that counter-knife engagement was not found to be significant for the WR chopper.

There was a direct relationship between counter-knife engagement and the specific energy requirements of the 2X3 and 3X3 choppers, and an indirect relationship between counter-knife engagement and the GML of MOG for all choppers. Engaged counter-knives do two things, they restrict the flow of plant material past the chopper, and they provide support (act as a counter-shear) to the plant material that is being cut. Both the restriction in flow of plant material and counter-shear support result in a greater degree of particle length reduction caused by the chopper. The greater degree of particle length

reduction comes at a cost of an increased amount of energy consumed to transport, compress and cut the plant material.

The interaction between counter-knife engagement and straw moisture content had a significant effect on the specific energy required to process straw with all of the choppers tested. When straw with higher moisture content was processed, both the specific energy requirement and the GML of MOG were more sensitive to counter-knife engagement. When dry straw was processed by the combine harvester, it is believed that it underwent extensive particle length reduction in the threshing rotor and feeder. Thus, by the time the straw reached the chopper it was already short enough that the chopper had little effect on the GML regardless of whether or not the counter-knives were inserted in the chopper. The majority of the energy consumed by the chopper was due to transporting the dry material instead of cutting it. Conversely, it is believed that when high moisture content straw was processed by the combine harvester the straw experienced very little particle length reduction in the threshing rotor and feeder. Thus, when the straw reached the chopper it was long enough that the chopper could still reduce the GML. Further, the degree to which the counter-knives were inserted in the chopper had a greater influence over the specific energy requirement of the choppers as well as the degree of particle length reduction because, the counter-knives act as a counter-shear and provide support to the plant material during the cutting process. The increased specific energy demand of the choppers was not only due to an increase in the amount of energy consumed to cut the plant material, but also to transport the plant material because the dynamic coefficient of friction increased with increasing straw moisture content.

6.1.4 Summary

After performing the field trials the following general trends were observed for all choppers tested:

1. an increase in counter-knife engagement resulted in a decrease in the GML and an increase in specific energy,
2. an increase in throughput caused little effect on the GML and an increase in specific energy,

3. an increase in moisture content caused an increase in both the GML and specific energy and
4. The GML and specific energy requirements of all choppers were more sensitive to counter-knife engagement when higher moisture content straw was processed.

The exceptions to the general trends were:

1. an inverse relationship was not observed between counter-knife engagement and the GML of MOG when the WR chopper was used,
2. the specific energy of the WR chopper was found to be independent of counter-knife engagement,
3. the specific energy requirement of the WR chopper was found to be inversely related to throughput, however the power required to process cereal straw with the WR chopper was directly related to throughput, and
4. the specific energy requirements of the 3X3 chopper were independent of throughput which is attributed to a lack of distinct high and low level throughputs during the 3X3 trials.

The first and second exceptions to the general trend are believed to be attributed to a relatively small range in counter-knife engagement explored while using the WR chopper and the moisture content of straw processed by the WR chopper was relatively low. Further, the instrumentation used during the field trials likely limited the tests ability to indicate that the counter-knife engagement did in fact have a significant effect on the specific energy required by the WR chopper.

6.1.5 Conclusions

The purpose for completing the HSCP RFCS field trials was to identify which parameters should be included in the analytical model, validate the model and identify the parameters that should be included in the stochastic model. The material properties of the cereal straw processed with the combine harvester were quantified with the material properties test stand so that the field data could be used to validate the analytical model.

In general, the specific energy requirement of the HSCP RFCS of all choppers tested was affected by counter-knife engagement, straw moisture content and throughput. The interaction of counter-knife engagement and straw moisture content was found to have a significant effect on the specific energy required by the HSCP RFCS. The magnitude of the effect of counter-knife engagement (on the specific energy required by the HSCP RFCS) increased when straw at a higher moisture content was processed with the HSCP RFCS. The inclusion of counter-knife engagement as an input parameter in the analytical and stochastic model is dependent on the moisture content of the straw that is processed by the HSCP RFCS. If the models are to be used to predict the power or specific energy required by the HSCP RFCS when dry straw is processed, counter-knife engagement does not need to be included as an input parameter in the model. However, if the models are to be used to predict the power demand or energy required by the HSCP RFCS when wet straw is processed, counter-knife engagement will need to be included in the analytical model. Typically, the HSCP RFCS is used to process plant material at varying moisture contents, thus it would be advantageous to include counter-knife engagement and plant material moisture content as an input parameter in the models.

Throughput had a significant effect on the specific energy required by the HSCP RFCS. It is common for the HSCP RFCS to be used to process cereal straw at a range of throughputs. Therefore it would also be advantageous to include throughput as an input parameter in the analytical model. However, the GML of MOG did not appear to be affected by the throughput of cereal straw, thus the parameter does not need to be included in the stochastic model.

7 ANALYTICAL MODEL

The 5th LSCP objective and the 2nd HSCP objective were to develop an analytical model to predict the power demand of the RFCS. The purpose of developing the analytical model was to give future designers of a RFCS a tool that they could use to quantify the effect of changing the design parameters of the RFCS on the power demand of the RFCS. Without the model, the designer of the RFCS would be forced to quantify the effect of changing the design parameters on the power demand of the RFCS by completing costly field or laboratory experiments. Optimistically, the need for completing future experiments to identify the effect of the design parameters on the power demand of a RFCS would be eliminated. More realistically, the required number of experiments will be substantially reduced.

In the first section of this chapter, the development of the analytical model is discussed. The model development is based on the concept that the total energy consumed by the RFCS, is the sum of the energy required to transport, compress and cut the plant material. Following the development of the model, the application of the model in terms of the LSCP and HSCP RFCS is discussed separately. The application of the model to the two different RFCS is discussed in separate sections because, the geometry of the two RFCS is different and the input parameters of the model are a function of the geometry of the RFCS. In both the HSCP and LSCP sections, the quantification of the input parameters, validation of the model and a sensitivity analysis are discussed. The conclusions drawn from the analytical model and the recommendations for future work on improvements to the model are provided at the end of this chapter.

The analytical model, though derived based on the governing laws of physics, is limited because the effect of the governing laws on some of the input parameters is not fully understood. Subsequently the governing equations describing the relationship between these parameters could not be defined from the governing laws of physics. Instead simplifying assumptions were made so that the equations could be defined. As will be discussed later in this chapter, not all of the input parameters of the governing equations used in the analytical model could be directly quantified or derived from first principles. These parameters were approximated by fitting the model to a subset of the

data collected with the rotary feeding and cutting systems. Because the analytical model was solved numerically to quantify the indeterminate parameters some may dispute whether the analytical model is in the truest sense of the definition an analytical model. A more accurate definition of the model may be - a limited analytical model.

7.1 Development

The development of the analytical model was done with the assumption that the plant material was cut between the counter-knives and the rotating elements on the chopper or rotor. Chancellor (1957) performed a comprehensive review of impact cutting and found that typically, speeds in the range of 43 to 84 m/s are required to cut plant material without a counter-shear. Therefore the model could not be applied to the 2X3, 3X3, or 2X0.5 choppers, because their average peripheral speed was 60 m/s, which is fast enough to cause impact cutting. The average peripheral speed (or cutting speed) of the WR chopper and rotor on the LSCP test apparatus was 17 and 2 m/s, respectively. The combination of the slow peripheral speed and the lack of sharp rotating elements on the WR chopper and rotor on the LSCP test apparatus prevented the WR chopper and LSCP RFCS rotor from performing impact cuts. Therefore, the analytical model is applicable to both the WR chopper and the LSCP test apparatus.

The analytical model was designed so that the output of the model would be the power demand of the RFCS as a function of the angular position of the rotor over a range of 360° (one full revolution of the rotor). This type of output was selected because the power demand for both the LSCP test apparatus and the HSCP test apparatus were measured with a one degree resolution. This format of output allowed for the effect of the geometry of the RFCS to be observed.

The number of cuts the RFCS made was defined as the number of times the leading edge of a tine pair passed the leading edge of the counter-knife that protruded into the tine pair. Because there were three tine pairs for each counter-knife (spaced 120° apart), the number of cuts the RFCS made over one revolution of the rotor was three times the number of counter-knives. Therefore the LSCP test apparatus, which was described in section 4.1, made 15 cuts per revolution of the rotor, and the HSCP test apparatus with

the WR chopper, which was described in section 4.2, made a total of 78 cuts per revolution of the rotor. The cut number was identified with the subscript *m*. Throughout this section "cut number" is used to refer to a specific cut made by the RFCS.

For each cut made by the RFCS, the boundary between the compression and cutting stages that the plant material experienced needed to be identified. The boundary between the stages of cutting needed to be identified because the governing equations used to quantify the force associated with cutting and compressing the plant material are different. Because of the geometry of the RFCS, the boundary between compressing and cutting the plant material was a function of the rotor's angular position and location of the plant material along the tine's leading edges (with respect to the rotor's axis of rotation). During operation (when the rotor was rotating) the base of the tine passed the leading edge of the counter-knife before the tip of the tine. The base of the tine refers to the leading edge of the tine closest to the axis of rotation of the rotor. Conversely, the tip of the tine is the leading edge of the tine furthest from the axis of rotation of the rotor. Therefore, plant material located at the base of the tine was compressed and cut before the plant material located at the tip of the tine. A side view of the RFCS showing the direction of rotation of the rotor, the direction of plant material entering the RFCS and the location of the base and tip of the tine is shown in Figure 7.1.

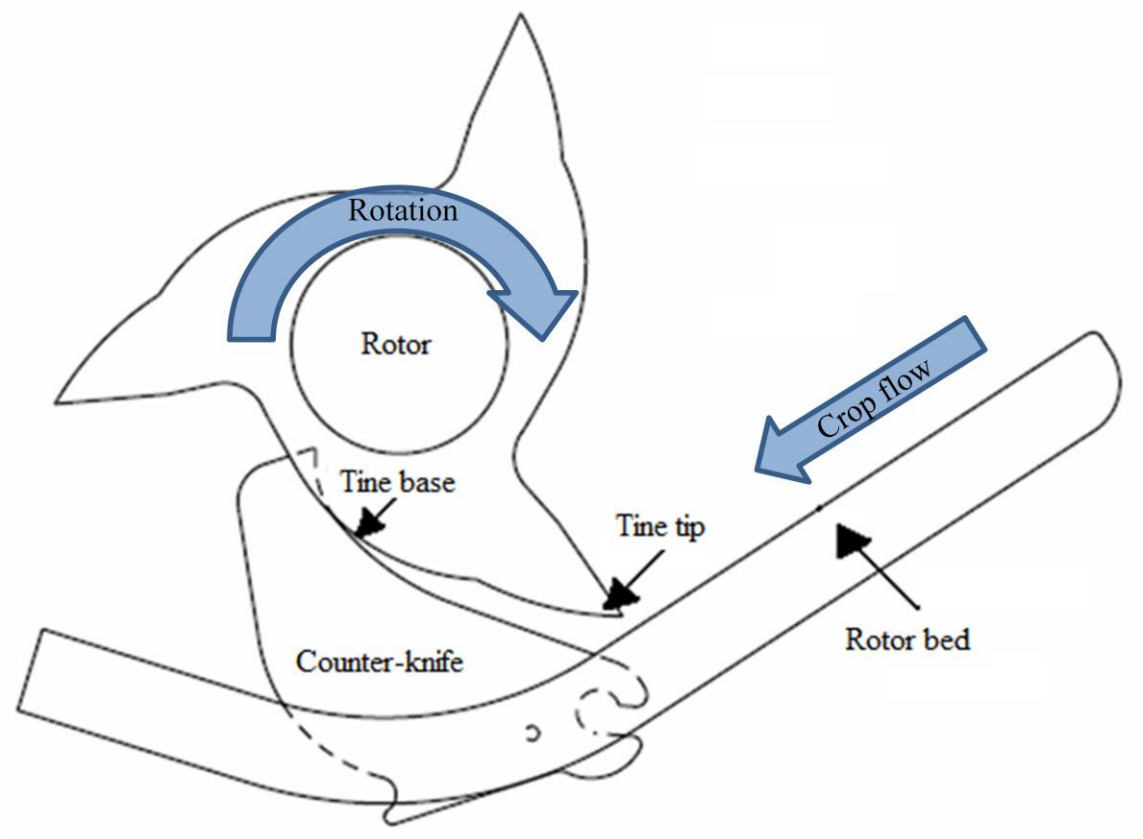

Figure 7.1 Drawing of a side view of a rotor tine, counter-knife and the rotor bed which shows that plant material at the base of a tine is compressed and cut prior to the plant material at the tip of a tine.

Because the compression and cutting stages of the plant material was a function of the location of the plant material with respect to the axis of rotation of the rotor, a series of 10 zones were created. It was assumed that the boundary between the compression and cutting stages the plant material experienced within each zone was only a function of the rotor's angular position. The zones were numbered 1 through 10, as shown in Figure 7.2 and are identified throughout this section with the subscript *n*. The difference between the radii of adjacent zone boundaries was approximately 12.5 mm.

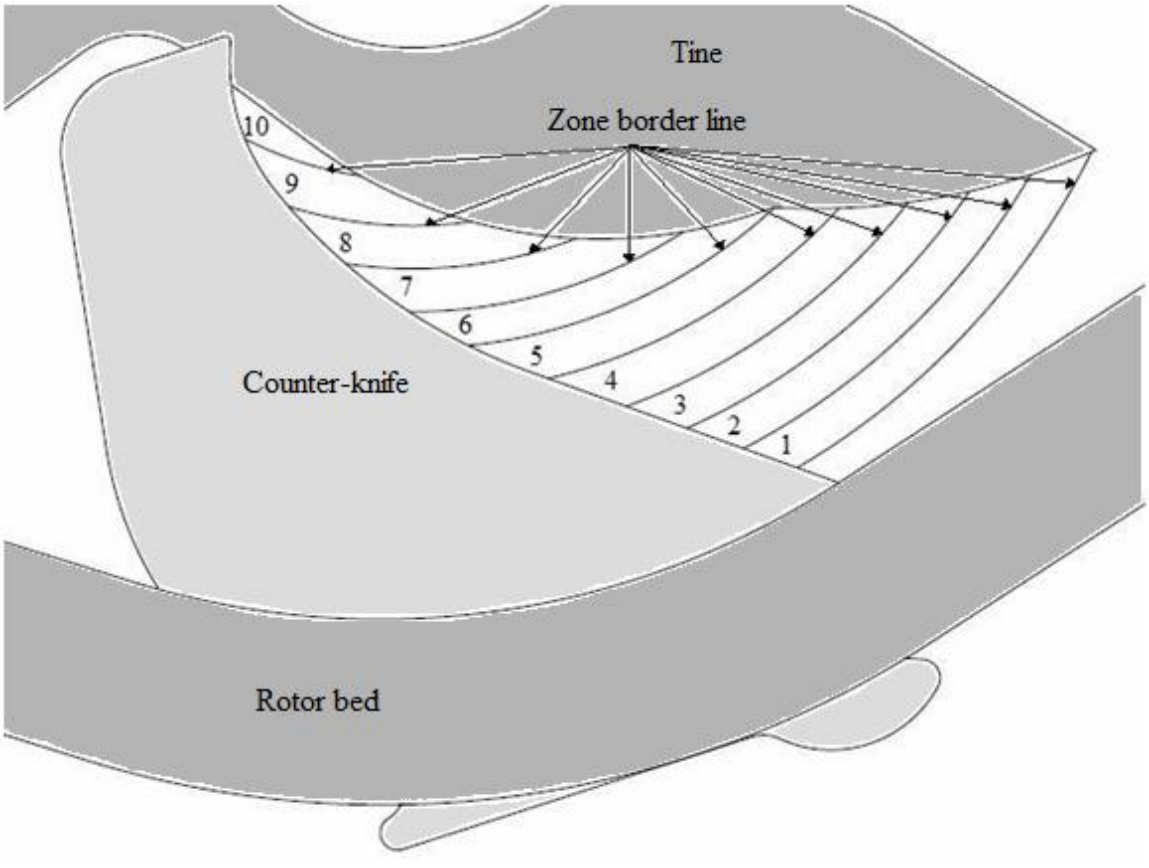

Figure 7.2 Drawing of a side view of a rotor tine, counter-knife and the rotor bed which shows the ten zones in wich the counter-knife leading edge/ tine leading edge was seperated.

The approach of the model development was to define the power required to compress, cut and transport the plant material over one full revolution of the rotor. The total power demand of the RFCS was found by the summation of the power required to: compress and cut plant material between the leading edge of the tines and counter-knives, transport plant material along the leading edge of the tines, transport plant material along the sides of the counter-knives, transport plant material along the rotor bed and to spin the rotor without crop flow. The power required to compress and cut plant material between the leading edge of the counter-knives and tines, transport plant material along the leading edge of the tines and transport plant material along the sides of the counter-knives were a function of the zones in which the plant material was located. Thus, the total

power required to cut and compress plant material between the leading edge of the counter-knives and tines, transport plant material along the leading edge of the tines and to transport plant material along the sides of the counter-knives was found by summing the power required to accomplish each task in each of the 10 zones for all cuts made by the RFCS (over a single revolution of the rotor). The power requirements of each task completed by the RFCS will be discussed in detail. First, to quantify the power required to compress the plant material, the magnitude of the compression force needed to be quantified.

7.1.1 Compressive force (plant material in the n^{th} zone of the m^{th} cut)

It was assumed that the compressive stress in the plant material being processed by the RFCS could be defined by Hooke's Law,

$$\sigma = E\varepsilon, \quad \textbf{(7.1)}$$

where:

$$\sigma = F_t/A, \quad \textbf{(7.2)}$$

$$\varepsilon = \Delta l/lo, \quad \textbf{(7.3)}$$

σ is the normal stress of the plant material (Pa),

E is the Young's modulus of the plant material (Pa),

ε is the strain of the plant material,

F_t is the force required to achieve a given level of strain (N),

A is the cross-sectional area of compression (m^2),

Δl is the change in depth of the plant material (m) and

lo is the initial depth of the plant material (m).

By combining equations (7.2) and (7.3) into (7.1) and solving for, F_t, the force required to compress plant material is given by,

$$F_t = AE\ \Delta l/lo \quad \textbf{(7.4)}.$$

The force required to compress the plant material in the n^{th} zone for the m^{th} cut was determined using the following,

$$F_{compress_{m_n}} = \delta_n w E_{m_n} \varepsilon_{m_n} \quad \textbf{(7.5)}$$

where:

$F_{compress_{m_n}}$ is the force required to compress the plant material in the n^{th} zone of the m^{th} cut (N),

δ_n is the arc length of the tine in the n^{th} zone (m),

w is the width of compression (m),

E_{m_n} is the Young's modulus of the plant material in the n^{th} zone of the m^{th} cut (Pa) and

ε_{m_n} is the strain of the plant material in the n^{th} zone of the m^{th} cut.

The Young's modulus of the plant material processed by the RFCS, E_{m_n}, is a function of the strain it experiences. Therefore, the Young's modulus had to be defined in terms of the zone and cut number because, the level of strain in each zone for a given rotor position was a function of the zone and cut number. The Young's modulus of plant material was defined using the following equation,

$$E_{m_n} = a_3 \varepsilon_{m_n}^3 + a_2 \varepsilon_{m_n}^2 + a_1 \varepsilon_{m_n} + a_0, \quad \textbf{(7.6)}$$

where:

$a_{3\ to\ 0}$ are the coefficients of the third order polynomial used to define the Young's modulus of a given plant material (Pa).

The polynomial relationship, instead of one of the standard methods (for example the secant method) of reporting the Young's modulus was used because, the stress-strain curve calculated with a polynomial relationship more accurately represented the measured average stress-strain curve of the plant material. If the secant method of reporting Young's modulus would have been used, the calculated stress required to

achieve a given level of strain (for a strain of zero up to the value used to calculate the secant Young's modulus) would have been substantially higher than the actual stress. This would ultimately result in the analytical model over-estimating the force, energy and power required to compress the plant material.

The strain of the material in n^{th} zone for the m^{th} cut was defined using the following equation,

$$\varepsilon_{m_n} = \frac{\Delta l_n}{lo_m} = \begin{cases} \frac{\pi r_n}{180\ lo_m}\left[\theta + \alpha_n - \left(\gamma_n - \frac{180 lo_m}{\pi r_n}\right)\right], \gamma_n - \frac{180\ l_{0_m}}{\pi r_n} < \theta + \alpha_n < \gamma_n \\ 0 \quad , \quad else \end{cases}, \quad (7.7)$$

where:

Δl_n is the change in depth of plant material in the n^{th} zone (m),

lo_m is the initial depth of plant material for the m^{th} cut (m),

r_n is the midpoint radius of the n^{th} zone (m),

θ is the angle of the tine with respect to the datum (°),

γ_n is the angle between the datum and the midpoint on the leading edge of the counter-knife of the n^{th} zone (°) and

α_n is the angle between the leading and lagging edge of the tine at the midpoint of the n^{th} zone (°).

The plant material in the n^{th} zone only experiences strain when two constraints are met. First, the n^{th} zone on the tine must be in contact with plant material. The first constraint was defined as,

$$\theta + \alpha_n > \gamma_n - \frac{180\ lo_m}{\pi r_n} \quad (7.8).$$

It was assumed that the gravitational force acting on the plant material forced the plant material to be in contact with the counter-knife before it was in contact with the tine. The second constraint was that the compression of plant material in the n^{th} zone could only continue up to the point when the leading edge of the tine was coincident with the leading

edge of the counter-knife (at the midpoint radius of the n^{th} zone). This constraint was based on the assumption that the plant material was cut (or sheared) once the leading edge of the tine passed the leading edge of the counter-knife or, before the leading edge of the tine passed the leading edge of the counter-knife. The second constraint was defined as,

$$\theta + \alpha_n < \gamma_n \qquad (\mathbf{7.9}).$$

The following parameters were quantified based upon the geometry of the RFCS: r_n, γ_n, α_n and δ_n. In order for γ_n and θ to be quantified a datum needed to be defined. The geometric parameters for zone 1, θ and the datum are shown in Figure 7.3. The width of compression, *w*, was assumed to be a function of counter-knife sharpness, with a sharper counter-knife having a smaller width of compression than a dull counter-knife. It was assumed that the initial depth of plant material, lo_m, was equal across all ten zones for the m^{th} cut, and lo_m was proportional to the throughput of plant material in the RFCS. The force that was required to compress the plant material between the leading edge of the tine and the counter-knife was discussed in this section. In the following section, the force required to cut the plant material between the tine and the counter-knife will be discussed.

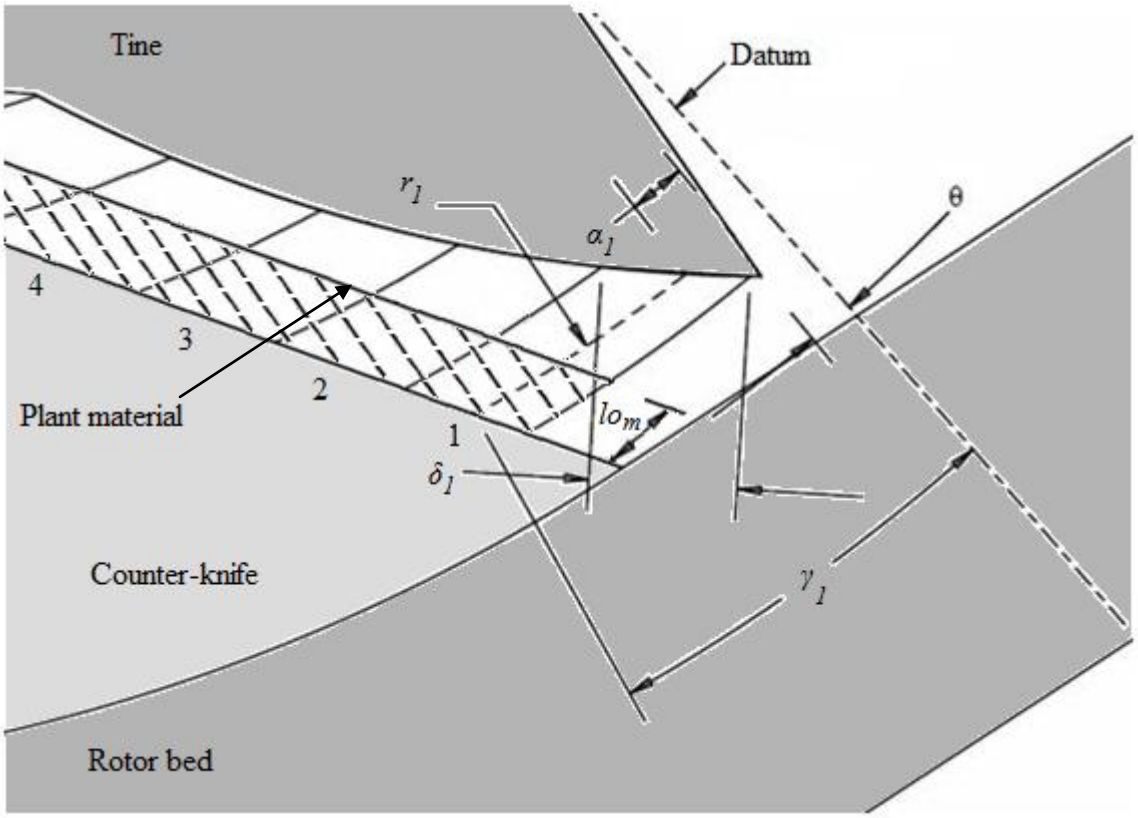

Figure 7.3 Drawing of a side view of the RFCS showing the variables required to define the force required to compress plant material in the n^{th} zone for the m^{th} cut, (r_1 is the midpoint radius of zone 1, lo_m is the initial depth of plant material for the m^{th} cut, α_1 is the angle between the leading and lagging edge of the tine at the midpoint of zone 1, δ_1 is the arc length of the leading edge of the tine in zone 1, θ is the angular position of the tine with respect to the datum and γ_1 is the angle between the datum and the midpoint on the leading edge of the counter-knife in zone 1).

7.1.2 Cutting force (plant material in the m^{th} cut)

Shear stress by definition is,

$$\tau = F_{shear}/A_{shear}, \quad \textbf{(7.10)}$$

where:

τ is the shear stress of the material (Pa),

F_{shear} is the force applied parallel to the cross-sectional area A_{shear} (N) and

A_{shear} is the cross sectional area of shear (m^2).

The force required to cut, or shear, the plant material for the m^{th} cut was determined by,

$$F_{cut_m} = \tau_{max} A_{sm}, \quad \textbf{(7.11)}$$

where:

F_{cut_m} is the force required to cut the plant material of the m^{th} cut made by the RFCS (N),

τ_{max} is the maximum shear strength of the plant material (Pa) and

A_{sm} is the cross-sectional area of the plant material when it was cut (m^2).

As with w, it was assumed that A_{sm} was affected by the sharpness of the counter-knives used in the RFCS. It was assumed that a sharper counter-knife would require less force to cut a given plant material than a dull counter-knife. Thus, a sharper counter-knife would result in A_{sm} being smaller than when a dull counter-knife is used to cut a given plant material.

Halyk and Hurlbut (1968) found that the maximum shear strength of plant material, τ_{max}, was linearly related to the dry-mass density of the plant material. The maximum shear strength of plant material processed by the RFCS, τ_{max} was described by,

$$\tau_{max} = \rho_{dm} \tau_{slope} + \tau_{int}, \quad \textbf{(7.12)}$$

where:

ρ_{dm} is the dry-mass density of the plant material when it was cut (kg/m^3),

τ_{slope} is the slope of the linear equation that relates τ_{max} to ρ_{dm} (Pa $(kg\ m^{-3})^{-1}$) and

τ_{int} is the intercept of the linear equation that relates τ_{max} to ρ_{dm} (Pa).

It was assumed that the dry-mass density of plant material when cut was a function of the initial depth of plant material of the m^{th} cut, lo_m. Thus, the dry-mass density of plant material when cut in the RFCS was found using the following equation,

$$\rho_{dm} = \rho lo_m \quad \textbf{(7.13)}$$

where:

ρ is the coefficient that relates ρ_{dm} to lo_m (kg m^{-3} m^{-1}).

By combining equations (7.11), (7.12) and (7.13) the force required to cut plant material for the m^{th} cut made by the RFCS is given by,

$$F_{cut_m} = \left(\rho lo_m \tau_{slope} + \tau_{int}\right) A_{sm} \quad \textbf{(7.14)}.$$

In this section, the equation used to quantify the force required to cut the plant material in the RFCS was discussed. The combined force to compress and cut the plant material with the RFCS will be discussed in the next section.

7.1.3 Compressive and cutting force (plant material in the n^{th} zone of the m^{th} cut)

Equation (7.5) was used to quantify the force required to compress plant material in the n^{th} zone of the m^{th} cut made by the RFCS, and equation (7.14) was used to quantify the force required to cut the plant material of the m^{th} cut made by the RFCS. The boundary between the compression and cutting force needed to be defined in terms of the angular position of the tine. The force to compress and cut the plant material in the n^{th} zone of the m^{th} cut was found using the following,

$$F_{cs_{m_n}} = \begin{cases} F_{compress_{m_n}}, & 0 \leq F_{compress_{m_n}} < F_{cut_m} \\ F_{cut_m}, & F_{compress_{m_n}} \geq F_{cut_m} \end{cases} \quad \textbf{(7.15)}$$

where:

$F_{cs_{m_n}}$ is the force required to compress and cut plant material in n^{th} zone of the m^{th} cut made by the RFCS (N).

The combined force to compress and cut the plant material with the RFCS was discussed in this section. In the next section, the frictional force caused by plant material sliding across the leading edge of the tine will be discussed.

7.1.4 Friction force (between plant material and the tine leading edge in the n^{th} zone of the m^{th} cut)

It was assumed that whenever plant material was in contact with the tine, the plant material was sliding on the tine's leading-edge. The frictional force acting on a tine can be found using the following equation,

$$F_{f_{m_n}} = F_{cs_{m_n}} \mu \,, \tag{7.16}$$

where:

$F_{f_{m_n}}$ is the frictional force acting on the tine leading edge in the n^{th} zone of the m^{th} cut (N) and

μ is the dynamic coefficient of friction between the plant material and the tine.

The value of the dynamic coefficient of friction was assumed to be constant for a given plant material at a given moisture content. The equations used to determine the force to compress and cut plant material in the RFCS, as well as the frictional force due to plant material sliding along the leading edge of a tine has been identified. The power required to compress, cut and transport the plant material along the leading edge of a tine are discussed in the following section.

7.1.5 Compress, cut and transport power (plant material along the leading edge of the tine in the n^{th} zone of the m^{th} cut)

The magnitude of the compression, cutting and frictional force has been defined, but in order for the forces to be represented as a torque on the rotor, the location and direction of the forces needed to be defined. It was assumed that the force to compress and cut plant material, $F_{cs_{m_n}}$, acted at the midpoint of the n^{th} zone through the center of curvature of the rotor tine leading edge. The center of curvature of the leading edge of the tine for all zones is shown in Figure 7.4.

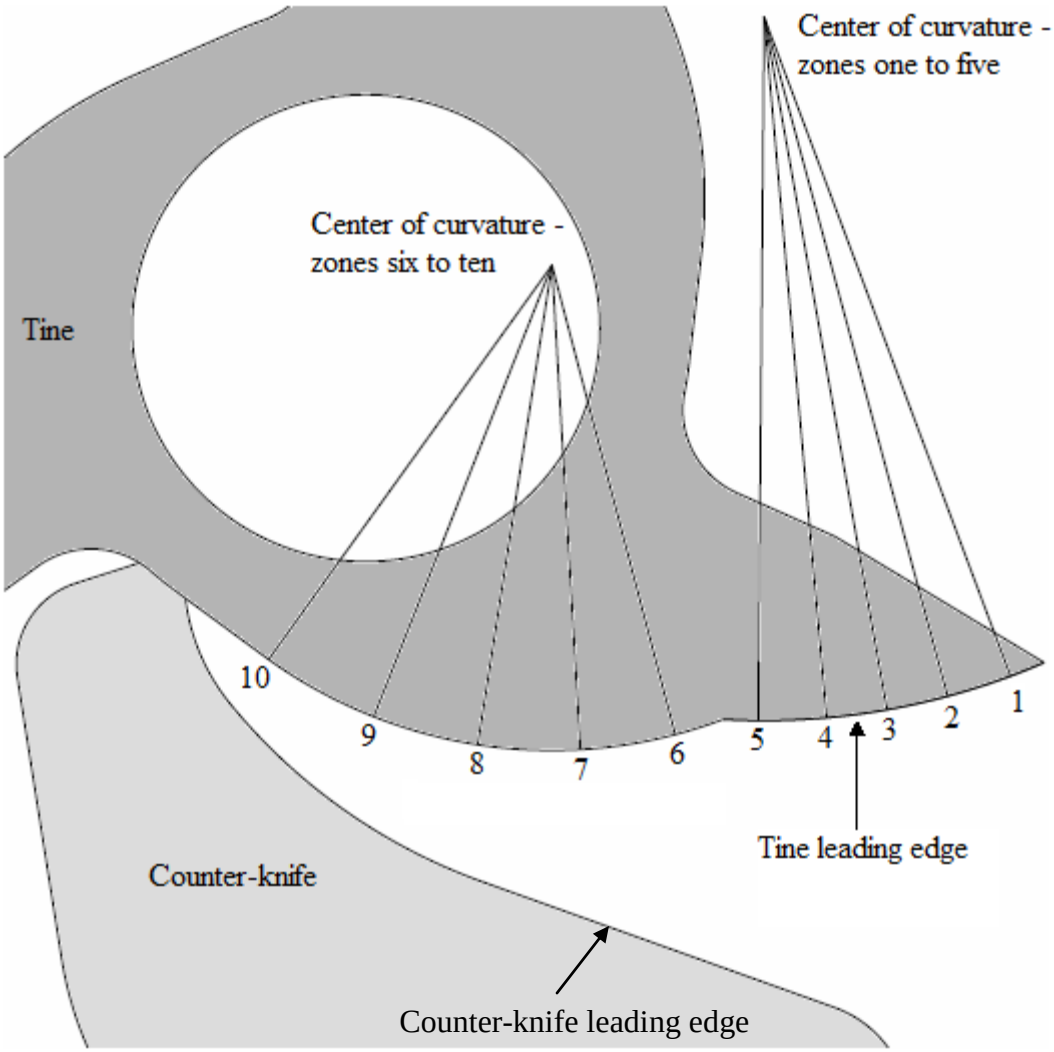

Figure 7.4 Drawing of a side view of the RFCS showing the center of curvature of the tine leading edge in zones one to ten.

The frictional force $F_{f_{m_n}}$ acted perpendicular to the $F_{cs_{m_n}}$, and in a direction that opposed the movement of plant material along the leading edge of the tine. It was assumed that the centrifugal force caused the plant material to move away from the center of rotation of the rotor. Therefore, the frictional force, caused by the plant material sliding along the leading edge of the tine was in a direction that opposed the rotation of the rotor. It was assumed that the bearing supporting the rotor was ideal and therefore the torque required to spin the rotor was not affected by the rotor's radial load. The torque

that must be applied to the rotor to compress, cut and overcome the friction force between the plant material and the leading edge of the tine in the n^{th} zone was found using the following equation,

$$T_{m_n} = \left(F_{cs_{m_n}} Sin\zeta_n + F_{f_n} Cos\zeta_n\right) r_n \,, \qquad (\mathbf{7.17})$$

where:

T_{m_n} is the torque that must be applied to the rotor to compress, cut and overcome the friction force between the plant material and the leading edge of the tine in the n^{th} zone of the m^{th} cut (N·m) and

ζ_n is the angle between the radial unit vector (which has an origin at the midpoint of the zone on the leading edge of the tine and is directed to the axis of rotation of the rotor) and $F_{cs_{m_n}}$ in the n^{th} zone (°).

As an example, $F_{f_{m_n}}$, $F_{cs_{m_n}}$, ζ_n and the radial and tangent unit vectors ($\hat{r}$ and $\hat{t}$, respectively) are shown in Figure 7.5 for zone 1.

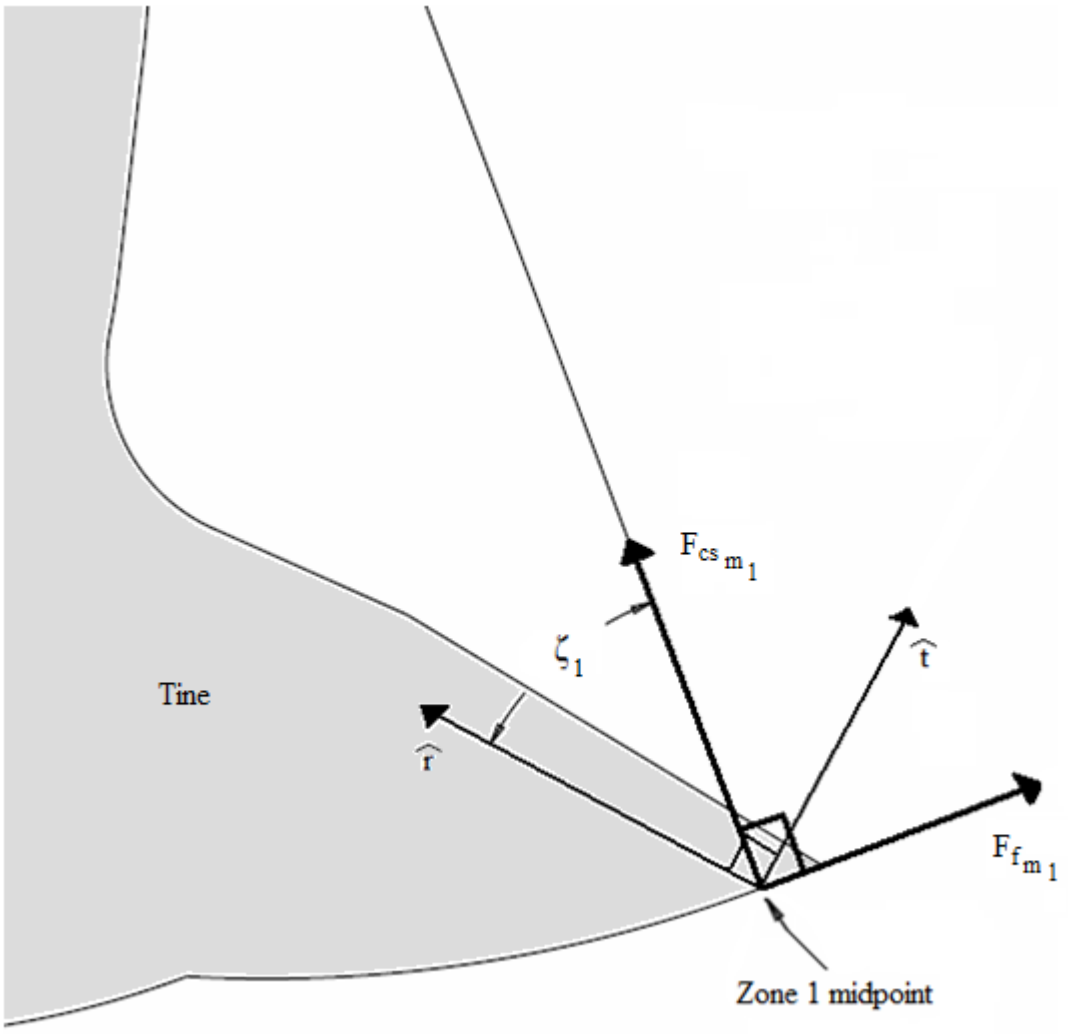

Figure 7.5 Drawing of a side view of the RFCS showing the direction of the radial, $\hat{r}$, and tangent, $\hat{t}$, unit vectors at the midpoint of zone 1, the direction of the force to compress and cut plant material in zone 1, $F_{cs_{m_1}}$, the frictional force caused by plant material sliding along the leading edge of the tine in zone 1, $F_{f_{m_1}}$, and the angle between the radial unit vector and the $F_{cs_{m_n}}$, ζ_1.

The power required by the rotor to compress, cut and overcome the frictional forces on the leading edge of the tine in the n^{th} zone for the m^{th} cut was determined using the following equation,

$$P_{cs_{m_n}} = T_{m_n} N \quad (7.18)$$

where :

$P_{cs_{m_n}}$ is the power required to compress, cut and overcome the frictional force between the plant material and the leading edge of the tine in the n^{th} zone for the m^{th} cut (W) and

N is the rotational speed of the rotor (rad/s).

The power required to compress, cut and transport the plant material along the leading edge of the tine was discussed in this section. The power required to transport plant material along the side of the counter-knife will be discussed in the following section.

7.1.6 Transport power (plant material along the side of a counter-knife in the n^{th} zone for the m^{th} cut)

Footage from a high-speed camera recorded during the completion of the LSCP laboratory trials revealed that plant material was squeezed between the tine pairs (the tine pairs are shown in Figure 4.1) and slid along the sides of the counter-knives. The force required to slide plant material along the sides of the counter-knife only occurred when the counter-knife was between the tine pair. The angular position of the rotor when the counter-knife protrudes between the tine pair was not the same for all zones. Thus the frictional force caused by sliding plant material along the sides of the counter-knife was defined on a per zone basis. The frictional force caused by sliding plant material along the sides of a counter-knife in the n^{th} zone of the m^{th} cut was found using the following equation,

$$F_{t_{m_n}} = P_{m_n} \mu, \quad (7.19)$$

where:

$F_{t_{m_n}}$ is the frictional force acting on the tine in the n^{th} zone for the m^{th} cut (N) and

P_{m_n} is the compressive force caused by plant material between the tine pair and the sides of the counter-knife in the n^{th} zone of the m^{th} cut (N).

It was assumed that compressive force P_{m_n}, caused by the presence of the material between the sides of a counter-knife and tine pair was proportional to the initial depth of plant material, lo_m. The compressive force, P_{m_n} is given by,

$$P_{m_n} = \begin{cases} P_f lo_m, & \theta + \alpha_n > \gamma_n \; and \; \theta < \lambda_n \\ 0, & else \end{cases}, \quad (\mathbf{7.20})$$

where:

P_f is the coefficient that relates the initial depth of plant material to the compressive force caused by plant material between the sides of a counter-knife and the tine pair (N/m).

It was assumed that the compressive force, P_{m_n}, only acts when two constraints were met. First, the leading edge of the tine in the n^{th} zone has to be past the leading edge of the counter-knife in n^{th} zone. The first constraint can be written as,

$$\theta + \alpha_n > \gamma_n \quad (\mathbf{7.21}).$$

Second, the lagging edge of the tine in the n^{th} zone has not yet passed the lagging edge of the counter-knife in the n^{th} zone. The second constraint can be written as,

$$\theta < \lambda_n \quad (\mathbf{7.22}).$$

The angles θ, α, and γ for zone 1 are shown in Figure 7.3. The angle between the model datum and the lagging edge of the counter-knife in the n^{th} zone is represented by, λ_n. The angle at which the rotor tine will pass the counter knife in zone 1, λ_1, is shown in Figure 7.6. It was assumed that the frictional force, $F_{t_{m_n}}$, acted at the midpoint radius of the n^{th} zone tangent to the axis of rotation of the rotor and in a direction that resisted the rotation of the rotor.

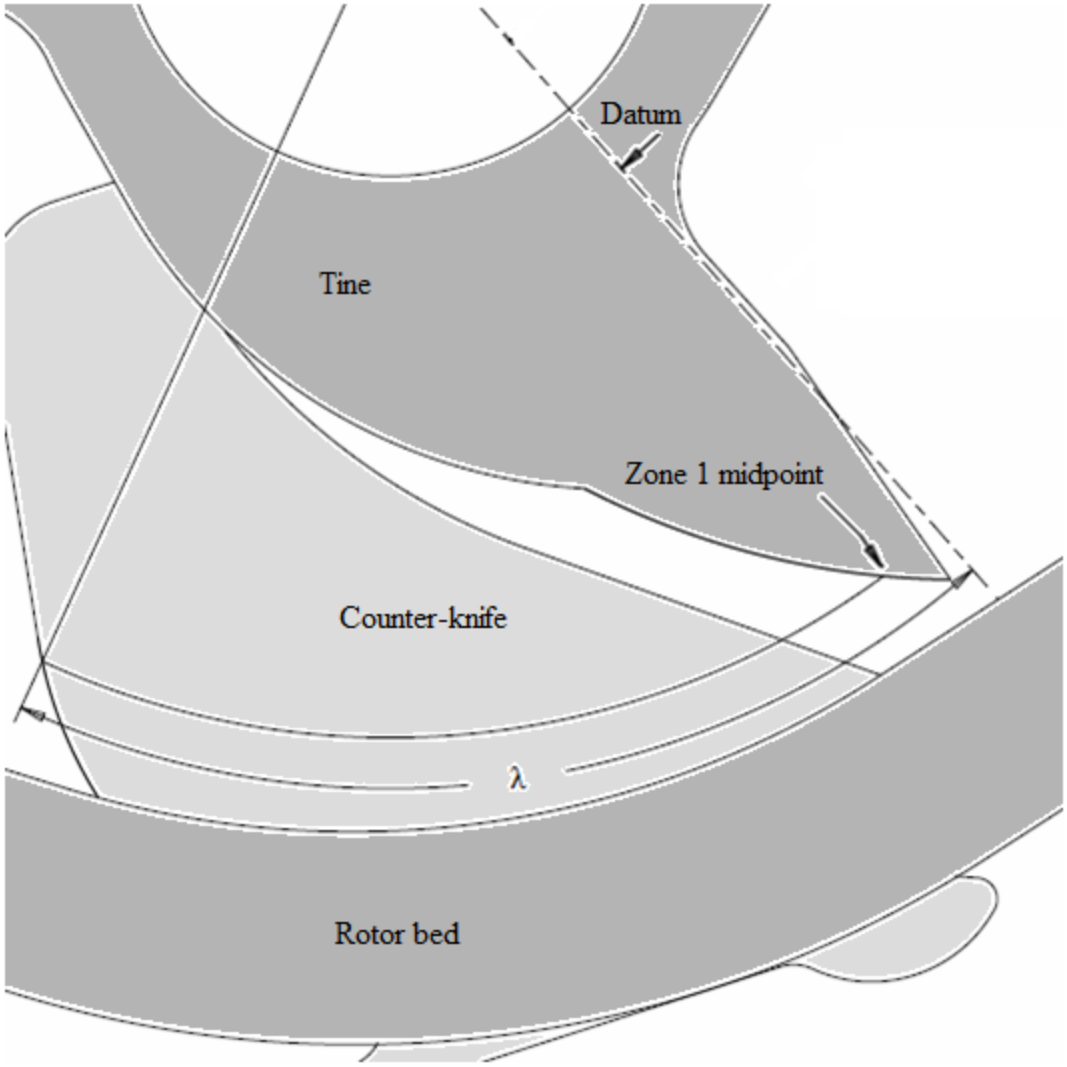

Figure 7.6 The angle between the datum and the lagging edge of the counter-knife in zone 1, λ_1.

The torque that needed to be applied to the rotor to overcome the frictional force to transport plant material along the sides of the counter-knife in the n^{th} zone of the m^{th} cut was found using the following equation,

$$T_{t_{m_n}} = F_{t_{m_n}} r_n, \qquad \textbf{(7.23)}$$

where:

$T_{t_{m_n}}$ is the torque the must be applied to the rotor to overcome the frictional force of sliding plant material along the sides of a counter-knife in the n^{th} zone for the m^{th} cut (N·m).

The power required to transport plant material along the sides of a counter-knife in the n^{th} zone of the m^{th} cut was found using the following equation,

$$P_{t_{m_n}} = T_{t_{m_n}} N, \quad (7.24)$$

where:

$P_{t_{m_n}}$ is the power required to overcome the frictional force of sliding plant material along the sides of a counter-knife in the n^{th} zone of the m^{th} cut (W).

The zone-dependent power demand of the RFCS has been completely defined. The power required to transport plant material along the side of a counter-knife, compress and cut plant material between the leading edge of a tine and counter-knife and transport plant material along the leading edge of a counter-knife are all zone dependent. The power required to transport plant material along the rotor bed was not zone dependent. The power required to transport material along the rotor bed will be discussed in the next section.

7.1.7 Transport power (plant material along the rotor bed)

The power required to transport material along the rotor bed was determined by quantifying the frictional forces between the rotor bed and plant material. The normal force between the plant material and rotor bed was determined using the following equation,

$$F_{rb} = m\frac{v^2}{R}, \quad (7.25)$$

where:

F_{rb} is the normal force of the material on the rotor bed (N),

m_{wet} is the mass of plant material (kg),

v is the velocity of plant material tangential to the radius of curvature of the rotor bed (m/s) and

R is the radius of curvature of the rotor bed (m).

The frictional force between the plant material and rotor bed was determined using the following equation,

$$F_{f_{rb}} = F_{rb}\mu, \quad \textbf{(7.26)}$$

where:

$F_{f_{rb}}$ is the frictional force between the plant material and the rotor bed (N).

The velocity of plant material along the rotor bed was not known. The average peripheral speed of the RFCS was used as a reasonable approximation of the speed of the plant material along the rotor bed. The velocity of the plant material along the rotor bed was approximated using the following equation,

$$v = Nr_5, \quad \textbf{(7.27)}$$

where:

r_5 is the midpoint radius of the 5th zone (m).

By definition power as,

$$P_{wr} = \frac{F*d}{t}, \quad \textbf{(7.28)}$$

where:

P_{wr} is the power required to transport a given body (W),

F is force required to transport the body (N),

d is distance the body is moved (m) and

t is the period of time in which the body is moved (s).

The power required to transport plant material along the rotor bed was found by combining equations (7.25), (7.26), (7.27) and (7.28) and replacing, *d*, with the rotor bed arc length, l_{rb}, and *m/t* with throughput, *T*. The power required to transport plant material along the rotor bed was determined using the following equation,

$$P_{rb} = \frac{T\,(Nr_5)^2 \mu l_{rb}}{R}, \qquad \textbf{(7.29)}$$

where:

P_{rb} is the power required to transport plant material along the rotor bed (W),

T is the throughput (on a wet-mass basis) of plant material (kg/s) and

l_{rb} is the rotor bed arc length (m).

The rotor bed radius of curvature, *R*, and arc length, l_{rb}, are shown in Figure 7.7, and both were quantified by the geometry of the RFCS. The total power requirements of the rotor were determined by summing the power required to compress and cut plant material between the leading edge of all tines and counter-knives, transport plant material along the leading edge of all tines, transport plant material along the sides of all the counter-knives, transport plant material along the rotor bed and spin the rotor without crop flow. The method used to determine the total power requirements of the RFCS will be discussed in the following section.

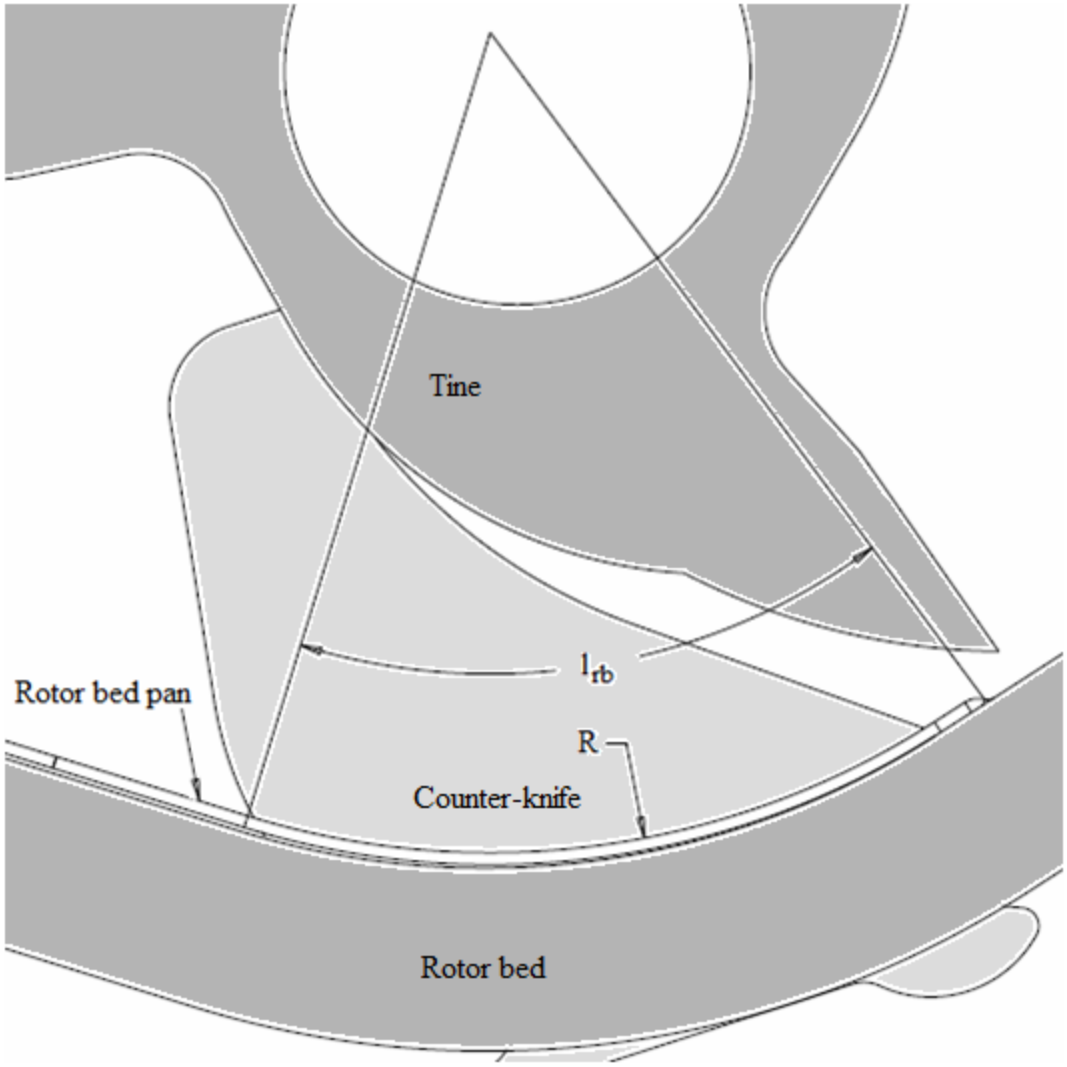

Figure 7.7 Drawing of a side view of a rotor tine, counter-knife and the rotor bed which shows the rotor bed radius of curvature, R, and the rotor bed arc length, l_{rb}.

7.1.8 Total power required by the RFCS

The total power demand of the RFCS was determined by summing the power required to compress, cut and transport plant material along the leading edge of all tines, the power to transport the plant material along the sides of all counter-knives, the power to transport plant material along the rotor bed and the power to spin the rotor without crop flow. A visual basic program was written to quantify the total power demand of the RFCS. A series of five loops in the visual basic program were used to sum the power

demand of the RFCS and create a model output that was a function of the rotor's angular position.

The five loops that were used to quantify the power demand of the RFCS and create the desired model output were titled: Angle, Zone, Cut, **V** to **Z** transfer and **Z** to **P** transfer. The matrices **V** and **Z** were used to store intermediate calculations while the matrix **P** was used to store the model output. The "Angle" loop was nested within the "Zone" loop and the "Zone" loop was nested within the "Cut" loop. The **V** to **Z** "Transfer" loop was also nested within the "Cut" loop and the **Z** to **P** "Transfer" loop occurred after the "Cut" loop was executed. The deepest nested loop, the "Angle" loop, was used to cycle through the angular position of -80 to 109°. Within this loop both $P_{cs_{m_n}}$ and $P_{t_{m_n}}$ were quantified and temporarily stored in the matrix **V**. The limits of the loop were chosen based upon the following assumptions. First, the lower limit of -80° was selected based on the assumption that the initial depth of material for the m^{th} cut, lo_m, would not exceed 230 mm (based on the current geometry of the tine and counter-knife). Second, the upper limit of 109° was chosen under the assumption the angle between the model datum and the lagging edge of the counter-knife in the n^{th} zone, λ_n, would not exceed 109°, in any of the zones. The "Zone" loop was used to cycle through all ten zones and sum the $P_{cs_{m_n}}$ and $P_{t_{m_n}}$ and, the Cut loop was used to cycle through and sum the $P_{cs_{m_n}}$ and $P_{t_{m_n}}$ for all of the cuts that the RFCS made during one revolution of the rotor. The **Z** matrix was used to temporarily store the power demand of the individual cuts made by the RFCS, while the **P** matrix was used to store the model output. The model output was the sum of the power required for the individual cuts made by the RFCS plus P_{rb} and P_{base} (the power required to spin the rotor without crop flow). The angular offset between tines that cut on adjacent counter-knives, AO_T, needed to be defined to create the **Z** matrix. Further, the angular offset between the model and trial rotor, AO_{MT}, needed to be defined to create the **P** matrix. The flowchart showing the loops used to create the model output for the LSCP RFCS is shown in Figure 7.8. The LSCP Syntax used to create the visual basic LSCP model is given in Appendix D.1.

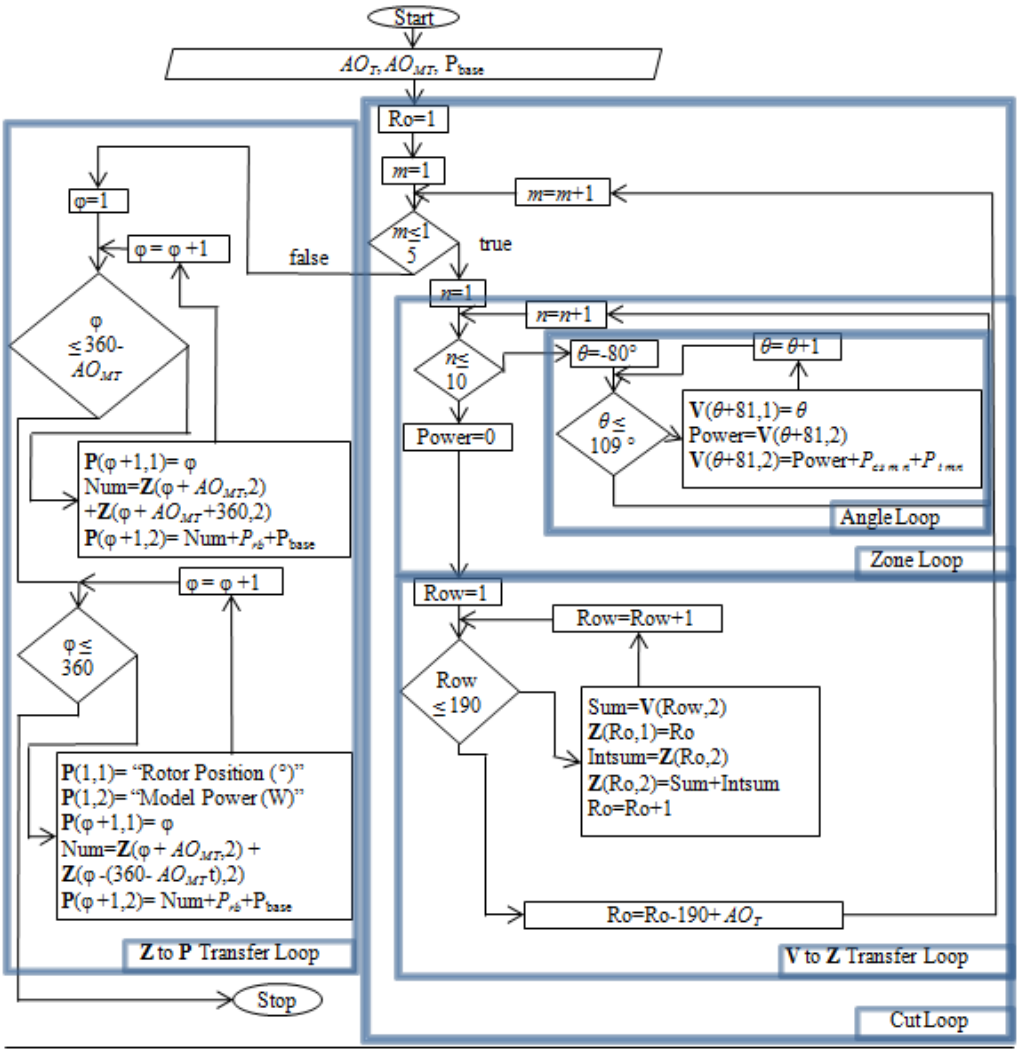

Legend

Num, Sum, Intsum and Power are all intermediate summation variables
Ro is an indexing variable
P_{base} is the power required to spin the rotor without crop flow
P_{rb} is the rotor bed transport power
P_{cutn} is the power required to compress, cut and overcome the frictional force between the plant material and the leading edge of the tine in the n^{th} zone of the m^{th} cut
P_{tmn} is the power required to overcome the friction force of sliding plant material along the sides of a counter-knife in the n^{th} zone of the m^{th} cut
AO_T is the angular offset between the tines that cut on adjacent counter-knives and
AO_{MT} is the angular offset between the model and trial rotor.

Figure 7.8 Flowchart of the visual basic program used to quantify the total power demand of the LSCP RFCS. (θ, n, m, Row and Φ are the index variables used in the Angle, Zone, Cut, **V** to **Z** Transfer and **Z** to **P** Transfer loops, respectively. **V**, **Z** and **P** are all matrices).

The approach taken to develop the LSCP and HSCP analytical models was the same, however there were a few differences between the models. The differences between the two models are attributed to the differing geometry and operational parameters of the two cutting devices. The differences between the two models include the following: the number of cuts made during one revolution of the rotor, the tine geometry, the initial depth of plant material on a pert cut basis, the pattern of tines on the rotor and the angular offset between the model and trial rotor. The difference in the number of cuts made during one revolution of the rotor, the tine geometry, and the angular offset between the trial and model datum could be accounted for with the LSCP analytical model, however the difference in initial depth of plant material on a per cut basis and the pattern of tines on the rotor could not be accounted for with the LSCP analytical model. The ramifications of the differing initial depth of plant material of the two RFCS and the different pattern of tines on the two RFCS is discusses below.

The geometry of the tines used on the HSCP and LSCP RFCS were approximately the same. For a single degree of rotation, the change in position of the midpoint in zone 1 (the zone that is farthest away from the rotational axis of the rotor, and therefore moves the farthest distance for a given angular rotation) was approximately 4 mm. For the LSCP RFCS a 4-mm change in depth was acceptable because, the minimum initial depth of plant material for the lowest throughput tested was estimated at 40 mm. However, the increased width of the HSCP RFCS and the higher rotational speed of the rotor on the HSCP RFCS suggested that the minimum initial depth of plant material would be significantly less in the HSCP RFCS than the LSCP RFCS. The minimum initial depth of plant material, for the lowest throughput tested, in the HSCP RFCS was estimated at 4 mm. To achieve the same ratio between the change in initial depth to the expected minimum initial depth of plant material the power demand of the rotor in the HSCP RFCS was calculated on a 1/40th degree interval size. In order to implement the change of the incremental rotor position, the "Angle" loop of the HSCP model was modified so that the $P_{cs_{m_n}}$ and $P_{t_{m_n}}$ were calculated over the range of -80.5 to 119.5° in 0.025° increments. As with the LSCP RFCS model, it was assumed that the initial depth of plant material would not exceed 230 mm in the HSCP RFCS model, which set the lower limit of the angle loop to -80.5°. The upper limit of the angle loop for the HSCP RFCS model

was not the same value used in the LSCP RFCS model because the orientations of the counter-knives in the two rotary feeding and cutting systems were not the same. The upper limit of the "Angle" loop in the HSCP RFCS model was chosen under the assumption that the lagging edge of the counter-knife, λ_n, would not exceed 119.5° in any of the zones. An additional matrix, **X**, was also created to store the $P_{cs_{m_n}}$ and the $P_{t_{m_n}}$ due to all of the zones and cuts the RFCS made during one revolution. Finally, an additional nested loop was added to the model, the Average loop, in which the values in the **X** matrix were averaged on a per degree basis and stored in the **Z** matrix.

There were 5 tine pairs on the LSCP RFCS rotor into which counter-knives protruded, as shown in Figure 4.1. Thus there were 5 planes (perpendicular to the axis of rotation of the rotor) in which plant material would be cut by the LSCP RFCS. Each tine pair had 3 sets of protrusions (numbered 1, 2 and 3) spaced equally around the circumference of the rotor that worked in concert with a counter-knife to cut plant material. A cut occurred when the leading edge of a tine pair passed the leading edge of the counter-knife which protruded between the tine pair. Therefore, 3 cuts occurred on each counter-knife during each full revolution of the rotor (assuming that there was plant material between the leading edge of the tine pair and the counter-knife). The leading edges of the tine and the counter-knife are shown in Figure 7.4.

The tines on the LSCP RFCS were in a "linear pattern". The planes in which plant material were cut were labeled A through to E, A being the farthest left (when looking at the RFCS from the front). The "linear pattern" means that during one-third of a revolution of the rotor, the order in which the tine leading edges passed the leading edge of a counter-knife were A_1, B_1, C_1, D_1, E_1. The pattern would repeat twice more over a full revolution of the rotor. The angular offset between adjacent tine pairs (A_1 to B_1, B_1 to C_1, C_1 to D_1, D_1 to E_1, $E_1$to A_2 …) was 24°.

Conversely, there were 26 tine pairs on the HSCP RFCS (WR chopper) into which counter-knives protruded, as shown in Figure 4.14 D. Thus there were 26 planes (perpendicular to the axis of rotation of the rotor) in which plant material would be cut by the WR chopper. As with the LSCP RFCS each tine pair on the WR chopper had 3 leading edges (numbered 1, 2 and 3) that were used to cut plant material on the leading

edge of the counter knife. The tines on the WR chopper were in a "V pattern". If the tine pairs were labeled A through Z, A being the farthest left tine pair (when looking at the RFCS from the front) the outside tine pairs, A and Z, were at the same angular orientation. Working from the outside towards the center of the chopper, the tine pairs were at the same angular orientation (the tine pairs at the same angular orientation were A and Z, B and Y…. L and O, M and N). The order in which the tine pairs passed the counter-knives over a one third revolution of the rotor was A_1 and Z_1 (and indicating that the tine pairs pass the counter-knife at the same time), B_1 and Y_1, C_1 and X_1, D_1 and W_1, E_1 and V_1, F_1 and U_1, G_1 and T_1, H_1 and S_1, I_1 and R_1, J_1 and Q_1, K_1 and P_1, L_1 and O_1, M_1 and N_1. The pattern would repeat twice more over a full revolution of the rotor. The angular offset between the adjacent tine pairs, for example A_1 and B_1, was 8° and the angular offset between the tine pairs located at the center and end of the chopper, for example N_1 (or M_1) and Z_2 (or A_2) was 24°.

To address the differences between the tine pair pattern of the HSCP RFCS the following modifications were made to the LSCP model. Instead of a single AO_T value in the LSCP model two AO_T values were defined for the HSCP model, AO_T and AO_{T2}. AO_T was used to identify the angular offset between the tines that cut on adjacent counter-knives and, AO_{T2} was used to identify the angular offset between the tines on the center and end of the rotor. Two conditional statements were added to the model, one immediately before both "Angle" loops and the other after one of the "Angle" loops. The flowchart showing the loops used to create the model output for the HSCP RFCS is shown in Figure 7.9. The HSCP syntax used to create the visual basic HSCP model is given in Appendix D.2.

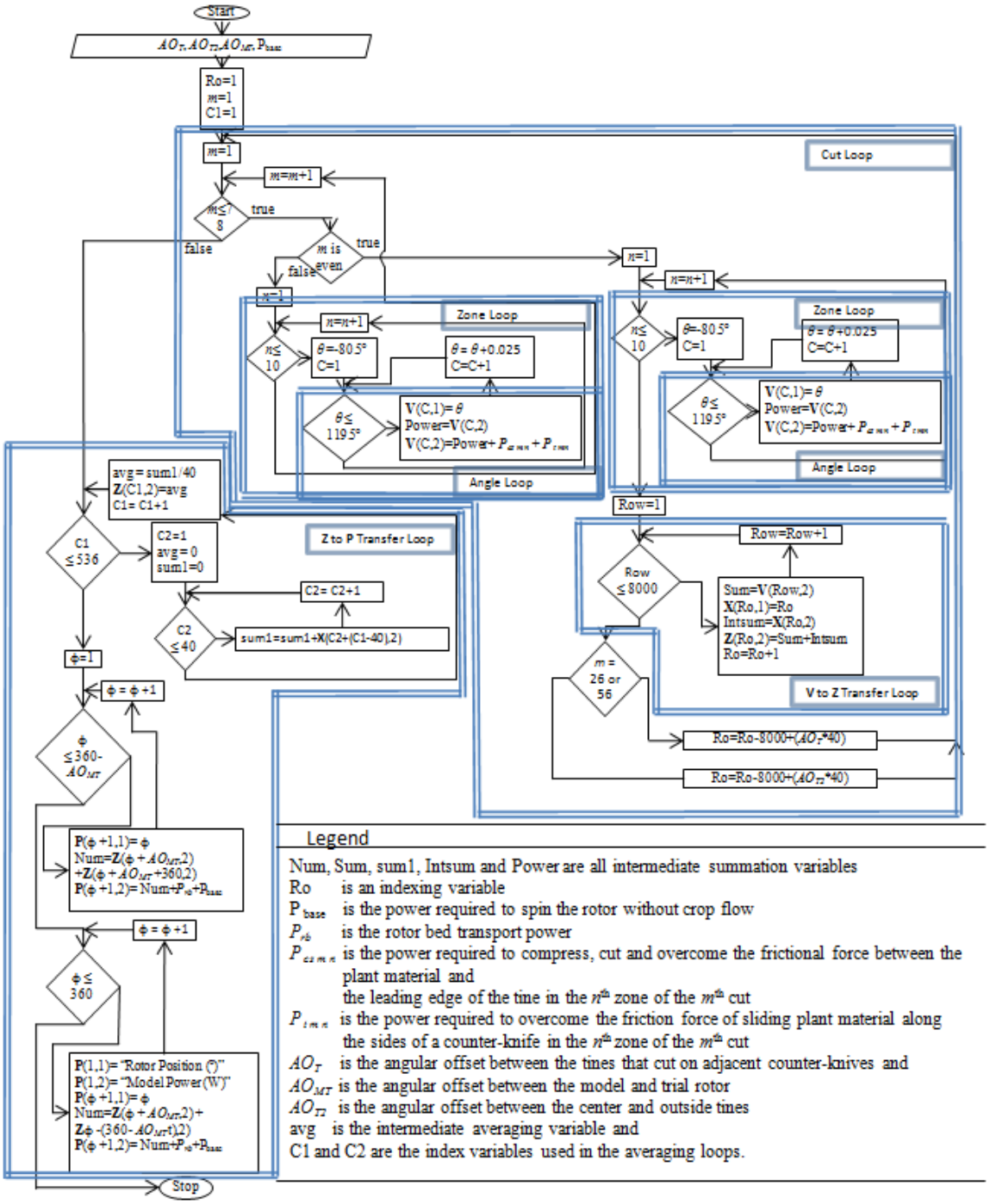

Figure 7.9 Flowchart of the visual basic program used to quantify the total power demand of the HSCP RFCS. (θ and C are indexing variables used in the Angle loop. *n*, *m*, Row and Φ are the index variables used in the Zone, Cut, **V** to **Z** Transfer and **Z** Transfer and **Z** to **P** Transfer loops, respectively. **V**, **Z**, **P** and **X** are matrices).

7.1.9 Summary

The analytical model was developed by quantifying the power required to compress, cut and transport the plant material with the RFCS. A series of zones were defined because the compression and cutting stages of the plant material was a function of the location of the plant material with respect to the axis of rotation of the rotor. The power required to compress, cut and transport plant material along the leading edge of a tine as well as the power required to transport the plant material along the side of a counter-knife was defined on a per zone basis for each cut made by the RFCS. The total power demand of the RFCS was found by summing the power demand of each zone of each cut made by the RFCS plus the power to transport the plant material along the rotor bed and the power to spin the rotor without crop flow. The assumptions that were made to develop the model were:

- the cutting process was divided into 3 distinct phases, the plant material was compressed, then it was cut and finally it was transported out of the RFCS,
- the plant material was cut between the counter-knives and the tines,
- the gravitational force acting on the plant material forced the plant material to be in contact with a counter-knife, before it was in contact with a tine,
- the plant material being compressed by the RFCS followed Hooke's Law,
- the width of compression, w, was assumed to be a function of counter-knife sharpness,
- the initial depth of material, lo_m, was equal across all ten zones for the m^{th} cut,
- lo_m was proportional to the throughput of plant material through the RFCS,
- initial depth of material for the m^{th} cut made by the RFCS, lo_m, would not exceed 230 mm,
- the plant material was cut prior to or once the leading edge of a tine passed the leading edge of a counter knife,
- the relationship between maximum shear strength and dry-mass density was linear,
- the density of the plant material when it was cut was linearly related to the initial depth of plant material, lo_m,

- the shear area, A_{sm}, was constant for a given plant material and a function of the counter-knife sharpness,
- when plant material was in contact with the tine, the plant material was always sliding along the leading edge of the tine, and the centrifugal force caused the plant material to move away from the center of rotation of the rotor,
- the bearings supporting the rotor were ideal and therefore the torque required to spin the rotor was not affected by the rotor's radial load,
- the force to compress, cut and transport the plant material along the leading edge of the tine, $P_{cs_{m_n}}$, in the n^{th} zone acted at the midpoint of n^{th} zone on the tine leading edge, and through the center of curvature of the tine leading edge in the n^{th} zone,
- the angle between the lagging edge of the counter-knife and the model datum, λ_n, would not exceed 109 and 119.5° in any of the zones for the LSCP and HSCP rotary feeding and cutting systems, respectively,
- the dynamic coefficient of friction between the plant material and the RFCS was a function of the plant material type and plant material moisture content,
- the frictional force caused by sliding plant material along the side of a counter-knife, $P_{t_{m_n}}$ was linearly related to the initial depth of plant material, lo_m, and a function of the type of plant material, and
- the frictional force caused by sliding plant material along the side of a counter-knife, $P_{t_{m_n}}$, acted at the midpoint of the n^{th} zone.

The parameters of the analytical model were separated into three categories, Global, Material and Zone-dependent Inputs. A complete list of the model input parameters, their symbol, description and unit of measure is given in Table 7.1.

Table 7.1 The analytical model input parameters, their symbol, description and unit of measure.

Symbol	Description	Units
	GLOBAL INPUTS	
N	Rotor rotational speed	rpm
T	Throughput	kg/s
w	Compression width	m
l_{rb}	Rotor bed arc length	m
R	Rotor bed radius of curvature	m
A_{sm}	Cross-sectional area of the material when it was cut	m^2
ρ	Coefficient that relates the dry-mass density of plant material to the initial depth of plant material	$(kg\ m^{-3})m^{-1}$
Pf	Coefficient that relates the initial depth of plant material to the compressive force caused by plant material between the side of a counter-knife and the tine pair	N/m
P_{base}	Power required to spin the rotor without crop flow	W
AO_T	Angular offset between adjacent tine pairs	°
AO_{T2} *	Angular offset between the center and side tine pairs	°
AO_{MT}	Angular offset between model and trial rotor	°
	PLANT MATERIAL INPUTS	
μ	Dynamic coefficient of friction	--
τ_{slope}	Slope of maximum shear strength	$kPa\ (kg\ m^{-3})^{-1}$
τ_{int}	Intercept of maximum shear strength	kPa
a	Young's modulus coefficient 0	kPa
a_1	Young's modulus coefficient 1	kPa
a_2	Young's modulus coefficient 2	kPa
a_3	Young's modulus coefficient 3	kPa
lo_m	Initial depth of plant material for the m^{th} cut	m
	ZONE-DEPENDENT INPUTS	
δ_n	Arc length of tine in the n^{th} zone	m
r_n	Midpoint radius in the n^{th} zone	m
γ_n	Angle between datum and leading knife edge in the n^{th} zone	°
α_n	Angle between leading and lagging edge of tine in the n^{th} zone	°
ζ_n	Angle between the radial unit vector and compressive/cutting force in the n^{th} zone	°
λ_n	Angle of the rotor when the tine passes the counter knife in the n^{th} zone	°

*****only for the HSCP analytical model.

7.1.10 Parameter quantification

The parameters listed in Table 7.1 fell into two categories, measurable and indeterminate parameters. The indeterminate parameters were w, A_{sm}, ρ, P_f and lo_m. The A_{sm} and ρ were indeterminate because no sensor currently exists that could be used to directly measure the parameters. Currently, sensors do exist that can be used to measure pressure and length, the parameters that needed to be measured to quantify w, P_f and lo_m. However, the sensors used to quantify w, P_f and lo_m would have been quickly damaged during operation of the RFCS because of the location in which the sensors needed to be mounted. The indeterminate parameters were quantified by minimizing the sum of squared error between the model output and a subset of the trials data collected with both the LSCP and HSCP RFCS test apparatuses. The way in which the measurable and indeterminate parameters were quantified is discussed below.

The plant material input parameters (the dynamic coefficient of friction, Young's modulus and maximum shear strength) were quantified with the material properties test stand which was described in section 4.3. The procedure used to quantify the material properties parameters is detailed in Appendix B. The geometric parameters: l_{rb}, R, AO_T, AO_{T2} and all of the zone-dependent input parameters were quantified with 3D CAD models of both the LSCP and HSCP RFCS. The throughput and rotor speed were both controlled and measured during the experiments completed with both the HSCP and LSCP RFCS. The way in which the throughput was measured in the HSCP and LSCP RFCS was discussed in detail in section 4.2 and 5.1.1, respectively. Similarly, the way the speed of the rotor was measured in the HSCP and LSCP RFCS was discussed in detail in section 4.2 and 4.1, respectively. P_{base} was determined for each of the RFCS tested. P_{base} for the LSCP test apparatus was determined during each trial, because the data logging event started before the plant material had entered the RFCS and finished after the plant material had passed through the RFCS. For the HSCP test apparatus, P_{base} was determined by recording the speed and torque of the chopper without crop flow during separate trials. AO_{MT} was quantified by identifying the angle that the rotor in the analytical model needed to be rotated to line it up with the absolute zero position (defined by the Z channel on the optical encoded attached to the rotor) of the rotor on the HSPC and LSCP RFCS test apparatus.

In this section the development of both the LSCP and HSCP RFCS analytical models was discussed. In the following sections, the discussion of the LSCP and HSPC analytical models has been separated. For both models, the input parameters, the model validation and the sensitivity analysis will be discussed.

7.2 Low Speed Cutting Process (LSCP)

Based on the conclusions drawn from the LSCP RFCS laboratory trials, presented in chapter 5, the specific energy requirements of the LSCP RFCS were significantly affected by counter-knife sharpness, serrations, thickness and bevel angle. Although counter-knife bevel angle, serrations and thickness were found to have a significant effect on the specific energy requirements of the RFCS, they were not included as parameters in the analytical model. Bevel angle was not included as an input parameter because the bevel angle on the counter-knives is already in the optimum range of values indicated by Chancellor (1988), Persson (1987) and Ige et al. (1976). Counter-knife thickness was not included as an input parameter because the use of counter-knives that were thinner than 5-mm in an industrial cutter was unacceptable by manufacturing design standards, due to their lack of robustness. Counter-knife serrations were not included in the model because there is a tendency in industry to use serrated counter-knives as they do not wear as fast and therefore remain sharper for a longer period of use. Counter-knife sharpness was included in the analytical model, because it is common for industrial cutters to have varying levels of counter-knife sharpness (new counter-knives are sharp but with use the counter-knives become dull). It was assumed that counter-knife sharpness affected w, and A_{sm}. Throughput did not have a significant effect on the specific energy requirements of the RFCS however, the power demand of the RFCS was affected by the throughput of both alfalfa and cereal straw. Throughput was assumed to affect the power required to transport the plant material along the rotor bed, P_{rb}, and it was assumed that the initial depth of plant material, lo_m, was affected by throughput. Alfalfa moisture content had a statistically significant effect on the specific energy requirement of the RFCS, however the magnitude of the effect was relatively small and therefore the model validation was completed at only one level of alfalfa moisture content. Based on the conclusions drawn from the LSCP RFCS laboratory trials, and to make the model applicable to the RFCS

currently used in industry, the trial data that were used to quantify the indeterminate parameters and validate the model were from the trials completed with 5-mm thick counter-knives that were both serrated and beveled and used to process alfalfa (at a moisture content of 53% w.b.) and cereal straw (at a moisture content of 8.9% w.b.).

Before the LSCP RFCS analytical model could be validated, the input parameters were quantified. The input parameters have been separated into two categories, the input parameters that could be measured during the laboratory trials, the measurable parameters, and the indeterminate input parameters (or the input parameters that could not be measured during the laboratory trials). Once the input parameters were quantified the model output was compared to a different subset of the trial data to show how well the model predicted the measured power demand of the RFCS. In the following section, the quantification of the input parameters of the analytical model will be discussed.

7.2.1 Input parameter quantification

Measurable input parameters: The plant material properties of both cereal straw and alfalfa were quantified using the material properties test stand, which was described in section 4.3. As identified in the analytical model development section, the plant material properties of interest were Young's modulus, dynamic coefficient of friction between the plant material and steel and the maximum shear strength of the plant material. The procedure used to quantify the plant material properties is described in Appendix B. The alfalfa that was processed with the material properties test stand was obtained from the same source (and at the same time) as the alfalfa that was processed with the LSCP RFCS. It was believed that the material properties of the alfalfa would change with time, because the alfalfa was actively growing when it was cut in the field. Thus, the plant material was processed with the LSCP RFCS and the material properties test stand as close to the same time as possible. This was done to ensure that the material properties of the alfalfa processed by the LSCP RFCS were the same as the material properties quantified with the material properties test stand. The cereal straw processed by the LSCP RFCS and the material properties test stand were not obtained from the same field. However, the same variety and moisture content of cereal straw were processed by both the LSCP RFCS and the material properties test stand. Because the cereal straw had

senesced and had dried prior to processing, it was assumed that the material properties of the cereal straw would not change with time. Thus, even though the cereal straw was not obtained from the same field it was believed that the cereal straw processed by the LSCP RFCS and the material properties test stand had the same material properties.

A total of five replicates were completed with the material properties test stand to quantify the Young's modulus of alfalfa and cereal straw. An average stress-strain curve was created from the five replicates for each material type. The average stress-strain curve was used to define a third-order polynomial which related the Young's modulus of the plant material to strain. The coefficients of the polynomials were quantified by minimizing the sum of squared error between the measured stress-strain curve and the stress-strain curve created from the polynomial. The average and modeled stress-strain curve for alfalfa and cereal straw is shown in Figure 7.10. The equation that describes the relationship between the Young's modulus of alfalfa and strain is,

$$E_a = 416{\varepsilon_a}^3 - 394{\varepsilon_a}^2 + 99\varepsilon_a \,, \qquad \textbf{(7.30)}$$

where:

E_a is the Young's modulus of the alfalfa processed by the RFCS (kPa) and

ε_a is the strain experienced by the alfalfa.

The equation that describes the relationship between the Young's modulus of cereal straw and strain is,

$$E_s = -484{\varepsilon_s}^3 + 1097{\varepsilon_s}^2 - 496\varepsilon_s + 65 \,, \qquad \textbf{(7.31)}$$

where:

E_s is the Young's modulus of the cereal straw processed by the RFCS (kPa) and

ε_s is the strain experienced by the cereal straw.

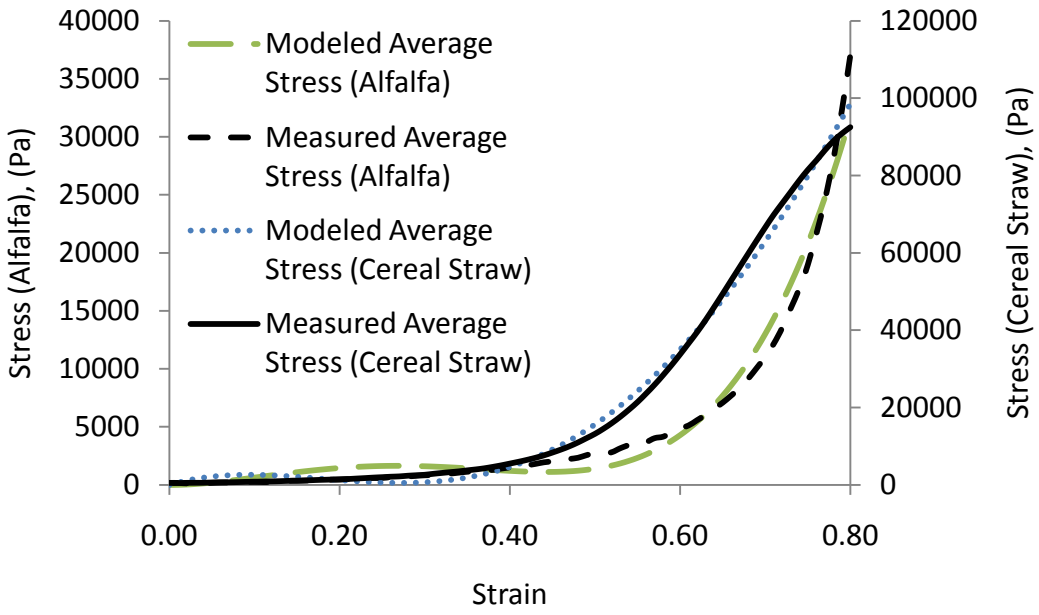

Figure 7.10 Comparison of the average measured stress-strain relationship and the modeled stress-strain relationship of alfalfa and cereal straw.

Previously reported research indicated that the Young's modulus of alfalfa was in the range of 0.79 to 3.99 GPa (Galedar et al., 2008). It is important to note that the value reported by Galedar et al. (2008) was for an individual stem of alfalfa. The bulk Young's modulus of alfalfa and cereal straw was quantified with the material properties test stand. The reason that the bulk Young's modulus was quantified was to account for plant material interaction, which occurs in the RFCS. Using the secant method (with a strain of 0.8), the bulk Young's modulus of alfalfa measured with the material properties test stand was 46.3 kPa, which is substantially lower than the values reported by Galedar et al. (2008). The previously reported research indicated that the Young's modulus of cereal straw was in the range of 0.33 to 6.59 GPa (Tavakoli et al., 2009 and O'Dogherty et al., 1995). It is important to note that the range of values reported by Tavakoli et al. (2009) and O'Dogherty et al. (1995) was for an individual stem of cereal straw. Using the secant method (with a strain of 0.8), the bulk Young's modulus of the cereal straw measured with the material properties test stand was 116.0 kPa, which is substantially lower than the values reported by Tavakoli et al. (2009) and O'Dogherty et al. (1995).

The lower bulk Young's modulus (for both cereal straw and alfalfa) was likely due to the voids between the individual stems of the plant material, which simultaneously increase the initial volume of the plant material and decrease the resistance to deformation, which had a combined effect of decreasing the stress required to achieve a given level of strain.

A total of five replicates were used to quantify the dynamic coefficient of friction between cereal straw & steel and alfalfa & steel. The dynamic coefficient of friction between cereal straw and steel, quantified by the material properties test stand, was slightly lower than the values previously reported in literature. The average coefficient of friction between cereal straw and steel was 0.26 at an average moisture content of 8.9% w.b. Richter (1954) found that the dynamic coefficient of friction of chopped straw ranged from 0.28 to 0.33, however the moisture content of the material during testing was not documented. Likely the moisture content of the chopped straw processed by Richter (1954) was slightly higher than 8.9% w.b., which would cause the dynamic coefficient of friction to be higher than the value quantified with the material properties test stand. The dynamic coefficient of friction between alfalfa and steel, quantified by the material properties test stand, was slightly higher than the values previously reported in literature. The average coefficient of friction between alfalfa and steel was 0.66 at an average moisture content of 54.0% w.b. Shinners et al. (1991) found that the dynamic coefficient of friction between alfalfa and steel was 0.53 at a moisture content of 54.0% w.b. According to ASABE D251.2 (ASABE Standards, 2008) the dynamic coefficient of friction between alfalfa and steel was 0.60 at a moisture content of 53.0% w.b. The differences in the values reported in literature and the value found with the material property test stand could be due to the slight differences in the surface preparation of the steel surface on which the plant material was slid.

The bulk maximum shear strengths of alfalfa and cereal straw were determined at two levels of dry-mass density, with five replicates at each of the dry-mass densities tested. The relationship between maximum shear strength (for both cereal straw and alfalfa) and dry-mass density followed the trend established by previous research; the bulk maximum shear strength had a direct relationship with dry-mass density. The average bulk maximum shear strength of alfalfa and cereal straw at two levels of dry-mass density is

given in Table 7.2. The linear equation that was used to describe the relationship between dry-mass density and shear strength for alfalfa (using the data from Table 7.2) was,

$$ms_a = \rho_{dm_a} 5.0 \times 10^{-3} + 3.34 \quad \textbf{(7.32)}$$

where:

ms_a is the maximum shear strength of alfalfa (MPa) and

ρ_{dm_a} is the dry-mass density of the alfalfa (kg/m^3).

The linear equation that was used to describe the relationship between dry-mass density and shear strength for cereal straw (using the data from Table 7.2) was,

$$ms_s = \rho_{dm_s} 30.0 \times 10^{-3} + 2.16 \quad \textbf{(7.33)}$$

where:

ms_s is the maximum shear strength of cereal straw (MPa) and

ρ_{dm_s} is the dry mass-density of the cereal straw (kg/m^3).

Table 7.2 The average bulk maximum shear strength of alfalfa and cereal straw at two levels of dry-mass density.

Material type	**Dry-mass density (kg/m^3)**	**Shear strength (kPa)**
Alfalfa	14.3	3420
	40.0	3554
Cereal Straw	30.0	3058
	90.0	4853

Bright and Kleis (1964) found the relationship between the bulk maximum shear strength and dry-mass density had a slope of 44 MPa (kg m^{-3})$^{-1}$ and an intercept of 0.87 MPa. The difference between the values reported by Bright and Kleis (1964) and the one found with the material properties test stand was likely attributed to the storage period of the alfalfa. The value reported by Bright and Kleis (1964) was for alfalfa after a 3 month

storage period however the value quantified with the material properties test stand was determined using fresh cut alfalfa (processed the same day it was cut from the field).

O'Dogherty et al. (1989) found that the mean ultimate shear strength was in the range of 5.39 to 6.98 MPa for five varieties of winter wheat and was equal to 8.53 MPa for spring wheat with a moisture content that ranged from 10.0 to 15.0% w.b. The values at which O'Dogherty arrived for the maximum shear strength was based on data obtained from shearing individual stems of wheat. O'Dogherty (1995) found that the shear strength of individual wheat stems at varying positions along the length of the stem at maturity ranged from 4.91 to 7.26 MPa. At a dry mass density of 90 kg/m^3, the maximum shear strength of cereal straw was 4.85 MPa, which was slightly lower than the value reported by O'Dogherty et al. (1989) but within the range of values reported by O'Dogherty (1995). The difference in the values was likely attributed to the method used to quantify the maximum shear strength. O'Dogherty et al. (1989) and O'Dogherty (1995) quantified the maximum shear strength of individual stems while the material properties test stand was used to quantify the bulk maximum shear strength.

The rotational speed of the rotor and the throughput of plant material were both measured and controlled during the experiments completed with the LSCP RFCS. The rotational speed of the rotor was measured with an optical encoder during the trials, and the throughput of plant material was measured by placing a known mass of plant material on the conveyor (that was used to feed the LSCP RFCS) that traveled at a constant speed. A more detailed description of how the rotor speed was measured and controlled was given in section 4.1 and a more detailed description of how throughput was quantified and controlled was given in section 5.1.1. The power required to spin the rotor without crop flowing through the RFCS, P_{base} was measured on a per trial basis and averaged across all trials. The angular offset between the model and trial rotor was quantified by measuring the angle of rotation required to line the trial data rotor up with the model rotor. The rotor bed arc length and radius of curvature, the angular offset between adjacent tine pairs as well as all of the zone-dependent inputs were quantified by measuring the geometry of the LSCP RFCS. The zone-independent model input

parameters are given in Table 7.3 and the zone-specific input parameters are given in Table 7.4.

Table 7.3 Measurable zone-independent input parameters of the LSCP RFCS analytical model.

Symbol	Description	Units	Value
N	Rotor rotational speed	rpm	140
T	Throughput	kg/s	2.5, 3.75 and 5.0
l_{rb}	Rotor bed arc length	m	0.340
R	Rotor bed radius of curvature	m	0.250
P_{base}	Power required to spin the rotor without crop flow	W	951.5
AO_T	Angular offset between adjacent tine pairs	°	24
AO_{MT}	Angular offset between model and trial rotor	°	25

Table 7.4 Zone-dependent input parameters of the n^{th} zone for the LSCP RFCS analytical model including: arc length of the tine, δ_n, midpoint radius, r_n, angle between datum and leading knife edge, γ_n, angle between the leading and lagging edge of the tine, α_n, angle between the radial unit vector and the compressive/cutting force, ζ_n, and the angle of the rotor when the tine passes the counter-knife, λ_n.

		Zone #									
Parameter		**1**	**2**	**3**	**4**	**5**	**6**	**7**	**8**	**9**	**10**
δ_n	mm	15	14	14	13	13	13	13	13	13	13
r_n	mm	205	195	185	175	165	155	145	135	125	115
γ_n	°	10	14	19	24	29	35	41	48	55	64
α_n	°	1	4	7	10	13	16	19	22	26	30
ζ_n	°	45	46	48	49	50	50	51	51	52	52
λ_n	°	71	75	80	83	83	83	83	83	83	84

Indeterminate input parameters: The indeterminate parameters were: w, A_{sm}, ρ, P_f, and lo_m. The indeterminate parameters were quantified by adjusting the values of the indeterminate parameters to minimize the sum of squared error between a subset of the data collected with the LSCP RFCS and the analytical model output. As previously

discussed, the trial data that were used to quantify the indeterminate parameters and validate the analytical model were from the trials completed with 5-mm thick, serrated and beveled counter-knives, while processing both cereal straw and alfalfa at three levels of throughput. Data were collected with the LSCP RFCS when alfalfa was processed with sharp and dull counter-knives and when cereal straw was processed with sharp counter-knives. Three replicates were completed for each combination of counter-knife sharpness, material type and throughput. The subset of trial data that was used to quantify the indeterminate parameters was chosen by randomly selecting one of the three replicates. An average of the other two replicates was later used to compare the analytical model output to the measured power demand of the LSCP RFCS.

To compare the trial data (discussed in chapter 5) to the analytical model output, the trial data needed to be in the form of a power curve as a function of the rotor position ranging from 0 to 359°. During the analysis of the data in chapter 5 a power curve for each replicate was created. The calculations that were performed to create the power curves were discussed in detail in section 5.1.2. The signal from the optical encoder was used in conjunction with the power curve (created during the analysis of the LSCP trials, and discussed in detail in section 5.1.2) to create an orientation-dependent power curve using the following equation,

$$P_{i_{ave}} = \sum_{n=0}^{k}(P_{i+360n})/k \qquad \textbf{(7.34)}$$

where:

$P_{i_{ave}}$ is the position-specific power demand of the rotor at the angular position *i*,

i is the rotor position which ranges from 0 to 359°and

k is the number of revolutions the rotor made during the trials while crop was being processed.

Solver in Excel was used to minimize the sum of squared error between the power curve defined by the analytical model and the measured power curve defined using equation (7.34). The numerical method used by the Solver is a generalized reduced gradient algorithm. The exact values of the indeterminate parameters were unknown.

However, the range of the indeterminate parameters was known. Therefore, a series of constraints was placed on the values that each of the indeterminate parameters could have. The constraints of each of the indeterminate parameters are discussed in detail below.

The width of compression, *w*, was assumed to be a function of the sharpness of the counter-knife, with a sharper counter-knife resulting in a smaller width of compression. For both a sharp and dull counter-knife, the width of compression was constrained to values in the range of 0.1 to 71.4-mm. The lower limit of 0.1 mm was set equal to the width of the leading edge of a sharp counter-knife. In order for the plant material to be cut, the plant material would have to be in contact with the leading edge of the counter-knife. Thus, it would be impossible for the width of compression to be less than the leading edge of the counter-knife. The upper limit was set to the distances between adjacent counter-knives. The width of compression could not exceed 71.4-mm with the assumption that the plant material would only be compressed once by the RFCS. If the width of compression was equal to 71.4-mm, the entire width of the windrow of plant material entering the RFCS would have been compressed. The width of compression was indicated by w_{sharp} when sharp counter-knives were used in the RFCS and, by w_{dull} when dull counter-knives were used in the RFCS.

The length of the shear area was assumed to be 13.3 mm, the average value of the arc length of the leading edge of the tine, δ_n, in all 10 zones. The width of the shear area was assumed to be between 1.0 and 0.01-mm. Thus, A_{sm} was constrained to a range of values from 1.0×10^{-5} to 1.0×10^{-7} m^2. The shear area was also constrained so that the maximum compressive force in each zone for each cut made by the RFCS would exceed the force required to cut the plant material in each zone for each cut. This constraint ensured that the plant material in each zone of each cut made by the RFCS was cut before or when the leading edge of the tine passed the leading edge of the counter-knife. It was assumed that the cross-sectional area of material, when cut, was a function of the sharpness of the counter-knife because the sharpness of the counter-knife was expected to affect the force required to cut the plant material. The cross-sectional area of compression when sharp and dull counter-knives were used was indicated by $A_{sm\ sharp}$ and $A_{sm\ dull}$, respectively.

The coefficient that relates dry-mass density of plant material when it was cut, to the initial depth of plant material for the m^{th} cut, ρ, was constrained so that the maximum dry-mass density of plant material when it was cut would be approximately 10 times the initial dry-mass density of the plant material when it entered the RFCS. This constraint suggests that the force required to shear the plant material will be reached before the plant material experiences a strain of 90%. The initial dry-mass density of both alfalfa and cereal straw was approximately 20 kg/m^3 when it entered the RFCS, thus the maximum dry-mass density of plant material was constrained to a value of 200 kg/m^3.

The coefficient that relates the initial depth of plant material for the m^{th} cut to the compressive force caused by plant material between the side of a counter-knife and the tine pair, P_f, was constrained to a value between zero to 2400 N/m for both cereal straw and alfalfa. The lower limit was set to zero because it was impossible for P_f to be a negative value. The P_f value for cereal straw and alfalfa was assumed to be different because, the force required to achieve a given level of deformation in each material was not the same, as can be seen with the differing Young's modulus of the two plant-types. The force required to achieve a given level of deformation with cereal straw was significantly higher than with alfalfa. The P_f values for cereal straw and alfalfa was identified by $P_{f\ straw}$ and $P_{f\ alfalfa}$, respectively. The tine pairs did not undergo any measurable permanent deformation due to plant material between the side of the counter-knife and tine. In order for the tine pairs to be permanently deformed, due to a bending load caused by plant material between the side of a counter-knife and the tine, P_f would have had to be in excess of 2400 N/m and the initial depth of plant material would have had to be equal to 230 mm.

It was assumed that the relationship between lo_m and throughput was a function of the type of material being processed. The reason for this was that the initial depth of cereal straw (on the conveyor used to feed the plant material into the LSCP RFCS) was higher than the initial depth of alfalfa, at the same level of throughput. Thus it was expected that for a given throughput, the initial depth of plant material on the counter-knife would have been larger for cereal straw than for alfalfa.

After observing the average power curves created using equation (7.34), it became apparent that the power demand of the RFCS was not constant as a function of the rotor position. Instead the alfalfa power curves all had three distinct peaks and valleys during one revolution of the rotor. The cereal straw power curves did not display the trend to the same extent as the alfalfa, however there were still fluctuations in the cereal straw power curves as a function of the rotor position. The variations in the power demand of the RFCS were believed to be attributed to variations in the instantaneous throughput of plant material during the laboratory trials. The variations in the instantaneous throughput of plant material during the trials were caused by the pattern of the tines on the rotor. The average throughput during the trials completed with the LSCP RFCS was controlled, however the instantaneous throughput was not.

It was assumed that the depth of plant material for the 15 cuts made by the RFCS at throughputs of 3.75 and 5.0 kg/s would be a multiple of the depth of plant material made by the RFCS at a throughput of 2.5 kg/s. In theory if there was a linear relationship between throughput and the depth of plant material, the depth of plant material at a throughput of 5.0 kg/s would have been twice the depth of plant material at a throughput of 2.5 kg/s. Similarly, the depth of plant material at a throughput of 3.75 kg/s would have been one and a half times the depth of plant material at a throughput of 2.5 kg/s. Further, the depth of plant material at a throughput of zero would have also been zero. The depth of alfalfa for the m^{th} cut made by the RFCS at a throughput of 3.75 and 5.0 kg/s were assumed to be described by,

$$lo_{m_{3.75\ alfalfa}} = \chi_{3.75\ alflafa} lo_{m_{2.5\ alfalfa}} \text{ and} \quad \textbf{(7.35)}$$

$$lo_{m_{5.0\ alfalfa}} = \chi_{5.0\ alflafa} lo_{m_{2.5\ alfalfa}}, \quad \textbf{(7.36)}$$

where:

$lo_{m\ 2.5\ alfalfa}$ is the initial depth of alfalfa for the m^{th} cut made by the RFCS when processing alfalfa at a throughput of 2.5 kg/s (m),

$lo_{m\ 3.75\ alfalfa}$ is the initial depth of alfalfa for the m^{th} cut made by the RFCS when processing alfalfa at a throughput of 3.75 kg/s (m),

$lo_{m\ 5.0\ alfalfa}$ is the initial depth of alfalfa for the m^{th} cut made by the RFCS when processing alfalfa at a throughput of 5.0 kg/s (m),

$\chi_{\ 3.75\ alfalfa}$ is the coefficient that relates the initial depth of alfalfa at a throughput of 2.5 kg/s to the initial depth of alfalfa at a throughput of 3.75 kg/s and

$\chi_{\ 5.0\ alfalfa}$ is the coefficient that relates the initial depth of alfalfa at a throughput of 2.5 kg/s to the initial depth of alfalfa at a throughput of 5.0 kg/s.

Similarly, the depth of cereal straw for the m^{th} cut made by the RFCS at a throughput of 3.75 and 5.0 kg/s were assumed to be described by,

$$lo_{m_{3.75\ straw}} = \chi_{3.75\ straw} lo_{m_{2.5\ straw}} \ , \qquad \textbf{(7.37)}$$

$$lo_{m_{5.0\ straw}} = \chi_{5.0\ straw} lo_{m_{2.5\ straw}} \ , \qquad \textbf{(7.38)}$$

where:

$lo_{m\ 3.75\ straw}$ is the initial depth of cereal straw for the m^{th} cut made by the RFCS when processing cereal straw at a throughput of 3.75 kg/s (m),

$lo_{m\ 2.5\ straw}$ is the initial depth of cereal straw for the m^{th} cut made by the RFCS when processing cereal straw at a throughput of 2.5 kg/s (m),

$lo_{m\ 5.0\ straw}$ is the initial depth of cereal straw for the m^{th} cut made by the RFCS when processing cereal straw at a throughput of 5.0 kg/s (m),

$\chi_{\ 3.75\ straw}$ is the coefficient that relates the initial depth of cereal straw at a throughput of 2.5 kg/s to the initial depth of cereal straw at a throughput of 3.75 kg/s and

$\chi_{\ 5.0\ straw}$ is the coefficient that relates the initial depth of cereal straw at a throughput of 2.5 kg/s to the initial depth of cereal straw at a throughput of 5.0 kg/s.

Solver in Excel was used to change the initial depth of plant material for the 15 cuts made by the RFCS at a throughput of 2.5 kg/s for both cereal straw and alfalfa and the throughput-initial depth coefficients ($\chi_{\ 5.0\ straw}$, $\chi_{\ 3.75\ straw}$, $\chi_{\ 5.0\ alfalfa}$ and $\chi_{\ 3.75\ alfalfa}$). The upper limit of lo_m was constrained to 230 mm because during the development of the analytical model it was assumed that the initial depth would not exceed this value. The

lower limit of lo_m was set to a value of zero, because it was impossible for the initial depth of material to be a negative value.

The values of the indeterminate parameters are given in Table 7.5. The coefficient that related the force between the side of the counter-knife and the tine, P_f, was larger for cereal straw than for alfalfa. This was expected because the Young's modulus of cereal straw was larger than the Young's modulus of alfalfa, and the plant material was being subjected to the same level of deformation, as the gap between the side of the tine and the counter-knife was not affected by the type of plant material that was processed. As expected the width of compression of plant material, w, when dull counter-knives were employed was larger than when sharp counter-knives were used. The relationship between the dry-mass density of plant material when it was cut and the initial depth of plant material was found to be equal to 652 (kg m^{-3}) m^{-1}. The maximum initial depth of plant material was 222 mm, therefore the maximum dry-mass density of plant material was 145 kg/m^3, which was less than the 200 kg/m^3 constraint placed on the value. The cross-sectional area of the plant material, when cut, was larger when dull counter-knives were used as opposed to sharp counter-knives. This was a predictable phenomenon because it meant that the force required to cut a given plant material was higher when a dull counter-knife was used as opposed to a sharp counter-knife.

Table 7.5 The indeterminate input parameters of the LSCP RFCS analytical model.

Symbol	Description	Units	Value
w_{sharp}	Compression width (sharp counter-knife)	m	0.001
w_{dull}	Compression width (dull counter-knife)	m	0.051
$A_{sm\ sharp}$	Cross-sectional area of shear (sharp counter-knife)	m^2	1.6E-07
$A_{sm\ dull}$	Cross-sectional area of shear (dull counter-knife)	m^2	6.3E-06
ρ	Relationship between dry-mass density and lo_m	$(kg\ m^{-3})\ m^{-1}$	652
$\chi_{3.75\ alfalfa}$	Relationship between lo_m and alfalfa throughput at 2.5 and 3.75 kg/s	--	1.22
$\chi_{5.0\ alfalfa}$	Relationship between lo_m and alfalfa throughput at 2.5 and 5.0 kg/s	--	1.51
$\chi_{3.75\ straw}$	Relationship between lo_m and straw throughput at 2.5 and 3.75 kg/s	--	1.59
$\chi_{5.0\ straw}$	Relationship between lo_m and straw throughput at 2.5 and 5.0 kg/s	--	2.40
$P_{f\ alfalfa}$	Relationship between force on the side of a counter-knife and lo_m for alfalfa	N/m	329
$P_{f\ straw}$	Relationship between force on the side of a counter-knife and lo_m for straw	N/m	840

As expected, the relationships between the depth of plant material and throughput for both cereal straw and alfalfa were direct, which meant that the depth of plant material increased with an increase in throughput ($\chi_{3.75\ alfalfa} < \chi_{5.0\ alfalfa}$ and $\chi_{3.75\ straw} < \chi_{5.0\ straw}$). The average initial depth of alfalfa at each level of throughput tested was lower than the average initial depth of cereal straw. The reason that the initial depth of cereal straw was larger than the initial depth of alfalfa is believed to be attributed to the lower bulk density of cereal straw. During the trials, when the same mass of plant material was placed on the conveyor, the height of the cereal straw was larger than the height of the alfalfa.

The amount the initial depth of cereal straw increased when the throughput was increased was larger than the amount the initial depth of alfalfa increased for the same increase in throughput. (Put differently, $\chi_{3.75\ alfalfa} < \chi_{3.75\ straw}$ and $\chi_{5.0\ alfalfa} < \chi_{5.0\ straw}$). The

reason that the depth of cereal straw increased more than the depth of alfalfa, over the same range of throughputs, was likely a result of cereal straw having a relatively low coefficient of friction (between the cereal straw and the conveyor) and the fact that the tip speed of the tines on the RFCS was 3.0 m/s while the conveyor speed was only 2.0 m/s. The combined effect of the lower coefficient of friction between the conveyor and cereal straw, and the faster tip speed of the tines on the RFCS in relation to the conveyor caused the cereal straw to slide into the RFCS (across the conveyor) at a speed closer to the tip speed of the RFCS, thereby causing the throughput of cereal straw to be slightly higher than measured values of 2.5, 3.75 and 5.0 kg/s. The higher throughput of cereal straw resulted in an increase in the initial depth of cereal straw. Conversely, the throughput of alfalfa into the RFCS was less than the throughput of cereal straw, and closer to the intended values of 2.5, 3.75 and 5.0 kg/s because of the relatively high friction coefficient between the conveyor and the alfalfa. The friction coefficient between the alfalfa and conveyor was high enough to prevent the entire mat of alfalfa from sliding into the RFCS at a speed equal to the tip speed of the RFCS.

The initial depth of alfalfa varied more than the initial depth of cereal straw. The initial depth of alfalfa and cereal straw as a function of the m^{th} cut made by the LSCP RFCS is shown in Figures 7.11 and 7.12, respectively. The larger variation in the depth of alfalfa relative to the depth of cereal straw can be explained by the same phenomenon that caused $\chi_{3.75\ alfalfa} < \chi_{3.75\ straw}$ and $\chi_{5.0\ alfalfa} < \chi_{5.0\ straw}$. . The low static coefficient of friction between the cereal straw and the conveyor allowed the mat of cereal straw to slide into the RFCS at a relatively constant speed that was dictated by the rotational speed of the rotor on the RFCS. This caused a relatively constant cereal straw throughput (during the laboratory trials). The variations in the depth of cereal straw for the m^{th} cut made by the LSCP RFCS were likely caused by variations in the mass-density of cereal straw across the width and length of the conveyor. Conversely, the higher static coefficient of friction between the alfalfa and conveyor prevented the entire mat of alfalfa from being fed into the RFCS at a rate dictated by the RFCS alone. Instead a portion of the mat of alfalfa on the conveyor was slid into the RFCS at a rate dictated by the tine tip speed, which caused a temporary increase in the throughput and initial depth of alfalfa. The temporary increase in the depth of alfalfa was followed by a temporary decrease in

the throughput and depth of alfalfa because of the time it took for the remaining mat of alfalfa on the conveyor to reach the path of the tines on the rotor. The three temporary increases and decreases in the throughput and depth of alfalfa were likely attributed to the pattern of tines on the rotor. In general it appeared that the relationship between throughput and the initial depth of plant material was affected by the speed of the rotor, the pattern of tines on the rotor, the plant material type and the device used to feed the plant material into the RFCS.

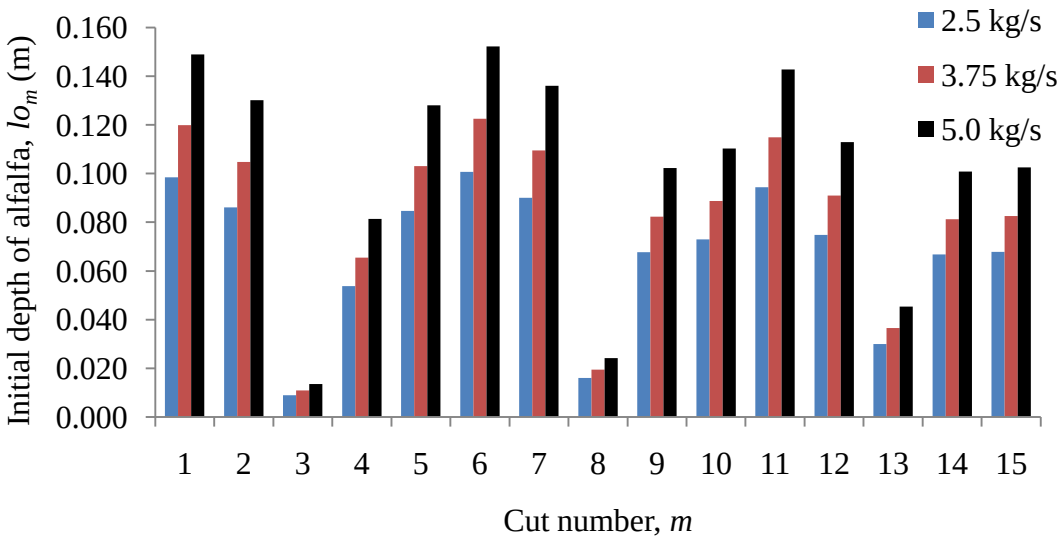

Figure 7.11 The initial depth of the m^{th} cut made by the LSCP RFCS while processing alfalfa at a throughput of 2.5, 3.75 and 5.0 kg/s.

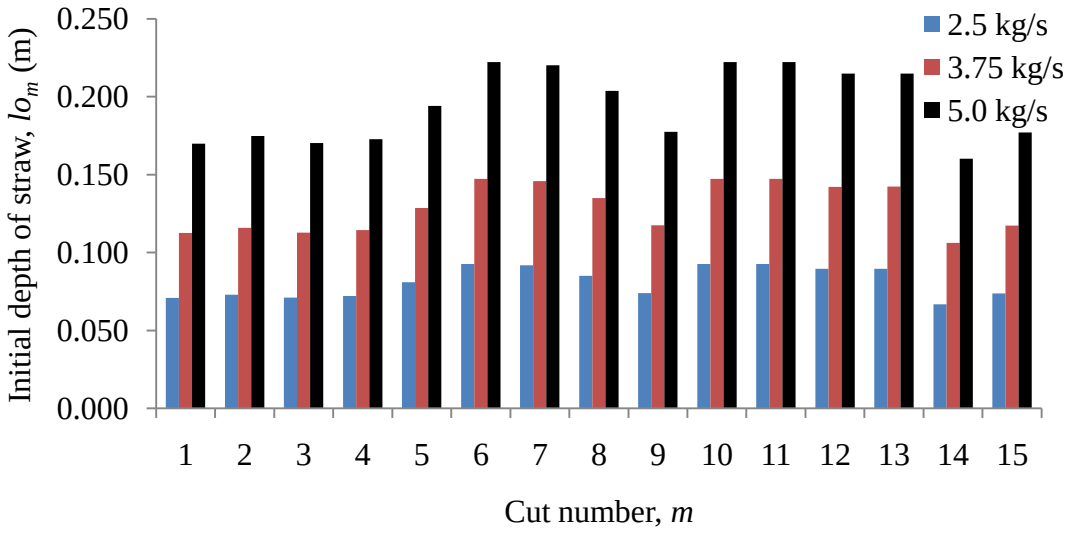

Figure 7.12 The initial depth of the m^{th} cut made by the LSCP RFCS while processing cereal straw at a throughput of 2.5, 3.75 and 5.0 kg/s.

7.2.2 Validation

In the previous section the measurable and indeterminate model inputs were quantified. Recall that the indeterminate inputs were quantified by minimizing the sum of squared error between the analytical model output and a subset of the data collected with the LSCP RFCS. Three replicates were completed with the LSCP RFCS during the trials that investigated the effect of throughput, counter-knife sharpness and plant material type. One of the replicates was used to quantify the indeterminate parameters while an average of the other two replicates was used to validate the model.

The model output, average and the 95% confidence interval of the measured power demand of the RFCS for processing alfalfa at three levels of throughput, with sharp and dull counter-knives is shown in Figures 7.13 and 7.14, respectively. Similarly, the model output, average and the 95% confidence interval of the measured power demand of the RFCS for processing cereal straw at three levels of throughput with sharp counter-knives is shown in Figures 7.15. The 95% confidence interval was included to show the magnitude of the variation of the average power demand of the RFCS.

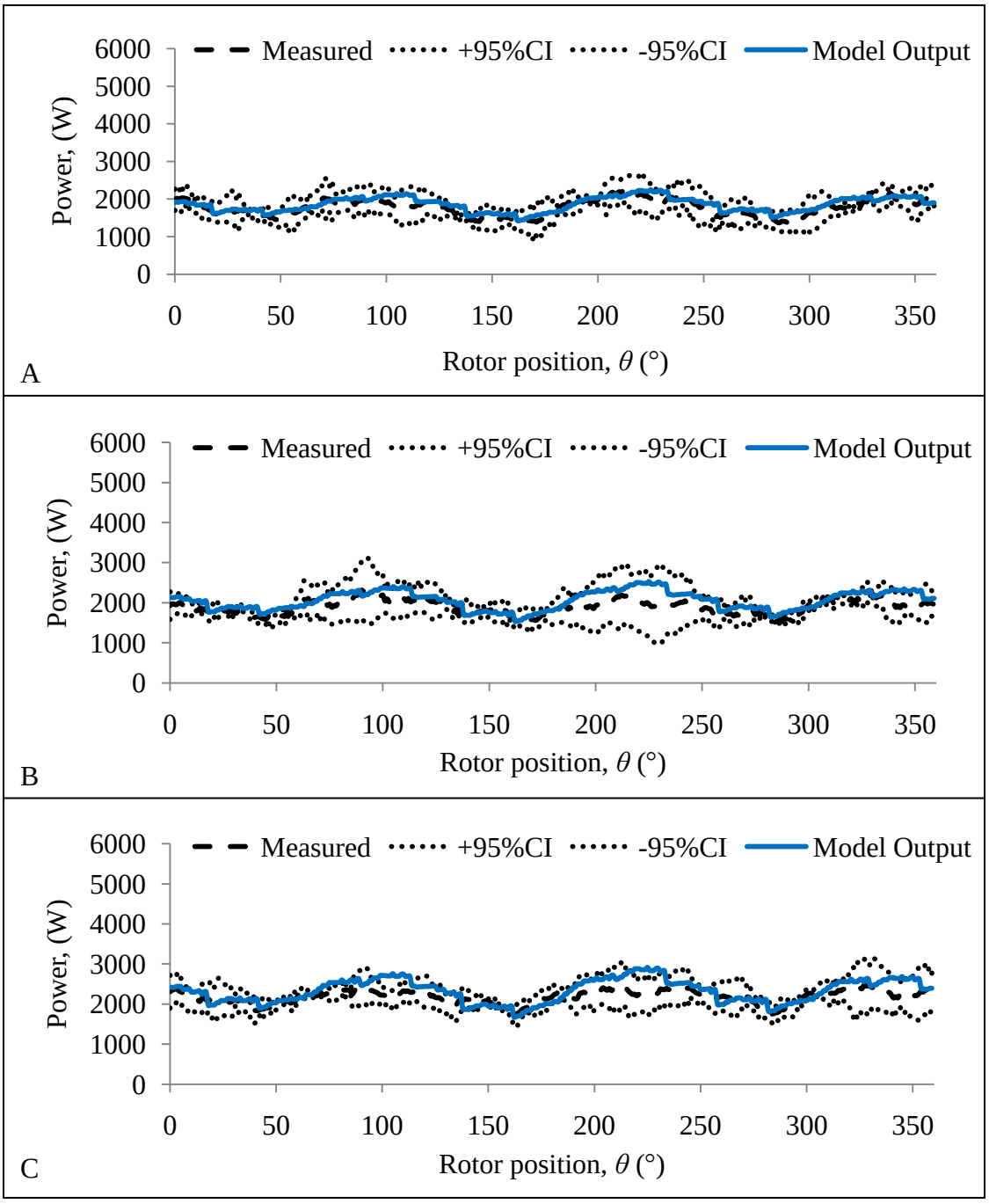

Figure 7.13 The average and ± 95% confidence interval (CI) of the measured power demand of the LSCP RFCS, and the analytical model output when sharp counter-knives were used to process alfalfa at a throughput of (A) 2.5, (B) 3.75 and (C) 5.0 kg/s.

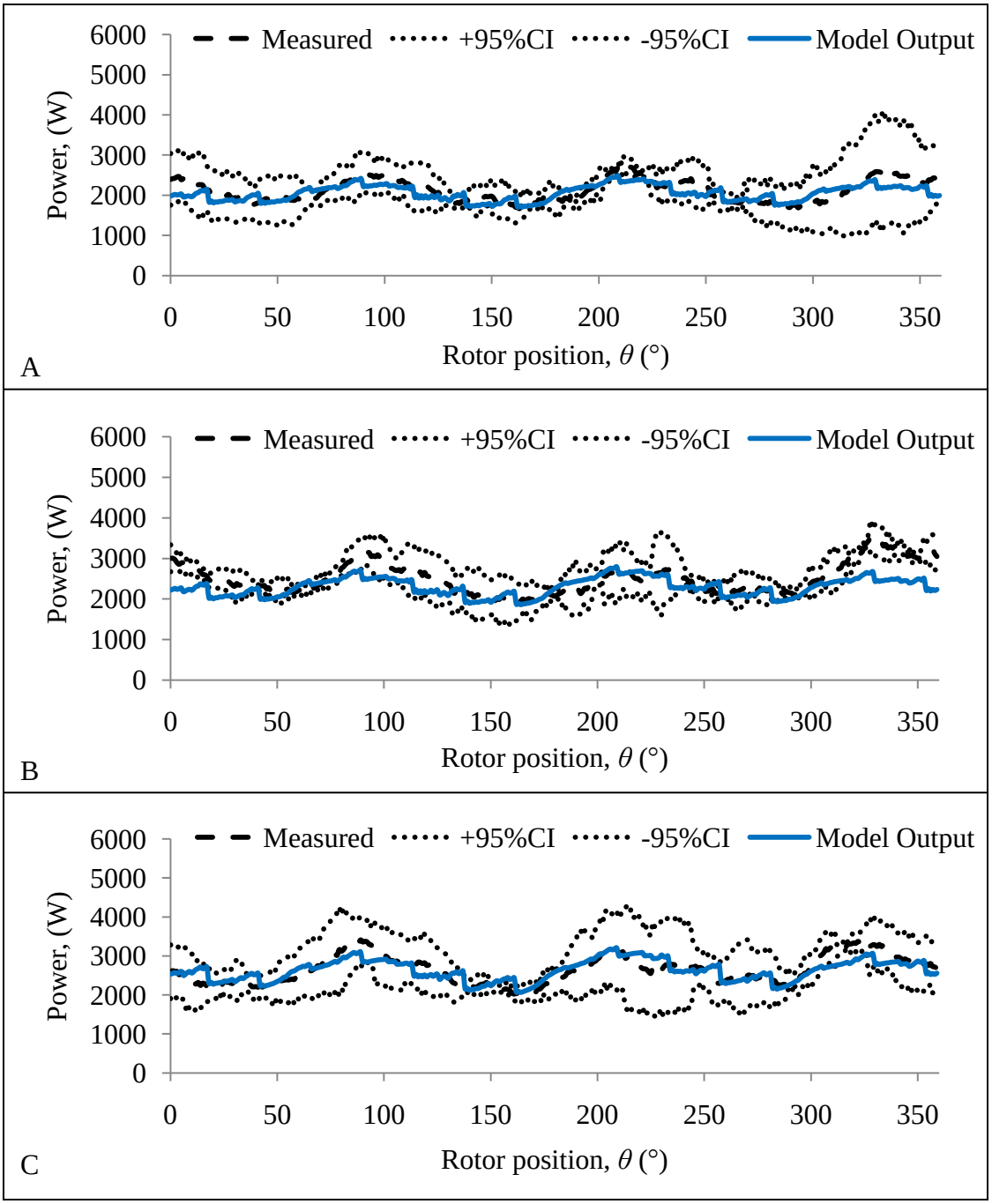

Figure 7.14 The average and ± 95% confidence interval (CI) of the measured power demand of the LSCP RFCS, and the analytical model output when dull counter-knives were used to process alfalfa at a throughput of (A) 2.5, (B) 3.75 and (C) 5.0 kg/s.

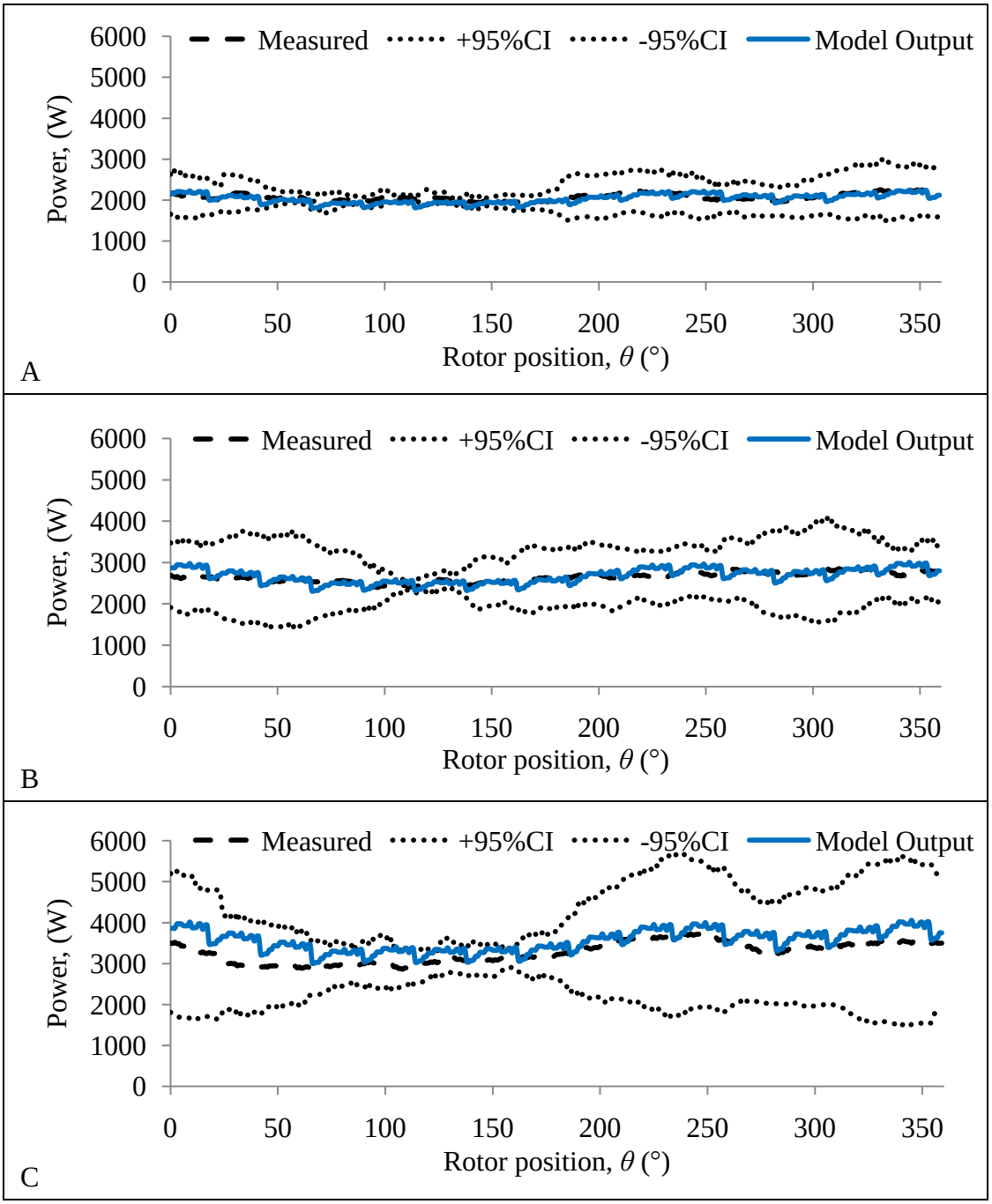

Figure 7.15 The average and ± 95% confidence interval (CI) of the measured power demand of the LSCP RFCS, and the analytical model output when sharp counter-knives were used to process straw at a throughput of (A) 2.5, (B) 3.75 and (C) 5.0 kg/s.

A common trend was present in all of the alfalfa trials in that there were three distinct peaks and valleys in the power demand of the rotor as a function of the rotor position. The same trend was not observed for the trials completed with cereal straw. The average power demand of the rotor when cereal straw was processed remained relatively constant. The cause of the peaks and valleys in the power demand of the rotor while processing alfalfa was attributed to variations in the instantaneous throughput of plant material, which caused variations in the initial depth of alfalfa processed by the RFCS. The average throughput of plant material in the RFCS was a controlled parameter, however the instantaneous throughout (or the throughput during the trial) was not a controlled parameter. Conversely, the power demand of the rotor remained relatively constant during the trials completed with the cereal straw because the throughput and initial depth of cereal straw remained relatively constant during the trials. The cause of the variations in the initial depth of alfalfa, and the reason the initial depth of cereal straw remained relatively constant was previously discussed at the end of section 7.2.1.

The magnitude of the variation of the power demand of the RFCS as a function of the rotor position, represented by the 95% CI presented in Figures 7.13 to 7.15 was likely due to the variation of the instantaneous throughput of plant material. Rotor angular positions that have a large variation in the instantaneous throughput of plant material were depicted in Figures 7.13 to 7.15 by having a larger 95% CI. For example when straw at a throughput of 5.0 kg/s was processed with sharp counter-knives the variation in the instantaneous throughput when the rotor was at an angular position of 150° was far less than when the rotor was at an angular position of 250°.

A harmonic shape in all of the model outputs was present – most noticeably when cereal straw was processed with sharp counter-knives as shown in Figure 7.15. The harmonic shape was a result of the number of cuts made by the RFCS during one full rotation of the rotor, a total of 15. A total of 15 “valleys” and “plateau peaks” were present in the model output, again most noticeably in Figure 7.15. During the “plateau peaks” the compression force had exceeded the force required to cut the plant material, and therefore the force and power required to cut the plant material became constant. The decrease in the model power demand of the RFCS immediately following the

"plateau peak" was caused by the decrease in the force, and power required to cut the plant material (because the plant material between the counter-knife and tine had been cut). The following increase in the model power was caused by the increase in the force and power required to compress the plant material between the adjacent tine and counter-knife.

The reason that the harmonic shape was not present in the average measured power is somewhat complex. Recall that analytical model was developed under the assumption that the initial depth of plant mateiral in each zone on each counter-knife was equal for the m^{th} cut. During the laboratory trials the depth of plant material within each zone on each counter-knife was not measured and may not have been constant. Further, the power demand of the RFCS (based on the analytical model output) was calculated based on the power required to make 15 cuts into plant material of discrete initial depths. Conversely, the measured power demand of the RFCS was converted with equation (7.34) to give the average positionally-specific power demand of the RFCS. The positionally-specific average power demand of the RFCS at the i^{th} angular position was based on the average power required to cut plant material at 3 to 5 different plant material initial depths. If the instantaneous throughput of plant material was constant during the trials it is believed that the harmonic shape present in the model output would also be present in the average power demand of the RFCS. Further, if the instantanious throughput of plant material was constant during the trials the variation in the average power demand as a function of rotor position would also substantially decrease which would be reflected by a decrease in the 95% CI.

During a single trial completed with the LSCP RFCS the rotor made anywhere from 3 to 5 full revolutions. The power data, collected during the trials as a function of time was converted with equation (7.34), to quantify the position-specific power demand of the LSCP RFCS. This means that the measured power demand, shown in Figures 7.13 to 7.15 is the average power demand of the LSCP RFCS for making anywhere from 45 to 60 cuts. Conversely, the output of the model is based on the power required to make 15 cuts over one full revolution of the rotor. In theory, by controlling the throughput of the plant material during the trials the depth of plant material for each cut made by the LSCP

RFCS should have been the same. However, even though the average throughput during the trial was a controlled parameter, the instantaneous throughput was varying. The variation in the instantaneous throughput caused variations in the depth of plant material being cut. The variation (at a given angular orientation) in the position-specific power demand of the RFCS (for all material types and throughputs) is believed to be largely attributed to variation in the instantaneous throughput of plant material (at the given angular orientation). The variation in the position-specific power demand of the RFCS is shown in Figures 7.13 to 7.15 by the 95% confidence interval. Computing the correlation coefficient, comparing the model output to the measured position-specific power demand of the RFCS indicated that the strength or "goodness of fit" of the model was poor. However, the poor strength is largely attributed to the inability to control the instantaneous throughput (and the depth of the plant material) during the trials.

The error between the average measured power and model output (both averaged across the full revolution of the rotor) ranged from positive 8.7 to negative 8.5%. The analytical model output typically fell within the envelope of the ±95% confidence interval for the trials completed with alfalfa at three levels of throughput while using sharp and dull counter-knives. Similarly, the analytical model output typically fell within the envelope of the ±95% confidence interval for the trials completed with straw at three levels of throughput while using sharp counter-knives. Thus, the analytical model can be used by future designers of the RFCS to quantify the power demand of the LSCP RFCS, if it is acceptable to have an absolute error of less that 8.7%. If the designer requires a more accurate model additional work will need to be completed to improve the analytical model.

7.2.3 Sensitivity analysis

The purpose of completing the sensitivity analysis was to identify which parameters had the greatest influence on the power demand of the RFCS. The sensitivity analysis completed was a one-factor-at-a-time sample-based analysis. This analysis involved defining the high, medium, and low values of all of the factors included in the analysis. The sensitivity of a given factor was determined by setting all other factors of the analysis equal to their medium level and quantifying the average power demand of the

RFCS when the factor of interest was set to its low, medium and high levels. The sensitivity of a given factor was found using the following equations:

$$\eta = \frac{\%\Delta\text{Output}}{\%\Delta\text{Input}} \ , \tag{7.39}$$

$$\%\Delta\text{Output} = \left(\frac{P_{avg\ high} - P_{avg\ low}}{P_{avg\ medium}}\right) \times 100 \ , \tag{7.40}$$

$$\%\Delta\text{Input} = \left(\frac{F_{high} - F_{low}}{F_{medium}}\right) \times 100 \ , \tag{7.41}$$

where:

η is the sensitivity of the factor,

$P_{avg\ high}$ is the average power demand of the rotor over 360° when the factor of interest is set to its upper limit (W),

$P_{avg\ low}$ is the average power demand of the rotor over 360° when the factor of interest is set to its lower limit (W),

$P_{avg\ medium}$ is the average power demand of the rotor over 360° when the factor of interest is set to the medium value (W),

F_{high} is the value of the upper limit of the factor of interest,

F_{low} is the value of the lower limit of the factor of interest and

F_{medium} is the average of the upper and lower limit of the factor of interest.

The initial depth of plant material for the m^{th} cut made by the RFCS, lo_m, was found to be affected by the speed of the rotor, the pattern of tines on the rotor, the type and throughput of plant material and the system used to feed the plant material into the RFCS. The effect of these parameters and the interaction of these parameters on lo_m are not fully understood. Therefore, rotor speed and the angular offset between tine pairs were not included in the sensitivity analysis, because changing them would likely change the previously defined lo_m. It is also believed that the profile of the leading edge of the tines and counter-knives would affect the distribution of the plant material along the leading edge of the tine and counter-knife. The analytical model was developed under the

assumption that the plant material along the leading edge of the tine and counter-knife was uniform. The zone-dependent input parameters were not included in the sensitivity analysis, because it is believed that changing the zone-dependent parameters would change the distribution of plant material along the leading edge of the tine and the counter-knife. Rotor bed arc length and rotor bed radius of curvature were also left out of the sensitivity analysis because it would only be logical to change them if the radius of the tines were changed, and the radius of the tines is a zone-dependent parameter. A separate sensitivity analysis was completed for the RFCS while processing cereal straw and alfalfa because lo_m, was different for each material.

Cereal straw: The high, medium and low levels of the factors included in the LSCP RFCS analytical model sensitivity analysis while processing cereal straw is given in Table 7.6.

Table 7.6 The high, medium and low levels of the factors included in the LSCP RFCS analytical model sensitivity analysis while processing cereal straw.

Symbol	Description	Units	Low	Medium	High
T	Throughput	kg/s	2.50	3.75	5.00
w	Compression width	m	0.001	0.026	0.051
A_{sm}	Cross-sectional area of the material when it was cut	m^2	1.6E-07	3.2E-06	6.3E-06
ρ	Coefficient that relates the dry-mass density of plant material to the initial depth of plant material	$(kg\ m^{-3})m^{-1}$	500	652	800
P_f	Coefficient that relates the initial depth of plant material to the compressive force caused by plant material between the side of a counter-knife and the tine pair	N/m	680	840	1000
μ	Dynamic coefficient of friction	--	0.14	0.31	0.47
τ_{int}	Intercept of maximum shear strength	kPa	2160	3080	4000
E	Young's modulus (at 80% strain)	kPa	111	123	140

The power demand of the RFCS was most sensitive to the throughput of plant material, which meant that lo_m had a large influence on the power demand of the RFCS. Out of the three material properties, the RFCS analytical model was most sensitive to the dynamic coefficient of friction, followed by the Young's modulus and the maximum shear strength of the plant material. Therefore focusing efforts on decreasing the dynamic coefficient of friction between the cereal straw and the RFCS would be an effective way in decreasing the power demand of the RFCS. The power demand of the RFCS is also relatively sensitive to P_f, which indicated that implementing design changes to the RFCS that would decrease the amount of plant material that becomes entrapped between the tine pairs and the sides of the counter-knives would also be an effective way to decrease the power demand of the RFCS. The compression width, w, and cross-sectional area of the material when it was cut, A_{sm}, were not independent, because both were affected by the sharpness, or leading edge width of the counter-knives. Therefore, the sensitivity of compression width, w, and shear area, A_{sm}, were not identified separately in Table 7.7. The power demand of the RFCS was approximately five times less sensitive to the w and A_{sm} than the dynamic coefficient of friction of the plant material. The RFCS was least sensitive to the coefficient that related the dry-mass density of plant material to the initial depth of plant material, ρ. Recall that the value of ρ indirectly affects the force required to cut the plant material. The fact that the RFCS was least sensitive the τ_{int} and ρ suggest that an ineffective approach to decreasing the power demand of the RFCS, while processing cereal straw, would be to focus design efforts on decreasing the power associated with cutting the plant material. The sensitivity of the factors included in the sensitivity analysis of the LSCP RFCS analytical model, while processing cereal straw is given in Table 7.7.

Table 7.7 Sensitivity of the LSCP RFCS analytical model while processing cereal straw.

Symbol	Description	Units	Sensitivity
T	Throughput	kg/s	0.96
μ	Dynamic coefficient of friction	--	0.59
P_f	Coefficient that relates the initial depth of plant material to the compressive force caused by plant material between the side of a counter-knife and the tine pair	N/m	0.56
E	Young's modulus (at 80% strain)	kPa	0.12
w	Compression width	m	0.12
A_{sm}	Cross-sectional area of the material when it was cut	m^2	
τ_{int}	Intercept of maximum shear strength	kPa	0.05
ρ	Coefficient that relates the dry-mass density of plant material to the initial depth of plant material	$(kg\ m^{-3})m^{-1}$	0.04

The total average power (power to transport, compress and cut) required by the RFCS while processing cereal straw at a throughput of 3.75 kg/s with dull counter-knives was 3.20 kW. The power required to compress and cut the plant material along the leading edge of the counter-knives was 0.494 kW. The power required to transport the plant material was 1.76 kW. Of that amount, 1.64 kW was required to transport the plant material along the sides of the counter-knives, 0.008 kW was required to transport the plant material along the rotor bed and 0.111 kW was required to transport the plant material along the leading edge of the tines. Because the transport power was much larger than the power required to compress and cut plant material with the RFCS, decreasing the transportation power requirements will drastically improve the efficiency of the RFCS. Further, the power required to transport the plant material along the side of the counter-knives is much larger than the power required to transport the plant material along the leading edge of the tines and along the rotor bed. Thus, the efficiency of the RFCS will drastically improve if the power required to transport the plant material along the tines is reduced.

The power required to transport plant material along the sides of the counter-knives is a result of plant material "hair pinning" around the leading edge of the counter-knife and being subsequently wedged between the sides of the counter-knife and the tine. The power to transport the plant material along the sides of the counter-knives could be eliminated if the plant material was prevented from getting between the sides of the counter-knives and tines. To accomplish this while using a side beveled counter-knife ,as shown in Figure 4.4A, the clearance between the "shearing" tine and the shearing surface on the counter-knife would need to be minimized (to less than a 1-mm clearance) and the second tine would be removed. This may present issues with maintaining the flow of plant material through the LSCP RFCS, which could potentially be addressed by adding a transporting surface to the "shearing" tine. A "shearing" tine, transport surface, side beveled counter-knife and the tine to be removed is shown in Figure 7.16. Assuming that the power required to transport the plant material along the side of the counter-knife and the tine could be reduced by one half, the average power required to process cereal straw at a throughput of 3.75 kg/s with dull counter-knives would be reduced from 3.20 kW to 2.38 kW, a 26% decrease in the power demand of the RFCS.

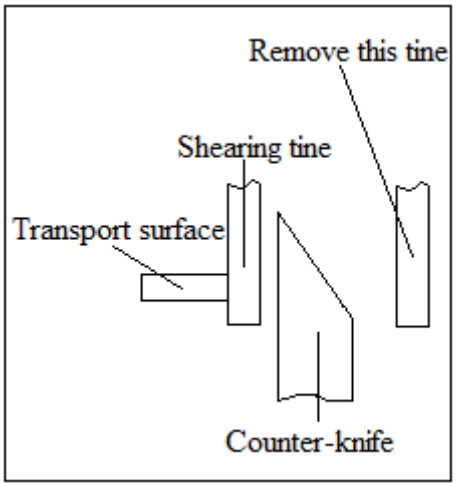

Figure 7.16 The "shearing" tine, transport surface and the tine to be removed to decrease the power required to transport plant material along the side of a counter-knife.

The power required to transport the plant material along the side of the counter-knives could be decreased by coating the inside surfaces of the tines, as shown in Figure 7.17,

with a material that would decrease the dynamic coefficient of friction. If the sides of the tines were coated with Baked Teflon® the friction coefficient between the LSCP RFCS and the cereal straw would be reduced from 0.26 to 0.18. The average total power required by the LSCP RFCS to process cereal straw at a throughput of 3.75 kg/s with dull counter-knives without the Baked Teflon® coating is 3.20 kW and with the coating 2.70 kW. Thus the power requirements of the RFCS could be reduced by 16% by coating the sides of the tines with Baked Teflon®.

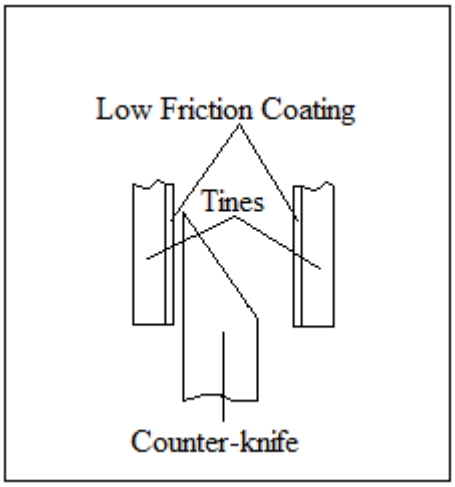

Figure 7.17 The location of the low friction coating that could be used to decrease the power required to transport plant material along the sides of the counter-knives.

The transportation power could also be reduced by decreasing the length of the counter-knife and or the length of the tine. In terms of the analytical model, decreasing the length of the tine or the length of the counter-knife would be accomplished by decreasing the angle of the rotor when the tine passes the counter-knife, λ_n. If λ_n was decreased by removing material from the counter-knife, as shown in Figure 7.18, the average total power requirement of the LSCP RFCS while processing cereal straw at a throughput of 3.75 kg/s with dull counter-knives would decrease by 0.547 kW, which is a 17% reduction in the average power demand of the LSCP RFCS. This reduction in power is based on the assumption that the distribution of the plant material along the leading edge of the tine and the counter-knife would not be affected by changing λ_n.

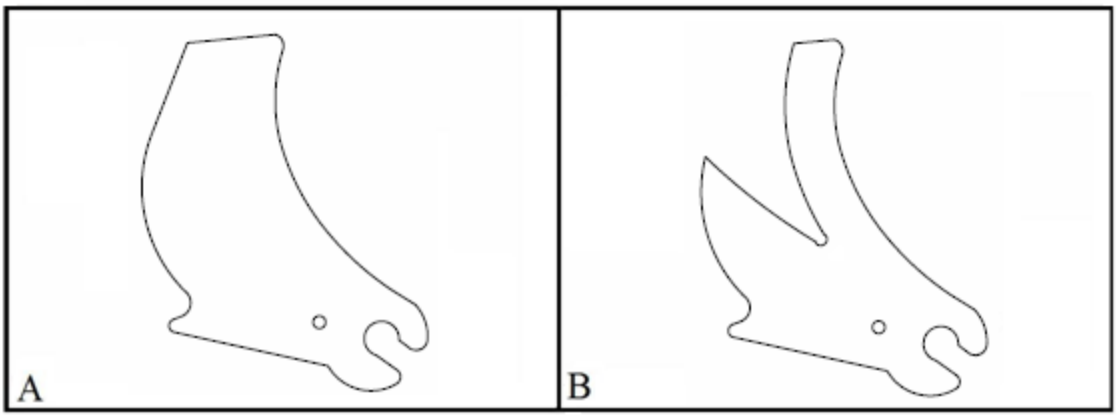

Figure 7.18 (A) the counter-knife used during the completion of the RFCS laboratory trials, and (B) the counter-knife that could be used to decrease the power requirements of the RFCS.

Alfalfa: The same levels of throughput, compression width, shear area and ρ were used for the alfalfa sensitivity analysis and the cereal straw sensitivity analysis. The high, medium and low levels of the factors included in the LSCP RFCS analytical model sensitivity analysis while processing alfalfa are given in Table 7.8.

Table 7.8 The high, medium and low levels of the factors included in the LSCP RFCS analytical model sensitivity analysis while processing alfalfa.

Symbol	Description	Units	Low	Medium	High
T	Throughput	kg/s	2.50	3.75	5.00
w	Compression width	m	0.001	0.026	0.051
A_{sm}	Cross-sectional area of the material when it was cut	m^2	1.6E-07	3.2E-06	6.3E-06
ρ	Coefficient that relates the dry-mass density of plant material to the initial depth of plant material	$(kg\ m^{-3})m^{-1}$	500	652	800
P_f	Coefficient that relates the initial depth of plant material to the compressive force caused by plant material between the side of a counter-knife and the tine pair	N/m	169	329	489
μ	Dynamic coefficient of friction	--	0.20	0.66	0.7
τ_{int}	Intercept of maximum shear strength	kPa	2221	3348	4127
E	Young's modulus (at 80% strain)	kPa	23	40	58

The rank of the material properties parameters based on their sensitivity are similar when the LSCP RFCS was used to process cereal straw and alfalfa. Out of the three material properties parameters, the RFCS analytical model was most sensitive to the dynamic coefficient of friction, followed by the maximum shear strength and the Young's modulus of the plant material. Therefore focusing efforts on decreasing the dynamic coefficient of friction between the alfalfa and the RFCS would be an effective way in decreasing the power demand of the RFCS. As was the case when the RFCS was used to process cereal straw, the sensitivity of the RFCS to P_f was also relatively high when used to process alfalfa. Therefore an effective strategy to decreasing the power demand of the RFCS would be to implement a design change that would prevent plant material from becoming entrapped between the side of the counter-knives and the tine pairs. As with the cereal straw RFCS sensitivity analysis, the compression width, *w*, and

shear area, A_{sm}, were not independent, because both were affected by the sharpness, or leading edge width of the counter-knives. Therefore the sensitivity of compression width, w, and shear area, A_{sm}, were not identified separately in Table 7.9. The sensitivity of the factors of the LSCP RFCS analytical model while processing alfalfa is given in Table 7.9.

Table 7.9 Sensitivity of the LSCP RFCS analytical model while processing alfalfa.

Symbol	Description	Units	Sensitivity
μ	Dynamic coefficient of friction	--	0.53
P_f	Coefficient that relates the initial depth of plant material to the compressive force caused by plant material between the side of a counter-knife and the tine pair	N/m	0.50
T	Throughput	kg/s	0.36
w	Compression width	m	0.06
A_{sm}	Cross-sectional area of the material when it was cut	m^2	
τ_{int}	Intercept of maximum shear strength	kPa	0.03
E	Young's modulus (at 80% strain)	kPa	0.02
ρ	Coefficient that relates the dry-mass density of plant material to the initial depth of plant material	$(kg\ m^{-3})m^{-1}$	3.1E-03

The total average power (power to transport, compress and cut) required by the RFCS while processing alfalfa at a throughput of 3.75 kg/s with dull counter-knives was 2.26 kW. The power required to compress and cut the plant material along the leading edge of the counter-knives was 0.159 kW. The power required to transport the plant material was 1.15 kW. Of that amount, 1.04 kW was required to transport the plant material along the side of the counter-knife, 0.020 kW was required to transport the plant material along the rotor bed and 0.091 kW was required to transport the plant material along the leading edge of the tines. As was concluded from the sensitivity analysis for cereal straw (discussed in the previous "cereal straw" sub-section), the power required to transport the alfalfa along the sides of the counter-knives was relatively large compared to the power required to transport the alfalfa along the rotor bed and along the leading edge of the

tines. The three options that were presented to decrease the power demand of the RFCS while processing cereal straw could also be used to decrease the power demand of the RFCS while processing alfalfa.

The three options were to eliminate a tine and possibly add a transport surface to the "shearing" tine as shown in Figure 7.16, to coat the inside surfaces of the tine with Baked Teflon®, as shown in Figure 7.17 and/or to decrease the length of the counter-knife, as shown in Figure 7.18. Option 1, the removal of a tine, would result in a decrease of 0.520 kW in the power demand of the LSCP RFCS which corresponds to a 23% decrease in the total average power demand of the LSCP RFCS, when processing alfalfa at a throughput of 3.75 kg/s. Assuming that the dynamic coefficient of friction between the tine and the alfalfa could be reduced to 0.38 by coating the tines with Baked Teflon®, the power demand of the LSCP RFCS would decrease by 0.441 kW, which corresponds to a 20% decrease in the total average power demand of the LSCP RFCS. The final option presented was to decrease the length of the counter-knife which would decrease the power demand of the LSCP RFCS by 0.347 kW, which corresponds to a 15% decrease in the total average power demand of the LSCP RFCS when processing alfalfa at a throughput of 3.75 kg/s.

7.3 High Speed Cutting Process (HSCP)

Based on the conclusions drawn from the HSCP RFCS field trails, presented in chapter 6, the specific energy requirements of the HSCP RFCS were significantly affected by straw moisture content and throughput. The statistical analysis indicated that counter-knife engagement did not have a statistically significant effect on the energy consumption of the RFCS. However the interaction between counter-knife engagement and straw moisture content was significant. When dry straw was processed the effect of counter-knife engagement on the specific energy requirement of the choppers was minimal, conversely when wet straw was processed the specific energy requirement of the choppers was affected by counter-knife engagement. The HSCP RFCS analytical model was developed so that the effect of throughput, counter-knife engagement and straw moisture content on the power demand of the RFCS could be assessed. However, the model could not be completely validated, because of the relatively low moisture

content of straw processed by the WR chopper during the field trials. The high level moisture content trials were used to validate the HSCP RFCS model because, the energy consumption of the RFCS was more sensitive to counter-knife engagement when high moisture content plant material was processed with the RFCS. The low moisture content trials completed with the WR chopper were not used to validate the model. The trials completed with three levels of counter-knife engagement (100, 89, 78%) and two levels of throughput (5.55 and 3.33 kg/s) while processing cereal straw at an average moisture content of 10.7% w.b. were used to validate the HSCP RFCS analytical model.

As was done with the LSCP RFCS analytical model validation, the input parameters of the HSCP RFCS needed to be quantified. The input parameters have been separated into two categories, the input parameter that could be measured during the field trials, the measurable parameters, and the input parameters that could not be measured during the field trials, the indeterminate input parameters. The indeterminate parameters were quantified by minimizing the sum of squared error between the model output and a subset of the trial data by adjusting the indeterminate parameters. Once the input parameters were quantified, the model output was compared to a different subset of the trial data to show the model accuracy. In the following section the quantification of the input parameters of the analytical model will be discussed.

7.3.1 Input parameter quantification

Measurable input parameters: The plant material properties of cereal straw used during the HSCP analytical model validation were the same material properties that were quantified in section 7.2.1. The cereal straw processed by the HSCP RFCS and the material properties test stand were obtained from the same field. The Young's modulus of cereal straw was defined with equation (7.31). The maximum shear strength of cereal straw was defined with equation (7.33). The dynamic coefficient of fiction between cereal straw and steel was found to be 0.27 while processing cereal straw at an average moisture content of 10.7% w.b.

The rotational speed of the rotor and the throughput of plant material were both measured and controlled during the experiments completed with the HSCP RFCS. The rotational speed of the rotor was measured with an optical encoder during the trials. The

throughput of plant material was measured by quantifying the mass of MOG that exited the combine while the harvester was traveling at a constant velocity. A more detailed description of how the rotor speed was measured and how throughput was quantified was given in section 4.2. P_{base} was measured once before the completion of the field trials. P_{base} was quantified by averaging the power demand of the chopper during a five-second interval during which the rotor spun at its normal operational speed with no crop flowing through the RFCS. The angular offset between the model and trial rotor was quantified by measuring the angle of rotation required to align the WR chopper with the model rotor. The rotor bed arc length & radius of curvature, the angular offset between adjacent tine pairs, the angular offset between the center and side tine pairs as well as all of the zone- dependent parameters were all quantified by measuring the geometry of the HSCP RFCS. The zone-independent model input parameters are given in Table 7.10. The zone- dependent input parameters of the HSCP RFCS analytical model that were not affected by counter-knife engagement are given in Table 7.11. and the zone-dependent input parameters that were affected by counter-knife engagement are given in Table 7.12. The angles of -90° shown in Table 7.12 in zones 8, 9 and 10 at varying levels of counter-knife engagement were not the actual angles of the angle between the datum and leading knife edge, γ_n, and the angle of the rotor when the tine passes the counter-knife, λ_n. Instead the angle of -90° indicates that the zone is inactive.

Table 7.10 The measurable zone-independent input parameters of the HSCP RFCS analytical model.

Symbol	Description	Units	Value
N	Rotor rotational speed	rpm	940
T	Throughput	kg/s	3.33 and 5.55
l_{rb}	Rotor bed arc length	m	0.370
R	Rotor bed radius of curvature	m	0.318
P_{base}	Power required to spin the rotor without crop flow	W	9900
AO_{T1}	Angular offset between the center and side tine pairs	°	24
AO_{T2}^{*}	Angular offset between adjacent tine pairs	°	8
AO_{MT}	Angular offset between model and trial rotor	°	64

Table 7.11 Zone-dependent input parameters of the n^{th} zone for the HSCP RFCS analytical model including: arc length of the tine, δ_n, midpoint radius, r_n, angle between the leading and lagging edge of the tine, α_n, and the angle between the radial unit vector and the compressive/cutting force, ζ_n.

		Zone #									
Parameter		**1**	**2**	**3**	**4**	**5**	**6**	**7**	**8**	**9**	**10**
δ_n	mm	22	21	21	20	25	28	36	35	40	67
r_n	mm	242	228	214	199	183	169	157	143	128	114
α_n	°	2	6	11	15	20	28	38	51	65	86
ζ_n	°	41	42	44	45	45	23	24	24	23	18

Table 7.12 Zone-dependent input parameters of the n^{th} zone for the HSCP RFCS analytical model as a function of the level of counter-knife engagement including: the angle between the datum and the leading knife edge, γ_n, and the angle of the rotor when the tine passes the counter-knife, λ_n.

Counter-knife engagement (%)	Parameter		Zone # 1	2	3	4	5	6	7	8	9	10
100	γ_n	°	16	22	27	33	39	45	50	55	61	-90
	λ_n	°	65	68	71	76	80	79	78	77	75	-90
89	γ_n	°	19	26	32	39	46	52	57	62	-90	-90
	λ_n	°	66	70	74	76	76	75	74	72	-90	-90
78	γ_n	°	24	31	38	45	52	58	63	-90	-90	-90
	λ_n	°	68	73	73	73	72	71	70	-90	-90	-90

Indeterminate input parameters: The same parameters that were indeterminate for the LSCP analytical model were indeterminate for the HSCP analytical model. These parameters included: compression width, w, cross-sectional area of the material when it was cut, A_{sm}, the coefficient that related dry-mass density of plant material, when cut, to the initial depth of plant material, ρ, the coefficient that related the initial depth of plant material to the compressive force caused by plant material between the side of a counter-knife and the tine pair, P_f, and the initial depth of plant material for the m^{th} cut, lo_m.

The same method was used to quantify the indeterminate HSCP parameters as was used to quantify the LSCP indeterminate parameters. The indeterminate parameters were adjusted using Solver in Excel to minimize the sum of squared error between the power curve defined by the analytical model and the measured power curve. The trial data that were used to quantify the indeterminate parameters and validate the analytical model were extracted from the trials completed with two levels of throughput (3.33 and 5.55 kg/s) with three levels of counter-knife engagement (100, 89 and 78%) while processing high-level moisture content cereal straw (10.7% w.b.). To compare the trial data to the analytical model output, the trial data needed to be in the form of a power curve as a function of the rotor position ranging from 0 to 359°. Equation (7.34) was used to create

the orientation-dependent power curves. Three replicates were completed for each combination of counter-knife engagement and throughput. The subset of trial data that was used to quantify the indeterminate parameters was chosen by randomly selecting one of the three replicates. An average of the other two replicates was later used to compare the analytical model output to the measured power demand of the HSCP RFCS.

The same constraints were placed on w, A_{sm}, ρ and P_f as were placed on the parameters to quantify them for the LSCP RFCS. The values of the constrains and a discussion of constraints was given in section 7.2.1. As was done during the quantification of the LSCP indeterminate parameters, it was assumed that the depth of plant material for the 78 cuts made by the RFCS at throughputs of 5.55 kg/s would be a multiple of the depth of plant material made by the RFCS at a throughput of 3.33 kg/s. The depth of cereal straw for the m^{th} cut made by the RFCS at a throughput of 5.55 kg/s was assumed to be described by,

$$lo_{m_{5.55\ straw}} = \chi_{5.55\ straw} lo_{m_{3.33\ straw}}\ , \qquad \textbf{(7.42)}$$

where:

$lo_{m\ 3.33\ straw}$ is the initial depth of cereal straw for the m^{th} cut made by the RFCS at a throughput of 3.33 kg/s,

$lo_{m\ 5.55straw}$ is the initial depth of cereal straw for the m^{th} cut made by the RFCS at a throughput of 5.55 kg/s and

$\chi_{\ 5.55\ \ straw}$ is the coefficient that relates the initial depth of cereal straw at a throughput of 3.33 kg/s to the initial depth of cereal straw at a throughput of 5.55 kg/s.

Solver was allowed to change the initial depth of plant material for the 78 cuts made by the RFCS at a throughput of 3.33 kg/s and the throughput-initial depth coefficient, $\chi_{\ 5.55\ straw}$ as well as w, A_{sm}, ρ and P_f.

The values of the indeterminate HSCP parameters are given in Table 7.13. The width of compression, w, was found to be larger when cereal straw was processed by the HSCP RFCS as opposed to the LSCP RFCS (with sharp counter-knives in both the HSCP and LSCP RFCS). The width of compression, w, of the HSCP and LSCP rotary feeding and

cutting systems (while using sharp counter-knives) was the same. However, the faster loading rate and/or the larger gap between the tine pairs on the HSCP RFCS, caused the cereal straw to exhibit a larger Young's modulus, when processed with the HSCP RFCS. Cereal straw would have exhibited a larger Young's modulus because it was visco-elastic in nature, and a faster loading rate would have caused the force required to achieve a given level of deformation to increase. An increased width of compression yielded the same effect as an increased Young's modulus. An increase in the compression width increased the force required to achieve a given level of deformation. Similarly an increase in the Young's modulus increased the force required to achieve a given level of deformation. The average linear speed of the tines on the HSCP RFCS was 18 m/s while the average speed of the compression plate (used to quantify the Young's modulus of plant material) on the material properties test stand was only 0.44 m/s. The Young's modulus of cereal straw was not quantified at a loading rate of 18 m/s, because the maximum sustainable speed of the compression plate (while in contact with the plant material) on the material properties test stand was 0.44 m/s. The increased width of compression could also be attributed to the larger tine-pair gap. The tine-pair gap on the HSCP RFCS and LSCP RFCS was 12 and 9 mm, respectively. The larger gap between the shearing surfaces on the HSCP RFCS could have caused the width of compression in the HSCP RFCS to be larger than the LSCP RFCS.

Table 7.13 The indeterminate input parameters of the HSCP RFCS analytical model.

Symbol	Description	Units	Value
w_{sharp}	Compression width (sharp counter-knife)	m	0.015
$A_{sm\ sharp}$	Cross-sectional area of shear (sharp counter-knife)	m^2	6.21E-07
ρ	Relationship between dry-mass density and lo_m	$(kg\ m^{-3})\ m^{-1}$	1000
$\chi_{5.55\ straw}$	Relationship between lo_m throughput at 3.33 and 5.55 kg/s	--	1.30
P_f	Relationship between force on the side of a counter-knife and lo_m	N/m	746

The relationship between the dry-mass density of plant material at the time it was cut and the initial depth of plant material was found to be equal to 1000 $(kg\ m^{-3})\ m^{-1}$. The

maximum initial depth of plant material was 196 mm, therefore the maximum dry-mass density of plant material was 196 kg/m^3, which was equal to the upper limit of the constraint on the dry-mass density of the cereal straw at the time it was cut.

The cross-sectional area of the plant material at the time it was cut was slightly larger when sharp counter-knives were used in the HSCP RFCS as opposed to the LSCP RFCS. The A_{sm} value for the LSCP RFCS was 1.6E-07 m^2 and 6.2E-07 m^2 for the HSCP RFCS. This means that the force and energy required to cut cereal straw was slightly higher when it was cut with the HSCP RFCS as opposed to the LSCP RFCS. This phenomenon has been observed in the past. Chancellor (1988) found that a major increase in the speed of cutting elements caused a slight increase in the energy required to cut the plant material.

Both the LSCP and HSCP rotary feeding and cutting systems had a direct relationship between the initial depth of cereal straw and throughput. It was expected that there would be a linear relationship between the initial depth of plant material and throughput, and a throughput of zero would correspond to an initial depth of plant material of zero. A throughput of 5.55 kg/s is approximately 1.67 times the throughput of 3.33 kg/s, thus it was expected that $\chi_{5.55\ straw}$ would have been equal to 1.67, however $\chi_{5.55\ straw}$ was found to be equal to 1.30. The flow of the cereal straw out of the threshing rotor and into the chopper may have been impeded at higher throughputs causing $\chi_{5.55\ straw}$ to be 1.30 instead of 1.67. Further experiments with the focus of this variable are necessary to confirm this hypothesis.

The P_f value for the LSCP RFCS while processing cereal straw was 840 N/m and the value for the HSCP RFCS was 746 N/m. The reason that the P_f value was not the same for the LSCP and HSCP RFCS is attributed to the difference in the gap between the tine pairs on the HSCP and LSCP RFCS. The tine-pair gap was 12 mm on the HSCP RFCS and 9 mm on the LSCP RFCS. Because 5-mm thick counter-knives were used in both RFCS, the clearance between the tine-pair and the side of the counter-knife was 3-mm less on the LSCP than the HSCP RFCS. Given the same depth of plant material in both systems (LSCP and HSCP RFCS), the force required to compress the plant material between the tine and the counter-knife on the LSCP RFCS would be larger than the force

required to do the same on the HSCP RFCS because of the smaller clearance between the counter-knife and the tine pair.

The average initial depth of cereal straw that was processed by the HSCP RFCS was significantly lower than the average initial depth of plant material processed by the LSCP RFCS. The average initial depth of cereal straw that was processed at a throughput of 5.55 kg/s with the HSCP RFCS was 26 mm while the average initial depth of cereal straw processed by the LSCP RFCS at a throughput of 5.0 kg/s was 194 mm. The reason that the initial depth of cereal straw was significantly lower when processed by the HSCP RFCS as opposed to the LSCP RFCS is attributed to the difference in the working width and operational speed of the two rotary feeding and cutting systems. The working width of the LSCP RFCS was 286 mm while the working width of the HSCP RFCS was 1015 mm. Given approximately the same level of throughput in the two systems, and assuming that the bulk density of the plant material flowing into the systems was the same and uniformly distributed across the working width of the system, the depth of plant material would be 3.5 times less in the HSCP RFCS than the LSCP RFCS. The geometry of the tines on the HSCP and LSCP RFCS were approximately the same, however the rotational speed of the rotor in the HSCP RFCS was 940 rpm while the LSCP RFCS rotor rotational speed was 140 rpm. The depth of plant material is inversely related to the rotational speed of the rotor because, the amount of plant material that enters the path of the tines is inversely proportional to the rotational speed of the rotor (given the same throughput). The initial depth of cereal straw as a function of the m^{th} cut made by the HSCP RFCS (WR chopper) is shown in Figure 7.19.

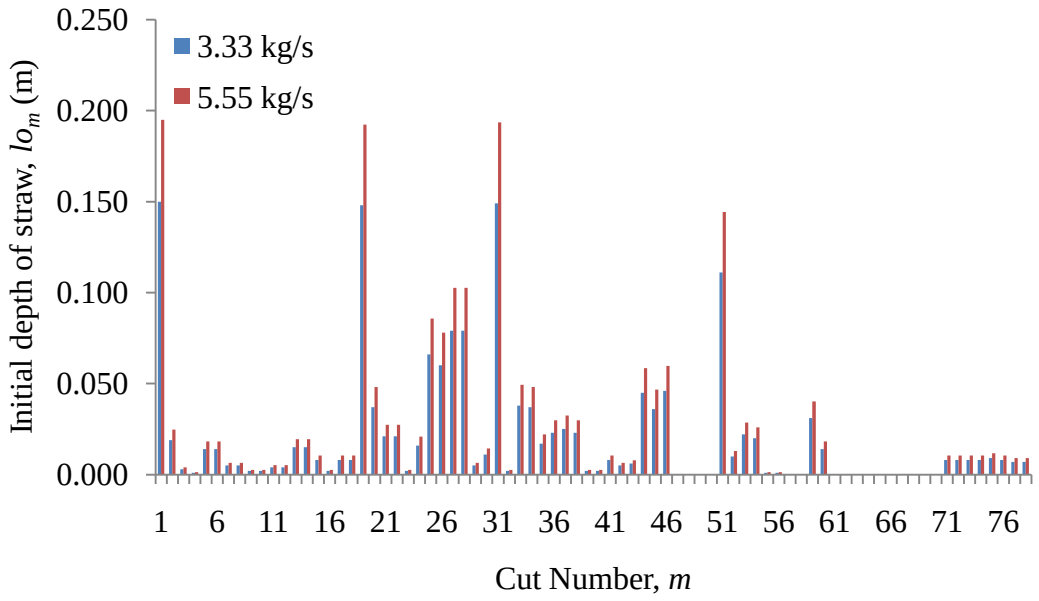

Figure 7.19 The initial depth of the m^{th} cut made by the HSCP RFCS while processing cereal straw at a throughput of 3.33, and 5.55 kg/s.

7.3.2 Validation

The indeterminate inputs were quantified by minimizing the sum of squared error between the analytical model output and a subset of the data collected with the HSCP RFCS. Three replicates were completed with the HSCP RFCS during the trials that investigated the effect of throughput and counter-knife engagement. One of the replicates was used to quantify the indeterminate parameters while the average of the other two replicates was used to validate the model. In the previous section the measurable and indeterminate model inputs were quantified. In this section the output of the analytical model and the measured power demand of the RFCS are compared.

The model output, average and the 95% confidence interval of the measured power demand of the RFCS while processing cereal straw at two levels of throughput, with three levels of counter-knife engagement is shown in Figures 7.20 to 7.22. The 95% confidence interval was included to show the magnitude of the variation of the average power demand of the RFCS. As with the LSCP RFCS it is believed that the variation in the average power demand of the HSCP RFCS at a given angular position of the rotor is

due to variations in the instantaneous throughput of plant material, which caused variations in the initial depth of plant material.

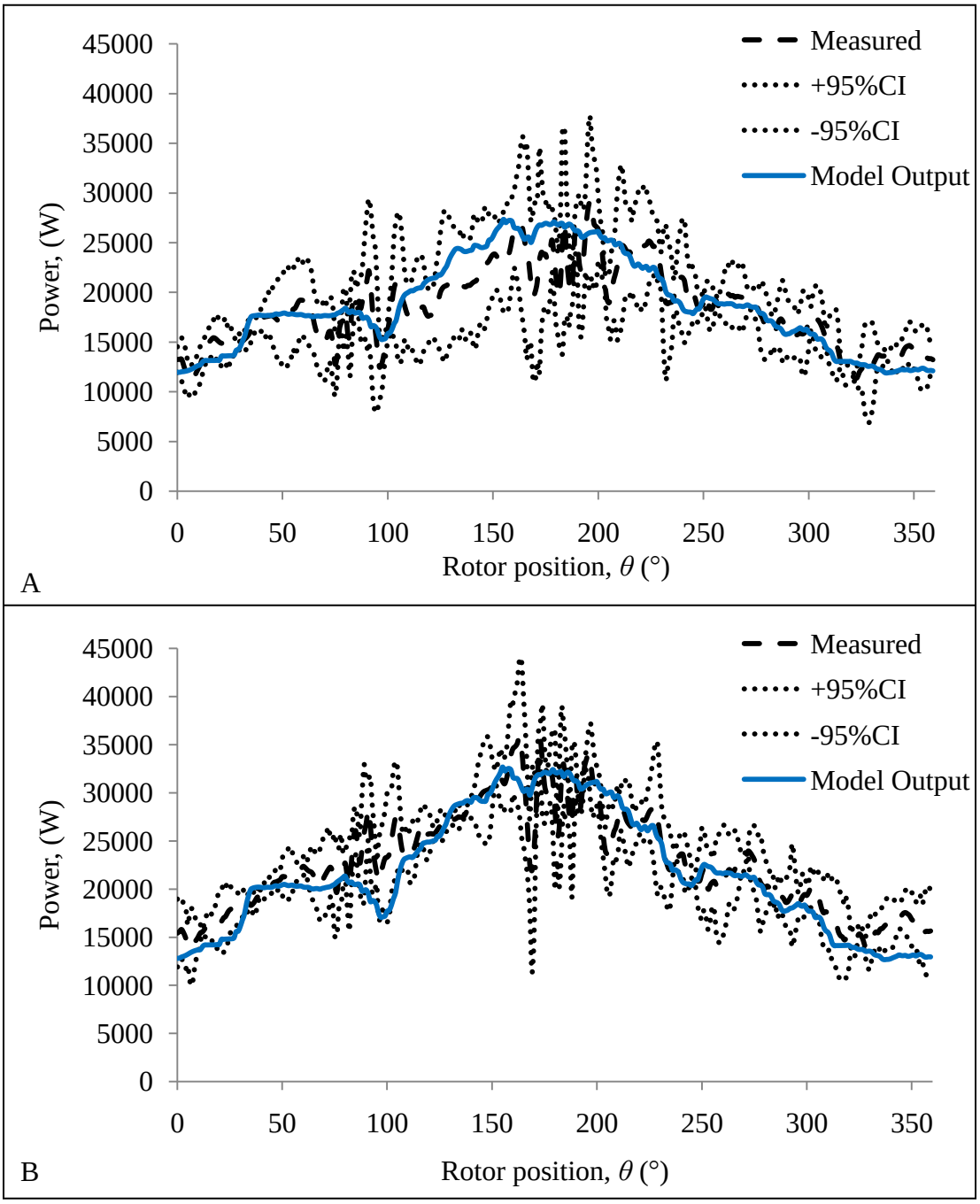

Figure 7.20 The average and ± 95% confidence interval (CI) of the measured power demand of the HSCP RFCS, and the analytical model output when 100% inserted counter-knives were used to process straw at a throughput of (A) 3.33 and (B) 5.55 kg/s.

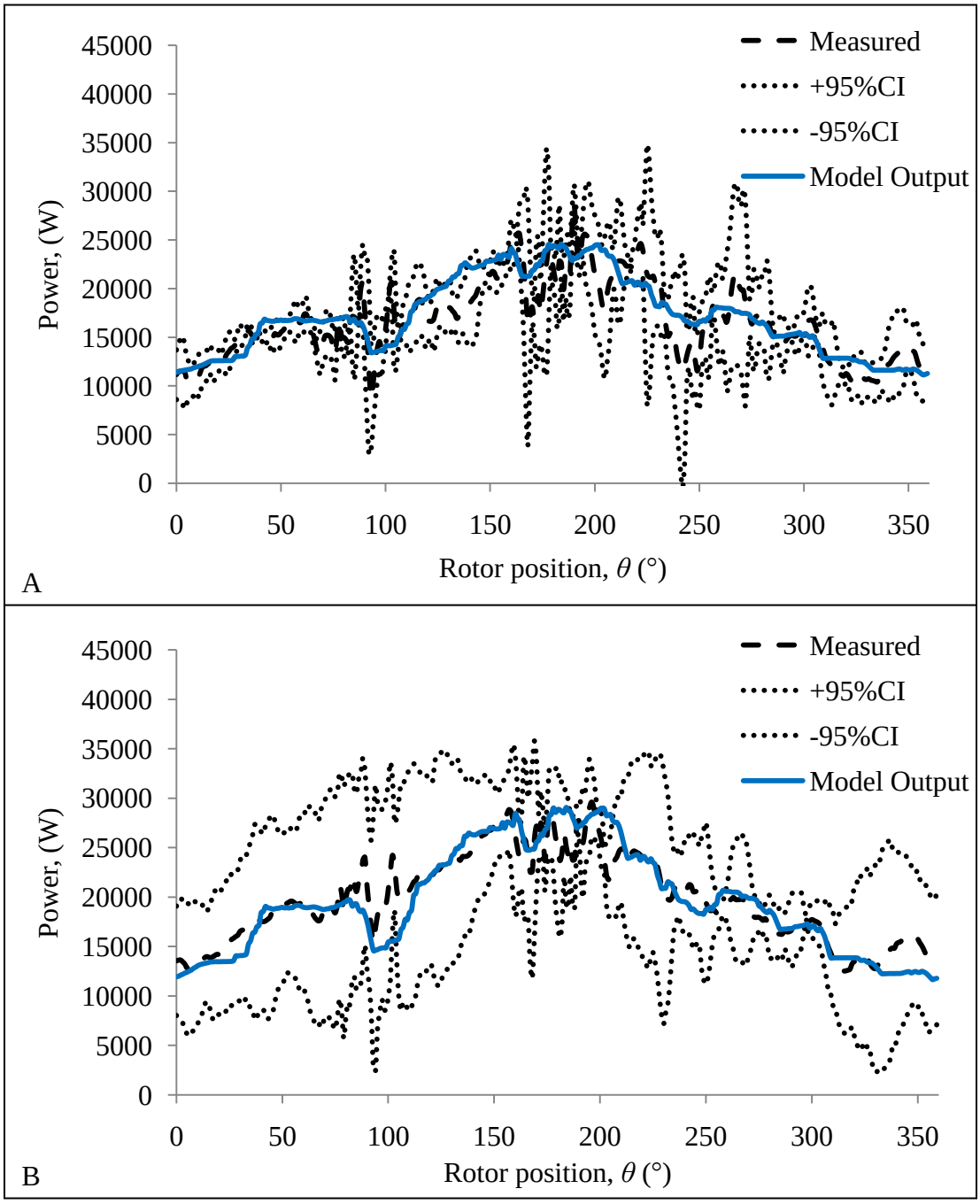

Figure 7.21 The average and ± 95% confidence interval (CI) of the measured power demand of the HSCP RFCS, and the analytical model output when 89% inserted counter-knives were used to process straw at a throughput of (A) 3.33 and (B) 5.55 kg/s.

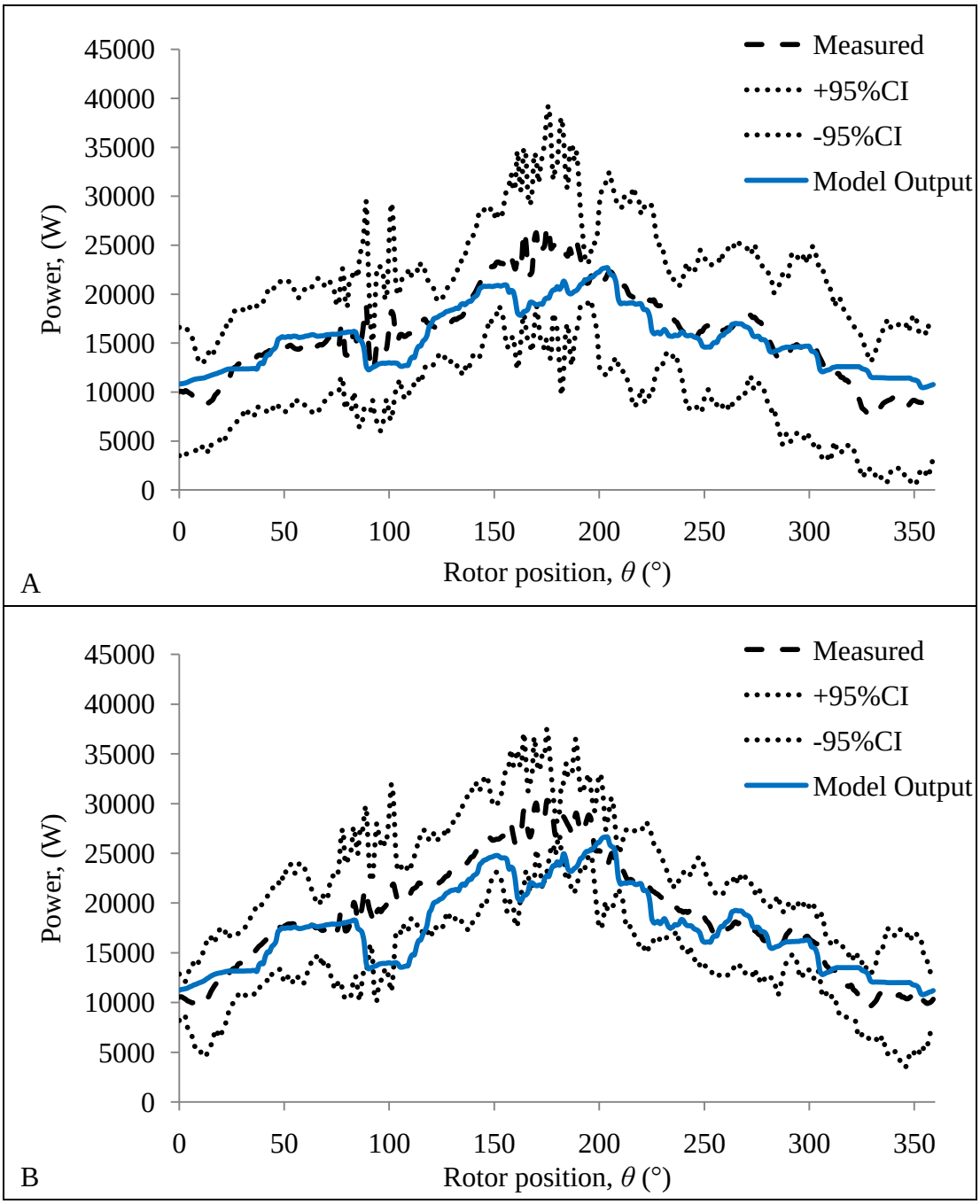

Figure 7.22 The average and ± 95% confidence interval (CI) of the measured power demand of the HSCP RFCS, and the analytical model output when 78% inserted counter-knives were used to process straw at a throughput of (A) 3.33 and (B) 5.55 kg/s.

A common trend was present in all the HSCP trials, in that the average power demand of the HSCP RFCS was concave downward with the maximum occurring at a rotor

position of 150 to 200°. This phenomenon is believed to be attributed to variations in the instantaneous throughput of plant material entering the RFCS. Variation in the instantaneous throughput of plant material has a direct correlation with the initial depth of plant material being cut by the RFCS. The variations in the instantaneous throughput are believed to be attributed to the systems used to convey the plant material to the chopper, mainly the threshing rotor. The threshing rotor had two "flightings" on the front of the threshing rotor and two "evacuating" elements on the rear of the threshing rotor. The configuration of the crop engaging elements on the threshing rotor was expected to cause the plant material exiting the threshing rotor to occur in two "bursts" (over a single rotation of the threshing rotor). Because the speed of the threshing rotor and chopper were approximately 1100 and 940 rpm respectively, during the field trials, it was expected that the initial depth of plant material would have 2 to 3 maxima during a single rotation of the chopper. The initial depth of plant material on a per cut basis over one revolution of the chopper is shown in Figure 7.23 for a throughput of 3.33 kg/s. In Figure 7.23, it is apparent that there are two sets of maxima when the chopper was at an angular position of 0 to 120° and 121 to 240°. These sets of maxima are attributed to the orientation of the crop engaging elements on the threshing rotor. The initial depth of the plant material on a per cut basis over one full revolution of the chopper at a throughput of 5.55 kg/s is a scaled version of the initial depth of plant material at a throughput of 3.33 kg/s, as it was assumed that $\chi_{5.55\ straw}$ was 1.30. Thus, the location of the two sets of maxima at a throughput of 3.33 and 5.55 kg/s occurred at the same angular orientations and on the same counter-knives. It should also be noted that the series of vanes that are typically installed inside the top of the rotor cage (the cylindrical structure within which the threshing rotor rotates) to facilitate the movement of plant material past the threshing rotor were not installed. The lack of the vanes could have caused the flow of crop material to be more sporadic than if the vanes were installed.

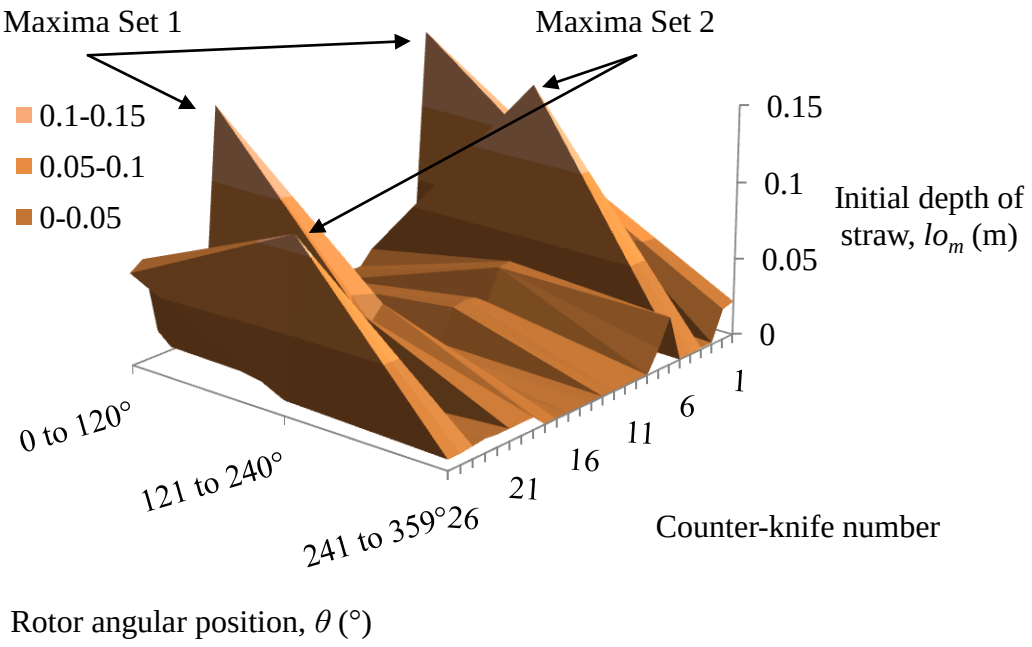

Figure 7.23 The initial depth of cereal straw in the HSCP RFCS with a throughput of 3.33 kg/s as a function of the counter-knife number (counter-knife 1 being the farthest left counter-knife in the combine) and the rotor angular position.

The telemetry system that was used to transfer the signal from the strain gages mounted on the chopper to the data logger could have attributed to the magnitude of the 95% CI. If the signal strength from the transmitter becomes weak the signal out of the receiver would become noisy. If the signal from the transmitter was completely lost the signal out of the receiver was set to drop to zero. The signal from the transmitter was not lost because the measured power demand of the chopper never dropped to zero. However, the increase in the magnitude of the 95% CI could be attributed to a weak transmitter signal strength during the trials completed with a counter-knife engagement of 78% and, the high throughput trials that were completed with a counter-knife engagement of 89%. The other factor that was believed to have an effect on the magnitude of the 95% CI was variations in the instantaneous throughput during the trial. The implication

of the variation in the instantaneous throughput and their effect on the 95% CI were discussed in section 7.2.2.

As with the LSCP RFCS the correlations coefficient was not used as an indication of the accuracy of the HSCP RFCS model. The correlation coefficient of the HSCP RFCS was also low, and as with the LSCP RFCS the low value is believed to be largely attributed to the inability to control the instantaneous throughput (and depth of plant material) during the trials.

The error between the average measured power and model output (both averaged over the full revolution of the rotor) ranged from positive 6.6 to negative 3.2%. Further, the analytical model output typically fell within the envelope of the ±95% confidence interval for the trials completed at two levels of throughput, with counter-knives at three levels of engagement. Thus, the analytical model can be used by future designers of the RFCS to quantify the power demand of the HSCP RFCS, if it is acceptable to have an absolute error of less that 6.6%. If the designer requires a more accurate model additional work will need to be completed to improve the accuracy of the analytical model.

7.3.3 Sensitivity analysis

The same type of sensitivity analysis (a one-factor-at-a-time sample-based analysis) that was completed on the LSCP RFCS' analytical model was also completed on the HSCP RFCS' analytical model. The sensitivity analysis was completed to identify which factors had the largest influence on the power demand of the RFCS. The sensitivity of each factor included in the HSCP RFCS analytical model sensitivity analysis was determined using equation (7.39). It was concluded that lo_m for the LSCP RFCS was affected by rotor speed, the pattern of tines on the rotor and throughput of plant material. It would be logical to expect that lo_m for the HSCP RFCS would also be affected by the same factors. Therefore, rotor speed and the pattern of tines on the rotor were excluded from the sensitivity analysis because changing these factors would likely change the previously defined relationship between lo_m and throughput. Further, as with the LSCP RFCS analytical model the HSCP FRCS model was developed under the assumption that the initial depth of plant material in all 10 zones of the m^{th} cut were equal. The zone-

specific input parameters were not included in the sensitivity analysis because changing them would likely change the distribution of plant material along the leading edge of the counter-knives and violate the assumption that the initial depth of plant material in all 10 zones was equal. As with the LSCP RFCS analytical model sensitivity analysis, rotor bed arc length and rotor bed radius of curvature were also left out of the sensitivity analysis because it would only be logical to change them if the radius of the tines was changed, and the radius of the tines was a zone specific parameter. The high, medium and low levels of the factors included in the HSCP RFCS analytical model sensitivity analysis is given in Table 7.14.

Table 7.14 The high, medium and low levels of the factors included in the HSCP RFCS analytical model sensitivity analysis.

Symbol	Description	Units	Low	Medium	High
T	Throughput	kg/s	3.33	3.33	5.55
--	Counter-knife engagement	%	78	89	100
ρ	Coefficient that relates the dry-mass density of plant material to the initial depth of plant material	$(kg\ m^{-3})m^{-1}$	850	1000	1150
P_f	Coefficient that relates the initial depth of plant material to the compressive force caused by plant material between the side of a counter-knife and the tine pair	N/m	593	746	913
μ	Dynamic coefficient of friction	--	0.14	0.31	0.47
τ_{int}	Intercept of maximum shear strength	kPa	2160	3080	4000
E	Young's modulus (at 80% strain)	kPa	111	123	140

The power demand of the HSCP RFCS was most sensitive to counter-knife engagement. The sensitivity of the HSCP RFCS to throughput was similar to the sensitivity of the LSCP RFCS (while processing alfalfa). As was observed with the LSCP RFCS the power demand of the HSCP RFCS was considerably more sensitive to the dynamic coefficient of friction between cereal straw and the RFCS than the Young's

modulus or maximum shear strength of cereal straw. As with the LSCP RFCS, an effective way to decrease the power demand of the HSCP RFCS would be to decrease the coefficient of friction between the cereal straw and the HSCP RFCS. The coefficient that relates the initial depth of plant material to the compressive force caused by plant material between the side of the counter-knife and the tine, P_f, also had a relatively large influence on the power demand of the HSCP RFCS. Similar to the LSCP RFCS, the power demand of the HSCP RFCS would benefit from a design change that prevented plant material from being entrapped between the side of the counter-knives and the tine pair. As was observed with the LSCP RFCS, the HSCP RFCS was least sensitive to the coefficient that relates the dry-mass density of plant material to the initial depth of plant material, ρ. Recall that the value of ρ indirectly affects the force required to cut the plant material. The fact that the HSCP RFCS was least sensitive to both the intercept of maximum shear strength, τ_{int}, and ρ suggests that design changes to decrease the energy required to cut the plant material would be relatively ineffective in decreasing the total power demand of the HSCP RFCS. The sensitivity of the factors in the HSCP RFCS analytical model is given in Table 7.15.

Table 7.15 Sensitivity of the HSCP RFCS analytical model while processing cereal straw.

Symbol	Description	Units	Sensitivity
--	Counter-knife engagement	%	0.85
Pf	Coefficient that relates the initial depth of plant material to the compressive force caused by plant material between the side of a counter-knife and the tine pair	N/m	0.43
μ	Dynamic coefficient of friction	--	0.38
T	Throughput	kg/s	0.23
E	Young's modulus (at 80% strain)	kPa	0.01
τ_{int}	Intercept of maximum shear strength	kPa	0.01
ρ	Coefficient that relates the dry-mass density of plant material to the initial depth of plant material	$(kg\ m^{-3})m^{-1}$	0.01

The total average power (power to transport, compress and cut) required by the HSCP RFCS at a throughput of 5.55 kg/s with sharp counter-knives that were fully inserted was 21.7 kW. The power required to compress and cut the plant material along the leading edge of the counter-knives was 0.333 kW. The power required to transport the plant material (along the leading edge of the tines, the rotor bed and the side of the counter-knives) was 11.5 kW. Of that amount, 10.8 kW was required to transport the plant material along the sides of the counter-knives, 0.547 kW was required to transport the plant material along the rotor bed and 0.128 kW was required to transport the plant material along the leading edge of the tines. As was concluded from the sensitivity analysis, the power required to transport cereal straw along the sides of the counter-knives was relatively large compared to the power required to transport the cereal straw along the rotor bed and along the leading edge of the tines. The three options that were discussed in section 7.2.3 could also be used to decrease the power demand of the HSCP RFCS.

The three options were to eliminate a tine and possibly add a transport surface to the "shearing" tine as shown in Figure 7.16, to coat the inside surfaces of the tine with Baked Teflon®, as shown in Figure 7.17 and to decrease the length of the counter-knives, as shown in Figure 7.18. Option 1, the removal of a tine would result in a decrease of 5.4 kW in the power demand of the HSCP RFCS which corresponds to a 25% decrease in the total average power demand of the HSCP RFCS. Assuming that the dynamic coefficient of friction between the tine and the counter-knife could be reduced to 0.18 by coating the tines with Baked Teflon®, the power demand of the HSCP RFCS would decrease by 3.3 kW, which corresponds to a 15% decrease in the total average power demand of the HSCP RFCS. The final option presented was to decrease the length of the counter-knife, as shown in Figure 7.18, which would decrease the power demand of the HSCP RFCS by 3.3 kW, which corresponds to a 15% decrease in the total average power demand of the RFCS.

7.4 Conclusions

The analytical model is valid for both the LSCP and HSPC RFCS because typically, but not always, the analytical model output fell within the ± 95% confidence interval of

the measured power demand of both the LSCP and HSCP RFCS. For the LSCP RFCS the analytical model can be used to quantify the effect of counter-knife sharpness, throughput and plant material type on the power demand of the LSCP RFCS. For the HSCP RFCS the analytical model can only be used to assess the power requirements of the WR chopper. The other choppers tested (2X3, 3X3 and 2X0.5) perform impact cuts which violates the principles on which the analytical model was developed. For the HSCP RFCS the analytical model can be used to quantify the effect of counter-knife engagement and throughput on the power demand of the HSCP RFCS.

Slightly more than 50% of the total power demand of the LSCP and HSCP rotary feeding and cutting systems is attributable to transporting plant material, and the majority of the transport power is attributable to transporting plant material along the side of the counter-knives. The reason that the power associated with transporting plant material along the side of the counter-knives is high is attributed to the relatively large clearance between the tine and the counter-knife. The large clearance allows plant material to wrap around the leading edge of the counter-knife and subsequently wedge between the sides of the counter-knife and the tine.

The power required to cut and compress the plant material in both the LSCP and HSCP RFCS was relatively small compared to the power required to transport the plant material. Only 2 to 15% of the total power demand of the rotary feeding and cutting systems was attributed to compressing plant material between the leading edge of the counter-knives and tines and cutting the plant material. Kepner et al. (1978), McRandal and McNulty (1978), as well as Ige and Finner (1976b) have all observed the same trend where only a small fraction of the total energy used by the cutting mechanism is used to cut the plant material.

Three different design modifications were suggested to decrease the power required to transport the plant material along the side of the counter-knives, because the majority of the total power demand of the RFCS was attributed to transporting plant material along the side of the counter-knives. The first suggestion was to remove one of the tines from each tine pair (shown in Figure 7.16), the second was to coat the inside surface of the tine with Baked Teflon® (shown in Figure 7.17) and the third suggestion was to modify the

profile of the counter-knife (as shown in Figure 7.18). Based on the analytical model, by implementing one of these suggested modifications the total power demand of both the LSCP and HSCP RFCS could be decreased by 15 to 26%.

7.5 Recommendations for future work

Because of the limitations of the analytical model, the following list of recommendations has been compiled to accelerate any future refinement of the analytical model:

1. In terms of improving the versatility and usefulness of the analytical model, it would be of great benefit for a study to be completed to determine what factors affect lo_m, and the effect of the profile of the leading edge of the counter-knife and tine on the distribution of plant material along the leading edge of the tine and counter-knife. Upon completion of this study the analytical model could be used to further improve the efficiency of the RFCS examined during this project by investigating the effect of changing all of the design parameters in the model. Based on the field and laboratory tests already completed with the RFCS, lo_m was affected by the throughput & type of plant material processed by the RFCS, the device used to feed plant material into the RFCS, the rotational speed of the rotor and the pattern of tines on the rotor.

2. The inclusion of counter-knife spacing as an input parameter to the model would be of benefit. In theory, decreasing the spacing between the counter-knives (and the spacing of the tines on the rotor) would be directly related to the magnitude of the particle length reduction that the plant material would experience.

3. The development of a model that could be used to quantify the degree of particle length reduction that plant material experiences as a result of being processed by the RFCS would also be of great benefit.

4. In order for the analytical model to be used to predict the power demand of a different RFCS (than the two that were investigated during this project) one of two tasks needs to be completed. A series of field trials could be completed during which the power demand of the RFCS would be measured. The field trial data could be used to quantify the indeterminate parameters (w, A_{sm}, lo_m, P_f and ρ). The second option would be to quantify the effect of all parameters on the indeterminate parameters. The second option is more attractive because of the versatility of the resulting model. However, the second option is much more complex than the first and would require a substantial investment in future research.

5. The development of an analytical model that could be used to predict the power demand of the 2X3, 2X0.5 and 3X3 choppers would be of benefit. The power demand of the aforementioned choppers could not be predicted with the analytical model described in section 7.1. The analytical model described in section 7.1 was developed under the assumption that the plant material would be cut between two surfaces (the leading edge of the tine and the leading edge of the counter-knife). Some of the plant material processed by the 2X3, 2X0.5 and 3X3 choppers was cut on the counter-knives, however because of the high speed and sharpness of the cutting elements on the choppers, some of the plant material was cut by the rotating elements alone. Because of this, the analytical model described in section 7.1 could not be used to predict the power demand of the choppers.

8 STOCHASTIC MODEL

The stochastic model was created to predict which of the four choppers tested in the combine harvester would have the best performance when subject to the same operating conditions. Within the realm of the stochastic model, the performance of the chopper refers to the specific energy requirement of the chopper and the geometric mean length (GML) of material other than grain (MOG) exiting the combine harvester when the chopper was employed. The best performance of a chopper would be one that consumed the least amount of specific energy to achieve the lowest acceptable GML of MOG. During the field trials (discussed in chapter 6) the choppers were not subjected to the same operating conditions, which prevented the best performing chopper from being directly identified from the field trial data. A stochastic model was well-suited for determining the best performing chopper because during normal operation, the chopper in the combine harvester was subjected to straw at varying throughputs and moisture contents. After processing the data collected from the field trials completed with the combine harvester, it was concluded that in general the specific energy requirement of the choppers was affected by the independent factors (counter-knife engagement, straw moisture content and throughput).

The relationship between the specific energy requirement of each chopper and the independent factors that had a significant effect on the specific energy requirement of the choppers was established using linear regression. Similarly, the relationship between the GML of MOG and the independent factors that had a significant effect on the GML of MOG was established using linear regression. The independent factors being counter-knife engagement, straw throughput and moisture content. The functional relationships were used to identify the specific energy requirement of each chopper, and the corresponding GML of MOG as a function of the significant independent factors, when each chopper was subjected to the same operating conditions. Ultimately, the output from the stochastic model was used to identify which chopper resulted in the minimum GML of MOG while consuming the least amount of specific energy, when subjected to the same operating conditions.

8.1 Development

8.1.1 Stochastic model

The stochastic model has three components: The inputs, the functional relationships and the output. Based on the conclusions drawn from the field data collected with the combine harvester (discussed in chapter 6), generally, the choppers' specific energy requirement was affected by counter-knife engagement and straw moisture content and throughput. Further, the GML of MOG was affected by counter-knife engagement, and straw moisture content. The inputs of the stochastic model were the moisture content and throughput of straw processed by the choppers. The functional relationships were defined using linear regression to relate the specific energy requirement of the chopper (at each level of counter-knife engagement) and the GML of MOG to the throughput and moisture content of the straw processed by the choppers. The simulated "normal" operating conditions to which each chopper was subjected was created by randomly selecting the throughput and moisture content of the straw during normal operating conditions. One hundred thousand different scenarios (combinations of straw throughput and moisture content) or operating conditions were defined and the specific energy requirement of each chopper and the GML of MOG were quantified. Histograms were created as the output of the model. The specific energy and GML data were compiled using histograms to identify at a 95% probability what the specific energy and GML of MOG would be for each chopper.

8.1.2 Functional relationships

The same data that was presented in chapter 6 were used to quantify the relationships between the dependent and independent factors. The independent factors included straw throughput, counter-knife engagement and straw moisture content, while the dependent factors were the specific energy required by the chopper and the GML of MOG. Because of a sensor malfunction, the specific energy demand of the 2X0.5 chopper could not be quantified, and therefore the relationship between the specific energy requirement of the 2X0.5 chopper and the independent factors could not be quantified. As discussed in chapter 6, it was impossible to complete tests with the 2X0.5 chopper again, because the maturity of the crop changed with time and in order to compare the performance of all

choppers the field trials needed to be completed in the least amount of time. A statistical analysis was not completed to identify the statistical significance of the independent factors on the GML of MOG. The reason for this is that there were no repeated measurements taken of the GML of MOG as a function of the independent factors.

A statistical analysis (ANOVA) was done to identify which of the independent factors had a significant effect on the specific energy requirements of the choppers. A probability of 0.05 was used as the criterion to accept or reject the null hypothesis. The statistical analysis and the results of the analysis are discussed in detail in chapter 6. The statistical analysis revealed that the specific energy requirement of the 3X3 chopper was significantly influenced by counter-knife engagement and straw moisture content. The specific energy required by the 2X3 chopper was significantly influenced by counter-knife engagement, throughput, and moisture content. Throughput and counter-knife engagement had a statistically significant effect on the specific energy requirements of the WR chopper. For all three choppers, the interaction between counter-knife engagement and straw moisture content had a significant effect on the specific energy requirement of the choppers.

The effect of straw moisture content on the specific energy requirement of the 2X3, 3X3 and WR chopper is shown in Figure 8.1. For all three choppers there appeared to be a direct relationship between the straw moisture content and the specific energy required by the choppers. The direct relationship between straw moisture content and the specific energy required by the straw choppers is attributed to two phenomena. First, dry straw behaved as a brittle material, and when processed by the combine harvester, the dry straw underwent extensive particle length reduction in the threshing rotor and feeder. Thus, when dry straw was processed, the majority of the straw that entered the chopper was likely short enough that it passed through the chopper without being cut. Conversely, when wet straw was processed, the straw experienced a lower proportion of particle length reduction due to the threshing rotor or feeder. Thus, when wet straw was processed, the chopper was responsible for a greater degree of particle length reduction. The increase in energy consumption of the choppers was due to an increase in the amount of particle length reduction caused by the choppers. Second, the increase in moisture

content of the straw caused the dynamic coefficient of friction of the straw to increase. The increase in the dynamic coefficient of friction (between the straw and steel) resulted in a greater amount of energy used to transport the straw through the chopper. The effect of straw moisture content on the GML of the straw that exited the combine harvester is shown in Figure 8.2. It appears that for all choppers there is a direct relationship between the GML of MOG and the moisture content of the straw processed by the choppers. The direct relationship between GML of MOG and straw moisture content is attributed to the fact that the wet straw was more ductile and underwent less particle length reduction in the threshing rotor, feeder and chopper.

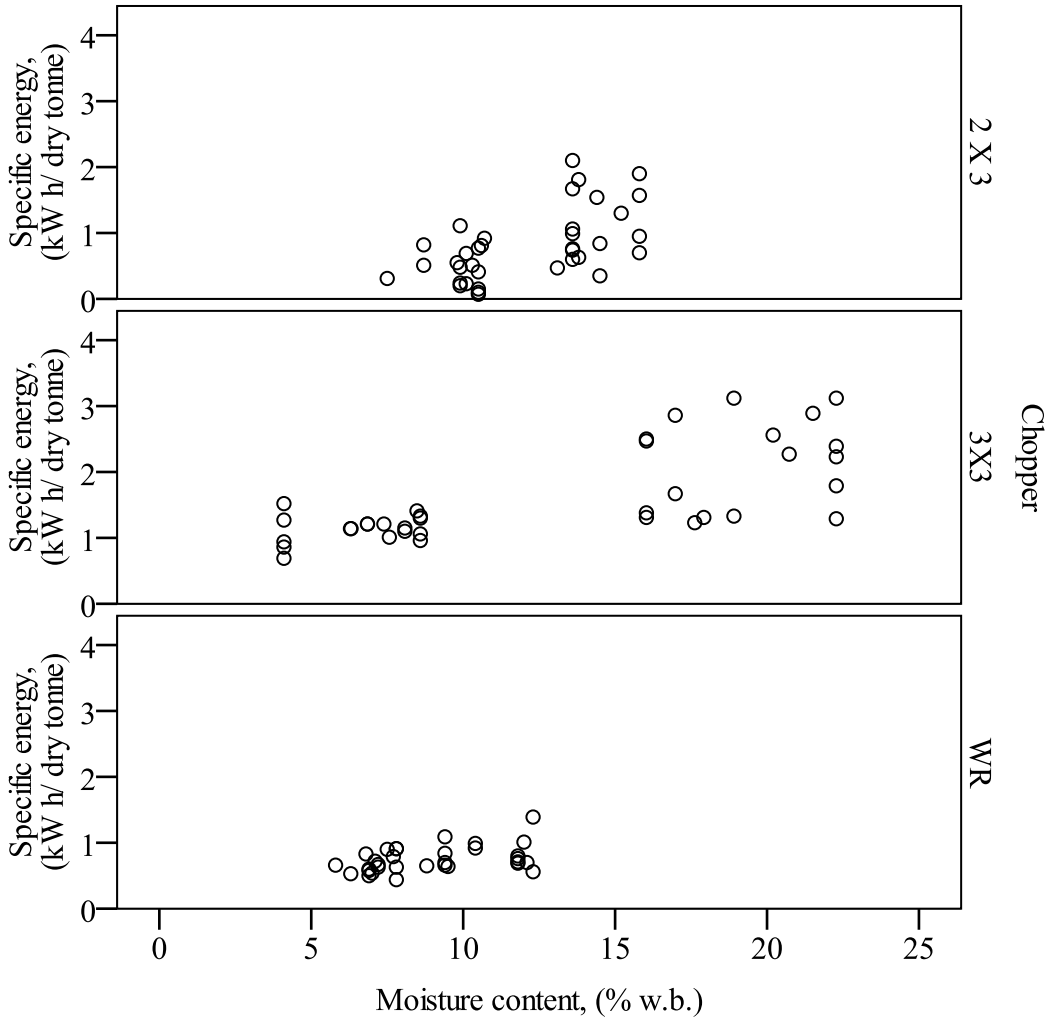

Figure 8.1 The specific energy requirements of the 2X3, 3X3 and WR chopper as a function of the moisture content of the straw processed by the choppers.

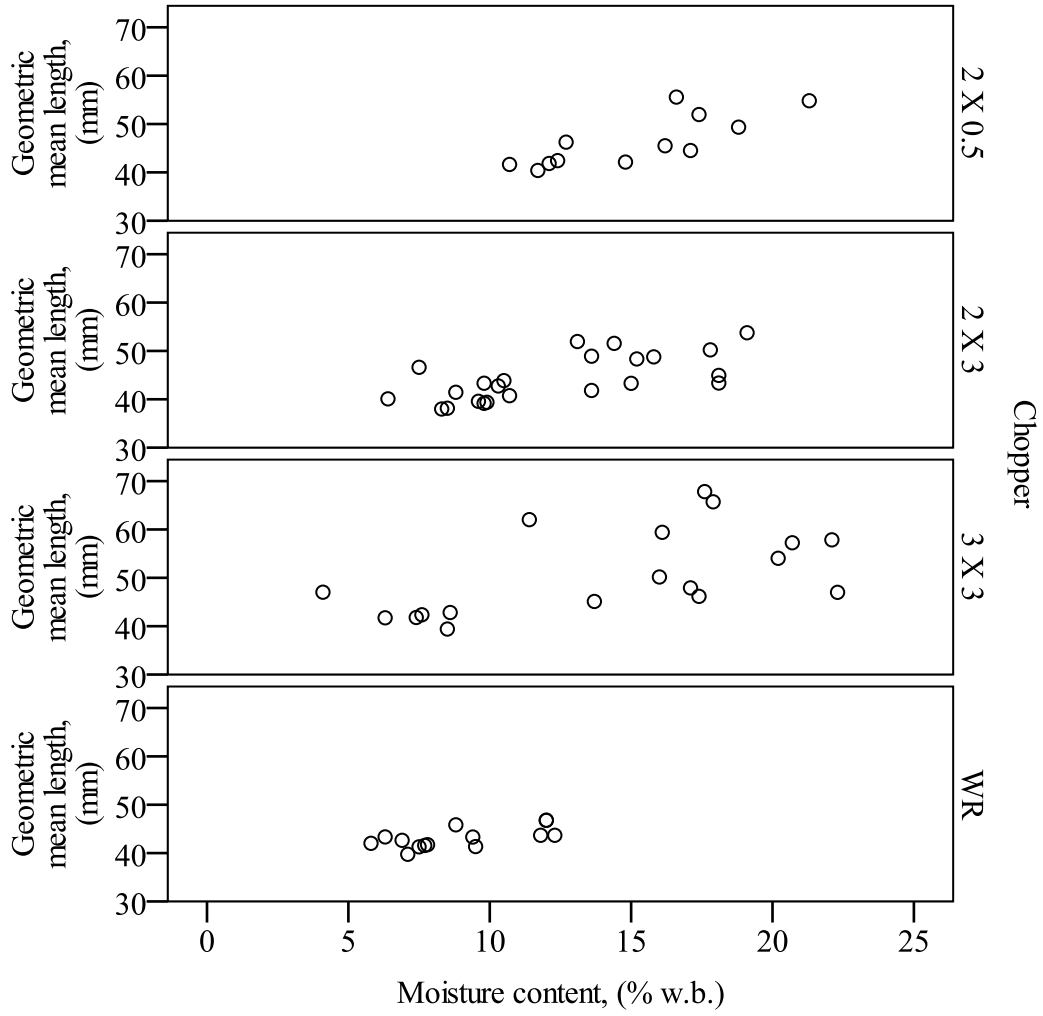

Figure 8.2 The geometric mean length (GML) of straw that exited the combine harvester as a function of the moisture content of the straw processed by the choppers while the 2X0.5, 2X3, 3X3 and WR chopper were installed in the combine harvester.

The effect of throughput on the specific energy requirement of the 2X3, 3X3 and WR choppers are shown in Figure 8.3. It appears that the specific energy requirements of the 2X3 and WR were independent of throughput. It also appears that there was an inverse relationship between throughput and the specific energy required by the 3X3 chopper. This inverse relationship is due to the correlation between straw moisture content and throughput. During the 3X3 trials, straw at relatively high moisture content was processed, as shown in Figures 8.1 and 8.2. During the high moisture content trials, the

throughput of the combine harvester had to be decreased to prevent the threshing rotor from plugging. It appears that the GML of plant material exiting the combine harvester was independent of throughput for all choppers tested, as shown in Figure 8.4.

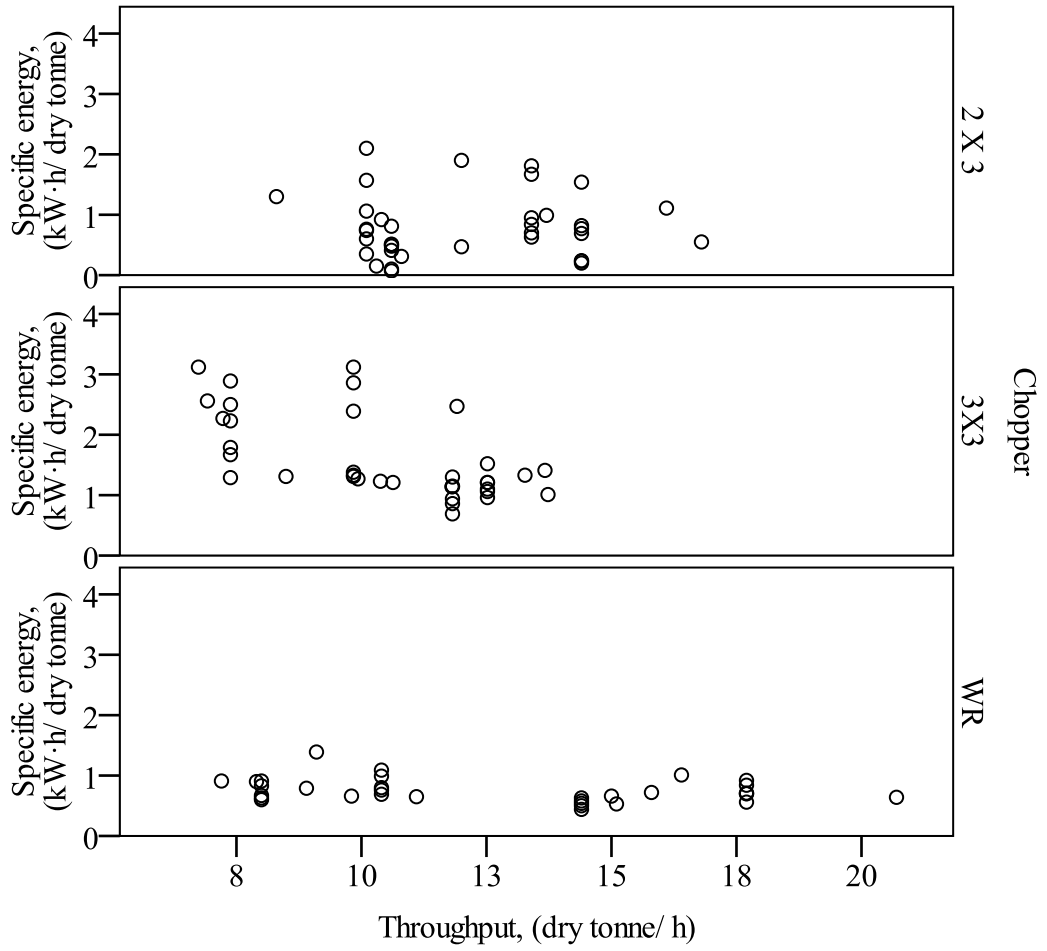

Figure 8.3 The specific energy requirements of the 2X3, 3X3 and WR chopper as a function of the throughput of straw through the choppers.

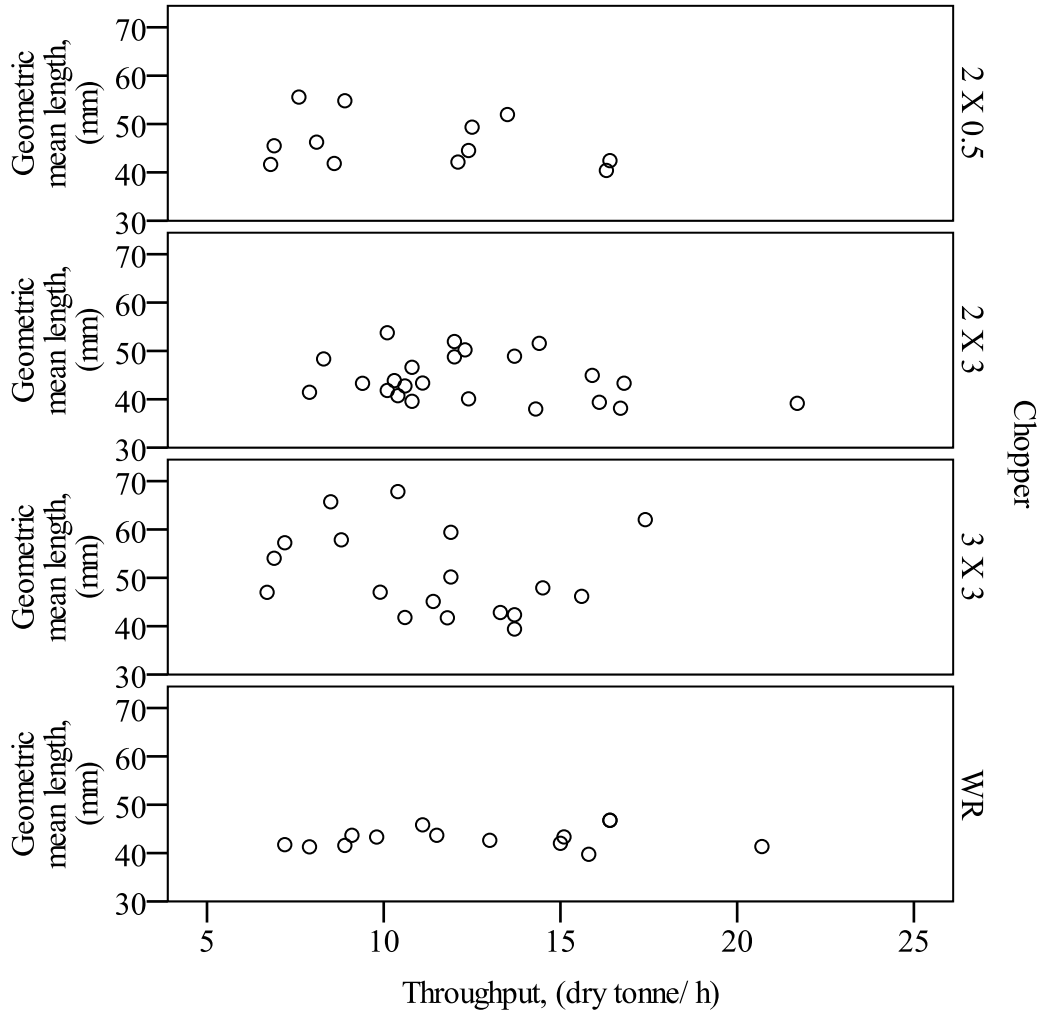

Figure 8.4 The geometric mean length (GML) of straw that exited the combine harvester as a function of the throughput of the straw through the choppers while the 2X0.5, 2X3, 3X3 and WR chopper were installed in the combine harvester.

The effect of the interaction between counter-knife engagement and straw moisture content, on the specific energy required by the 2X3, 3X3 and WR choppers is shown in Figure 8.5. For all three choppers, the effect of counter-knife engagement on the specific energy required by the chopper was subtle when low moisture content straw was processed. As previously discussed, dry straw behaved as a brittle material, and when dry straw was processed, the majority of the straw that entered the chopper was likely short enough that it passed through the chopper without being cut, regardless of the

position of the counter-knives. Conversely, the effect of counter-knife engagement was apparent when high moisture content straw was processed. When high moisture content straw was processed, the chopper was responsible for a greater degree of the straw length reduction. The counter-knives acted as a counter-shear and interrupted the flow of straw past the chopper until further straw length reduction was achieved. Because the counter-knives aided the cutting process at higher straw moisture contents, the effect of counter-knife engagement was more noticeable. For the 3X3 and 2X3 choppers, when straw was processed that had a moisture content in excess of 12% w.b., the specific energy requirement of the choppers was directly related to counter-knife engagement. The reason for this was that engaged counter-knives accomplished two things, they restricted the flow of plant material past the chopper, and they provided support (acted as a counter-shear) to the plant material that was being cut. Both the restriction in the flow of plant material past the chopper and counter-shear support of the plant material resulted in a greater degree of particle length reduction caused by the chopper. The greater sensitivity of the GML of straw exiting the combine harvester to counter-knife engagement (when high moisture content straw was processed) is shown in Figure 8.6. The greater degree of particle length reduction came at a cost of an increased amount of energy consumed to transport, compress and cut the plant material, instead of simply transporting the plant material through the chopper (when the counter-knives were fully removed).

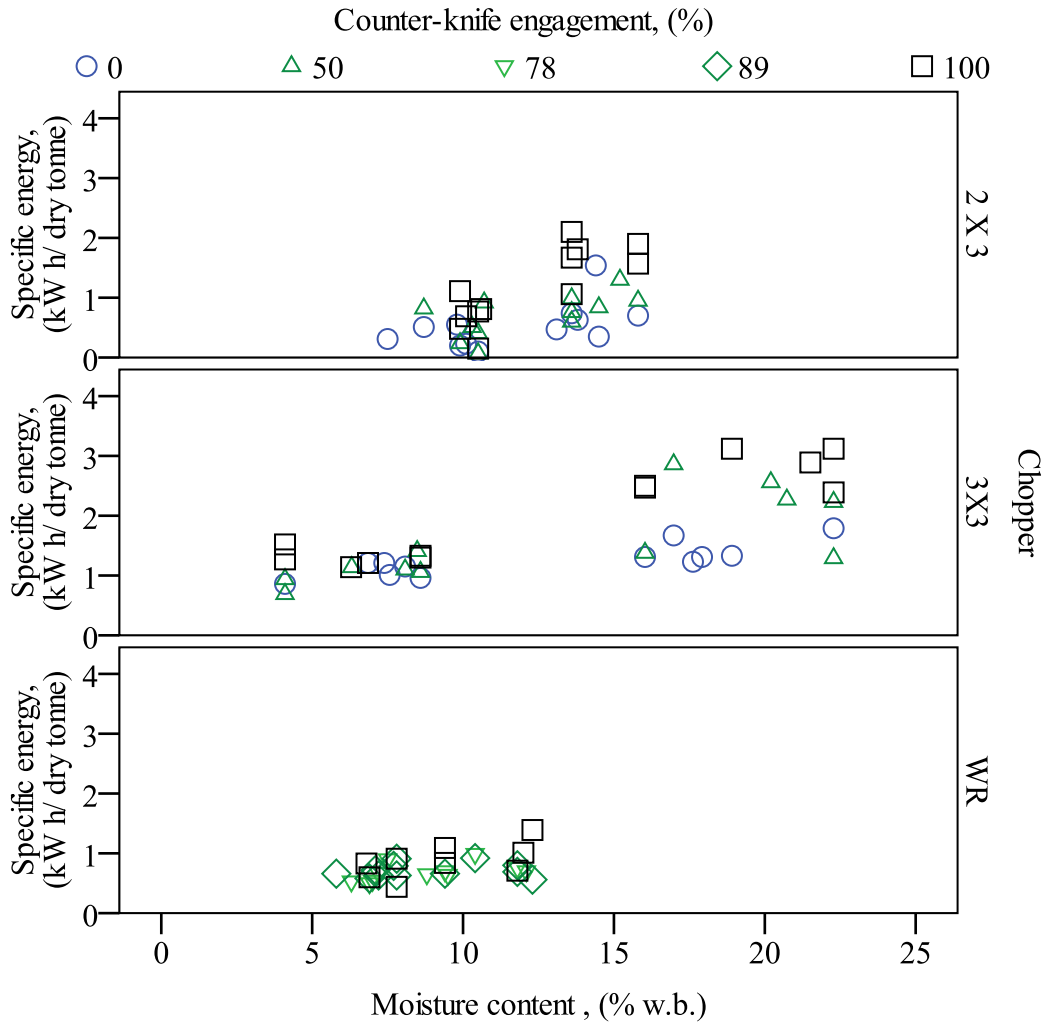

Figure 8.5 The specific energy required by the 2X3, 3X3, and WR chopper as a function of counter-knife engagement and, the moisture content of the straw processed by the choppers.

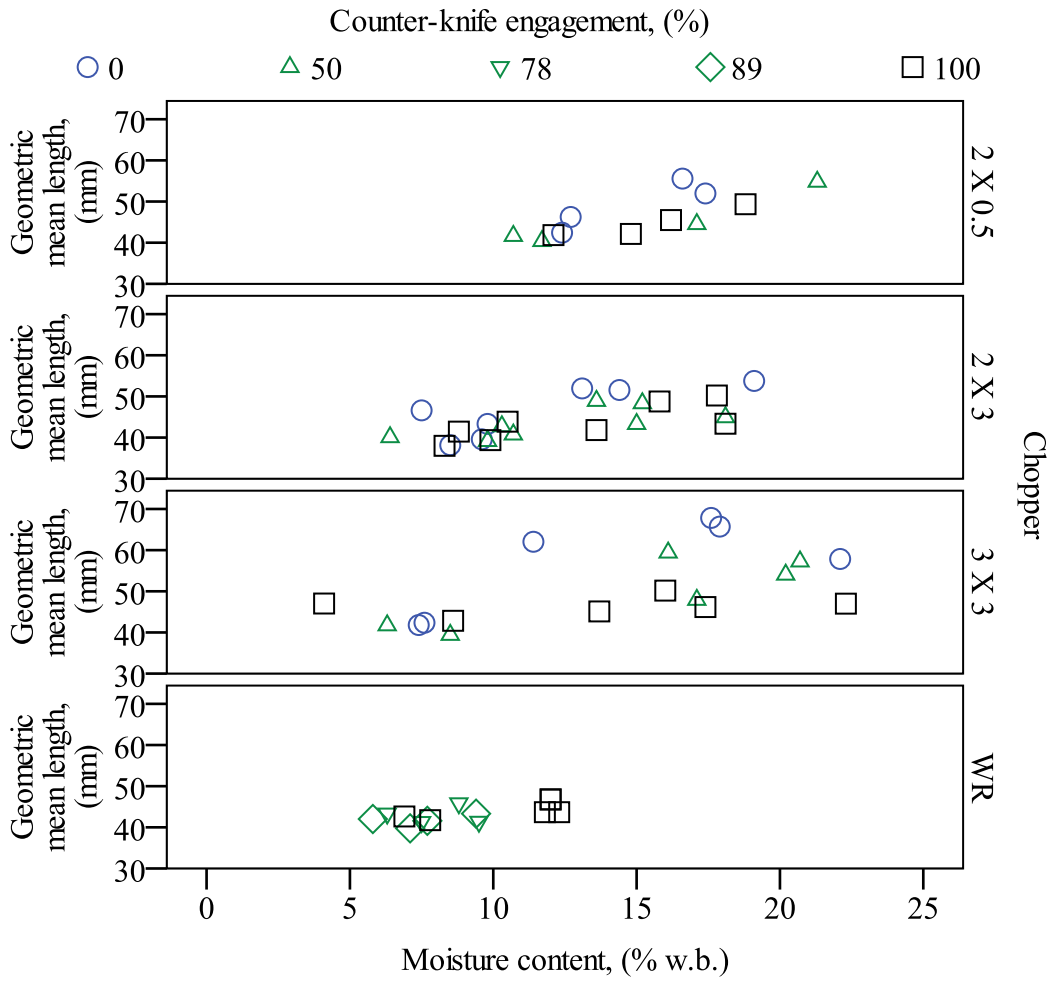

Figure 8.6 The geometric mean length, GML of straw that exited the combine harvester for the 2X0.5, 2X3, 3X3 and WR chopper as a function of counter-knife engagement and the moisture content of the straw processed by the choppers.

The field trials completed with the choppers dictated the type of relationship that could be established between the dependent factors and the independent factors. Plant material at two levels of moisture content and two levels of throughput was processed by each chopper with three levels of counter-knife engagement during the field trials. A regression analysis was used to establish a functional relationship between the specific energy demand of each chopper and the significant independent factors, and between the GML of MOG and the significant independent factors. SPSS 17 (IBM Corporation,

Somers, NY) was used to complete a stepwise linear regression analysis. The probability of F was used as the criteria to include or remove a factor from the relationship. In order for a given factor to be included in the relationship the probability of F had to be less than 0.05 and in order for a factor to be removed, the probability of F had to be greater than 0.10. The equations that were used to quantify the relationship between the independent factors that affected the specific energy demand of the choppers and the specific energy of the choppers is given in Table 8.1. It is interesting to note that for the 2X3 and 3X3 choppers, the magnitude of the effect of counter-knife engagement on the specific energy requirement of the chopper increased when the choppers were used to process straw at a higher moisture content. This effect is demonstrated in Table 8.1 as the magnitudes of the slope of the linear equations increase with increasing counter-knife engagement. The relationships between the moisture content of the straw processed by the choppers and the GML of MOG for each chopper are given in Table 8.2.

Table 8.1 The equations used to quantify the specific energy, *SE* in (kW·h/dry tonne) required by each chopper, as a function of counter-knife engagement, straw moisture content, *M* in (% wet basis) and throughput, T_{dry} in (dry tonne/h) of material other than grain.

	Counter-knife engagement		
Chopper	**Low**	**Medium**	**High**
2X0.5		-	
2X3	SE=0.08M-0.36	SE=0.09M-0.40	SE=0.22M-1.53
3X3	SE=0.04M+0.80	SE=0.07M+0.61	SE=0.10M+0.71
WR		SE=0.59+0.05M-0.02T_{dry}	

High	100% engaged, or fully inserted for all choppers
Medium	50% engaged (2X3, 3X3 and 2X0.5) 89% (WR)
Low	0% engaged or fully removed (2X3, 3X3 and 2X0.5) 78% engaged (WR)

Table 8.2 The equations used to quantify the geometric mean length, *GML* in (mm) of material other than grain that exited the combine harvester, as a function of counter-knife engagement, chopper type and straw moisture content, *M* in (% wet basis).

	Counter-knife engagement		
Chopper	**Low**	**Medium**	**High**
2X0.5	GML=2.0M+19.0	GML=1.2M+26.7	GML=1.2M+26.6
2X3	GML=1.2M+32.1	GML=0.7M+35.3	GML=0.8M+32.9
3X3	GML=1.4M+36.5	GML=1.1M+33.0	GML=0.3M+40.6
WR		GML=0.5M+38.5	

High 100% engaged, or fully inserted for all choppers
Medium 50% engaged (2X3, 3X3 and 2X0.5) 89% (WR)
Low 0% engaged or fully removed (2X3, 3X3 and 2X0.5) 78% engaged (WR)

It was assumed that the equations presented in Table 8.1 and 8.2 were valid for a straw moisture content of 8 to 23 % w.b. and a straw throughput of 2 to 20 dry tonne/h. The moisture content of the straw that was processed by the 2X3 and 3X3 choppers during the field trials very nearly covered the moisture range of 8 to 23 % w.b. However, the maximum moisture content of the straw processed by the WR chopper was only 12.3% w.b. Thus, it was assumed that the relationships defined between the specific energy requirement of the WR chopper and straw moisture content, over a range of 5.8 to 12.3% w.b. would hold when the WR chopper was used to process straw with a moisture content of 12.3 to 23% w.b. Similarly, it was assumed that the relationships defined between the GML of straw that exited the combine while the WR chopper was used, and straw moisture content, over a range of 5.8 to 12.3% w.b. would hold when the WR chopper was used to process straw with a moisture content of 12.3 to 23% w.b.

Even though the analysis of variance indicated that the 2X3 chopper was significantly influenced by throughput at the 0.05 level, it was not a factor that was included in the relationship used to define the specific energy required by the chopper. The analysis of variance indicated that the effect of throughput on the specific energy required by the 2X3 chopper was on the verge of significance ($p = 0.031$). The stepwise linear regression indicated that at each level of counter-knife engagement, throughput had an insignificant effect on the specific energy required by the 2X3 chopper ($p > 0.393$). Throughput was not included in the relationship that was used to define the specific energy required by the

2X3 chopper because the ANOVA analysis indicated that the factor was on the verge of significance and the stepwise linear regression indicated that the factor had an insignificant effect on the specific energy required by the 2X3 chopper. In contrast, throughput was included in the relationship that was used to define the specific energy required by the WR chopper because the ANOVA indicated that throughput was significant ($p < 0.001$) and the stepwise linear regression indicated that the factor was significant ($p = 0.010$).

8.1.3 Model inputs

The variation of the moisture content of the straw that was contained in the field typically followed a cyclical pattern. The straw dried during the day because of the heat from the sun and the drying process was expedited by the presence of wind. During mid afternoon the straw was typically at its driest. Conversely, the straw moisture content increased during the evening and at night because, as the temperature of the air decreased the ability for the moisture to remain suspended in the air decreased, which ultimately causes dew to form on the straw. Of course after a precipitation event, the moisture content of the straw in the field would rapidly increase. It was assumed that during normal operation, the harvester would be subject to straw at a moisture content that followed a normal distribution with an average of 15% w.b. and a standard deviation of 2% w.b. A histogram and cumulative probability of the expected moisture content of straw processed by the harvester during normal operating conditions is shown in Figure 8.7.

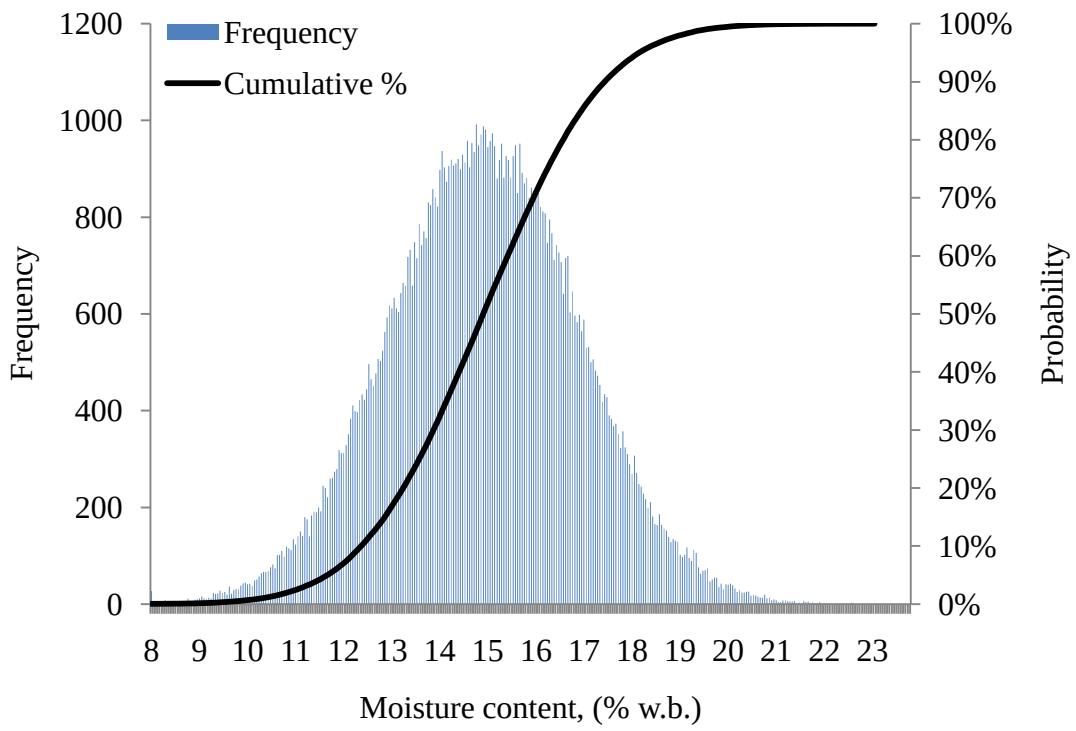

Figure 8.7 Histogram and cumulative probability of the moisture content of straw used as an input for the stochastic model.

It was assumed that during normal operation of the harvester, the operator of the harvester "opened up the field", which meant that when a new field was started the crop around the entire perimeter of the field would be harvested (creating a border around the entire field) and an additional pass along each of the headlands was completed. After the field was "opened," the operator of the harvester would continue to harvest the crop that remained between the headlands of the field until all of the crop in the field was harvested. The headlands were used by the pilot to reverse the direction of the harvester, while ensuring that it did not travel outside the border of the field nor travel over uncut crop within the field border. While the harvester reversed travel direction at the headlands, the throughput of MOG would temporally decrease to zero. As the harvester travelled between the headlands the pilot of a combine harvester continually adjusted the forward velocity of the combine, while maintaining a full (or as close to full as possible) cut width to maximize the throughput of the combine harvester. The cut width was

defined as the distance measured perpendicular to the direction of travel of the harvester in which standing plant material in the field is cut and subsequently processed by the harvester. The probability density function that defined the throughput of MOG would have a positive skew, because the experienced operator tried to maximize the throughput of the harvester while harvesting between the headlands. The probability density function would also have a long lower tail, caused by the temporary decrease in throughput when the harvester's direction was reversed at the headlands.

The throughput of MOG was limited by the available power of the harvester. Of all the crop-material engaging components of the combine harvester, the threshing rotor of the combine harvester consumed the most power. The power consumption of the threshing rotor was sensitive to the moisture content of the straw processed by the harvester because, the coefficient of friction between the straw and the threshing rotor was directly proportional to the straw moisture content. The maximum sustainable throughput (or the throughput that ensures that the threshing rotor will not plug) of the threshing rotor decreased when higher moisture content straw was processed because the increase in the coefficient of friction between the straw and threshing rotor increased the power demand of the threshing rotor. When dry straw (straw with a moisture content of less than 13% w.b.) was processed with the 7010 combine harvester, the throughput of MOG could be maintained in excess of 20 dry tonne/h without plugging. However, when wet straw was processed (straw with a moisture content in excess of 13% w.b.) with the harvester, the throughput of MOG was limited in some cases to approximately 10 dry tonne/h or less. Therefore the upper bound of the probability density function that defined the throughput of MOG was affected by the straw moisture content. A higher straw moisture content yielded a lower upper bound of the probability density function.

It was assumed that the throughput of MOG during normal operation would follow a beta distribution with alpha, beta and the lower bound of 12, 3 and 0 dry tonne/h, respectively. The upper bound of the beta function was assumed to be a function of the moisture content of straw processed by the harvester. The upper bound was described with the following equation,

$$J = -0.67M + 25.3, \quad \textbf{(8.1)}$$

where:

J is the upper bound of the throughput of MOG (dry tonne/h) and

M is the moisture content of straw processed by the harvester (% w.b.)

A histogram and cumulative probability of the expected throughput of MOG during normal operation when straw with a moisture content of 8% w.b. and 23% w.b was processed, is shown in Figure 8.8. Note that the probability density function has a positive skew regardless of the straw moisture content and the upper bound of the throughput is inversely related to the straw moisture content.

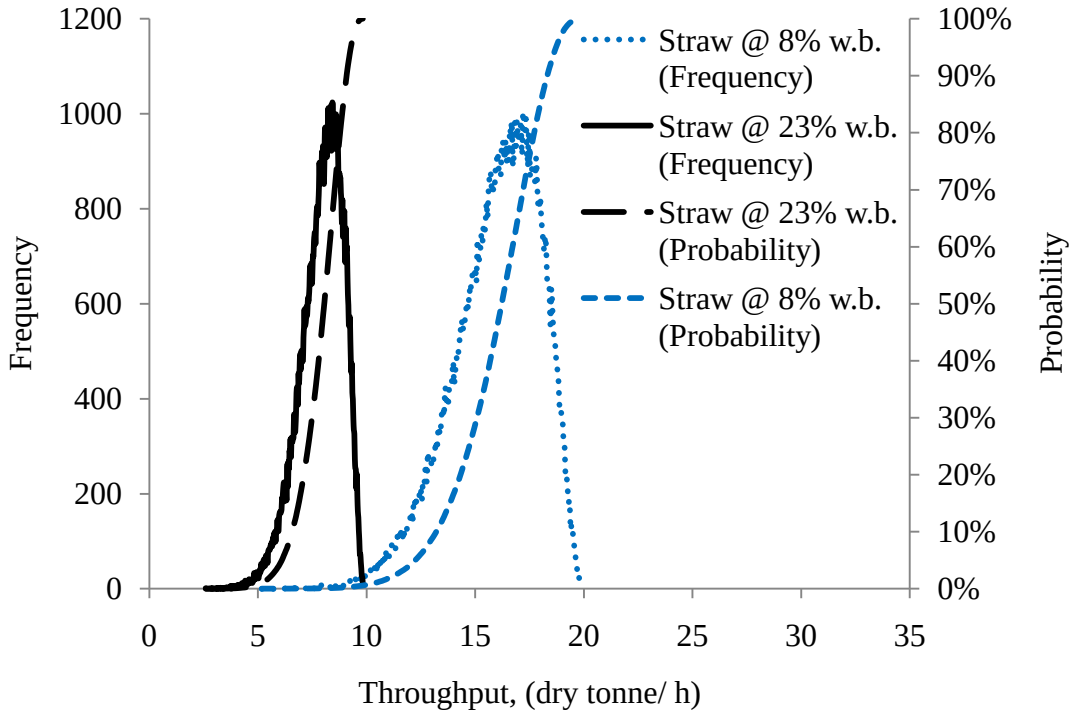

Figure 8.8 Histogram and cumulative probability of the throughput of MOG when straw at a moisture content of 8 and 23% w.b. is processed.

The straw throughput and moisture content during normal operating conditions was defined using a random number generator. The straw moisture content values used as the model input were defined using the random number generator which selected numbers based on a normal distribution with a mean of 15 and a standard deviation of 2. The straw

throughput values used as the model input were defined using the random number generator which selected numbers based on a beta distribution with an alpha value of 12, a beta value of 3 , a lower bound of zero and a upper bound defined using equation (8.1). A total of one hundred thousand straw moisture content and throughput values were quantified. The functional relationships defined in Table 8.1 and 8.2 were used to quantify the specific energy requirement of the 2X3, 3X3 and WR chopper and the GML of MOG for the same choppers. Histograms were created to quantify at a 95% probability what the specific energy and GML of MOG when each chopper was used in the combine harvester.

8.2 Results and discussion

Based on the stochastic model, the simulated specific energy requirement of each chopper and the simulated GML of MOG at a 95% probability is shown in Figure 8.9. Out of all the choppers tested, the WR chopper resulted in the minimum GML of MOG while requiring the least specific energy. Therefore based on the stochastic model, the WR chopper was the best chopper to use in the combine harvester. This was based on the assumption that a 47.6-mm GML of MOG exiting the combine harvester was acceptable. If a 47.6-mm GML of MOG exiting the combine harvester was too long, the WR chopper could not be used and either the 2X3 or 3X3 chopper (with fully inserted counter-knives) would need to be used. The use of the 2X3 or 3X3 chopper, to achieve less than a 47.6-mm GML of MOG, would require approximately an additional 1.2 kW·h/dry tonne specific energy than the WR chopper.

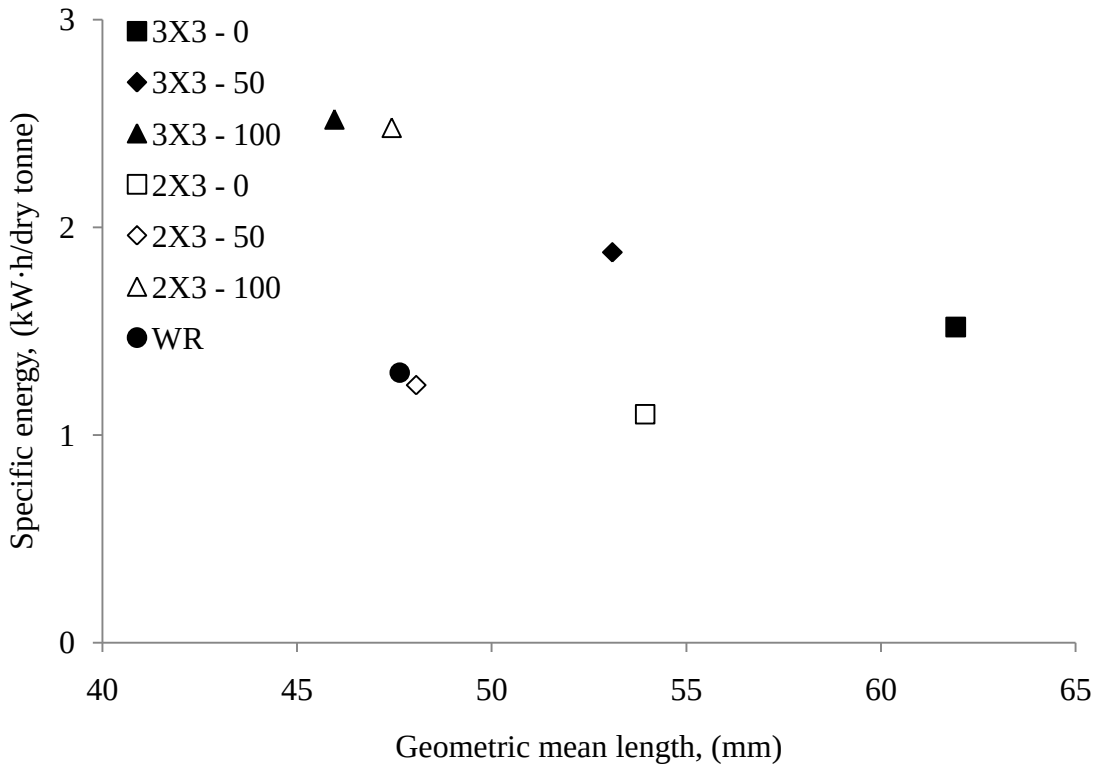

Figure 8.9 The specific energy requirements of the 3X3 and 2X3 (with counter-knives engaged at 0, 50 and 100%) and WR choppers with the corresponding geometric mean length of material other than grain exiting the combine harvester at the 95% probability.

It is important to note that the output of the stochastic model was based on the assumption that the functional relationships defined for each chopper were valid when straw at a moisture content of 8 to 23% w.b. was processed. Recall that the functional relationships of the WR chopper were defined with low straw-moisture-content field data. Further, the performance of all choppers tested was better when low moisture content straw was processed. Therefore, the functional relationships defined for the WR chopper may indicate that the performance of the WR chopper, when used to process high-moisture-content straw (straw moisture content in excess of 12 % w.b.), was better than the actual performance of the chopper. The implication of this in terms of the stochastic model was that the performance of the WR chopper indicated by the stochastic model would have been better than the actual performance of the WR chopper. However, the

2X3 and 3X3 choppers were both subject to straw at a moisture content that approximately encompassed the full range of 8 to 23% w.b. Thus it was reasonable to put a high level of confidence in the output of the stochastic model in terms of the 2X3 and 3X3 choppers.

The specific energy requirement increased and the GML of MOG decreased when the counter-knives were inserted into the chopper for both the 2X3 and 3X3 choppers. This type of relationship was expected because engaged counter-knives accomplished two things, they restricted the flow of plant material past the chopper, and they provided support (acted as a counter-shear) to the plant material that was being cut. As previously discussed, the restriction of flow of plant material past the chopper and counter-shear support of the plant material resulted in a greater degree of particle length reduction caused by the chopper. The greater degree of particle length reduction came at a cost of an increased amount of energy consumed to transport, compress and cut the plant material.

The specific energy requirement and the GML of MOG were similar for the 2X3 and 3X3 choppers, when the counter-knives were fully inserted. When the counter-knives were fully inserted the plant material entering the chopper was forced to travel into the path of the rotating knives on the chopper. The 3X3 chopper reduced the GML of MOG slightly more than the 2X3 chopper while consuming slightly more specific energy than the 2X3 chopper. The ability of the 3X3 chopper to reduce the GML of MOG was due to the additional rotating knives mounted on the 3X3 chopper. A total of 84 knives were mounted on the 2X3 chopper and 126 on the 3X3 chopper. The additional 42 knives mounted on the 3X3 chopper were able to reduce the GML of MOG. The 3X3 chopper required more specific energy than the 2X3 chopper because of the increased amounts of cutting that the 3X3 chopper completed.

When the counter-knives were not fully inserted the 2X3 chopper performed better than the 3X3 chopper because the use of the 2X3 chopper resulted in a shorter GML of MOG and the specific energy required by the 2X3 chopper was less than the specific energy required by the 3X3 chopper. The reason that the 2X3 chopper performed better than the 3X3 chopper, when the counter-knives were removed or 50% engaged was

attributed to the number and pattern of knives on the two choppers. The 84 knives on the 2X3 chopper were arranged in 6 rows (around the circumference of the chopper drum) across the width of the chopper as shown in Figure 4.14 (B). When rotating at the normal operating speed of 2900 rpm, the 6-row pattern on the 2X3 chopper allowed plant material to enter the path of the leading edge of the knives even when the counter-knives were fully removed. Conversely, when the 3X3 chopper, shown in Figure 4.14 (C), was rotating at the same operating speed, the tips of the 126 knives created a wall, which prevented the plant material from entering the path of the leading edge of the knives, and forced the plant material around the circumference of the circle created by the rotating knife tips. The larger specific energy required by the 3X3 chopper was due largely to the energy required to transport the plant material between the tip of the knives and the rotor bed.

8.3 Conclusions

The 5th HSCP objective was to identify which chopper resulted in the minimum GML of MOG for the same specific energy. During the field trials completed with the four different choppers the choppers were not subject to the same operating conditions (straw throughput and moisture content). The stochastic model was created so that the performance of the choppers could be compared when they were subjected to the same operating conditions. After the development of the stochastic model the following conclusions were drawn:

1. The use of the WR chopper would result in the shortest GML of MOG while also requiring the least amount of specific energy. Therefore, the WR chopper was the best chopper to use. This was based on the assumption that the functional relationships that were defined for the WR chopper when subjected to straw at a moisture content of 8 to 12.3% w.b. were valid when the WR was subject to straw at a moisture content of 12.3 to 23% w.b.
2. Aside from the WR chopper when the counter-knives were fully inserted, the performance of the 2X3 and 3X3 choppers were very similar, but the use of the 3X3 chopper did require slightly more specific energy and resulted in a shorter

GML of MOG. The minimum GML of MOG was achieved by using the 3X3 chopper with fully inserted counter-knives.

3. The performance of the 2X3 chopper was superior to the 3X3 chopper when the counter-knives were partially or fully removed from the path of the rotating knives on the choppers.

8.4 Recommendations for future work

It is believed that the particle length reduction of the plant material is not just caused by the chopper of the combine. The particle length of plant material is also reduced by the threshing rotor and feeder of the combine harvester (especially when straw with a moisture content lower than 12% w.b. was processed). During future studies it would be wise to quantify the length of plant material immediately before the plant material entered the RFCS and immediately after the RFCS so that the change in particle length due to the RFCS could be quantified. Furthermore, the effect of the chopper on the GML of MOG appeared to be minor when straw with a moisture content below 12% w.b. was processed because, the position of the counter-knives had little effect on the GML of MOG. Thus, during future studies completed to evaluate the performance of a chopper it would be advisable to limit the straw moisture content processed by the choppers to greater than 12% w.b.

During the field trials, discussed in chapter 6, the choppers were not subjected to the same operating conditions (straw throughput and moisture content) which prevented the best chopper from being directly determined from the field trial data. If the choppers were subjected to the same operating conditions – a challenging task to complete during field trials – there would be no need for the stochastic model. Because the choppers were not subjected to the same operating conditions, the stochastic model was used to identify the best chopper. The ability of the stochastic model to identify the best chopper to use in the combine harvester during normal operating conditions is dependent on how well the effect of the operating conditions on the performance of the chopper is understood. The functional relationships (the relationship between the GML of MOG and the specific energy required by the chopper as a function of straw throughput and moisture content) of the WR chopper were defined with low straw-moisture-content field data. Thus it was

assumed that the functional relationships defined with the low straw-moisture content data were valid when higher straw moisture content straw was processed with the WR chopper. In the future, when the performance of choppers is to be compared, the goal of the field trials should be to complete field trials with the choppers at as close to the same operating conditions as possible, as the accuracy of the stochastic model will improve in terms of the output of the model predicting the actual performance of the choppers.

9 SUMMARY

The rotary feeding and cutting system (RFCS) is used to transport and decrease the length of plant material (or cut plant material). Two different cutting devices were brought into focus during this project: the low speed cutting process (LSCP) RFCS and the high speed cutting process (HSCP) RFCS discussed in sections 4.1 and 4.2, respectively. The LSCP RFCS is an optional accessory on balers manufactured by Case New Holland (CNH Global N.V.). The RFCS decreases the length of plant material entering the bale forming chamber, resulting in bales of higher density. Heavier (more dense) bales can be transported and stored more cost effectively. Further, hay processed with an RFCS can also result in higher quality feed. The HSCP RFCS is an optional accessory on the combine harvesters manufactured by CNH. The advantage of using a RFCS on a combine harvester is that the length of the material other than grain (MOG) that exits the combine harvester is reduced considerably. Reducing the length of MOG is advantageous as it aids in the uniform distribution of MOG behind the combine, and it helps to ensure high productivity during subsequent seeding operations. In the past, the improvements to the RFCS were achieved by performing costly field or laboratory experiments. The general objective of this project was to develop an analytical model that could be used to quantify the effect of changing the levels of design parameters of the RFCS on the power required by the device. The analytical model could be used by future designers to assess design changes to the RFCS , while decreasing the required number of field or laboratory experiments.

When this project began, in 2006, there was no published work that indicated the factors that had a significant effect on the specific energy requirements, or the power demand of the RFCS. There had been extensive research completed, which identified the factors that affect the energy requirements of other cutting devices. Before the analytical model could be developed, the factors that had a significant effect on the energy requirements or power demand of the RFCS needed to be quantified. Thus a series of laboratory tests were completed to identify the significant parameters. These tests were discussed in section 5.1. The conclusions drawn in section 5.1 were used to identify which design parameters to include in the analytical model. The development of the

analytical model was discussed in section 7.1. After the analytical model was developed it became apparent that further trials needed to be completed to validate the LSCP analytical model. These model validation trials were discussed in section 5.2. To validate the analytical model the Young's modulus, dynamic coefficient of friction (between the plant material and steel) and the maximum shear strength of the plant material processed by the RFCS needed to be quantified. Plant material being visco-elastic in nature will behave differently, depending on the rate at which the material is loaded. Therefore it was important to quantify the material properties of the plant material at, or as close as practically possible, the loading rate it experienced in the RFCS. The material properties testing devices available at the time had a very low loading rate relative to the speed at which the plant material was loaded in either the LSCP or HSCP RFCS. Thus a material properties test stand that could load the plant material at a faster rate was used to quantify the aforementioned properties of the plant material. The test stand used to quantify the plant material properties was described in section 4.3. The analytical model development occurred before any of the field trials were completed with the HSCP RFCS. During the completion of the field trials the material properties of the cereal straw processed by the RFCS was quantified with the material properties test stand. Thus no additional trials needed to be completed with the HSCP RFCS to validate the model. The HSCP field trials were discussed in chapter 6.

The analytical model was used to quantify the amount of energy required to compress, cut and transport the plant material. For both cutting devices (LSCP and HSCP) the amount of energy required to transport the plant material was far greater than the energy required to compress or cut the plant material. The analytical model was used to quantify the effect of decreasing the coefficient of friction between the plant material and the RFCS, and decreasing the surface area over which the plant material was transported. Up to a 26% reduction in the total power required by the RFCS was achieved when either approach was adopted. The analytical model can be used to investigate the effect of changing some of the design parameters of the RFCS on the power demand of the device. However not all of the design parameters in the analytical model can be changed because changing them would change the flow of plant material into the RFCS. The indeterminate parameters were affected by the flow of plant material, therefore if the flow

of plant material into the RFCS was changed the values of the indeterminate parameters would no longer be known. To use the analytical model to its full potential the relationship between the indeterminate parameters and the design parameters need to be quantified. If the relationship between the design parameters and the indeterminate parameters was quantified the utility of the analytical model would greatly increase, as the shape of the leading and lagging edge of the tines and the counter-knives could be explored with the model and their effects on the total power demand of the RFCS quantified.

A stochastic model was also developed to identify which of the four choppers tested in the combine harvester had the best performance if they were subjected to the same operating conditions. It was found that the WR chopper had the best performance, or required the least amount of energy to result in the shortest geometric mean length (GML) of MOG exiting the combine harvester. However this conclusion is questionable because the WR was subject to relatively low moisture content plant material, relative to the other three choppers tested. The approach of the stochastic model development is sound. However, the confidence in the output of the model would be greatly increased if the effect of counter-knife engagement, material throughput and moisture content on the GML of MOG exiting the combine, and the specific energy consumption of the RFCS were better defined. The effect of counter-knife engagement, material throughput and moisture content on the GML of plant material exiting the combine harvester and the specific energy consumption of the RFCS could be better defined by performing additional field trials. During the additional field trials it would be important to expose the choppers to the same range of operating conditions. Further, during the trials the GML of MOG prior to and after being processed by the chopper should be quantified. Measuring the GML of MOG up-stream and down-stream of the chopper would quantify the effect of the chopper on the reduction of the GML of MOG, as opposed to assuming that the chopper is the only device in the combine that reduced the GML of MOG.

LIST OF REFERENCES

Afzalinia, S. 2005. Modeling and validation of the baling process in the compression chamber of a large square baler. Thesis (Ph.D.), University of Saskatchewan.

ASTM. 1992c. ASTM D 3108-89. Standard test method for coefficient of friction, yarn to solid material. In 1992 Annual Book of ASTM Standards, 7.01:822. Philadelphia, PA: ASTM.

ASAE Standard. 2008. D251.2 APR2003: Friction Coefficients of Chopped Forages. St. Joseph, MI: ASAE.

ASABE Standard. 2008. S358.2 DEC1988: Moisture Measurement-Forages. St. Joseph, MI: ASAE.

ASAE Standards. 2005 . D497.6 JUN2009: Agricultural machinery management data. St. Joseph, MI: ASAE.

ASAE Standard.2005. EP496.3 FEB2006: Agricultural machinery management. St. Joseph, MI: ASAE.

ASAE Standard. 2007. S424.1 MAR1992: Method of determining and expressing particle size of chopped forage materials by screening. St. Joseph, MI: ASAE.

Baird, E.D. 1956. An analysis of cutting forces in a mower. Thesis (M.Sc.), University of California.

Berge, O.I. 1951. Design and performance of characteristics of the flywheeltype forage harvester cutterhead. Agricultural Engineering 32(2): 85-91.

Blevins, Fredrick Z. 1954. Some of the component power requirements of field type forage harvesters. Reports from Purdue University, Lafayette, IN, May 13, 1954.

Blevins, F. Z. and H. J. Hansen. 1956. Analysis of forage harvester design, Agricultural Engineering 37(1): 21.

Bockhop, C.W. and K.K. Barnes. 1965. Power distribution and requirements of a flail-type forage harvester, Agricultural Engineering 36(7): 454.

Borreani G. and E. Tabacco. 2006. The effect of a baler chopping system on fermentation and losses of wrapped big bales of alfalfa. Agronomy Journal 98(1).

Bright, R.E. and R.W. Kleis. 1964. Mass shear strength of haylage. Transaction of the ASAE 7(2): 100-101.

Chancellor W.J. 1988. Cutting of biological material. In Handbook of Engineering in Agriculture. Vol. 1, pp. 35-63, CRC Press Inc., FL,

Chancellor, W. J. 1957. Basic Concepts of Cutting Hay, Ph.D. thesis, Cornell University, Ithaca, New York, 170.

Chancellor, W.J. 1958. Energy requirements for cutting forage, Agricultural Engineering 39(10): 633.

CNH America LLC. 2009. Axial-Flow® Combine Class V to IX [Brochure]. Racine, WI. Retrieved January 16, 2011 from http://www.caseih.com/northamerica/Products/Harvesting/AxialFlowCombines/Documents/Axial-Flow%28R%29%20Combine%20Brochure%20CIH1120901.pdf.

CNH America LLC. 2008. New Holland BR7000 Series Roll-Belt™ Round Balers [Brochure]. Racine, WI. Retrieved April 9, 2011 from http://agriculture.newholland.com/us/en/Products/Hay-and-Forage-Equipment/Roll-Belt-Round-Balers/Documents/NH6150703-2.pdf

CNH America LLC. 2004. AFX7010 Operators Manual. Racine, WI.

Colzani, G. 1968. Test of three mowers on Different Forages, Rep. No 33, Institute Sperimentale Di Meccanica Agraia, Milano, Italy, April, 30.

Elfes, L.E. 1954. Design and development of a high speed mower. Agricultural Engineering 35(3):147-149. St. Joseph, MI.

Esehaghbeygi, A., B. Hoseinzadeh, M. Khazaei and A. Masoumi. 2009. Bending and shearing properties of wheat stem of alvand variety. World Applied Science Journal 6(8):1028-1032.

Freitag, H. 1985. Beitrag zum Bemessung und Bewerten von Prozessen der Grunfuttersilierung (Contribution to the measurement and evaluation of processes of green forage ensiling). Arbeniten zur Mechanisierung der Landwirtschaft, Schlieben?Bornim No. 8, 1985. In McGechan M.B., 1990. Losses during conversion of grass forage. J. Agric. Eng. Res. 45:1-30.

Galedar, M.N., A. Tabatabaeefar, A. Jafari, A. Sharifi and S. Rafiee. 2008. Bending and shearing characteristics of alfalfa stems. Agricultural Engineering International: the CIGR Ejournal. Manuscript FP 08 001. Vol. X.

Goering, C.E., R.P. Rohrbach and A.K. Srivastava. 1993. Engineering Principles of Agricultural Machines, St-Joseph, MI.: ASAE.

Hall, J.W. and J.F. Husman. 1981. Correlating physical properties with combine performance. ASAE paper No. 81-3538. St. Joseph, MI:ASAE.

Halyk, R.M. and Hurlbut, L.W. 1968. Tensile and shear strength characteristics of alfalfa stems. Transactions of ASAE 11(2):256-257

Han K.J., M. Collins, M.C. Newman, and C.T. Dougherty. 2006. Effects of forage length and bale chamber pressure on pearl millet silage. Crop Sci. 46:337–344.

Harbage, R.P., and R.V. Morr. 1962. Development and design of a ten-foot mower. Agricultural Engineering 43(4): 208.

Hennen, J. J. 1971. Power Requirements for Forage Chopping, ASAE Paper No. 71-145. St. Joseph, MI: ASAE.

Huisman, W. 1978. Moisture content, coefficient of friction and modulus of elasticity of straw in relation to walker losses in a combine harvester. Proc. of the international grain and forage harvesting conference 1(78):49-54.

Hunt, D. 1986. Engineering models for agricultural production. Westport: Connecticut.

Ige, M. T. and M. F. Finner. 1976. Optimization of the performance of the cylinder-type forage harvester cutterhead, Transaction of the ASAE 19(3): 455.

Ige, M. T. and M. F. Finner. 1975. Effects and interactions between factors affecting the shearing characteristics of forage harvesters, Transaction of the ASAE 18(6): 1011.

Kadam, K.L., L.H. Forrest and W.A. Jacobson. 2000. Rice straw as a lignocellulosic resource:collection, processing, transportation, and environmental aspects. Biomass and Bioenergy. 18(2000) 369-389.

Kushwaha, R.L., A.S. Vaishnav and G.C. Zoerb. 1983. Shear strength of wheat straw. Canadian Agricultural Engineering. 25:163-166.

Kepner, R.A. 1952. Analysis of the cutting action of a mower. Agricultural Engineering 33(11): 693-697, 704.

Lambert, M.B. 1974. Evaluation of Power Requirements and Blade Design for Slash Cutting Machinery, ASAE Paper No. 74-1570. St. Joseph, MI: ASAE.

Liljedahl, J. B., G. L. Jackson , R. P. De Graff, and M. E. Schroeder. 1961. Measurement of shearing energy, Agricultural Engineering 42(6): 298.

McClelland, J.H. and R.E. Spielrein. 1958. A study of some design factors affecting the performance of mower knives, Agricultural Engineering 3(2): 137.

Moustafa, S. M. A., S. W. Searey, and G. H. Brusewitz. 1978. Development of a forage chopping energy standard procedure, Proc. 1st mt. Grain Forage Handling Conf, American Society of Agricultural Engineers, St. Joseph, MI., 261.

Negi, S.C, J.R. Ogilvie, and J.C. Jofriet. 1987. Some mechanical and rheological properties of silages. Canadian Agricultural Engineering 29:59-64.

Nieuwenhof P. 2003. Modeling of the energy requirements of a non-row sensitive corn header for a pull-type forage harvester. Thesis (M.Sc.), University of Saskatchewan.

O'Dogherty, M.J., J.A. Huber, J. Dyson and J. Marshall. 1995. A study of the physical and mechanical properties of wheat straw. Journal of Agricultural Engineering Research 62:133-142

O'Dogherty, H.G. Gilbertson, G.E. Gale. 1989. Measurements of physical and mechanical properties of wheat straw. Fourth International Conference on Physical Properties of Agricultural Materials, Rostock, German Democratic Republic, 4-8: 608-613.

Persson, S. 1987. Mechanics of cutting plant material. St. Joseph, MI: ASAE.

Prince, R. P., W. C. Wheeler, and D. A. Fisher. 1958. Discussion on energy requirements for cutting forage, Agricultural Engineering 39(10): 638.

Prince, R.P. and W.C. Wheeler. 1959. Some Factors Affecting the Cutting of Forage Crops, Prog. Rep. No. 37, Agricultural Experimentation Station, University of Conneticut, Storrs, 10.

Prince, R.P. and W.C. Wheeler. 1960. Factors affecting the cutting process of forage crops, ASAE paper No 60-611. St. Joseph, MI: ASAE.

Reznik, N. E. 1979. Teoriya Rezaniya Lezviem i Osnovy Rascheta Rezsushchikh Apparatov (Theory of Blade Cutting and Basis of the Calculations of Cutting Apparatus) Mashiostroenie, Moskova, 1975. (Translated from Russian for the U.S. Department of Agriculture and National Science Foundation, Washington, D.C. by the Al Ahram Center for Scientific Translation,)

Richey, C. B., P Jacobson, C. W. and Hall. 1961. Agricultural Engineers' Handbook, McGraw-Hill, New York.

Richter, D. 1954. Friction coefficients of some agricultural materials. Agricultural Engineering 35(6): 411-413.

Roberge, M. 1999. Design and evaluation of performance of a crop processor for a pull-type forage harvester. Thesis (PhD), McGill University.

Shinners, K.J., R.G. Koegel and L.L. Lehman. 1991. Friction coefficient of alfalfa. Transactions of ASAE 34 (1): 33-37.

Shinners, K.J. 2003. Engineering principles of silage harvesting equipment, p.361-403. In D.R. Buxton et al. (ed.) Silage science and technology. Agron. Monogr. 42. ASA, CSSA, Madison, WI.

Siemens, M.C., D.E.Wilkins. 2005. Effect of residue management methods on no-till drill performance. Applied Engineering in Agriculture 22(1):55-60

Springer, A. G., J. L. Smith, and R. E. Tribelhorn. 1976. Forage Harvester Cutterhead Kinetics, ASAE Paper No. 76-1008. St. Joseph, MI. ASAE.

Srivastava, A.K., W.T. Mahoney and N.L. West. 1990. The effect of crop properties on combine performance. Transactions of the ASAE 33(1): 63-72.

Srivastava A.K., C.E. Goering, R.P. Rohrbach, and D.R. Buckmaster. 2006. Hay and forage harvesting. In Engineering Principles of Agricultural Machines, 2nd edition. McCann, P, 325-401 St. Joseph, MI:ASAE.

Stroppel, Theodor. 1953. Studien uber den Verschleiss von Schneiden fur halmartiges Schnittgut. (Studies of the wear of edges for straw materials). In Grundlagen der Landtechnik 5(2):134-144. VDI-Verlag, Dusseldorf.

Stroshine R. 1998. Structure and composition. In Physical Properties of Agricultural Materials and Food Profucts.53-107.

Tavakoli, H., S.S. Mohtasebi, A. Jafari. 2008. Comparison of mechanical properties of wheat and barley straw. Agricultural Engineering International: the CIGR Ejournal. Manuscript CE 12002. Vol. 10.

Tavakoli, H., S.S. Mohtasebi, A. Jafari. 2009. Effect of moisture content, internode position and loading rate on the bending characteristics of barley straw. Research Agricultural Engineering 55(2): 45-51

Tribelhorn, R. E. and J. L. Smith. 1975. Chopping energy of a forage harvester, Transaction of the ASAE 18(3): 423.

Tuck, C.R. 1976. The effect of various design and operation parameters of rotary mowers on cutting performance. Phase 1976. NIAE Department Note no DN/FC/666/1355.

Tuck, C.R. 1977. The effect of various design and operating parameters of rotary mowers on cutting performance. Phase 1977. NIAE Department Note no DN/FC/771/1355.

Tuck, C.R. 1978. The effect of various design and operating parameters of rotary mowers on cutting performance. Phase 1978. NIAE Department Note no DN/FC/906/03001.

Usrey L.J., J.T. Walker, O.J. Loewer. 1992. Physical characteristics of rice straw for harvesting simulation. Applied Engineering in Agriculture 35(3): 923-930.

Von Bargen, K., L. R. Verma, and W. E. Foster. 1979. Particle Size Reduction of Alfalfa Hay by Cutting, ASAE Paper No. 79-1541. St. Joseph, MI: ASAE.

APPENDIX A - SENSOR CALIBRATION

A.1 LSCP Sensor calibration

The pressure transducers were calibrated using a deadweight tester. The range of pressure over which the transducers were exposed was zero, or atmospheric pressure, to 20.6 MPa, in 3.5 MPa increments. For each transducer, a linear equation was fit to the measured data. The coefficients of the line were obtained by minimizing the sum of squared error between the applied pressure and the measured data. For both pressure transducers, the R^2 values of the equations that relate pressure to voltage were 1.0. The equation that was used to convert the voltage signal from the down-stream pressure transducer to pressure was,

$$P_{DS} = 2861x - 11.61, \quad \textbf{(A.1)}$$

where:

P_{DS} is the down-stream pressure (kPa) and

x is the signal from the pressure transducer (V).

The equation that was used to convert the voltage signal from the up-stream pressure transducer to pressure was,

$$P_{US} = 2822x - 7.21, \quad \textbf{(A.2)}$$

where:

P_{US} is the up-stream pressure (kPa) and

x is the signal from the pressure transducer (V).

The relationship between voltage and pressure for both transducers are shown in Figure A.1.

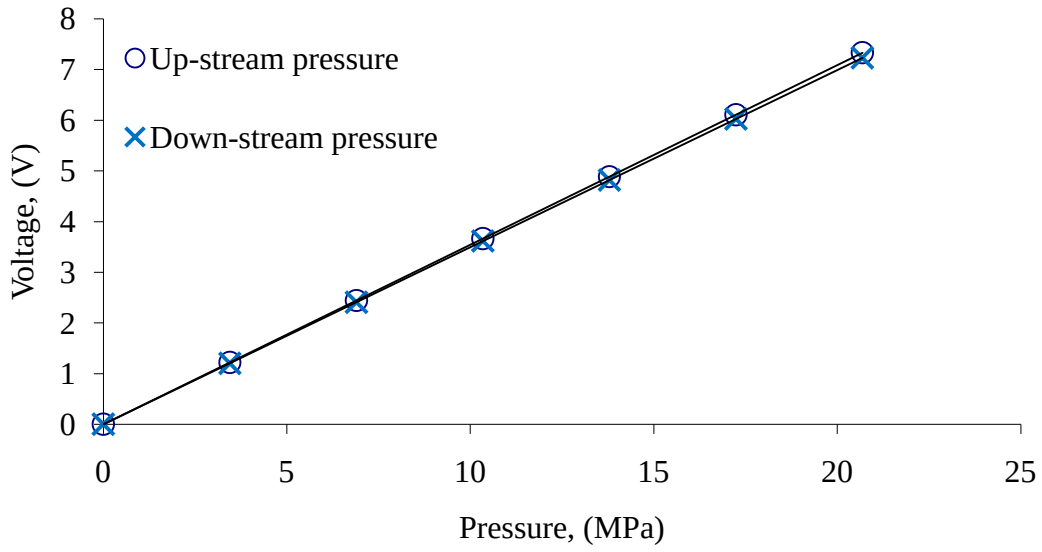

Figure A.1 Calibration curves for the pressure transducers used on the LSCP test stand.

The flow meters were calibrated using a negative feedback, closed-loop control system as shown in Figure A.2. Doug Bitner designed and developed the apparatus in the Fluid Power Lab at the University of Saskatchewan. The components of the system were a function generator, a proportional servo valve, a single-ended linear hydraulic actuator and a linear displacement transducer (LDT). The function generator was used to create a ramp function. Varying levels of flow rate were achieved by varying the period of the ramp function. The control system adjusted the proportional valve to minimize the error between the ramp function and the LDT signal.

The flow meters were placed in series with a nominal flow meter, and attached to the blank side of the hydraulic actuator. A linear displacement transducer (LDT) was attached to the hydraulic cylinder. The position of the cylinder was recorded with a time-stamp using a data acquisition system. The LDT data were used to calculate the actual flow rate of oil through the flow meters, after the calibration procedure. During the calibration procedure the approximate oil flow rate was quantified with the nominal flow meter.

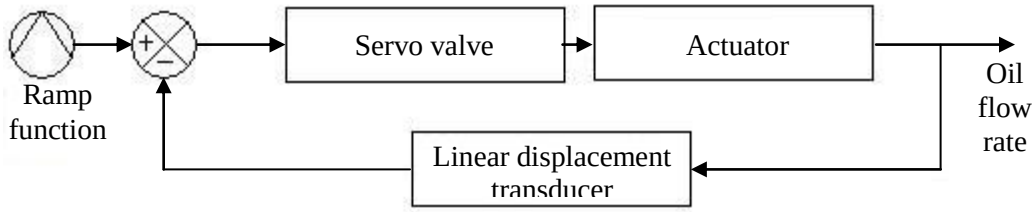

Figure A.2 Closed loop control system used to calibrate the flow meters used on the LSCP test stand.

The control system maintained a constant, steady-state cylinder speed corresponding to each of the levels of flow to which the meters were subjected. The range of flow to which the transducers were exposed was from 0 to 38.0 L/min, in approximately 3.8-L/min increments. A curve was fit to the actual flow rate of oil through each transducer. The coefficients of the function were obtained by minimizing the sum of squared error between the flow rate and the measured data. For both flow meters, the R^2 values of the equations that related oil flow to voltage were 1.0. The equation that was used to convert the voltage signal from Flow Meter 1 to oil flow was,

$$Q_{Flow\,1} = 19.29x^{0.34} + 0.90x - 6.06, \quad \textbf{(A.3)}$$

where:

$Q_{Flow\,1}$ is the oil flow rate through Meter 1 (L/min) and

x is the signal from the flow meter (V).

The equation that was used to convert the voltage signal from Flow Meter 2 to oil flow was,

$$Q_{Flow\,2} = 17.79x^{0.43} + 1.50x - 3.93, \quad \textbf{(A.4)}$$

where:

$Q_{Flow\,2}$ is the oil flow rate through Meter 2 (L/min) and

x is the signal from the flow meter (V).

The relationships between voltage and flow rate for both transducers are shown in Figure A.3.

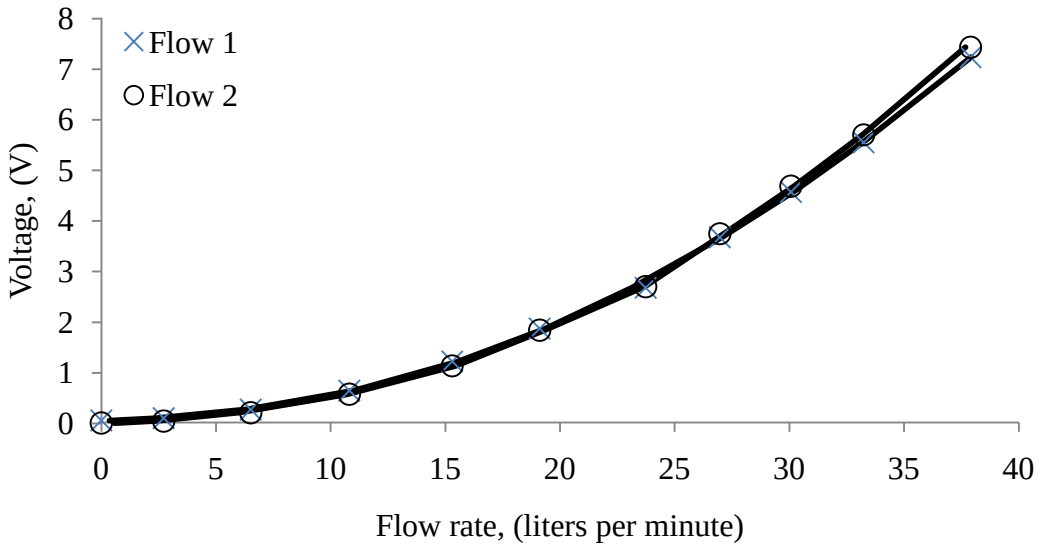

Figure A.3 Calibration curves for the flow meters used on the LSCP test stand.

A.2 HSCP Sensor calibration

All four of the choppers were calibrated prior to the completion of the field trials. The data logging system used during the calibration procedure was the same one used during the field trails. A torsional load of 0 to 400 N·m in 100-N·m intervals, was applied to the 2X0.5, 2X3 and 3X3 choppers. The range of load was selected based on previous testing, which suggested that the maximum power required by the choppers was 120 kW, while the chopper was rotating at approximately 2900 rpm. For the WR a torsional load of 0 to 800 N·m in 100-N·m intervals was applied. The range of the torsional load applied to the WR was selected based on previous testing, which suggested that the maximum power required by the chopper was 80 kW, while the chopper was rotating at approximately 940 rpm. The WR was also subject to a torsional load that mimicked a load from the cleaning system with a range of 0 to 300 N·m in 100-N·m intervals.

The choppers were individually calibrated by applying varying static loads with a known moment arm to the choppers to achieve the prescribed torsion load. A set of brackets were fabricated so that the choppers could be supported by bearings atop a bench and rotate freely. To simulate a chopper load, a block was placed under the center knife of the chopper to prevent the chopper from rotating. To simulate a cleaning system load, (only for the WR chopper) the cleaning system drive, shown in Figure 4.16, was fixed to prevent the chopper from rotating. The signal from the Wheatstone bridge on each chopper, shown in Figure 4.17, was recorded during the calibration procedure. For each chopper, a linear equation was used to relate the voltage from the bridge (during the calibration procedure) and the applied torque. The coefficients of the linear fit were obtained by minimizing the sum of squared error between the predicted and measured data. The coefficients of the equations, and the corresponding R^2 value for each chopper are listed in Table A.1. The voltage output as a function of the applied torque to the 2X0.5, 3X3, and WR cleaning system is shown in Figure A.4. The voltage output as a function of the applied torque on the WR, due to a chopper load, and the 2X3 is shown in Figure A.5.

Table A.1 Chopper calibration curves with the corresponding R^2 values where, T_{rq}, is torque (N·m) on the chopper and V, is the signal from the Wheatstone bridge on the chopper (V).

Chopper	**Linear equation**	**R^2**
2X0.5	T_{rq} =134.2V-1.0	1.0
2X3	T_{rq} =-135.0V+1.9	1.0
3X3	T_{rq} =123.2V-9.6	1.0
WR chopper	T_{rq} =-424.3V+4.1	1.0
WR cleaning	T_{rq} =135982V-3141.6	0.90

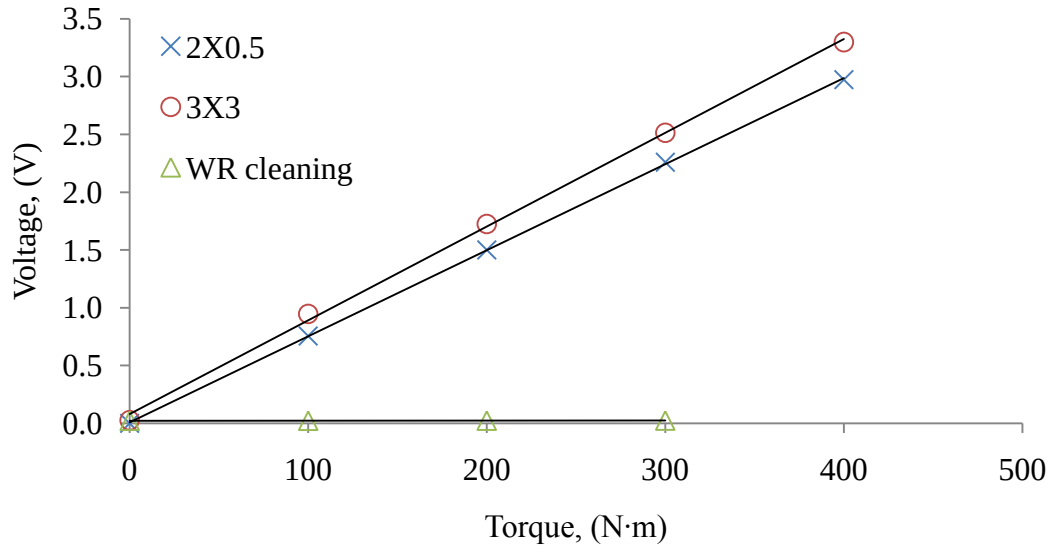

Figure A.4 Calibration curves for the 2X0.5, 3X3 choppers as well as the WR chopper subject to a cleaning system load.

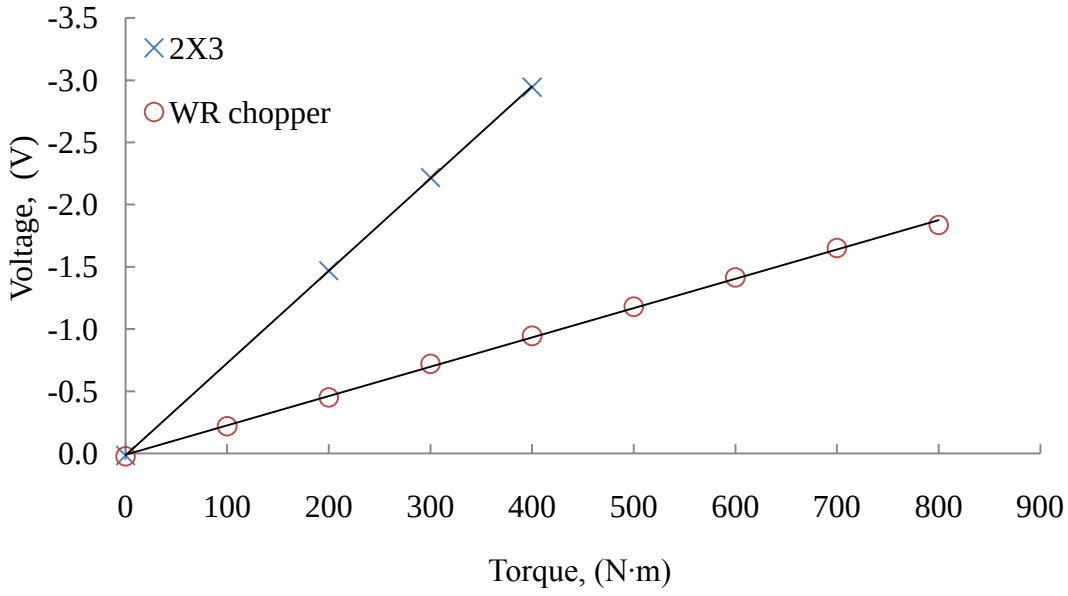

Figure A.5 Calibration curves for the 2X3 chopper and WR chopper subject to a load from the chopper.

The signal output from the Wheatstone bridge on the WR chopper was approximately three orders of magnitude smaller when a simulated “cleaning system load” was applied to the chopper rather than a simulated “chopper load”. The “cleaning system load” was used to mimic the load caused by the cleaning system on the WR chopper, while the “chopper load” was used to mimic the load caused by cutting plant material with the WR chopper. A simulated “cleaning system load” was applied to the chopper by applying a torsional load to the chopper drive, while the resistance to the torsional load was provided at the cleaning system drive. The location of the chopper drive and cleaning system drive are shown in Figure 4.16. Conversely, a simulated “chopper load” was applied to the chopper by applying a torsional load to the chopper drive, while the resistance to the torsional load was provided at the chopper drum. The location of the chopper drum is also shown in Figure 4.16. The WR chopper was not sensitive to a torsional load caused by the cleaning system because the signal from gages 5 to 8 canceled the signal from gages 1 to 4 when a “cleaning system load” was applied to the WR chopper. The location of gages 1 to 8 on the chopper is shown in Figure 4.17. However, when a “chopper load” was applied to the WR chopper, gages 5 to 8 did not experience any deformation, and therefore the signal from gages 5 to 8 did not cancel the signal from gages 1 to 4. Because the signal from the Wheatstone bridge was approximately three orders of magnitude smaller when a simulated “cleaning system load” was applied to the chopper than when a simulated “chopper load” was applied to the chopper, it was assumed that the signal from the WR was independent of the load caused by the cleaning system on the combine. The output from the Wheatstone bridge on the WR chopper was less sensitive than the output from the Wheatstone bridge on the 2X3, 3X3 and 2X0.5 choppers when the choppers were subject to a “chopper load”. The output from the Wheatstone bridge on the 2X3, 3X3 and 2X0.5 choppers was more sensitive to a “chopper load” because the diameter of the shaft to which the gages were mounted on the 2X3, 3X3 and 2X0.5 choppers was smaller than the diameter of the shaft on which the gages were mounted to the WR chopper.

APPENDIX B - MATERIAL PROPERTY TEST STAND PROCEDURES

B.1 Dynamic coefficient of friction

Note: for all tests the pressure relief valve on the test stand must be set to 18 MPa (2600 psi) shown in Figure B.1. This is done by closing the gate valve on the test stand and adjusting the pressure relief valve on the hydraulic power unit.

1. Set flow control valve to 0.6 to top dead center. Note both top dead center and 0.6 are scribes on the pressure-compensated flow control valve, which is shown in Figure B.2.
2. Install the Pulley, modified bolt, and box on the test stand. As shown in Figure B.3.
3. Open Labview program titled Eric's Dynamic coefficient of friction. The screen shot is shown in Figure B.4.
4. Cycle the program once. Proper execution would result in the cylinder making one cycle (starting from a fully extended position and ending in the fully extended position). Before the cylinder extends the program will ask you for the file name. The file contains the position and load data from the test stand for a 3 second interval.
5. Place 300 g of plant material into the box and place the red plate with the two masses on top of the plate as shown in Figure B.5. The combined load of the plate and two masses is 138 N. Thus the total load on the material (including straw is 141.1 N (3.1 N of material)
6. To get a consistent value for zero load press the accept zero when the cylinder is extended but when the box is at the end of its path of travel as shown in Figure B.6.
7. Pull the box to the start of its path and then press the start button.
8. Complete five replicates.

The dynamic coefficient of friction was quantified by dividing the average force to pull the plant material across a steel surface by the normal force applied to the plant material. The dynamic coefficient of friction was quantified by,

$$\mu_k = {}^{F_{AP}}/_{F_N} \quad \textbf{(B.1)}$$

where:

μ is the dynamic coefficient of friction between the plant material and steel,

F_N is the normal force exerted on the plant material (N) and

F_{AP} is the average force required to pull the plant material across a steel surface (N).

The data logging event did not start when the material and containment box was in motion, however it did end when the material was in motion. The pulling force increased at the beginning of the data logging event until the material and containment box reached a steady state velocity. The average pulling force, F_{AP}, was quantified over the period when the material was at a steady state velocity.

B.2 Young's modulus

Note: for all tests the pressure relief valve on the test stand must be set to 18 MPa (2600 psi) shown in Figure B.1. This is done by closing the gate valve on the test stand and adjusting the pressure relief valve on the hydraulic power unit.

1. Set flow control valve to 1.5 to top dead center. Note both top dead center and 1.5 are scribes on the pressure-compensated flow control valve, which is shown in Figure B.2.
2. Install the compression plate and box on the test stand. The compression box must be place in the lowest position possible while still being attached with 4 bolts as shown in Figure B.7.
3. Open Labview program titled Eric's Apparent Young's Modulus. The screen shot is shown in Figure B.8.
4. Cycle the program once. Proper execution would result in the cylinder making two cycles (starting from a fully retracted position and ending in the fully retracted

position). During the first extension the cylinder will pulse down until 22 N of force is exerted on the load cell. The cylinder will briefly stop record its position when it experiences the 22 N load, retract fully, extend fully, and finally retract fully. Before the final retract the program will ask you for the file name. The file contains the position and load data from the test stand for a 20 second interval. The file also contains the load which it stopped at (should be 22 N) and the initial depth of the material.

5. To compute the Young's modulus you will need the following information. The distance between the bottom of the compression plate and the bottom of the box when the cylinder is fully extended. This value should be around 2.7 mm. This value is used in two ways, first to determine the initial depth of material, second to identify the absolute position of the compression plate relative to the box. THIS VALUE MUST BE PUT INTO THE LABVIEW PROGRAM SO THAT THE CORRECT INITIAL DEPTH IS GIVEN AND RECORED FOR LATER USE. Also the signal when the cylinder is fully extended is -7.66V. (Note 1V=1 inch). The area of the compression plate was 77470 mm^2. The area was used to determine the stress.
6. Place 300 g of straw into the box.
7. Complete five replicates replacing the straw every time.

The stress and strain experienced by the plant material needed to be quantified so that the Young's modulus could be defined. The stress experienced by the plant material in the material properties test stand was quantified by,

$$\sigma = {F_{hc}}/{A_p} \qquad \textbf{(B.2)}$$

where:

σ is the normal stress experienced by the plant material (Pa),

F_{hc} is the force exerted on the plant material by the hydraulic cylinder (N) and

A_p is the cross-sectional area of the compression plate (m^2).

The strain experienced by the plant material was determined using the following equation,

$$\varepsilon = {(l_o - l_i)}/{l_o} \quad \textbf{(B.3)}$$

where:

ε is the strain experienced by the plant material,

l_o is the initial depth of plant material in the compression box (m) and

l_i is the instantaneous depth of plant material in the compression box (m).

A third-order polynomial curve was fit to the plant material stress-strain curve to define the Young's modulus. A curve was fit to the data instead of using the tangent, secant or cord method because the third-order polynomial curve was more accurate in defining the stress-strain relationship.

B.3 Maximum cutting force

Note: for all tests the pressure relief valve on the test stand must be set to 18 MPa (2600 psi) shown in Figure B.1. This is done by closing the gate valve on the test stand and adjusting the pressure relief valve on the hydraulic power unit.

1. Set flow control valve to 1.5 to top dead center. Note both top dead center and 1.5 are scribes on the pressure compensated flow control valve, which is shown in Figure B.2.
2. Install the max cutting force die and plunger. The cutting die must be place in the lowest position possible while still being attached with 4 bolts as shown in Figure B.9.
3. Open Labview program titled Eric's Maximum Cutting Force. The screen shot is shown in Figure B.10.
4. Cycle the program once. Proper execution would result in the cylinder making one cycle (starting from a fully retracted position and ending in the fully retracted position). Before retracting the program will ask you for the file name. The file contains the position and load data for a 1 second interval.

5. To achieve a density of 30, 90, kg/m^3 a mass of 9, 26 g must be placed in the cutting die.
6. Complete five replicates for each density level (10 measurements per sample) replacing the plant material every time.

The maximum shear force was quantified by dividing the maximum compressive force exerted by the hydraulic cylinder by the cross-sectional area of the punch. The maximum shear force was quantified by,

$$ms = {F_{CM}}/{A_{punch}} \quad \textbf{(B.4)}$$

where:

ms is the maximum shear strength of the plant material (Pa),

F_{CM} is the maximum compressive force exerted by the hydraulic cylinder (N) and

A_{punch} is the cross-sectional area of the punch used to shear the plant material (m^2).

It was assumed that there was a linear relationship between the maximum shear strength and the dry-mass density. The moisture content of the plant material was quantified after the trials were completed using the ASABE Standard S358.2 (ASABE Standards, 2008). The moisture content information was used to quantify the dry-mass density of the material at the time of processing.

Data Acquisition

- Set the two channels of the power supply to 15.01V.
- Connect LVDT signal to channel 0 on data logger, connect load cell to channel 1 on data logger

Figure B.1 Photograph of pressure transducer used to measure the pump pressure.

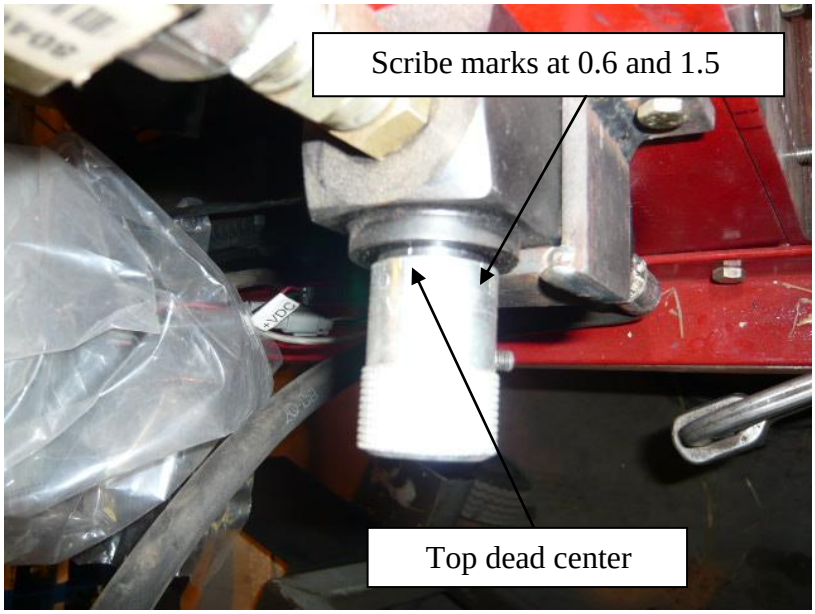

Figure B.2 Photograph of the pressure compensated flow control valve.

Figure B.3 Photograph of the dynamic coefficient of friction tool installed on the material properties test stand.

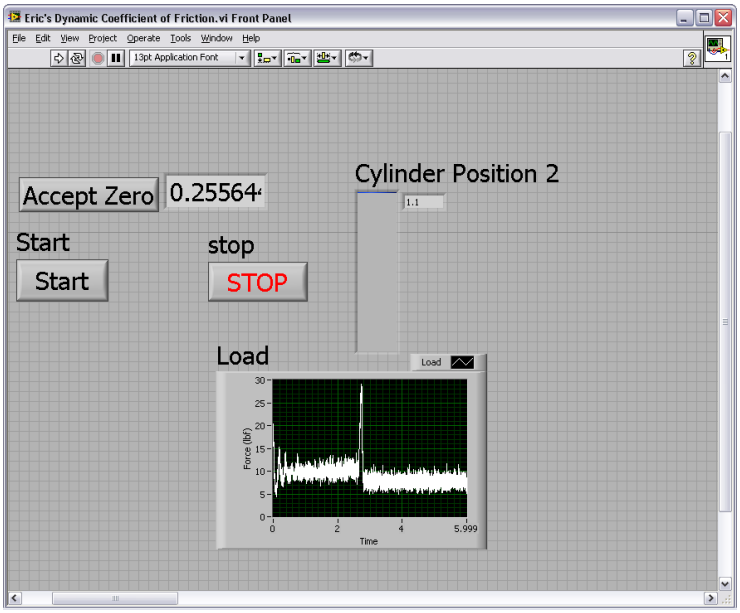

Figure B.4 Screenshot of the Labview program used to measure the dynamic coefficient of friction.

Figure B.5 Photograph of the compression plate and weights used to load the material to determine the dynamic coefficient of friction.

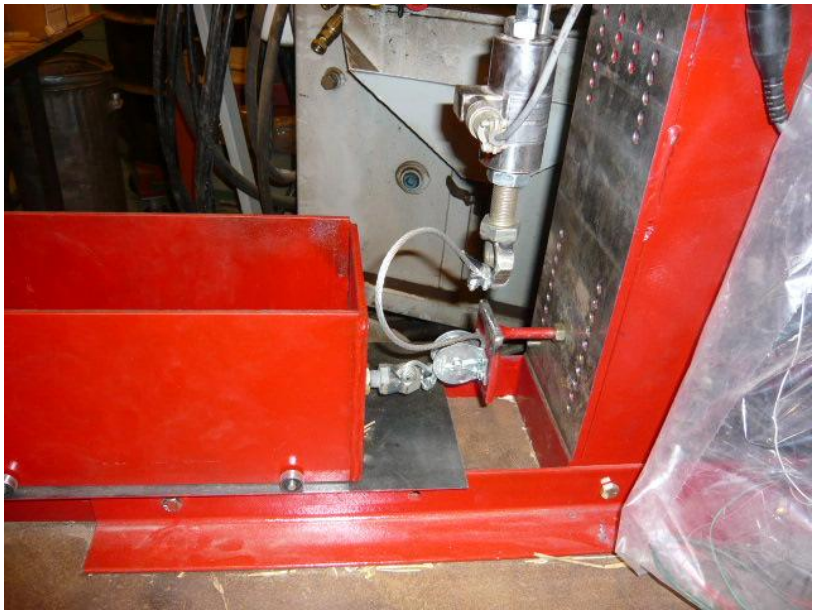

Figure B.6 Photograph showing the position of the box and cable when the “zero” value is accepted in the Labview program.

Figure B.7 Photograph showing the compression box and plate installed on the material properties test stand.

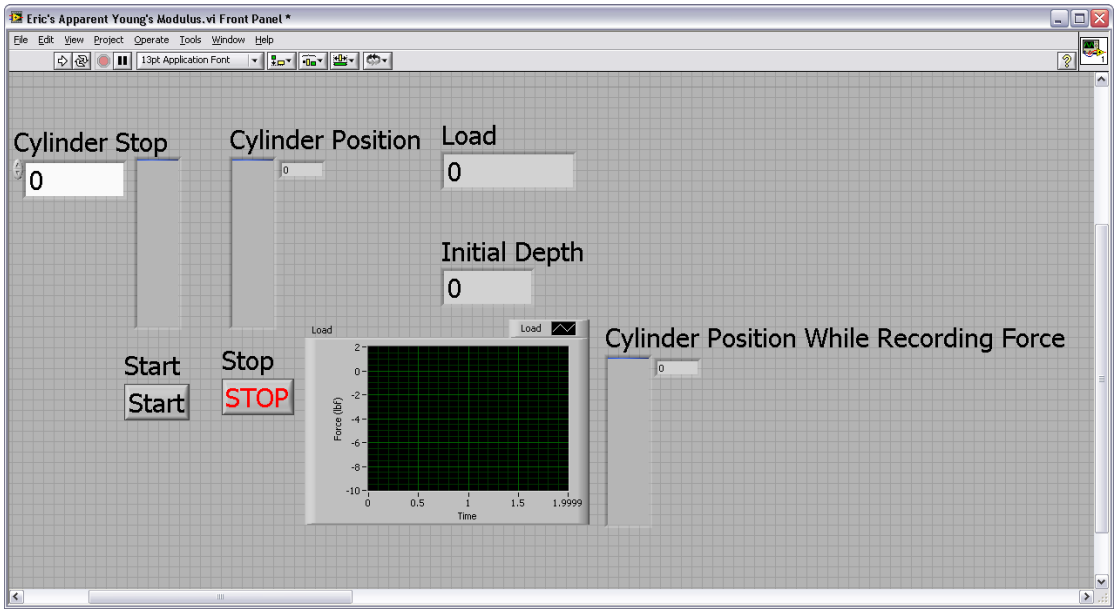

Figure B.8 Screenshot of the Labview program used to determine the apparent Young's modulus.

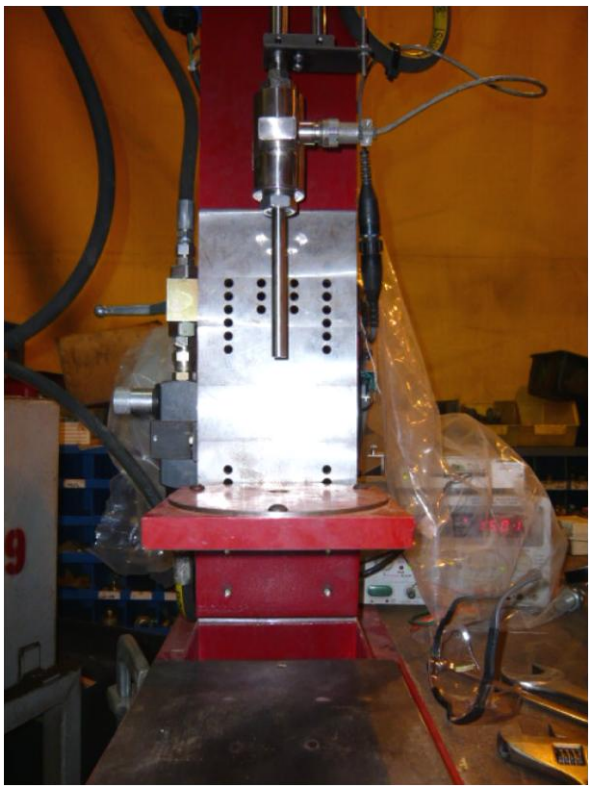

Figure B.9 Photograph of the plunger and die used to determine the maximum shear strength installed on the material properties test stand.

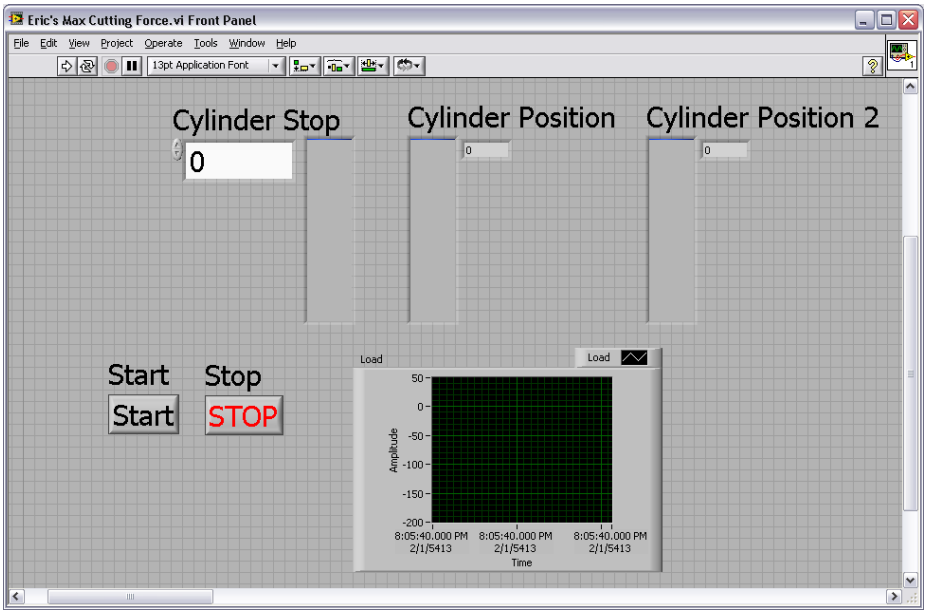

Figure B.10 Screenshot of the program used to determine the maximum shear strength.

APPENDIX C - TABLES OF ANALYSIS OF VARIANCE

C.1 Factors that affected the specific energy requirement of the LSCP RFCS

Table C.1 Analysis of variance of the data investigating the effect of counter-knife sharpness, rotor speed and cereal straw throughput on the specific energy requirement of the LSCP RFCS.

Source	Partial SS	df	Mean Square	F	Sig.
Model	1.8188	17	0.1070	6.94	<0.0001
Sharpness	1.1188	1	1.1188	113.49	0.0004
Whole Plot | Sharpness	0.0394	4	0.0099		
Rotor speed	0.0185	2	0.0093	0.60	0.5543
Throughput	0.0290	2	0.0145	0.94	0.4006
Rotor speed * Throughput	0.1569	4	0.0392	2.55	0.0592
Throughput * Sharpness	0.0698	2	0.0349	2.26	0.1209
Rotor Speed * Sharpness	0.0535	2	0.0268	1.74	0.1929
Error	0.4777	31	0.0154		
Total	2.2965	48	0.0478		

Table C.2 Analysis of variance of the data used to investigate the effect of counter-knife thickness, serrations and cereal straw throughput on the specific energy requirement of the LSCP RFCS.

Source	Partial SS	df	Mean Square	F	Sig.
Model	0.2307	19	0.0121	3.22	0.0109
Thickness	0.0237	1	0.0237	4.28	0.0723
Serrations	0.1126	1	0.1126	20.37	0.0020
Thickness * Serrations	0.0053	1	0.0053	0.95	0.3580
Whole Plot | Thickness * Serrations	0.0442	8	0.0055		
Throughput	0.0283	2	0.0141	3.76	0.0460
Thickness * Throughput	0.0046	2	0.0023	0.62	0.5518
Throughput * Serration	0.0066	2	0.0032	0.87	0.4378
Thickness* Throughput* Serration	0.0055	2	0.0027	0.73	0.4972
Error	0.0602	16	0.0038		
Total	0.2909	35	0.0083		

Table C.3 Analysis of variance of the data used to investigate the effect of counter-knife thickness, bevel angle and alfalfa moisture content and throughput on the specific energy requirement of the LSCP RFCS.

Source	Partial SS	df	Mean Square	F	Sig.
Model	1.3912	28	0.0497	34.88	<0.0001
Thickness	0.0201	1	0.0201	7.25	0.0133
Bevel	1.0877	1	1.0877	391.29	<0.0001
Moisture	0.0256	2	0.0128	4.61	0.0213
Whole Plot | Thickness*Bevel*Moisture	0.0612	22	0.0028		
Throughput	0.0028	2	0.0014	0.97	0.3851
Error	0.0727	51	0.0014		
Total	1.4638	79	0.0185		

Table C.4 Analysis of variance of the data used to investigate the effect of counter-knife sharpness, serrations and alfalfa throughput on the average power required by the LSCP RFCS.

Source	Partial SS	df	Mean Square	F	Sig.
Model	4.9549E+06	19	2.6079E+05	10.37	<0.0001
Sharpness	3.1821E+06	1	3.1821E+06	203.73	<0.0001
Serrations	2.2357E+05	1	2.2357E+05	14.31	0.0054
Sharpness * Serrations	2.5587E+05	1	2.5587E+05	16.38	0.0037
Whole Plot | Sharpness * Serrations	1.2495E+05	8	1.5619E+04		
Throughput	9.5205E+05	2	4.7602E+05	18.93	0.0001
Sharpness * Throughput	1.5207E+04	2	7.6037E+03	0.30	0.7432
Throughput* Serrations	5.9857E+04	2	2.9929E+04	1.19	0.3297
Sharpness*Throughput*Serrations	1.4136E+05	2	7.0681E+04	2.81	0.0899
Error	4.0238E+05	16	2.5149E+04		
Total	5.3573E+06	35	1.5307E+05		

C.2 Factors that affected the specific energy requirement of the HSCP RFCS

Table C.5 Analysis of variance of the data used to investigate the effect of cereal straw throughput, moisture content and counter-knife engagement on the specific energy requirements of the 3X3 chopper.

Source	Type III Sum of Squares	df	Mean Square	F	Sig.
Corrected Model	1.3942E+01	11	1.2670E+00	10.32	<0.0001
Intercept	9.4187E+01	1	9.4187E+01	766.72	<0.0001
Moisture	8.2270E+00	1	8.2270E+00	66.97	<0.0001
Throughput	7.0000E-03	1	7.0000E-03	0.06	0.8100
Counter-knife Engagement	3.5710E+00	2	1.7850E+00	14.53	<0.0001
Moisture * Throughput	1.7500E-01	1	1.7500E-01	1.43	0.2440
Moisture * Counter-knife Engagement	1.7830E+00	2	8.9100E-01	7.26	0.0030
Throughput * Counter-knife Engagement	1.4600E-01	2	7.3000E-02	0.59	0.5600
Moisture * Throughput * Counter-knife Engagement	3.3000E-02	2	1.7000E-02	0.14	0.8740
Error	2.9480E+00	24	1.2300E-01		
Total	1.1108E+02	36			
Corrected Total	1.6890E+01	35			

Table C.6 Analysis of variance of the data used to investigate the effect of cereal straw throughput, moisture content and counter-knife engagement on the specific energy requirements of the 2X3 chopper.

Source	Type III Sum of Squares	df	Mean Square	F	Sig.
Corrected Model	7.5900E+00	11	6.9000E-01	7.22	<0.0001
Intercept	2.3136E+01	1	2.3136E+01	242.04	<0.0001
Moisture	3.4230E+00	1	3.4230E+00	35.80	<0.0001
Throughput	5.0400E-01	1	5.0400E-01	5.27	0.0310
Counter-knife Engagement	2.7120E+00	2	1.3560E+00	14.18	<0.0001
Moisture * Throughput	0.0000E+00	1	0.0000E+00	0.00	0.9570
Moisture * Counter-knife Engagement	7.2000E-01	2	3.6000E-01	3.77	0.0380
Throughput * Counter-knife Engagement	1.9000E-02	2	1.0000E-02	0.10	0.9060
Moisture * Throughput * Counter-knife Engagement	2.1200E-01	2	1.0600E-01	1.11	0.3460
Error	2.2940E+00	24	9.6000E-02		
Total	3.3020E+01	36			
Corrected Total	9.8840E+00	35			

Table C.7 Analysis of variance of the data used to investigate the effect of cereal straw throughput, moisture content and counter-knife engagement on the specific energy requirements of the WR chopper.

Source	Type III Sum of Squares	df	Mean Square	F	Sig.
Corrected Model	8.4400E-01	11	7.7000E-02	4.38	0.0020
Intercept	1.6026E+01	1	1.6026E+01	914.10	<0.0001
Moisture	2.4000E-01	1	2.4000E-01	13.68	0.0010
Throughput	3.1000E-01	1	3.1000E-01	17.68	<0.0001
Counter-knife Engagement	8.6000E-02	2	4.3000E-02	2.45	0.1120
Moisture * Throughput	1.4000E-02	1	1.4000E-02	0.80	0.3810
Moisture * Counter-knife Engagement	2.1000E-01	2	1.0500E-01	5.98	0.0090
Throughput * Counter-knife Engagement	1.0000E-01	2	5.0000E-02	2.84	0.0820
Moisture * Throughput * Counter-knife Engagement	1.5000E-02	2	7.0000E-03	0.42	0.6640
Error	3.5100E-01	20	1.8000E-02		
Total	1.9120E+01	32			
Corrected Total	1.1950E+00	31			

APPENDIX D - ANALYTICAL MODEL VISUAL BASIC SYNTAX

D.1 LSCP analytical model visual basic syntax

```
Function BalerRotorPower(Thr As Double, Width As Double, Rotorbedarclenght As Double, Rotorbedradiusofcurvature As Double, Sheararea As Double, Slopedensityatshear As Double, Frictionfactor As Double, Pbase As Double, AOt As Integer, Dynamiccoefficientoffriction As Double, Slopemaxshear As Double, Interceptmaxshear As Double, Young0 As Double, Young1 As Double, Young2 As Double, Young3 As Double, Del As Variant, Mptrd As Variant, Gam As Variant, Alp As Variant, Zet As Variant, Lam As Variant, Idpth As Variant, Rotationalspeed As Double) As Variant

    'Define variables

    'Variables used to calculate power due to one tine and zone

    Dim Fcompress As Double 'Compressive force
    Dim Fshear As Double 'Shear force
    Dim Fcs As Double 'Force to compress and shear
    Dim Pcs As Double 'Power to compress and shear
    Dim Strain As Double 'The strain the plant material experiences
    Dim InitialDepth As Double 'Used to identify the initial depth of plant material
    Dim Cut As Integer ' Used to identify the cut number

    'Indicate that the force to compress plant material exceeds the force to cut plant material in each zone of each cut

    Dim Fcompressmax 'Variable used to identify that the compression force exceeds the shear force
    Dim CC As Boolean 'Variable used to identify that the compression force exceeds the shear force

    'Variables to define tine transport power

    Dim Lambda As Double 'Angle of rotor when the tine passes the counter knife
    Dim Ptt As Double 'Variable used to store the power to transport material by the counter-knife

    'Variables used to loop through zones

    Dim zone As Integer 'Used to identify the zone
    Dim Midpointradius As Double 'Mid point radius of zone
    Dim Zeta As Double 'Angle between the radial unit vector and compressive/shear force
    Dim Alpha As Double 'Angle between leading and lagging edge of tine
    Dim Gamma As Double 'Angle between datum and leading knife edge
    Dim Delta As Double 'Arc length of tine
    Dim Power As Double 'Used to store the power consumption of all 10 zones on a tine
    Dim V() As Variant 'Vector used to store the per degree power requirements of a tine
    ReDim V(1 To 190, 1 To 2) 'Zero the matrix


    'Vector to store total power for all zones

    Dim Z() As Variant
    ReDim Z(1 To 720, 1 To 2) 'Zero the matrix
    Dim Ro As Long
    Dim Row As Long
    Dim Intsum As Double

    'Variables used to copy tine power into total power

    Dim Sum As Double
    Dim Theta As Integer
```

```
Dim NumofCuts As Integer 'Total number of cuts made by RFCS during one revolution
Dim AOmt As Integer 'Angular offset between the model zero and the trial zeroth degree

'Variables to create the model output a 0 to 359 power curve

Dim P() As Variant
ReDim P(1 To 364, 1 To 2)
P(1, 1) = "RotorPosition, deg"
P(1, 2) = "Model Power, W"
Dim Phi As Integer

'Variables to define rotor bed transport power

Dim Prb As Double 'Rotor bed transport power
Dim Num As Double

'Quantify the dry mass density of plant material during shear

Dim maxIdpth As Double 'Maximum initial depth of plant material
Dim minIdpth As Double 'Minimum initial depth of plant material
Dim hy As Integer

'Initialize variables

Fcompressmax = 0
Fshear = 0
Fcompress = 0
Fcs = 0
Pcs = 0
Strain = 0
Power = 0
zone = 1
Ptt = 0
Ro = 1
Cut = 1
Intsum = 0
Theta = 1
Prb = 0
Num = 0
NumofCuts = 15  'Number of cuts made by RFCS during one revolution of the rotor
AOmt = 25 'Angular offset between model and trial data zeroth degree
Phi = 1
maxIdpth = 0
minIdpth = 100
hy = 1
CC = True

 'Start loops

For Cut = 1 To NumofCuts

InitialDepth = Idpth(1, Cut)

'Quantify the maximum and minimum initial depth of plant material and the corresponding dry mass density of plant material

maxIdpth = Application.WorksheetFunction.Max(Idpth)
For hy = 1 To NumofCuts
If Idpth(1, hy) > 0.001 And Idpth(1, hy) < minIdpth Then minIdpth = Idpth(1, hy)
Next hy

ReDim V(1 To 190, 1 To 2) 'Zero the V array
```

```
For zone = 1 To 10

   Midpointradius = Mptrd(1, zone)
   Zeta = Zet(1, zone)
   Alpha = Alp(1, zone)
   Gamma = Gam(1, zone)
   Delta = Del(1, zone)
   Lambda = Lam(1, zone)
   Theta = -80

   For Theta = -80 To 109

     V(Theta + 81, 1) = Theta + 81

        'Calculation of compress and shear power

           If (Theta + Alpha > (Gamma - (InitialDepth / (Midpointradius * (1.74532925199433E-02))))) And (Theta + Alpha < Gamma) Then Strain = Midpointradius * (0.017453293 * (Theta + Alpha - (Gamma - InitialDepth / (Midpointradius * (2 * 3.141592654 / 360))))) / InitialDepth Else: Strain = 0
           Fcompress = Delta * Width * 1000 * (Young0 + Young1 * Strain + Young2 * Strain ^ 2 + Young3 * Strain ^ 3) * Strain
           Fshear = (Slopemaxshear * (InitialDepth * Slopedensityatshear) + Interceptmaxshear) * Sheararea * 1000
           If Fcompress < Fshear Then Fcs = Fcompress Else Fcs = Fshear
           Pcs = Rotationalspeed * Midpointradius * Fcs * Sin(Zeta) + Dynamiccoefficientoffriction * Rotationalspeed * Midpointradius * Fcs * Cos(Zeta)

        'Ensure that fcompress exceeds fshear

           If Fcompress > Fcompressmax Then Fcompressmax = Fcompress

        'Calculation of tine transport power

           If (Theta + Alpha > Gamma) And (Theta < Lambda) Then Ptt = Frictionfactor * InitialDepth * Dynamiccoefficientoffriction * Midpointradius * Rotationalspeed Else Ptt = 0

        'Store power from previous zone

           Power = V(Theta + 81, 2)

        'Enter total power into array

      V(Theta + 81, 2) = Pcs + Power + Ptt

   Next Theta

'Ensure that fcompress exceeds fshear

If Fcompressmax < Fshear And Fcompressmax > 1 Then CC = False
Fcompressmax = 0

Next zone

   Power = 0

'Copy values from V matrix to Z matrix

For Row = 1 To 190

   Sum = V(Row, 2)
   Z(Ro, 1) = Ro
```

```
            Intsum = Z(Ro, 2)
            Z(Ro, 2) = Sum + Intsum
            Ro = Ro + 1

        Next Row

    Ro = Ro - 190 + AOt

    Next Cut

    'Define rotor bed power consumption

    Prb = Thr * (Rotationalspeed * Mptrd(1, 5)) ^ 2 * Dynamiccoefficientoffriction * Rotorbedarclenght / Rotorbedradiusofcurvature

    'Shift the matrix Z to the P matrix

    For Phi = 1 To 360 - AOmt

        P(Phi + 1, 1) = Phi
        Num = Z(Phi + AOmt, 2) + Z(Phi + AOmt + 360, 2)
        P(Phi + 1, 2) = Round(Num + Prb + Pbase, 0)

    Next Phi

    For Phi = 360 - AOmt + 1 To 360

        P(Phi + 1, 1) = Phi
        Num = Z(Phi + AOmt, 2) + Z(Phi - (360 - AOmt), 2)
        P(Phi + 1, 2) = Round(Num + Prb + Pbase, 0)

    Next Phi

        P(362, 1) = "Fcompress>Fcut"
        P(362, 2) = CC
        P(363, 1) = "Max drymass density, kg/m3"
        P(363, 2) = Round(Slopedensityatshear * maxIdpth, 0)
        P(364, 1) = "Min drymass density, kg/m3"
        P(364, 2) = Round(Slopedensityatshear * minIdpth, 0)

  BalerRotorPower = P

End Function
```

D.2 HSCP analytical model visual basic syntax

```
Function CombineRotorPower2(Thr As Double, Width As Double, Rotorbedarclenght As Double, Rotorbedradiusofcurvature As Double, Sheararea As Double, Slopedensityatshear As Double, Frictionfactor As Double, Pbase As Double, AOt As Integer, AOt2 As Integer, Dynamiccoefficientoffriction As Double, Slopemaxshear As Double, Interceptmaxshear As Double, Young0 As Double, Young1 As Double, Young2 As Double, Young3 As Double, Del As Variant, Mptrd As Variant, Gam As Variant, Alp As Variant, Zet As Variant, Lam As Variant, Idpth As Variant, Rotationalspeed As Double) As Variant

    'Define variables

    'Variables used to calculate power due to one tine and zone

    Dim Fcompress As Double 'Compressive force
    Dim Fshear As Double 'Shear force
    Dim Fcs As Double 'Force to compress and shear
    Dim Pcs As Double 'Power to compress and shear
    Dim Strain As Double 'The strain the plant material experiences
    Dim InitialDepth As Double 'Used to identify the initial depth of plant material
    Dim Cut As Integer ' Defines the number of cuts per revolution of rotor

    'Indicate that the force to compress plant material exceeds the force to cut plant material in each zone of each cut

    Dim Fcompressmax 'Variable used to identify that the compression force exceeds the shear force
    Dim CC As Boolean 'Variable used to identify that the compression force exceeds the shear force

    'Variables to define tine transport power

    Dim Lambda As Double 'Angle of rotor when the tine passes the counter knife
    Dim Ptt As Double 'Variable used to store the power to transport material on tine

    'Variables used to loop through zones

    Dim zone As Integer 'Used to identify the zone
    Dim Midpointradius As Double 'Mid point radius of zone
    Dim Zeta As Double 'Angle between the radial unit vector and compressive/shear force
    Dim Alpha As Double 'Angle between leading and lagging edge of tine
    Dim Gamma As Double 'Angle between datum and leading knife edge
    Dim Delta As Double 'Arc length of tine
    Dim Power As Double ' Used to store the power consumption of all 10 zones on a tine
    Dim V() As Variant ' Vector used to store the per degree power requirements of a tine
    ReDim V(1 To 8000, 1 To 2)
    Dim counter As Integer

    'Vector to store total power for all zones on a fraction of a degree basis

    Dim X() As Variant
    ReDim X(1 To 21440, 1 To 2) 'Zero the matrix
    Dim Ro As Long
    Dim Row As Long
    Dim Intsum As Double

    'Vector to store total power for all zones on a per degree basis

    Dim Z() As Variant
    ReDim Z(1 To 1072, 1 To 2) 'Zero the matrix
    Dim sum1 As Double
    Dim avg As Double
    Dim Count1 As Integer
    Dim Count2 As Integer
```

```
'Variables used to copy tine power into total power

Dim Sum As Double
Dim Theta As Double
Dim NumofCuts As Integer 'Total number of cuts made by RFCS during one revolution
Dim AOmt As Integer 'Angular offset between the model zero and the trial zeroth degree

'Variables to create a 0 to 359 power curve

Dim P() As Variant
ReDim P(1 To 364, 1 To 2)
P(1, 1) = "Rotor Position (°)"
P(1, 2) = "Model Output"
Dim Phi As Integer

'Variables to define rotor bed transport power

Dim Prb As Double 'Rotor bed transport power
Dim Num As Double

'Quantify the dry mass density of plant material during shear

Dim maxIdpth As Double 'Maximum initial depth of plant material
Dim minIdpth As Double 'Minimum initial depth of plant material
Dim hy As Integer

'Initialize variables

Fshear = 0
Fcompress = 0
Fcs = 0
Pcs = 0
Strain = 0
Power = 0
zone = 1
Ptt = 0
Ro = 1
Cut = 1
Intsum = 0
Theta = -80.5
Prb = 0
Num = 0
NumofCuts = 78 'Number of cuts made by RFCS during one revolution of the rotor
AOmt = 64 'Angular offset between model and trial data zeroth degree
Phi = 1
Fcompressmax = 0
counter = 1
sum1 = 0
avg = 0
Count1 = 1
Count2 = 1
maxIdpth = 0
minIdpth = 100
hy = 1
CC = True

'Start loops

For Cut = 1 To NumofCuts

InitialDepth = Idpth(1, Cut)
```

```
'Quantify the maximum and minimum initial depth of plant material and the corresponding dry mass density of plant material

maxIdpth = Application.WorksheetFunction.Max(Idpth)
For hy = 1 To NumofCuts
If Idpth(1, hy) > 0.001 And Idpth(1, hy) < minIdpth Then minIdpth = Idpth(1, hy)
Next hy

If Application.WorksheetFunction.IsOdd(Cut) Then

ReDim V(1 To 8000, 1 To 2) 'Zero the V array

  For zone = 1 To 10

    Midpointradius = Mptrd(1, zone)
    Zeta = Zet(1, zone)
    Alpha = Alp(1, zone)
    Gamma = Gam(1, zone)
    Delta = Del(1, zone)
    Lambda = Lam(1, zone)
    Theta = -80.5
    counter = 1

    For Theta = -80.5 To 119.5 Step 0.025

      V(counter, 1) = Theta


        'Calculation of compress and shear power

          If (Theta + Alpha > (Gamma - (InitialDepth / (Midpointradius * (1.74532925199433E-02))))) And (Theta + Alpha < Gamma) Then Strain = Midpointradius * (0.017453293 * (Theta + Alpha - (Gamma - InitialDepth / (Midpointradius * (2 * 3.141592654 / 360))))) / InitialDepth Else: Strain = 0


          Fcompress = Delta * Width * 1000 * (Young0 + Young1 * Strain + Young2 * Strain ^ 2 + Young3 * Strain ^ 3) * Strain
          Fshear = (Slopemaxshear * (InitialDepth * Slopedensityatshear) + Interceptmaxshear) * Sheararea * 1000
          If Fcompress < Fshear Then Fcs = Fcompress Else Fcs = Fshear
          Pcs = Rotationalspeed * Midpointradius * Fcs * Sin(Zeta) + Dynamiccoefficientoffriction * Rotationalspeed * Midpointradius * Fcs * Cos(Zeta)

        'Ensure that fcompress exceeds fshear

          If Fcompress > Fcompressmax Then Fcompressmax = Fcompress

        'Calculation of tine transport power

          If (Theta + Alpha > Gamma) And (Theta < Lambda) Then Ptt = Frictionfactor * InitialDepth * Dynamiccoefficientoffriction * Midpointradius * Rotationalspeed Else Ptt = 0

        'Store power from previous zone

          Power = V(counter, 2)

        'Enter total power into array

       V(counter, 2) = Pcs + Power + Ptt
       counter = counter + 1
```

```
        Next Theta

    'Ensure that fcompress exceeds fshear

    If Fcompressmax < Fshear And Fcompressmax > 1 Then CC = False
    Fcompressmax = 0

    Next zone

Else

    For zone = 1 To 10

      Midpointradius = Mptrd(1, zone)
      Zeta = Zet(1, zone)
      Alpha = Alp(1, zone)
      Gamma = Gam(1, zone)
      Delta = Del(1, zone)
      Lambda = Lam(1, zone)
      Theta = -80.5
      counter = 1
      For Theta = -80.5 To 119.5 Step 0.025

        V(counter, 1) = Theta

          ' Calculation of compress and shear power

            If (Theta + Alpha > (Gamma - (InitialDepth / (Midpointradius * (1.74532925199433E-02))))
And (Theta + Alpha < Gamma) Then Strain = Midpointradius * (0.017453293 * (Theta + Alpha - (Gamma -
InitialDepth / (Midpointradius * (2 * 3.141592654 / 360))))) / InitialDepth Else: Strain = 0
            Fcompress = Delta * Width * 1000 * (Young0 + Young1 * Strain + Young2 * Strain ^ 2 +
Young3 * Strain ^ 3) * Strain
            Fshear = (Slopemaxshear * (InitialDepth * Slopedensityatshear) + Interceptmaxshear) * Sheararea
* 1000
            If Fcompress < Fshear Then Fcs = Fcompress Else Fcs = Fshear
            Pcs = Rotationalspeed * Midpointradius * Fcs * Sin(Zeta) + Dynamiccoefficientoffriction *
Rotationalspeed * Midpointradius * Fcs * Cos(Zeta)

          'Ensure that fcompress exceeds fshear

          If Fcompress > Fcompressmax Then Fcompressmax = Fcompress

          ' Calculation of tine transport power

          If (Theta + Alpha > Gamma) And (Theta < Lambda) Then Ptt = Frictionfactor * InitialDepth *
Dynamiccoefficientoffriction * Midpointradius * Rotationalspeed Else Ptt = 0

          'Store power from previous zone

            Power = V(counter, 2)

          ' Enter total power into array

        V(counter, 2) = Pcs + Power + Ptt
        counter = counter + 1

      Next Theta

    'Ensure that fcompress exceeds fshear

    If Fcompressmax < Fshear And Fcompressmax > 1 Then CC = False
    Fcompressmax = 0
```

```
    Next zone

     'Copy values from V matrix to X matrix

    For Row = 1 To 8000

       Sum = V(Row, 2)
       X(Ro, 1) = Ro
       Intsum = X(Ro, 2)
       X(Ro, 2) = Sum + Intsum
       Ro = Ro + 1

    Next Row

If Cut = 26 Or Cut = 52 Then Ro = Ro - 8000 + (AOt2 * 40) Else Ro = Ro - 8000 + (AOt * 40)

End If

Next Cut

'Average the power to a per degree basis transferring values from the X matrix to the Z matrix

For Count1 = 1 To 536

   sum1 = 0
   avg = 0
   Count2 = 1

   For Count2 = 1 To 40

      sum1 = sum1 + X((Count2 + ((Count1 - 1) * 40)), 2)

   Next Count2
   avg = sum1 / 40
   Z(Count1, 2) = avg


Next Count1

'Define rotor bed power consumption

Prb = Thr * (Rotationalspeed * Mptrd(1, 5)) ^ 2 * Dynamiccoefficientoffriction * Rotorbedarclenght /
Rotorbedradiusofcurvature

'Shift the Z matrix to the P matrix

For Phi = 1 To 360 - AOmt

   P(Phi + 1, 1) = Phi
   Num = Z(Phi + AOmt, 2) + Z(Phi + AOmt + 360, 2)
   P(Phi + 1, 2) = Round(Num + Prb + Pbase, 0)

Next Phi


For Phi = 360 - AOmt + 1 To 360

   P(Phi + 1, 1) = Phi
   Num = Z(Phi + AOmt, 2) + Z(Phi - (360 - AOmt), 2)
   P(Phi + 1, 2) = Round(Num + Prb + Pbase, 0)

Next Phi
```

```
        P(362, 1) = "Fcompress>Fcut"
        P(362, 2) = CC
        P(363, 1) = "Max drymass density, kg/m3"
        P(363, 2) = Round(Slopedensityatshear * maxIdpth, 0)
        P(364, 1) = "Min drymass density, kg/m3"
        P(364, 2) = Round(Slopedensityatshear * minIdpth, 0)

  CombineRotorPower2 = P

End Function
```